Active Cooling for Electronics in a Wireline Oil-Exploration Tool

by

Aaron G. Flores

B.S.M.E., MIT (1991)

M.S.M.E., MIT (1992)

Submitted to the Department of

Mechanical Engineering

in Partial Fulfillment of the Requirements for the

Degree of Doctor of Philosophy

at the

MASSACHUSETTS INSTITUTE OF TECHNOLOGY

June, 1996

Signature of Author.....

Department of Mechanical Engineering June, 1996

Certified by.....

Peter Griffith

Professor, Mechanical Engineering

Chairman, Graduate Committee

Accepted by.....

Ain Sonin

Chairman, Departmental Committee on Graduate Students

Active Cooling for Electronics in a Wireline Oil-Exploration Tool

by

Aaron G. Flores

Submitted to the Department of Mechanical Engineering
in Partial Fulfillment of the Requirements for
the Degree of Doctor of Philosophy in
Mechanical Engineering

Abstract:

A low-cost, low-maintenance miniature active cooling system was successfully designed, built, and tested at temperatures up to 200°C for refrigeration in a downhole electronic chassis of a wireline oil-exploration tool with a maximum outside diameter of 0.0921 meter (3.625 inches). The downhole oil-exploration environment and operation constraints were applied to numerous potential cooling techniques, and the optimal method was selected in terms of performance, cost, size, and simplicity. A once-through mechanical vapor-compression cooler, with water as the working refrigerant, was invented. The cooler design is theoretically capable of maintaining an electronics chassis dissipating up to 50W within a Dewar flask at or below 125°C for extended periods of time (greater than 10 hours) in a 200°C borehole. The miniature cooling system consists of an evaporator, condenser, and compressor. Each component was designed, built, and tested at 200°C. The actual prototype is capable of 30W of cooling while maintaining the electronics chassis within a Dewar flask below 114°C, and the coefficient of performance (COP) of the system was approximately equal to one.

Thesis Supervisor: Dr. Peter Griffith
Title: Professor of Mechanical Engineering

Acknowledgments:

Many people and institutions have aided me in completing this investigation. On a personal level, I would like to thank my wife Valerie. She has sacrificed the majority of our first two years of marriage for this project. On an academic level, I would like to thank my advisor Professor Peter Griffith. I have had the opportunity and honor to work with him on two different research projects. From him I have gained a true appreciation of an order-of-magnitude analysis and the "gut" feeling an engineer should have about a given problem in the real world. I would also like to thank Professor Carl Peterson and John Brisson II for being on my committee. I would also like to thank Dipti Nevrekar who worked for me as an undergraduate engineering intern and produced a lot of useful work towards this investigation. On a professional level, I would like to thank Schlumberger Wireline and Testing management for allowing me the time and resources to perform this research. Dr. Bruce McCann, Tom Zimmerman, Dr. Andrew Kurkjian, and Mike Parsons all at one time or another had to okay this program from a management perspective. I also would like to thank the following Schlumberger engineers, designers, and technicians for their help and insights over the last two years: Mark Hinton, Tom Macdougall, Miles Jaroska, Mark Olender, Jack Followay, Mario Flores, Bill Grant, Duane LaDue, Dean Lauppe, Mike Perkins, Tom Langford, John Ratcliffe, Alan Sallwasser, Dan Stehling, Wayne Sundquist, and Wes Wofford. I would also like to thank Winona Junco for proof-reading the text of this document.

Table of Contents

Table of Contents (cont.)

List of Figures

List of Figures (cont.)

List of Tables

Chapter 1: Introduction

1.1: Motivation: Problem Statement

Schlumberger Wireline and Testing is an oilfield services company which designs and builds tools used for downhole oil exploration. Downhole tools can be exposed to temperatures as high as 200°C, possibly causing damage to or negatively affecting the performance of the electronic circuitry in the tools. Currently, sophisticated electronics, able to withstand these high temperatures, are used in the tools (i.e., high temperature electronics), but they are often very expensive and increasingly difficult to find. When tools not designed with the high temperature components are used in a hot borehole, their electronics are placed in Dewar flasks that insulate them. However, in the absence of a cooling system, the Dewar flask only provides a temporal solution, as short as three to four hours depending on the electronic power dissipation. The purpose of this research is to discover, design and build an inexpensive, low-maintenance miniature cooling system that allows standard "off-the-shelf" electronic components (i.e., electronics rated to 125°C) dissipating up to 50W of heat to be used in downhole wireline exploration tools in a hot borehole (200°C) for an extended length of time (i.e., greater than 10 hours).

1.1.1: Motivation: Costs of High Temperature

The oil-exploration industry is very competitive but for the most part saturated. Corporations such as Schlumberger Wireline and Testing tend to gain or maintain market share with better service and/or lower cost to their clients than their competitors. This service includes more sophisticated technology that provides superior results to those offered by competitors at a lower price. The accuracy of the results allows customers to better analyze their production capabilities and ultimately their revenues and profits. In this competitive market place, corporations must continually strive to make exploration tools with less capital but higher performance through low-cost innovation (Parsons, 1996).

Unlike industries such as the automotive or aerospace, the oil exploration industry sells their services to their clients, not their hardware. In other words, Schlumberger will produce exploration tools, train their own personnel on their use, and then sell the entire service to a customer on a per-job basis. This method of operation requires the seller to continually maintain their tools. Consequently, low-maintenance and low-cost components are sought when designing the exploration tools.

The costs of high temperature components in oil-exploration tools are apparent on three different levels. The three levels are (1) cost of man-years dedicated to development, searching, and characterization, (2) screening, and (3) maintenance. These costs can further be characterized as reoccurring for the life of the tool which can be well over a decade. When summed, the costs contribute to an overall price tag of the tool that is several factors greater than the equivalent low temperature component version.

An order-of-magnitude analysis of the first level of cost can be further explained by comparing the development times and selling prices of two similar functioning tools developed by Schlumberger in the last decade. The AIT* Array Induction Tool is a high temperature (i.e., 175°C) wireline tool. When compared to the newer, low temperature (i.e., 125°C) wireline tool that performs the same function, AIT-H* Array Induction Tool-Platform Express, some cost comparisons can be made. First of all, one can look at the electronic development times of five years for the AIT* tool versus one and one-half years for the AIT-H* tool with similarly sized project teams. This is basically a factor of three in development time and man-years. Although, one can rationalize the development time differences with the fact that a lot of the technology could be put into AIT-H* tool since its predecessor the AIT* tool was already developed, the general pricing scheme further verifies the cost differentiation. The price tag associated with the AIT* tool is approximately three times higher than the AIT-H* tool. Again, the factor of three in cost is reflected between the low and high temperature tools (Hazen, 1995).

There also exists a high price associated with the second cost level or part characterization and qualification. When developing a new high temperature tool or replacing a no-longer-functioning or obsolete part number within an existing tool, the engineer must perform several tasks. First, the engineer must find a component that works at the elevated temperatures of the tool. He usually starts with several similar components that are rated to 125°C and tests them until he finds one that continues to work at the high temperatures. After the part is found, it must be qualified with several tests such as heating cycles, as well as, calibrated for its high temperature behavior. This entire process costs several thousand dollars per part (Mathison, 1995).

In addition to finding a high temperature component, engineers many times must screen each component before it is assembled in a tool. The screening process can cost between $5 and $10 per part. Although not very expensive on a per-part level, one must consider each time the part is used the process must be repeated. Thus, the total capital expenditures quickly rise for the screening processes. In addition to part screening, the entire electronic assemblies must also be screened through a series of high temperature tests (Mathison, 1995).

Exploring the different areas of high component costs, it quickly becomes apparent how the high temperature tool can be several factors more expensive than those rated to lower temperature. Unfortunately, the future promises an even more difficult task of finding and maintaining high temperature components.

1.1.2: Motivation: High Temperature Component Availability: Present and Future

Design engineers are finding it increasingly difficult to find and maintain high temperature electronic components. The two main phenomena responsible are shortened manufacturing cycle times and the low temperature driven industrial market.

Manufacturing cycle times for electronics continue to shorten causing engineers to many times replace components that are presently used in high temperature tools. The cycle times now are roughly two years. The driving forces for the shorter cycle times are competition, performance enhancements, and lower manufacturing costs. The Schlumberger engineer usually discovers that the cycle has been altered when electronic components that had previously worked in tools no longer perform at elevated temperatures. Since the component is not originally specified from the manufacturer to work at the elevated temperatures, the new manufacturing processes may drastically alter the behavior of a component at high temperature. Consequently, a new low temperature component must be found, tested, qualified, etc. to the high temperature rating. The previously described sequence of events is constantly reoccurring today and will continue into the future (Jaroska, 1995).

One of the main reasons for the unavailability of high temperature components is the electronics market. High volume customers primarily drive the market. Today, the high volume customers are the computer and automotive industries. Neither of these industries use or require high temperature components. In the past, the military also was a market force and did include some high temperature electronics. However, with the shrinking defense in the United States and the end of the Cold War, the military is no longer driving a significant market sector. In fact, several electronic companies are dropping military standard components. These are the same military standard components that many times serve as the best starting point for finding high temperature components for the oil-exploration industry (Jaroska, 1995).

1.1.3: Motivation: Current Market

The oil-exploration market consists of both low and high temperature wells. Traditionally, tools have been designed to withstand both types. However, with the increasing costs of high temperature equipment, it is important to reexamine the well temperature distribution and market share as a function of temperature. The well distribution for both the World and North America is found in Figure 1.1. The resulting market share distributions are plotted in Figure 1.2. It is interesting to note that only 10% of the wells are above 125°C, but 20% of the exploration revenue is generated by those 10%. These figures display the obvious need for high temperature exploration, but not the requirement for all tools to meet the high temperature rating. An optimal compromise is an inexpensive add-on cooling unit that allows low temperature tools to perform in high temperature wells for the extended lengths of time necessary for exploration.

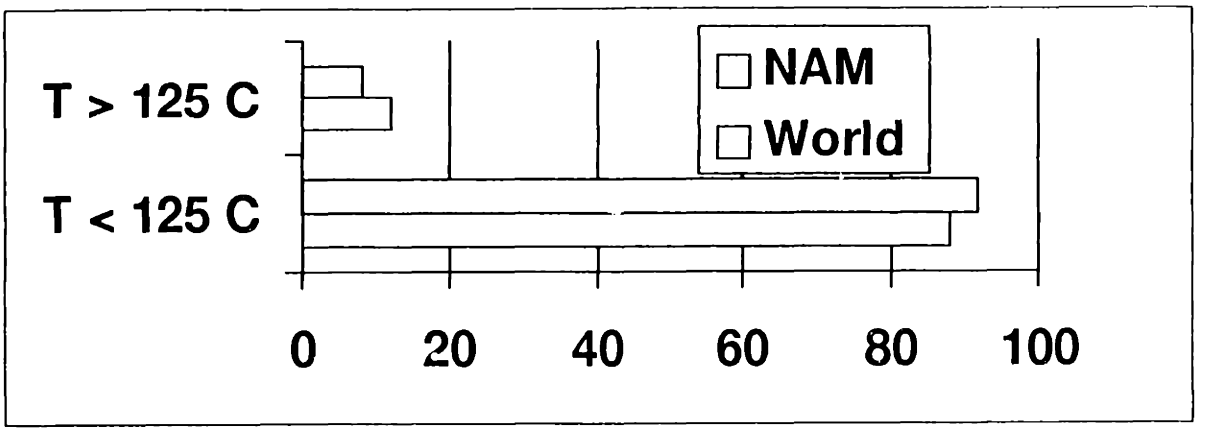

Figure 1.1: Number of Wells Percent vs. Temperature in North America and the World (Ardic, 1995)

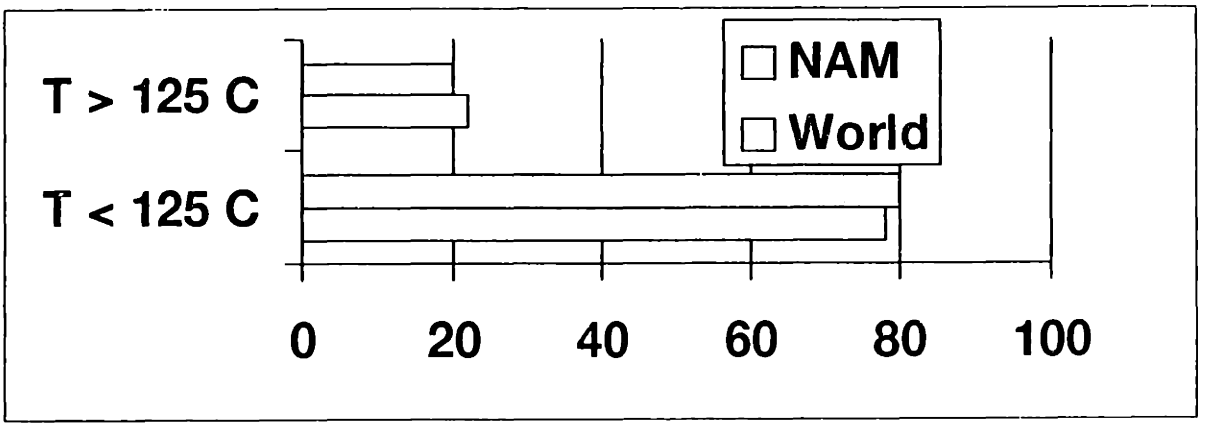

Figure 1.2: Market Share Percent vs. Temperature in North America and the World (Ardic, 1995)

1.1.4: Motivation: Potential Performance Enhancements

In addition to cost savings and lack of availability of high temperature components, a cooling system allowing the electronic chassis of the tool to remain at or below 125°C could allow designers to add new tool-enhancing performance components. High performance logic and/or processing components could be added to the downhole tool. Thus, better sensors and measurements would be available, as well as increased downhole control and processing. This would inevitably be a competitive advantage for the company using this technology (Jaroska, 1995).

1.2: Background

Historically, geothermal exploration, not oil exploration, has driven active downhole cooling development. Oil companies in the past have accepted the higher operating costs of the high temperature components and designed accordingly. The geothermal environment challenges engineers with temperatures in excess of 300°C. The selection of components that work at this level are much more difficult to develop than the high temperature oil-exploration components rated to 175°C or 200°C.

The state-of-the-art in downhole thermal protection in both industries is represented by the Dewar flask. Dewar flasks are passive devices that act to insulate the electronic chassis of the tool from the hot borehole (see Chapter 3). The behavior is similar to a large Thermos bottle. In many designs the Dewars are put in thermal communication with a heat sink of phase-change material. The addition of the heat sink extends the downhole residence time of the tool. In the average oil-exploration tool, a Dewar flask extends the downhole residence time by approximately two to four hours (Bennett, 1991, p.9). The previously mentioned passive systems are inherently limited by their heat sink size and cannot be made for extended downhole service.

Currently, development and research on active refrigeration systems for downhole tools in both industries are very limited. Development work on advanced cooling methods done by oil companies suffers from budget swings brought about by changes in oil prices. In addition, due to the competitive nature of the oil-exploration industry, any advancements or cooling system developments would be kept strictly confidential and as a trade secret (Bennett, 1991, p.8). To the author's knowledge, only two significant efforts have been attempted on active cooling methods, and both were for geothermal environments. Because of the technical promise of a vapor cycle-based active cooling system, the Division of Geothermal Energy of the Energy Research and Development Administration (ERDA) of the Department of Energy (DOE) funded a two-part development contract for a reciprocating water vapor compressor suitable for cooling a geothermal-exploration tool's electronics chassis in the late 1970's (United States, 1977 and 1979). Although a prototype compressor was built, it failed to function properly. A second and more in-depth effort occurred at Los Alamos National Labs and entailed a detailed search and analysis of several different cooling methods versus the geothermal exploration environment and constraints. Furthermore, an optimal method was chosen and designed. However, the research ended without an actual prototype (Bennett, 1991, p.1).

1.3: Course of Action

The present research effort was broken into several steps. First, the exploration and downhole environment of the tool was defined. Second, the available operation parameters, constraints, maintenance, and costs of the tools were identified. The thermal and hydraulic behaviors of the tools were then modeled with respect to the flow patterns, geometry, and downhole environment. With the above information, a matrix of possible cooling methods was developed, and the optimal method chosen for a downhole

refrigeration system. The optimal system was then designed and proved feasible on a component-by-component basis. Once the subsystems were proved feasible, a full-scale prototype was built and successfully tested at downhole temperatures. The prototype cooler was able to cool 30W of electronic heat between an electronics temperature at 114°C and a borehole temperature of 200°C with a coefficient of performance (COP) equal to one. The research was performed at two different locations. All steps, except for the modeling of the tool and cooling matrix evaluation, occurred at Schlumberger Well Services in Sugar Land, Texas. The remaining steps were performed at the Massachusetts Institute of Technology. The completion goal of the research was a working prototype in two years.

* Mark of Schlumberger

Chapter 2: Environment, Operation, and Design Constraints

To properly evaluate an optimal cooling method for downhole exploration tools, the investigator must define the environment, operation constraints, design constraints, maintenance, and cost limitations from which downhole tools are designed. In the following chapter an overall industrial description of these parameters is provided. Although some of these parameters differ from tool to tool and company to company, the average behavior is presented.

2.1: Environment

The environment that the downhole tools are exposed to is very harsh when compared to surface conditions. Pressures range from 1.01×10^5Pa to 1.38×10^8Pa at depths from 0m to 4572m. Downhole temperatures range from -20°C to 200°C. Wellbores are filled with a host of fluids and additives. The presence of different fluids is usually a function of the reserves sought, in-situ stress in the formation, and well economics. The majority of the fluid volumes can be classified into oils, water, gases, and muds. The muds can be further broken down into water and oil-based types with between 1% and 30% solid volume (Gray, 1981, pp. 11-23). Table 2.1 lists the major environmental parameters for downhole tools.

Table 2.1: Environment of Downhole Tools

1) Depth	0m (0ft)- 4572m (15,000ft)
2) Pressure	1.01×10^5Pa (14.7psi)-1.38×10^8Pa (20,000psi)
3) Temperature	-20°C - 200°C
4) Fluids	Oil, Water, Gas
5) Solids: Water and Oil-Based Muds	0 %-30 % Solid Volume

2.2: Operation Constraints

Downhole tools are also subject to several operation constraints that include hole sizes, shocks, and vibrations. Wellbore hole diameters in both cased and open holes range from 0.076m to 0.203m. The vibration levels in downhole logging tools range from 0g's to roughly 10g's on all three axes at frequencies from 0Hz to 250Hz where g is equal to acceleration due to gravity. Tools may also experience mechanical shocks up 100g's at 5msec when dropped in a borehole or the shop floor (Jaroska, 1995). The movements of the tool within a borehole range from zero velocity to a constant tool velocity between 0.5m/s and 1m/s depending on the job being performed (Sundquist, 1995). However, the majority of oil-exploration logging tools move in the 0.5m/s to 1m/s range, and the active cooling system of the tool will be designed accordingly (see Chapter 4). Table 2.2 sums the operating specifications for downhole tools.

Table 2.2: Operating Specifications of Downhole Logging Tools

1) Wellbore Diameters	0.076m (3in.)-0.203m (8in.)
2) Tool Speed	0m/s (Not Considered) & 0.5m/s (~1.5ft/s)-1m/s (~3.5ft/s)
3) Vibrations:	Sine and Random
X, Y, Z Axes	10g's @ 0Hz- 250Hz
4) Mechanical Shock	up to 100g's @ 5msec.

2.3: Design Constraints

Given a typical wireline logging tool, the investigator can estimate design specifications for a downhole refrigerator. A downhole wireline tool performs remote tasks in deep boreholes via a wireline cable with lengths equaling the depth of the hole (see Figure 2.1). The wireline cable transmits power and data to the tools, as well as data

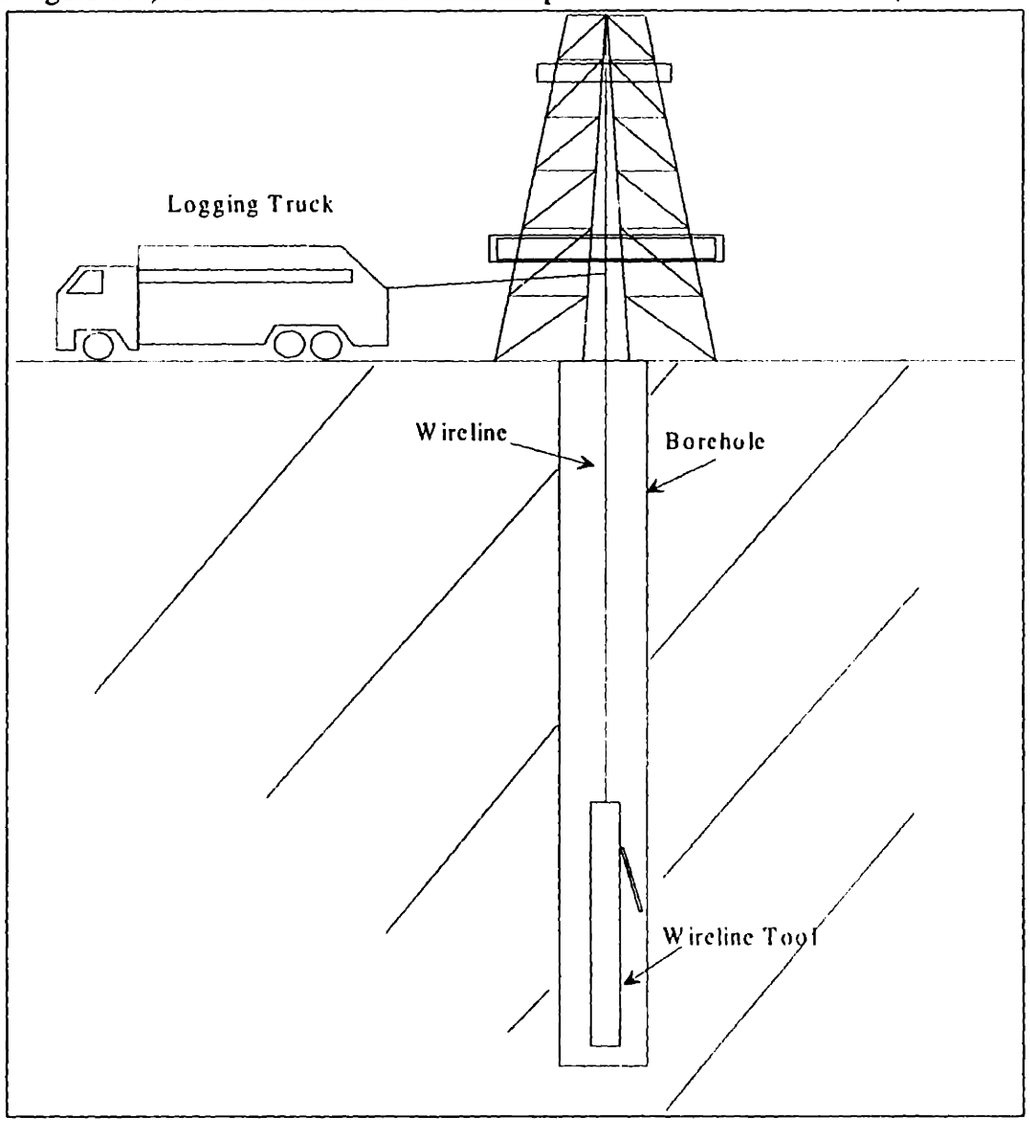

Figure 2.1: Wireline Evaluation Services

back to the user at the surface. Power available through the cable, and not used by the standard tool, ranges from 250W to 500W (Jaroska, 1995). The cooling unit should be no larger than 0.0921m (3.625in.) in diameter. This diameter represents the popular 0.0857m (3.375in.) diameter wireline tools with the addition of a Dewar flask. The length, although not as important as the diameter specification, is to be minimized and contribute to an overall weight as small as possible. Along with the physical design specifications, the investigator can derive the refrigeration parameters.

The refrigeration limits represent current worst-case-scenarios in wireline tools. Although, the downhole residence times of tools vary from tool to tool, a limit for the cooler is set for 10 hours in a 200°C borehole. This period would encompass the vast majority of downhole wireline tools (Head, 1995). The electronics chassis must be kept at or below 125°C at its hottest spots. Although 150°C could be tolerated, the 125°C goal is a common industrial component standard. The borehole is assumed to be at a worst-case 200°C. With 75-°C temperature difference, the conduction or heat flux through modern Dewar flasks is approximately 30W (see Chapter 3). The worst-case electronic power dissipation or heat generation in a wireline tool is approximately 50W (Jaroska, 1995). Thus, the total refrigeration load equals 80W between a cold reservoir of 125°C and a hot reservoir of 200°C.

The less tangible design constraints include simplicity, maintenance, and price. The refrigeration unit should be as simple as possible to development to do so in the funded two-year period. From the oil field perspective, the maintenance costs and requirements should be kept to a minimum with respect to labor and materials. In other words, the maintenance materials should be those that can be acquired easily at oilfield locations. Finally, the finished refrigeration unit should be priced at a fraction of the standard wireline tool. The author assumes a $10 thousand per unit price is reasonable. The design and development constraints are summed in Table 2.3.

Table 2.3: Design Constraints

1) Available Power	250W - 500W
2) Diameter	0.0921m (3.625in.)
3) Weight and Length	Minimized
4) Electronics Temperature (Cold Reservoir)	< 125°C
5) Borehole Temperature (Hot Reservoir)	200°C
6) Refrigeration Load: Total	80W
6a) Conduction through Dewar	30W
6b) Electronic Heat Generated	50W
7) Downhole Residence Time	10 Hours
8) Complexity	Minimized
9) Maintenance	Not Labor/Capital Intensive
10) Unit Price	~ $ 10,000

Chapter 3: Today's Solution

The oil industry today deals with high temperature boreholes in one of two ways. The first solution utilizes high temperature rated tools. These tools contain the costly, high temperature electronics described in Chapter 1. The second solution entails using a Dewar flask when the borehole is hotter than the temperature rating of the downhole tool. The critical electronic components of the tool are inserted into the Dewar and remain thermally isolated from the hot borehole. This solution attempts to buffer the electronics for the length of time required to explore the hole. Section 3.1 briefly describes a Dewar flask and Section 3.2 develops the thermal models for the flask within a borehole.

3.1: Dewar Flask Description

As stated in Chapter 1, Dewar flasks represent today's solution in thermal protection systems. The Dewar flask design entails a long, cylindrical steel outer housing that encases a thin vacuum-evacuated layer filled with low conductivity insulation (see Figure 3.1). The Dewar is closed on one end and is open on the other for the insertion of electronic boards, etc. In addition to the Dewar flask, several passive thermal systems contain phase change materials acting as heat sinks (see Chapter 4). Thus, the Dewar may also encompass heat sinks at either end.

The circuit boards of the tool are mounted on an electronics chassis and inserted into the center of the Dewar flask. The outer wall of the flask is then in contact with the wellbore surroundings. The insulation provides the barrier to heat flux into the flask. Interior to the insulation, there also exists a thin inner housing of steel that provides

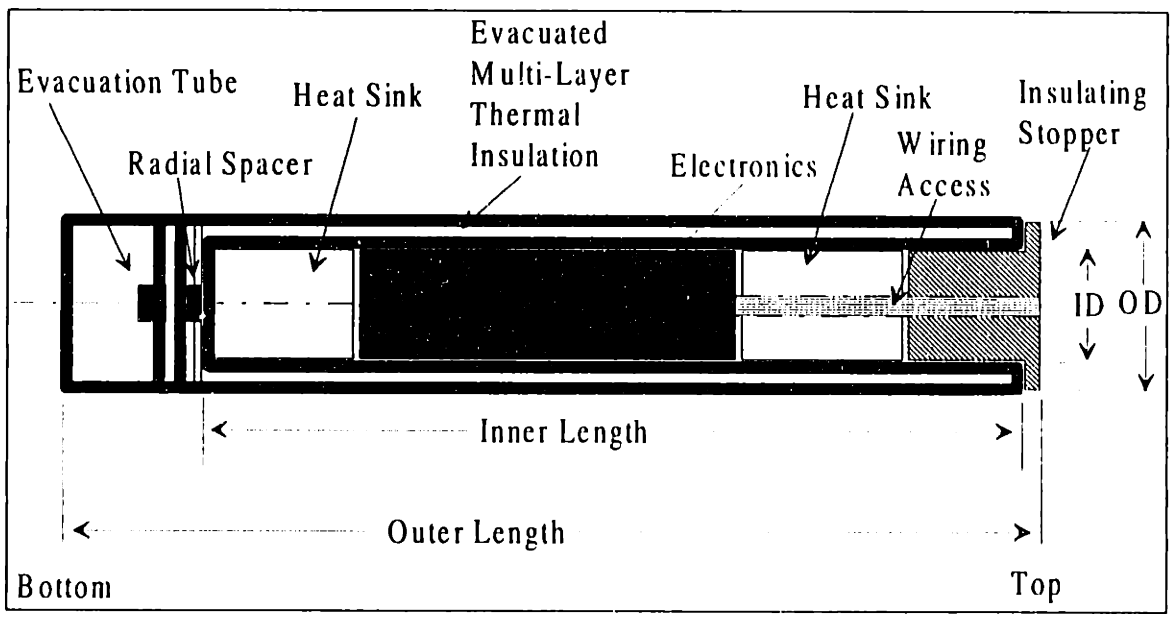

Figure 3.1: Passive Thermal Protection System (Blanton, 1986, p.36)

internal support. Heat transfer to the electronics of the tool occurs by conduction across the steel wall, insulation, and inner housing. Although no two Dewar flasks are exactly the same, due to the nature of their construction, companies screen them through a series of tests determining their usability (Followay, 1995). Figure 3.2 displays the common flask construction and dimensioning scheme used in the oil industry (see Tables 3.1-3.2). The screenings test for a minimum acceptable thermal conductivity through the walls of the flask. With knowledge of the geometry and thermal conductivity of the flask, as well as the proposed electronics and borehole temperatures, the investigator is able to derive the heat flux into the electronic chassis and resulting downhole residence time.

Table 3.1: Numerical Values for Flask Analysis

Material	Specific Heat (c_p) (J/kg-°K)	Conductivity (k) (W/m-°K)	Density (ρ) (kg/m^3)
Steel	470	13.4	8400
Aluminum	903	177	
Copper	385	401	
Titanium	522	21.9	
Electronics	~ 750		~1800
Super Insulation		~0.001 (conservative)	
Teflon™	1050	0.45	2200
Approximate Dimensions	in.	m	
r_4	1.819	0.046	
r_3	1.550	0.039	
r_2	1.440	0.037	
r_1	1.390	0.035	
L	66	1.676	
Steel Plate Width	0.5	0.013	
Steel Plate Wire Hole (22) Radius	~0.040	~0.001	
Steel Plate Radius	r_4		
Teflon Insulation Length	6	0.152	
Teflon Insulation Radius	r_4		

Table 3.2: Flask Analysis Constants

T_H(°C)	200
T_C(°C)	100
Max T_{elect}(°C)	125
Initial T_{elect}(°C)	25
Heat Dissipation, Q_{gen}(W)	50

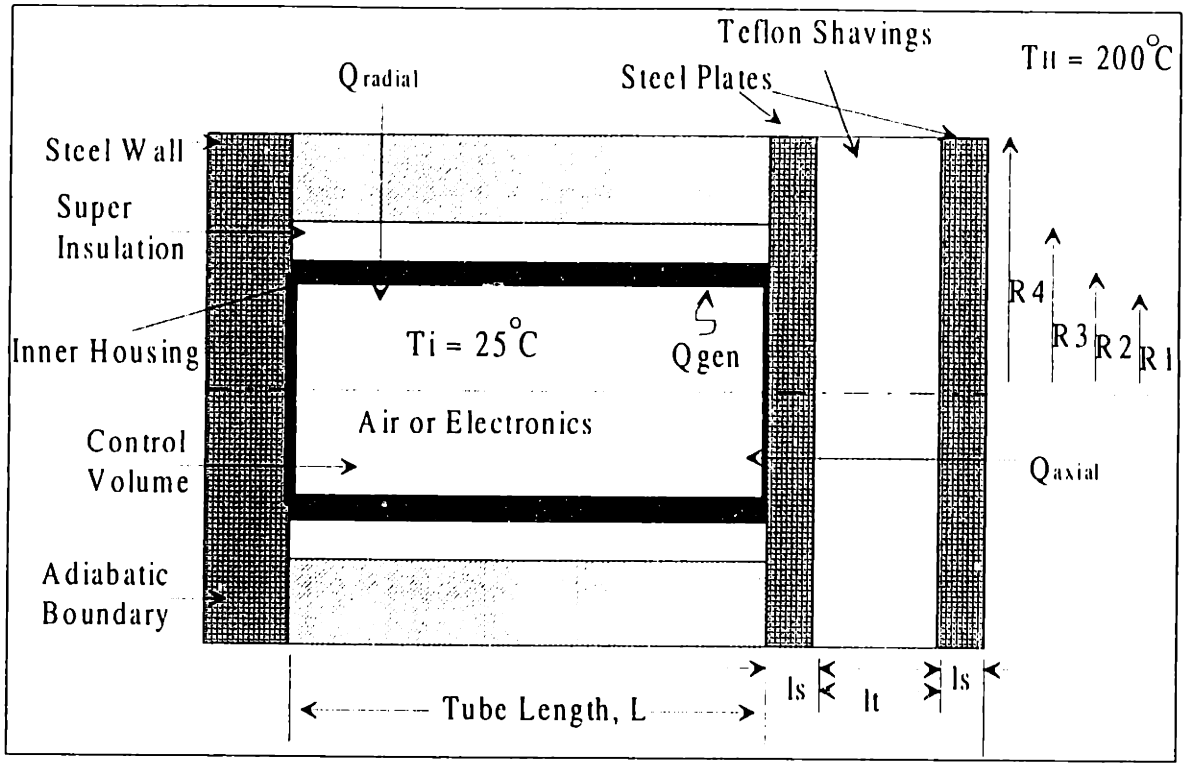

Figure 3.2: Oil-Exploration Dewar Flask (Radial View) (Nevrekar, 1996, p.12)

3.2: Dewar Flask Analysis

3.2.1: Temperature Rise of Dewar/Tool System (w/Electronic Heat Generation)

When placed into a hot wellbore, heat is conducted into the electronic chassis through the Dewar causing its internal temperature to rise. For an upper-bound estimate, the environment surrounding the flask is assumed to be at 200°C. To create a worst-case-scenario, the temperature at the exterior wall, T_H, is taken to be 200°C. In the actual system, the skin temperature would be less than or equal to 200°C as a function of convection interactions between the outer surface of the flask, borehole fluid, and tool speed. For this analysis, the internals of the electronics chassis and inner housing of the flask were assumed to be a lumped mass at the same temperature. The end effects are also neglected, and the flask and its internals are assumed to be homogeneous throughout its length. The validity of the assumption concerning the end effects is proved in a previously supervised study by this investigator performed at Schlumberger (Nevrekar, 1996, p.18).

Initially, at time, t, equal to 0sec., the temperature of the interior of the flask and the inner housing was assumed to be at the same temperature T_i equal to 25°C. At t > 0sec., the temperature of the interior and the inner housing of the flask increases. The internal temperature rise of the flask, as a function of time, is given by (see Appendix A)

$$T(t) = \left(T_i - T_H - Q_{gen}\,\Sigma R\right) e^{-\frac{t}{\left[(\rho V c_p)_{int} + (\rho V c_p)_{inner\ shell}\right]\Sigma R}} + T_H + Q_{gen}\,\Sigma R, \quad (3\text{-}1)$$

where Q_{gen} is the electronic heat generated, ΣR is the total thermal resistance of the Dewar flask, and ρ and V are the density and volume of the internal electronics and steel inner housing, respectively. The thermal resistances for the steel and insulation are given by

$$R_{st} = \frac{\ln\left(\frac{r_4}{r_3}\right)}{2\pi\, k_{st} L} \qquad \text{and} \qquad R_{ins} = \frac{\ln\left(\frac{r_3}{r_2}\right)}{2\pi\, k_{ins} L}. \quad (3\text{-}2)$$

The total effective resistance is found by combining the two expressions in eq. (3-2):

$$\Sigma R = R_{st} + R_{ins}. \quad (3\text{-}3)$$

Plots of the internal temperature of the flask versus time are shown in Figures 3.3 and 3.4. Two calculations are plotted assuming electronics fill the interior of the flask generating both 0W and 50W.

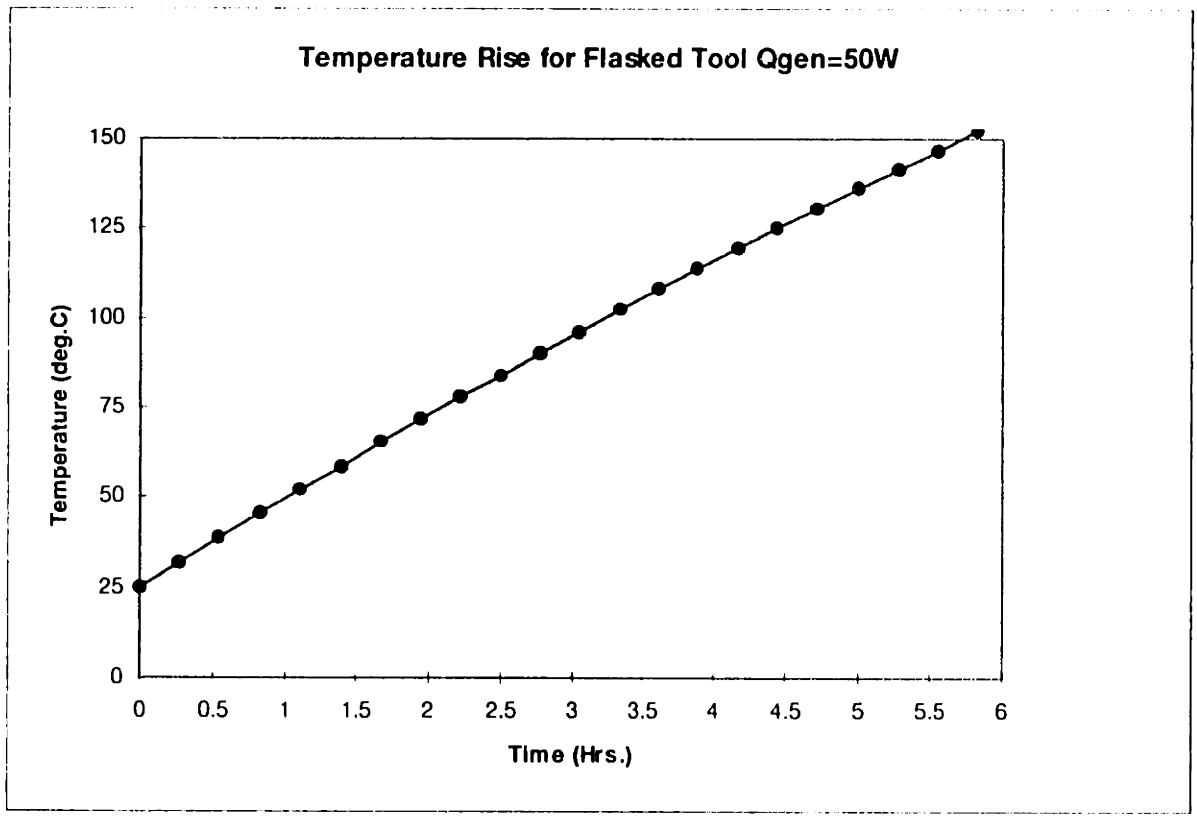

Figure 3.3: Temperature Rise of Flasked Electronics for Q_{gen}=50W

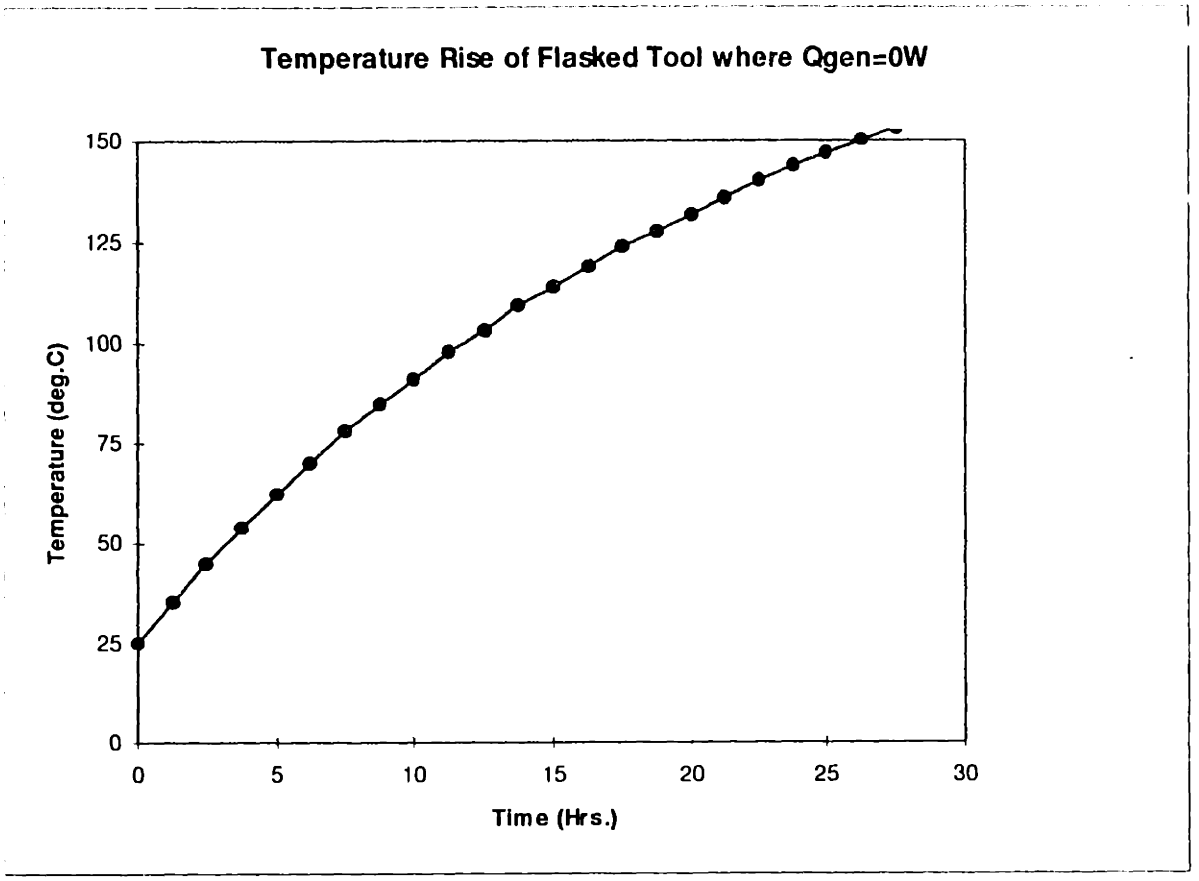

Figure 3.4: Temperature Rise of Flasked Electronics for Q_{gen}=0W

The curves show the electronics temperature reaching the 125°C mark at periods of approximately four hours when the electronic components generate 50W. In an optimal scenario, the heat generation by the electronics would be very low. Consequently, the standard flask would give the operator almost seventeen hours to explore the borehole. Because the majority of tools fall between these two curves, the active cooler development will account for the worst-case scenario.

3.2.2: Heat Flux into Dewar/Tool System with Refrigerator

The steady state heat flux conducted into the flasked and refrigerated electronics from the hot borehole must also be derived so that the total refrigeration load can be specified. The same constant values will be assumed, as well as, an electronic chassis cooled to 100°C. Equation(A-4) without the heat-generation term and equation(A-7) can be combined to give the heat flux conducted into the electronics as approximately 15W (see Appendix A). Thus, 30W conduction value is used for conservative design purposes when a safety factor of two is used.

Chapter 4: Borehole Analysis

To gain an estimate of heat exchanger sizes and heat transfer convection rates, the tool/borehole flow and heat transfer patterns are modeled. There are several borehole fluid models used in the oil-exploration industry. Three such models are discussed in this chapter for wireline tools: (1) Laminar, (2) Plug, and (3) Bingham-Plastic fluid models (see Figure 4.1). Heat transfer in the zero flow or stationary flow case is also developed. Different models are applicable as a function of the fluids within the borehole and movement of the tool. Turbulent models are not included in this analysis because of slow vertical velocities of wireline tools and the increased heat transfer rates in turbulent flows versus those of non-turbulent flows. In other words, if the components are designed to work properly with heat transfer rates in non-turbulent flows, they will also run with the higher heat transfer rates present in turbulent flows. The fluids present in boreholes can be both Newtonian, as well as, non-Newtonian with constant and varying properties. The plug and laminar flow models represent both lower and upper bound heat transfer models (see Section 4.5). The investigator does not develop the heat transfer behavior of the Bingham-Plastic flow, for it falls between the two bounds. With the fluid properties, flow models, and heat transfer models, the convective heat transfer coefficients are derived in the following sections.

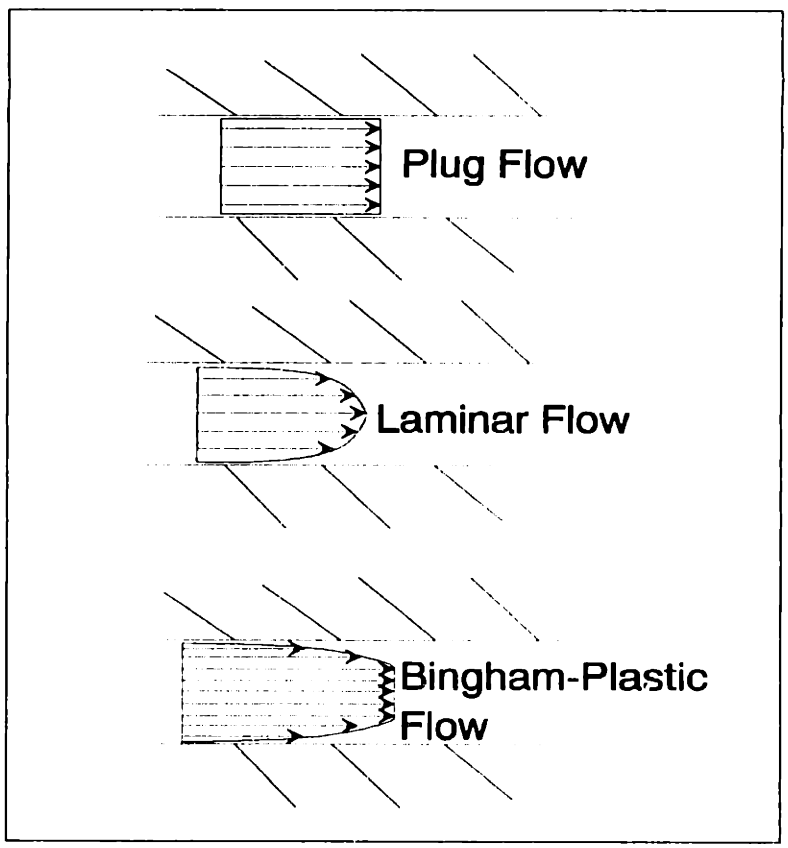

Figure 4.1: Flow Profiles

4.1: Borehole Fluids

Wellbores contain a host of fluids in several different combinations and conditions. These fluids are chosen as a function of the desired properties and reserves, as well as economics. The basic components are oils, water, gases, and muds. The oils present in wellbores range in properties from light-weight to heavy-weight types and display various viscosities. The water can be fresh or contain salt. The gases exist as foams, dry gases, or mists. Both water and oil-based muds are used in wells today with solid volume percentages up to 30%. Some of the more common muds are composed of clay-water and barite-oil mixtures. Additives such as cuttings and surfactants are also commonly added to the wellbore fluids. For the order-of-magnitude flow and heat transfer analyses, a few common wellbore fluids are considered (Gray, 1981, pp.1-37).

To simplify the modeling in these analyses, only a few common wellbore fluids will be included. The components include water, oil, clay, and barite. Muds composed of oil-clay, oil-barite, water-clay, and water-barite up to 30% volume are considered. Wellbores filled with gases will not be considered as candidates for an active cooling system because of the low convection rates attainable. Furthermore, the properties of the fluids are assumed constant. Table 4.1 lists the common components and some approximate values for their properties (Gray, 1981 p.6) (Thermophysical Properties, 1979).

Table 4.1: Common Wellbore Components and Approximate Properties

Material	Density, ρ,(kg/m^3)	Viscosity,μ ,(N-s/m^2)	Specific Heat, c_p, (J/kg-°K)	Thermal Conductivity, k, (W/m-°K)	Thermal Diffusivity, α, (m^2/s)
Water	1000	1.3×10^{-4}	4534	0.653	1.68×10^{-7}
Oil	800	4×10^{-3}	2500	0.13	6.6×10^{-8}
Barite	4300	-	550	0.37	1.7×10^{-7}
Clay	2500	-	6000	1.5	1×10^{-7}

In the cases modeled with fluid-solid combinations, the new properties are determined by volume percent. For example, say one has two materials: A and B. Material A is immersed in material B as 10% of the total volume mixture. The thermal conductivity of the mixture, k_{mix}, is derived by

$$k_{mix} = 0.9k_B + 0.1k_A \qquad (4\text{-}1)$$

Thus, it is assumed that materials A and B are well-mixed and represent a continuous solution.

4.2: Tool-Borehole Geometry

The following analysis of flow patterns assumes two different tool-borehole geometries. For a more realistic model in the laminar and plug-flow analyses, the tool is assumed off-center (Griffith, 1995). The resulting cross-sectional geometry is simplified into four sections with the perimeter of each section equal to one fourth the perimeter of the tool (see Figure 4.2). One section shows no gap between the borehole and the tool. The two sections surrounding the zero-gap section contain a gap equal to the difference

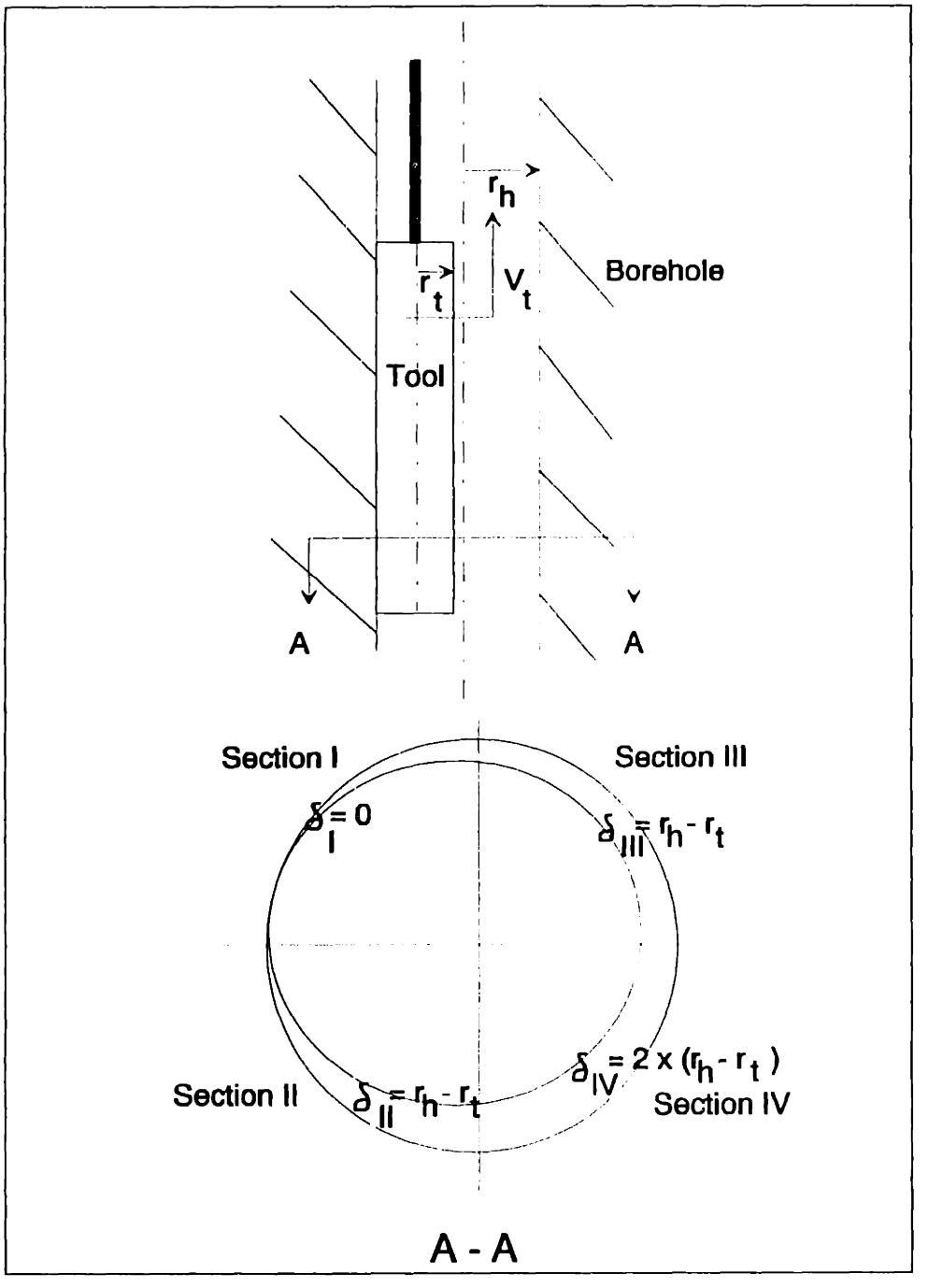

Figure 4.2: Model Description for Laminar and Plug Analysis

between the radii of tool and borehole. The fourth section contains a gap between the tool and borehole equal to the difference between the diameters of borehole and tool. The flows between each of the four sections are then treated as 1-D flows between parallel plates with the gap equal to δ. For simplicity in the more complex Bingham-Plastic flow analysis, however, the tool is assumed to be traveling in the center of the borehole.

4.3: Plug Flow

The plug-flow model describes a fluid in plastic flow with a yield stress equal to zero. This model will later be used to determine an upper bound limit on the heat transfer between tool and borehole. Plug flow is characterized with the entire fluid moving altogether at the same velocity, almost as if it were a rigid solid (see Figure 4.1). The assumptions used in the plug-flow analysis are listed in Table 4.2.

Table 4.2: Plug Flow Analysis Assumptions

1) Plastic Flow
2) Four Channels (see Figure 4.1)
3) Pressure Gradient in Borehole = 0
4) Neglect Gravity
5) Properties Constant
6) Incompressible Fluid
7) Tool Moving Up at Velocity V_t and the level of liquid in the borehole remains constant

With the previous assumptions, the analysis becomes trivial. Continuity gives an overall volumetric fluid flux, Q, between tool and borehole by

$$Q = \pi r_t^2 V_t. \tag{4-2}$$

The resulting fluid plug velocity, V_{plug} , is then

$$V_{plug} = \frac{r_t V_t}{2(r_h - r_t)} \tag{4-3}$$

where r_t, V_t, and r_h are defined in Figure 4.1.

4.4: Laminar Flow Analysis

The laminar flow model entails several assumptions and they are listed in Table 4.3

Table 4.3: Laminar Flow Analysis Assumptions

1) Laminar Flow
2) Four Channels (see Figure 4.1)
3) Pressure Gradient equal in the Four Channels and varies only in the vertical direction
4) Newtonian Fluid with Constant Properties
5) Fully Developed Flow
6) Tool Moving Up at Velocity V_t and the level of liquid in the borehole remains constant
7) Flow in Channels treated as 1-D Channel Flow
8) Boundary Conditions: No Slip condition at borehole's and tool's walls

The analysis for each of the four channels is the same except for the width between the tool and borehole. Figure 4.3 shows the geometry and coordinates for the laminar analysis. For a given channel with the previous assumptions the Navier-Stokes equations are reduced to

$$0 = -\frac{dP}{dx} + \rho g_x + \mu\left(\frac{d^2u}{dy^2}\right) \quad . \tag{4-4}$$

The resulting velocity profiles for the four sections are

$$u(y)_I = 0\,, \tag{4-5}$$

$$u(y)_{II\&III} = -\frac{6V_t r_H}{5(r_H - r_t)^3}\left[y^2 - (r_H - r_t)y\right] + V_t\left[\frac{y}{(r_H - r_t)} - 1\right], \tag{4-6}$$

and

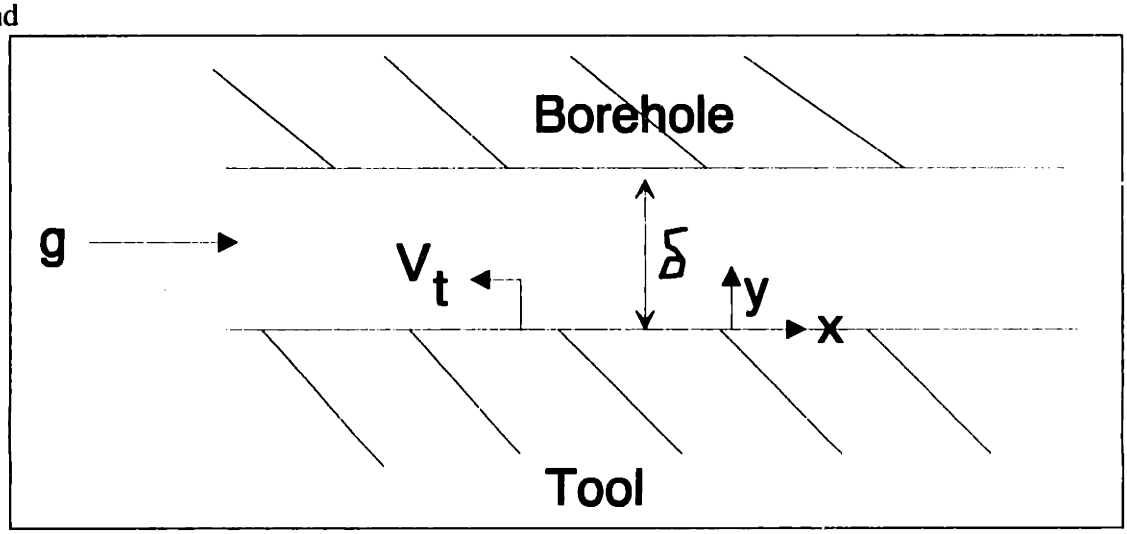

Figure 4.3: Laminar Flow

$$u(y)_{IV} = -\frac{6V_i r_{II}}{5(r_{II}-r_i)^3}\left[y^2 - 2(r_{II}-r_i)y\right] + V_i\left[\frac{y}{2(r_{II}-r_i)} - 1\right] \qquad (4\text{-}7)$$

where the variables are defined in Figure 4.3. These velocity profiles are later used in the heat transfer analysis.

4.5: Bingham-Plastic Flow Analysis

A Bingham-Plastic fluid is different from a Newtonian fluid in that it requires a finite stress to initiate flow. The equation for an ideal Bingham-Plastic fluid is

$$\tau - \tau_o = -\mu_p \frac{du}{dr} \qquad (4\text{-}8)$$

where τ_o is the stress required to initiate flow, and μ_p is the plastic viscosity, which is defined as the shear stress in excess of the yield stress that will induce a unit rate of shear (Gray, 1981, p.185). The consistency curve for a Bingham-Plastic fluid is shown in Figure 4.4.

As the figure displays, flow below the yield stress acts as plug flow. However, as the shear stresses on the fluid are increased past the yield point, the flow behaves in a laminar fashion with a viscosity equal to the plastic viscosity. Consequently, the earlier analysis of both plug and laminar flows should act as upper and lower bounds for this scenario. A Bingham-Plastic fluid analysis can be found in Appendix B and contains the much more complex flow profile formulation in cylindrical coordinates.

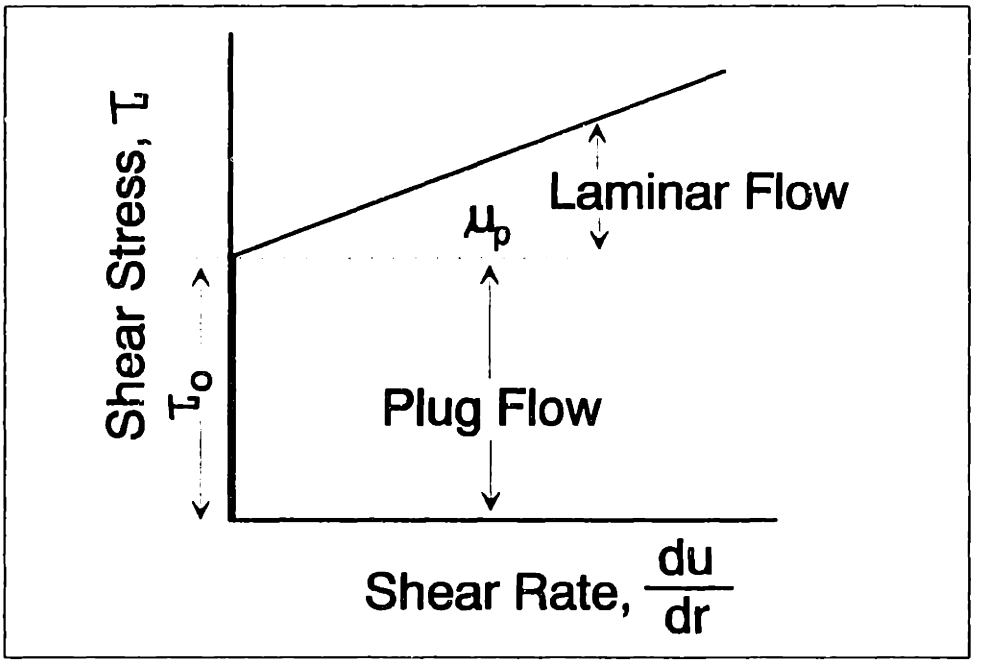

Figure 4.4: Ideal Bingham-Plastic Consistency Curve (Gray, 1981, p.186)

4.6: Heat Transfer Analysis: Moving Tool

Both plug and laminar profiles are considered in the heat transfer analyses. Figure 4.5 displays the heat transfer mode as a thermal boundary layer forms on the surface of the hot heat exchanger of the tool. The thermal boundary layer forms as the tool is pulled up at velocity V_t in the respective plug or laminar flow. An integral approach on the thermal boundary layer is used in the analysis with the thermal boundary layer starting at the hot heat exchanger (see Appendix C). The heat exchanger is assumed to have the same diameter as the tool and a length L. For simplicity, a linear temperature gradient is assumed in the thermal boundary layer. An overall heat transfer coefficient is developed for both laminar and plug velocity profiles and normalized to the convection area of the hot heat exchanger.

The heat transfer coefficient for the plug flow case with mixture properties k and α is given by

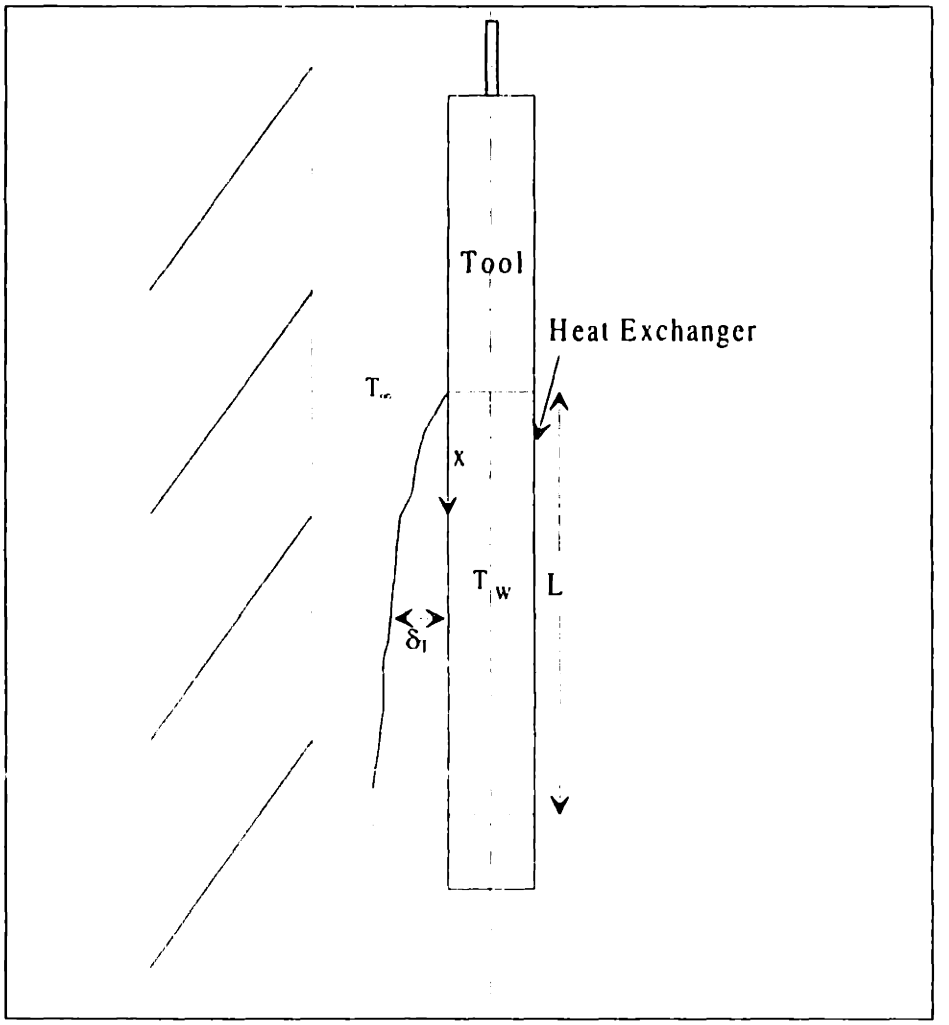

Figure 4.5: Thermal Boundary Layer Schematic

$$h_L = \frac{3}{4}\left[\frac{V_t k^2 (2r_H - r_t)}{2\alpha L(r_H - r_t)}\right]^{\frac{1}{2}}. \qquad (4\text{-}9)$$

The heat transfer coefficient for the laminar case with mixture properties k and α is given by

$$h_L = \frac{3k}{4}\left[\frac{2V_t}{90(r_H - r_t)^2 \alpha L}\right]^{\frac{1}{3}}\left[(11r_H - 5r_t)^{\frac{1}{3}} + \left[\frac{(29r_H - 5r_t)}{16}\right]^{\frac{1}{3}}\right]. \qquad (4\text{-}10)$$

Common tool sizes, borehole sizes, and fluid mixture properties are inserted into the heat transfer coefficient equations to gain a better understanding of the heat transfer coefficient values. Table 4.4 is calculated using the property values of Section 4.1, r_t equal to 0.046m, r_H equal to 0.064m, L equal to 1m, and V_t equal to 0.5m/s.

Table 4.4: Heat Transfer Coefficients: Estimated Values

Material	h_{slug} (W/m^2-°C)	$h_{laminar}$ (W/m^2-°C)
Water	1377	378
Oil	408	98.1
Barite	749	209
Clay	3797	982
Water Based Muds		
10% Barite	1484	392
30% Barite	1555	392
10% Clay	1595	434
30% Clay	2047	549
Oil Based Muds		
10% Barite	511	121
30% Barite	677	160
10% Clay	688	176
30% Clay	1270	336

The values in Table 4.4 show the heat transfer coefficient of the laminar velocity profile as a lower bound and the heat transfer coefficient of the plug velocity profile as an upper bound. Furthermore, wellbores filled with oil display the lowest convection rates of the fluids examined. Consequently, as a conservative design parameter, it is assumed oil, flowing with a laminar velocity profile, fills the borehole.

4.7: Stationary Tool Heat Transfer

In the stationary tool scenario, this investigator assumes the surrounding fluid also remains stationary. Since most wellbore fluids display a finite yield stress and because of the lack of data on natural convection in high pressure wellbores, a conservative no-flow case is developed. The borehole and tool heat exchanger are assumed to be at constant temperatures separated by the borehole fluid. The resulting heat transfer coefficient is given by

$$h_{stationary} = \frac{k}{r_{ti} - r_t}. \qquad (4\text{-}11)$$

Using the same tool and worst-case fluid (oil) values as the previous moving tool section, the heat transfer coefficient is approximately $7 W/m^2\text{-}°C$. Apparently, the no-flow case produces heat transfer coefficients an order-of-magnitude less than the flow cases. Therefore, for the operation parameters of the active cooler, the tool must move as specified in the plug and laminar analyses.

Chapter 5: Cooling Techniques vs. Downhole Constraints: Passive Systems

In an effort to determine the optimal methods of cooling for downhole electronics, several systems are evaluated. The systems must meet the predetermined specifications and performance criteria listed in the previous chapters. The potential cooling techniques are divided into two categories: active and passive. Passive systems are those requiring no external power supply. In other words, a passive system cannot operate indefinitely but only until all of the phase-change material has been heated to some temperature above which, the electronics will not function.

A simplified downhole passive system consists of an electronics chassis in a Dewar flask that contains a phase-change material acting as a heat sink. Historically, Cerro-metals have been used in downhole passive systems. The Cerro-metals then melt at a given temperature below that desired in the electronics of the tool. This method gives the user a period of time, referred to in this study as the downhole residence time, in which the temperature of the electronic components will be maintained below their rated temperature. The downhole residence time is a function of the thermal capacitance of the system. This chapter investigates potential passive systems including low temperature phase-change metals and constant volume and constant pressure water vaporization.

Several assumptions are made in the following order-of-magnitude derivations to isolate the behavior of the different passive systems. Heat pipes or other conductive materials or fluids are usually used for thermal communication between electronics and heat sinks (Bennett, 1991, p.7). In the present analysis, the thermal resistance of the heat pipes is assumed negligible. Furthermore, it is assumed the electronics and phase-change material, through the heating process, maintain a uniform temperature throughout their volumes. In other words, the entire system is modeled as a lumped thermal mass. For a conservative model, the thermal mass of the electronic component section and flask is also assumed to be much less than that of the phase change material and neglected. Thus, the mechanism controlling the behavior of the entire system is the passive heat sink material. The outside housing of the tool is assumed to be at a worst case 200°C and the cutoff temperature of the electronic components is 125°C. The total heat load into the tool is through conduction from the borehole and 50W of electronic heat dissipation. The initial temperature and pressure in the tool are atmospheric. Table 5.1 lists the approximations used for the passive systems analyses.

Table 5.1: Passive Analysis Assumptions

1) Thermal Resistance of Heat Pipes, etc. is negligible
2) Phase change material stays at uniform temperature (i.e., Lumped Mass: 1-D)
3) Lumped mass of Electronics / Flask neglected
4) Tool's skin temperature: 200°C
5) Cutoff Temperate of Electronics: 125°C
6) Electronic Heat Dissipation: 50W
7) Initial Conditions: Atmospheric

5.1: Water Vaporization

Water can be used as the phase-change heat sink material in the passive system. While in thermal communication with the electronic components of the tool, the temperature of the water would rise. At a certain temperature, depending on its initial pressure, the water would begin to vaporize. Two different water systems are modeled. The first system allows the water to vaporize at a constant pressure and would require a mechanism (steam compressor) to purge the steam from within the flask as it is created. The second system would simply allow the temperature and pressure to rise within the constant volume of the flask. Given an initial volume of water, the time it takes for each system to rise to the cutoff temperature of the electronics is the downhole residence time of the passive cooler.

The behavior of both water systems up to the point of vaporization is identical. With the previous assumptions, the problem becomes one dimensional and similar to the flask analysis in Chapter 3. The temperature rise of the water up to the point of vaporization is given by

$$T(t) = \left(T_i - T_H - Q_{gen}\sum R\right)e^{\frac{-t}{(\rho V c_p)_{water}\sum R}} + T_H + Q_{gen}\sum R, \qquad (5\text{-}1)$$

where the variables are defined in Chapter 3 and the water properties are listed in Table 5.2. Equation (5-1) is rearranged to solve for the time, t_{vapor}, it takes to reach vaporization temperature, T_{vap}, by

$$t_{vapor} = \left(\rho V c_p\right)_{water}\sum R\left[\ln\left(\frac{T_i - T_H - Q_{gen}\sum R}{T_{vap} - T_H - Q_{gen}\sum R}\right)\right]. \qquad (5\text{-}2)$$

Upon reaching the point of vaporization the two methods act in dissimilar fashions.

5.1.1: Constant Pressure Vaporization

The constant pressure vaporization system allows the water volume to stay at a constant pressure while steam is created. Atmospheric pressure would allow a vaporization temperature, T_{vap}, equal to 100°C which is a desirable temperature for most electronic components. Thus, it is assumed the water volume is maintained at atmospheric pressure via a compressor external to the flask and allowed to vaporize. The heat flux, Q, into the tool pertaining to these temperatures is given by (also see Chapter 3)

$$Q = \frac{T_H - T_{vap}}{\sum R} + Q_{gen}. \qquad (5\text{-}3)$$

The time required to vaporize the volume of water, t_{boil}, is equal to

$$t_{boil} = \frac{(\rho V)_{water} h_{fg}}{Q}, \qquad (5\text{-}4)$$

where h_{fg} is equal to the latent heat of vaporization of water at atmospheric pressure. The total downhole residence time of the constant pressure system is

$$t_{total} = t_{vapor} + t_{boil}. \qquad (5\text{-}5)$$

With the values in Table 5.2 and eq.(5-5), a total downhole residence time of 10 hours requires an initial volume of $0.001m^3$ or 1kg of water. This amount equals an added flask length of approximately 0.3m in a given system. The method, however, would require an active component, namely, the compressor. The power requirements and compressor sizing are further discussed in the active systems section in Chapter 6 (see section 6.5).

5.1.2: Constant Volume Vaporization

For a constant volume process, the system acts differently when it reaches the boiling point. As the substance is heated and begins to vaporize, its pressure rises. To determine the downhole residence time of the system, one must find the end state (state two) at which temperature equals the cutoff temperature and the specific volume equals the specific volume of the liquid at the onset of boiling (state one). To find the time it takes to reach the end state, the differences in the internal energies, u_i's, of the two states must be multiplied by the mass of the water and divided by an average heat flux:

$$t_{boil} = \frac{(\rho V)_{water}(u_2 - u_1)}{Q}. \qquad (5\text{-}6)$$

For a conservative estimate, the heat flux is set equal to eq.(5-3) with T_{vap} equal to 100°C. The total downhole residence time for this process is found by adding eq.(5-2) and eq.(5-6). A downhole residence time of 10hr. for this process requires a water volume of $0.0066m^3$ or approximately 6.5kg and extended internal flask length of over 2m.

5.2: Cerro-Metals

Cerro-metal or low-melt alloy passive systems work similarly to that of the water systems, and the same equations are used to determine the downhole residence times. However, instead of the material vaporizing, it changes from a solid to a liquid. Consequently, the heat of fusion, h_{if} ,should be substituted for the heat of vaporization in

the equations. The time it take to reach the melting temperature, $T_{melpt.}$, of the material is equal to

$$t_{melpt.} = (\rho V c_p)_{cmetal} \sum R \left[\ln \left(\frac{T_i - T_H - Q_{gen} \sum R}{T_{melt} - T_H - Q_{gen} \sum R} \right) \right], \qquad (5\text{-}7)$$

where the values of the Cerro-metals are given in Table 5.2. The time required to change the metal from a solid to a liquid, t_{melt}, is given by

$$t_{melt} = \frac{(\rho V)_{cmetal} h_{if}}{Q} \qquad (5\text{-}8)$$

where Q is determined by eq.(5-3) with T_{melt} substituted for T_{vap}. Summing eq.(5-7) and eq.(5-8) produces the downhole residence time. A downhole residence time of 10hr. requires a volume for the Cerro-metal equal to $0.0082m^3$ or 77kg, and an extended internal flask length of over 2m.

Table 5.2: Passive System Property Values (Cerro-Metal, 1995)
(Crahalvo, 1981, pp.522-530)

	$\rho(m^3/kg)$	c_p(J/kg-°K)	h_{gf}(J/kg)	T_{vapor} (°C)
Water	1000	4000	2.0867×10^6	100
	$\rho(m^3/kg)$	c_p(kJ/kg-°K)	h_{if}(kJ/kg)	T_{melt} (°C)
Cerro - Base	9411	0.130	16.880	124
Water	v (m^3/kg)	u(kJ/kg)	T(°C)	P(Pa)
State 1	0.0010435	418.94	100	1.01×10^5
State 2	0.0010435	494	120	30×10^6

Chapter 6: Cooling Techniques vs. Downhole Constraints: Active Systems

Several cooling techniques are evaluated to determine the best suited for downhole use. These systems must meet both the design and operation constraints discussed in the previous chapters. This chapter investigates performance and downhole potential versus the downhole criteria for several active cooling systems.

6.1: Ideal Refrigeration

To properly discuss the active systems, several terms require definition. First of all, in refrigeration terminology one often encounters terms such as hot and cold reservoirs, Carnot cycles, coefficient of performance (COP), etc. These terms are best explained through the ideal refrigeration or Carnot cycle. The Carnot cycle is often used to develop design criteria and provide performance bounds against which other systems can be graded.

The Carnot cycle is composed of reversible isothermal and adiabatic processes that occur while the system is in thermal communication with the hot and cold reservoirs. It serves as the ultimate performance limit when considering a hot and cold reservoir temperature differential. In the downhole case, the hot reservoir represents the borehole temperature, T_H, and the cold reservoir represents the desired electronics temperature, T_C. Figure 6.1 displays the energy interaction of the Carnot cycle where the rejected heat to the hot reservoir is equal to the sum of the absorbed heat from the cold reservoir plus the work into the refrigerator.

Performance of a given refrigerator is often measured with the coefficient of performance (COP). The COP defines the efficiency of the refrigeration system as the ratio of heat absorbed from the cold reservoir or cooling load, Q_{abs}, over the work required to operate the refrigerator, W:

$$COP = \frac{Q_{abs}}{W} \quad . \tag{6-1}$$

The COP of the Carnot cycle represents a best efficiency bound between any two reservoirs with

$$COP_{Carnot} = \frac{T_C}{T_H - T_C} \quad , \tag{6-2}$$

where the temperatures in this equation are in degrees Kelvin.

In a real refrigeration cycle, however, irreversibilities are always present and a temperature difference is required to transfer heat between the system and reservoirs.

Consequently, only a fraction of the COP_{Carnot} is ever actually attained in real refrigeration systems. Table 6.1 lists the refrigeration terms discussed as they are applicable to the downhole environment.

Table 6.1: Downhole Refrigeration Values

Hot Reservoir	200°C (473°K)
Cold Reservoir	125°C (398°K)
COP_{Carnot}	5.3
Allowable COP	80W/(250W to 500W) = ~0.16-0.32

6.2: Candidate Systems

Several cooling systems are used today in various applications. Bennett(1991) does a thorough job in her doctoral thesis of investigating the state-of-the-art for cooling systems used today versus geothermal conditions. Table 6.2 lists the candidate systems discussed in her investigation. From the results of her study, this author chooses only a few candidate systems for potential downhole use. These systems include thermoelectric cooling, the vapor-compression cycle, the Brayton cycle, and the Joule-Thompson cycle. The other systems are discounted for reasons of high cost for technology and development, complexity, maintenance, size constraints, and the current state-of-the-art. It should be kept in mind that the motivation of this author is to develop an inexpensive, functioning prototype of a downhole cooling system. Again, for a complete analysis and

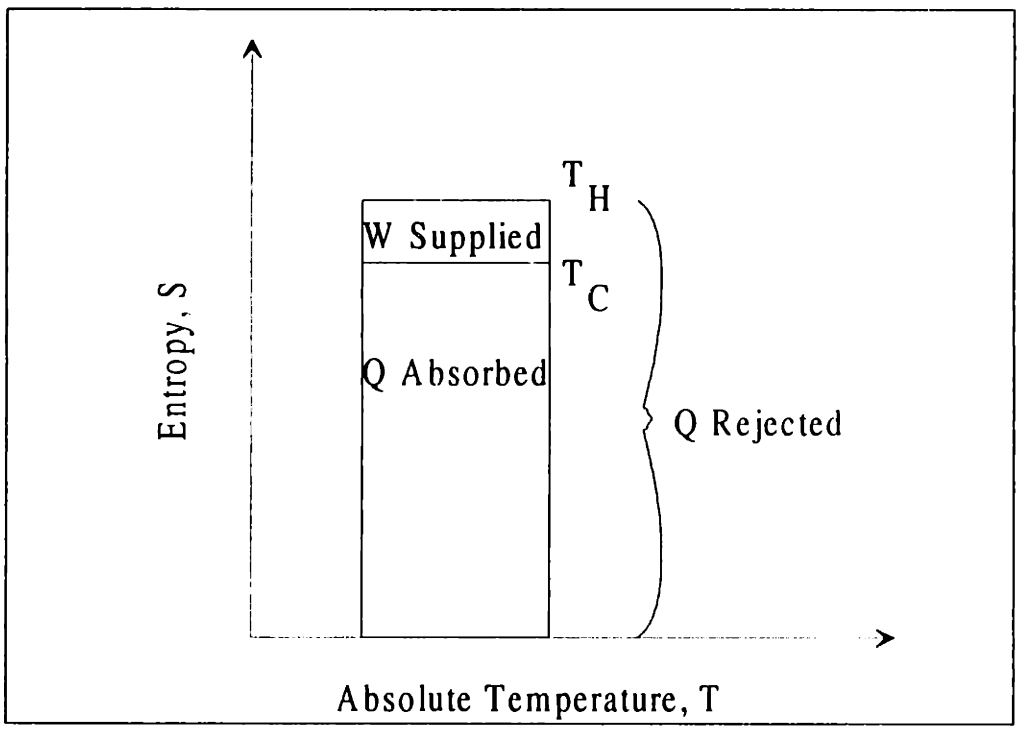

Figure 6.1: Carnot Cycle Temperature-Entropy Diagram
(Karlekar, 1983, p. 237)

description of these different systems the reader is referred to the Ph.D. dissertation of Bennett (1991).

Table 6.2: Matrix of Candidate Refrigeration Processes (Bennett, 1988, p.4)

Process Name	Energy Forms	Description	Refrigerant
Rankine	Heat-Mechanical	Phase change	Water, Freon
Brayton	Heat-Mechanical	Isentropic gas expansion	Air
Joule-Thompson	Heat-Mechanical	Isenthalpic gas expansion	N_2
Surface Heat Pumping	Heat-Acoustic	Polytropic gas expansion	He
Absorption	Heat-Chemical	Concentration change	NH_3-H_20 LiBr-H_20
Thermoelectric	Heat-Electricity	Peltier	Bi-Te, Sb-Te
Magnetocaloric	Heat-Magnetism	Magnetic field at Curie point	Gd
Electrocaloric	Heat-Polarization	Permittivity at Curie point	$BaTi0_3$
Fuel Cells	Electro-Chemical	Ion and charge	H/O

For each of the four cooling systems with potential use in downhole tools, an order-of-magnitude analysis and design are developed. Through the analyses, COP's for the systems are derived as a function of the downhole parameters. The following sections give a summary of each of the cooling systems, their analyses, and results.

6.3: Thermoelectric Cooling

Thermoelectric cooling employs the Peltier effect. In 1834 Jean Peltier found that if one passed an electric current across two dissimilar metals, a heating or cooling flux would occur between the two metals (ITI, 1992, p.19). The direction of the flux depends on the direction in which the current was passed. The major advantages of thermoelectric cooling include no moving parts, small size, and simple implementation. The greatest disadvantage of the cooling method is its very low operating efficiencies. This problem even worsens with increased temperature (Bennett, 1991, pp.63-74).

Today, there are several manufacturers of thermoelectric coolers. The low cost coolers are made with various semiconductor pairs such as Bismuth-Telluride (Bi_2Te_3), Lead-Telluride (PbTe), Silicon-Germanium (SiGe), and Bismuth-Antimony (Bi-Sb) (ITI, 1992, p.22). The effectiveness of the cooling or heating between the semiconductor pairs depends on three properties. These properties are commonly lumped into a Figure-of-Merit, Z, given by

$$Z = \frac{\alpha^2}{RK} \qquad (6\text{-}3)$$

where α is the Seebeck coefficient, R is the electrical resistance of the cooler, and K is a thermal conductivity value for the cooler (Goldsmid, 1964, pp.5-11).

6.3.1: Thermoelectric Cooler Theory

The theory, assumptions, and terminology used for this thermoelectric analysis are the same ones used by Bennett (1991, pp.63-74). Due to downhole diametric size constraints, only single and two-stage coolers are considered in this analysis, for a typical thermoelectric cooler is sized between 0.00254m and 0.0508m thick (ITI, 1992). Additionally, the other types of thermoelectric coolers, such as the segmented, are less efficient than the staged units (Bennett, 1991, pp.63-74). For each system, the ideal performance at given reservoir temperatures can be derived with only a few governing equations and semiconductor properties and without going into extreme detail (see Appendix D)(Goldsmid, 1964). Actual cooling devices, however, suffer from irreversibilties and thermal losses that contribute to a performance at approximately half that of the ideal case (ITI, 1992, p.57).

For each stage of the cooling device the maximum COP can be found and is given by

$$COP_{max} = \frac{T_c\left[\left(1+ZT_m\right)^{\frac{1}{2}} - \left(\frac{T_h}{T_c}\right)\right]}{\left(T_h - T_c\right)\left[\left(1+ZT_m\right)^{\frac{1}{2}} + 1\right]} \qquad (6\text{-}4)$$

where

$$T_m = \frac{T_h + T_c}{2}, \qquad (6\text{-}5)$$

and the subscripts h and c represent the hot and cold side of the cooler, respectively. The work or power, W, necessary to run the cooler is given by

$$W = \left(\alpha_2 - \alpha_1\right)\left(T_h - T_c\right)I + I^2R, \qquad (6\text{-}6)$$

where the current, I, is

$$I = \frac{\left(\alpha_2 - \alpha_1\right)\left(T_h - T_c\right)}{R\left[\left(1+ZT_m\right)^{\frac{1}{2}} - 1\right]}, \qquad (6\text{-}7)$$

and the subscripts 1 and 2 represent the semiconductor pair. For multistage coolers the cumulative COP is derived as

$$COP_{total} = \frac{Q_{st.1}}{W_{st.1} + W_{st.2} + \ldots}, \qquad (6\text{-}8)$$

where the abbreviation st. stands for stage.

6.3.2 Thermoelectric Cooler Results

From the Figures-of-Merit versus temperature, as well as component availability, it becomes apparent that the Bismuth-Telluride pairs are the best suited semiconductor pairs for temperatures between 100°C and 200°C (see Figure 6.2). Table 6.3 lists the properties and results of a single stage cooler (see Appendix D for the detailed analysis). The Figures-of-Merit and Seebeck coefficients at the listed temperatures are found in Goldsmid (1964) and Bennett (1988, pp.79-84). Knowing the outside film coefficient from the borehole to the tool is approximately equal to 100W/m^2-°C (see Chapter 4), the hot heat sink of the cooler could be designed such that the temperature difference required to transfer heat from itself to the environment is negligible. Thus, a hot reservoir temperature

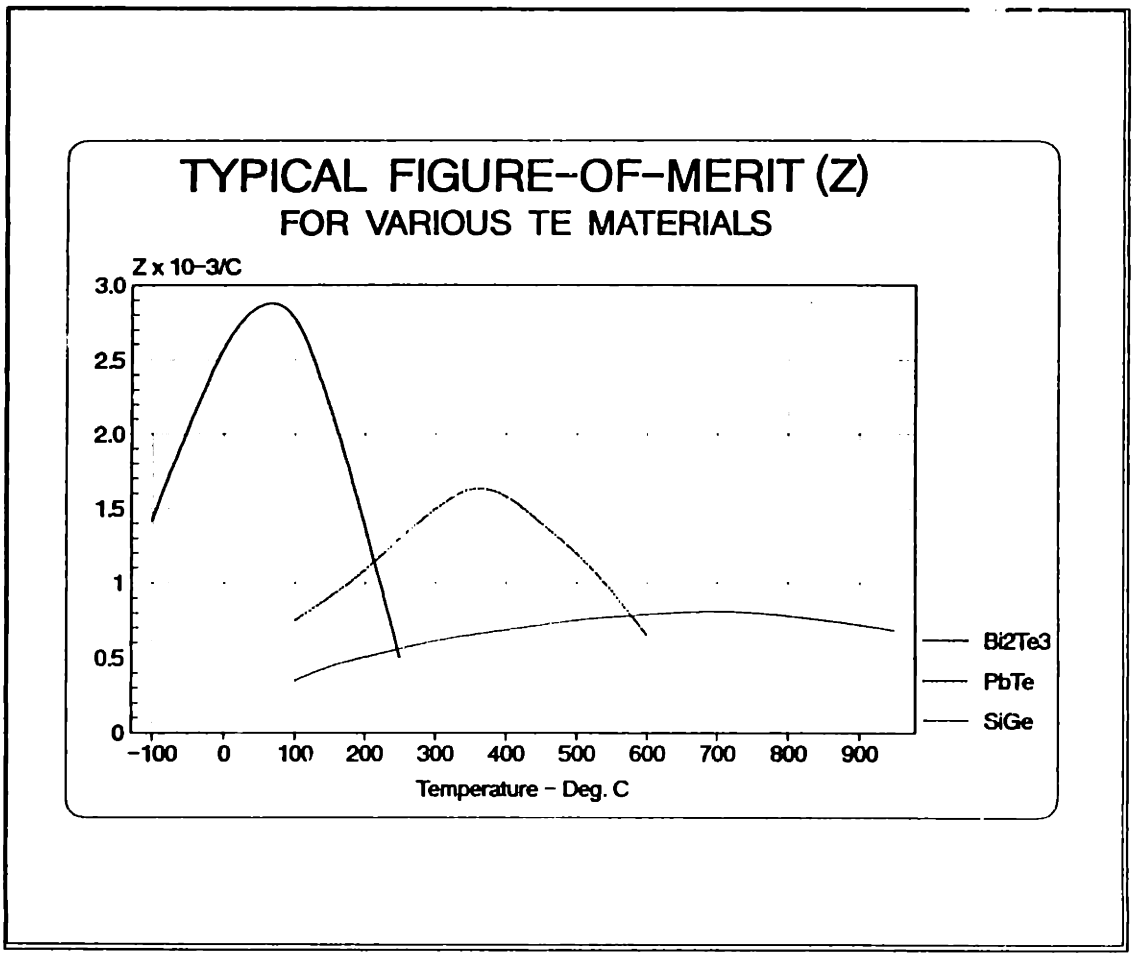

Figure 6.2: Performance of Thermoelectric Materials at Various Temperatures (ITI, 1992, p.22)

equal to 200°C is used for this analysis. The ideal maximum COP of the ideal single-stage cooler is approximately 7% Carnot COP.

Table 6.3: Single-Stage Thermoelectric Cooler Parameters and Results

T_h (°C)	200
T_c (°C)	125
COP_{max}	0.39
Q_{abs} (W)	80
W (W)	205

A two-stage thermoelectric cooler would also fit in the geometry of the downhole tools. The first stage must absorb the refrigeration load, and the second stage must absorb both the refrigeration load and the work of the first stage. Both pairs are Bismuth-Telluride. The first stage cools from 125°C to 190°C, and the second stage cools from 190°C to 200°C. Again, it is assumed that no temperature difference is required to conduct heat from hot heat sink to the hot reservoir. Table 6.4 lists the results of the two-stage cooler (see Appendix D for detailed analysis). The maximum COP of the ideal system is approximately 9% Carnot COP.

Table 6.4: Two-Stage Thermoelectric Cooler

Stage 1:	
T_h (°C)	190
T_c (°C)	125
COP_1	0.67
Q_{abs} (W)	80
W (W)	120
Stage 2:	
T_h (°C)	200
T_c (°C)	190
COP_2	6.0
Q_{abs} (W)	200
W (W)	33
Total System	
COP_{max}	0.5
Q_{abs} (W)	80
W (W)	153

6.4: Vapor Compression Cooling : Rankine Cycle

A vapor-compression cycle or Rankine cycle with a refrigerant fluid, run in reverse, provides the conventional refrigeration seen in most homes and automobiles (Karlekar, 1983, p.390). The basic vapor-compression cycle consists of two isobaric heat

exchange processes, an isentropic compression, and an isenthalpic expansion device. In their simplest forms, these four processes translate to an evaporator or cold heat exchanger, a condenser or hot heat exchanger, a compressor, and an expansion valve (see Figure 6.3).

This investigation considers only single-stage coolers. The added complexity of multiple stages, intercoolers, subcoolers, etc. far outweigh the benefits in a downhole environment. This is especially apparent when one considers the downhole size and environmental constraints. One only needs to look at the historical attempts at downhole mechanical refrigerators to see the problems associated in systems more complex than necessary (United States 1977 and 1979). Those interested in the more complex systems are referred to Bennett's (1991) investigation where several vapor-compression cycle variations other than the single-stage cycle are analyzed.

Water is the refrigerant of choice for the downhole mechanical refrigerators. Water is non-toxic, readily available even in remote field locations, and non-flammable. Water also displays good and well established thermodynamic properties that include high heat of vaporization and manageable pressure ranges (United States, 1977, p.12). Several studies have resulted in water being chosen as the optimal refrigerant in mechanical refrigerators in the downhole temperature range (Barger, 1955, p.23)(Bennett, 1988, p.14)(United States, 1977 and 1979).

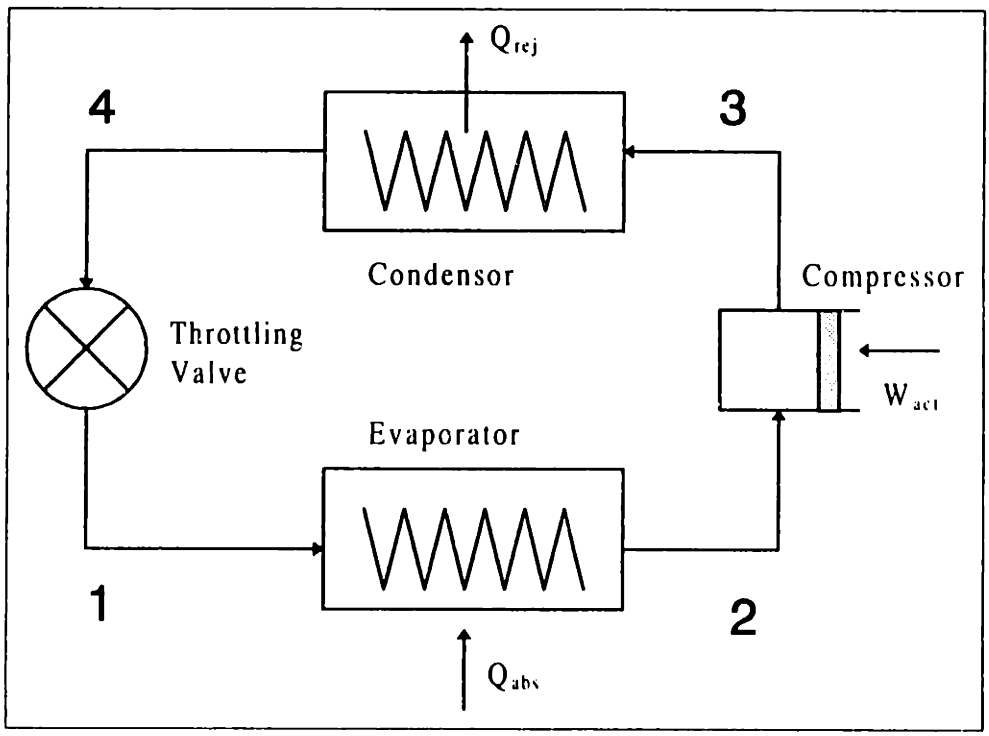

Figure 6.3: Vapor-Compression Cycle Cooler Components
(Karlekar, 1983, p.391)

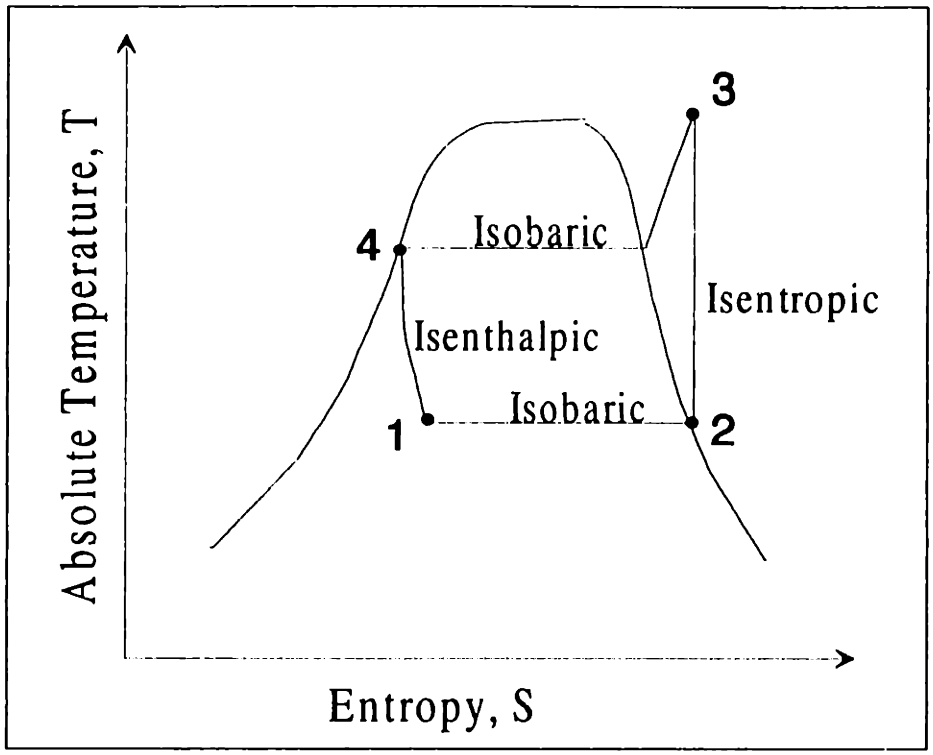

Figure 6.4: Vapor-Compression Cycle Cooler Temperature-Entropy Diagram (Karlekar, 1983, p.391)

6.4.1: Single-Stage Vapor-Compression Cycle Theory

The theory, assumptions, and terminology used for this vapor compression analysis follow that of Bennett (1991, pp.31-35). The vapor-compression cooler temperature-entropy, T-s, diagram is given in Figure 6.4.

The following theory is derived on a per-unit-mass flowing through the cycle, $\dot{m}$, basis (see Appendix E). The heat absorbed from the source or cooling load, q_{12}, is

$$q_{12} = h_2 - h_1, \qquad (6\text{-}9)$$

where the h_i's represent the specific enthalpies of the different states. The compression process between states two and three raises the vapor to a superheated condition isentropically. The work required, w_{23}, is

$$w_{23} = h_3 - h_2. \qquad (6\text{-}10)$$

Irreversibilities in the system cause the real value of work, w_{act}, in eq.(6-10) to increase. This inefficiency is accounted for by the compressor efficiency value, η, and expressed by

$$w_{act} = \frac{w_{23}}{\eta} \qquad (6\text{-}11)$$

Condenser heat rejected to the environment, q_{34}, between states three and four is

$$q_{34} = h_4 - h_3 \quad . \qquad (6\text{-}12)$$

From state four to state one the refrigerant expands isenthalpically resulting in an ideal COP of

$$COP = \frac{h_2 - h_1}{h_3 - h_2} \, . \qquad (6\text{-}13)$$

The total cooling capacity of the cycle, Q_{abs}, is then

$$Q_{abs} = \dot{m} q_{12} \quad , \qquad (6\text{-}14)$$

and the total compressor work, W_{23}, is

$$W_{23} = \dot{m} w_{23}. \qquad (6\text{-}15)$$

From an energy balance for the system, the total heat rejected, Q_{rej}, becomes

$$Q_{rej} \geq Q_{12} + W_{23}, \qquad (6\text{-}16)$$

where the actual value of Q_{rej} is larger than eq.(6-16) due to irreversibilities in the cycle and its components.

A preliminary analysis was conducted using water as the refrigerant in the downhole environment (see Appendix E), and the four points of the cooler are listed in Table 6.5. The results of the analysis are listed in Table 6.6.

Table 6.5: Fully Defined States for Vapor-Compression Cycle

Point	State	T(°C)	P(Pa)	quality	h(kJ/kg)	s(kJ/kg-°K)	v(m^3/kg)
1	Wet Vapor	125	232.1×10^3	0.149	851	2.40	0.00125
2	Sat. Vapor	125	232.1×10^3	1	2713.5	7.0775	0.7706
3	Super-Heated Vapor	351	1.58×10^6	1	3148	7.0775	0.177
4	Sat. Liquid	200	1.58×10^6	0	851	2.33	0.00116

Table 6.6: Vapor-Compression Cycle Results

Q_{abs}(W)	80
W (W)	18.7
COP	4.29
Heat Exchanger Length (m)	~ 1
Mass Flowrate (kg/s)	4.3×10^{-5} kg/s

6.5: Constant Pressure Vaporization: Once-Through Vapor-Compression Cooler

In this section, the constant pressure vaporization of water method from Section 5.1.1 is further explored. This system is very similar to the conventional vapor-compression cycle with the exception of the throttling valve. The cooler is comprised of a condenser, evaporator, and compressor (see Figure 6.5). Water is chosen as the working fluid for the same reasons as those of the original Rankine system. To the author's knowledge, the present system is a new concept for downhole use, and a patent application has been filed by the author for Schlumberger (see Appendix M).

6.5.1: Once-Through Vapor-Compression Cooler Theory

The cooler, as discussed in Section 5.1.1, allows a volume of water to vaporize at constant pressure. For downhole cooling purposes, this pressure corresponds to atmospheric. Consequently, the water vaporizes at a temperature of 100°C. To maintain this state of vaporization, the steam must be removed from within the flask and electronic components as it is generated. Following its removal, the steam must be compressed via a

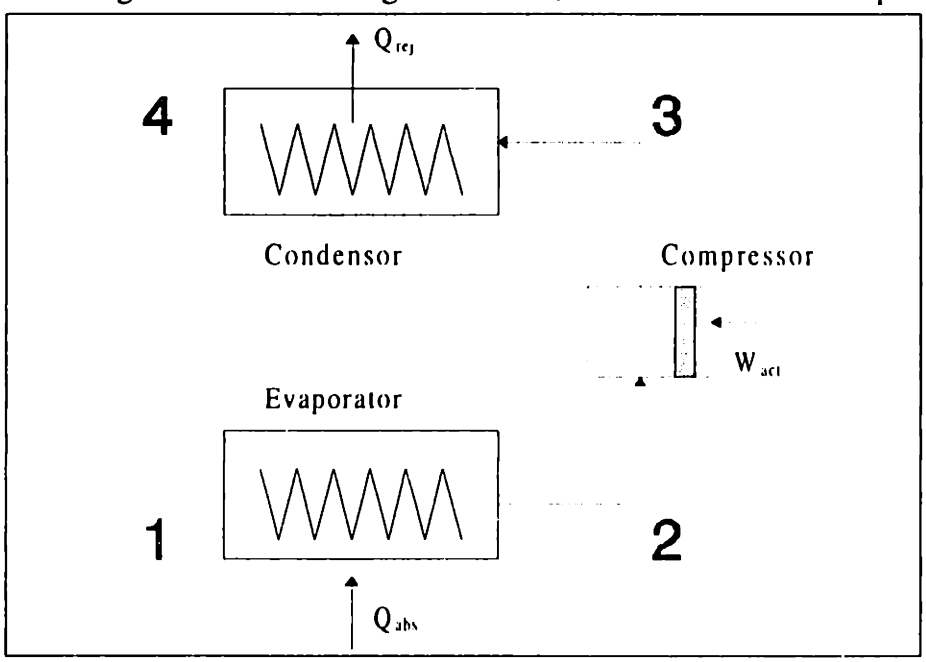

Figure 6.5: Once-Through Vapor-Compression Cooler Components

compressor into a hot heat exchanger or condenser in thermal communication with the hot borehole at 200°C. The outlet pressure of the compressor must be equal to or greater than the saturation pressure of water corresponding to the temperature of the hot reservoir. Schematics explaining the system are shown in Figures 6.5 and 6.6. The states of the system are determined assuming the conservative 80-W cooling load (see Table 6.7).

Except for the selection of the end states and the isenthalpic process, the theory of this cooler is identical to that of the conventional vapor-compression cycle. The heat absorbed from the source or cooling load, q_{12}, is

$$q_{12} = h_2 - h_1. \qquad (6\text{-}17)$$

The compression between states two and three raises the vapor to a super-heated vapor isentropically. The work required for the compression, w_{23}, is

$$w_{23} = h_3 - h_2. \qquad (6\text{-}18)$$

However, irreversibilities in the system cause the real value of work, w_{act}, in eq.(6-18) to increase. The compressor efficiency, η, denotes this and is expressed by

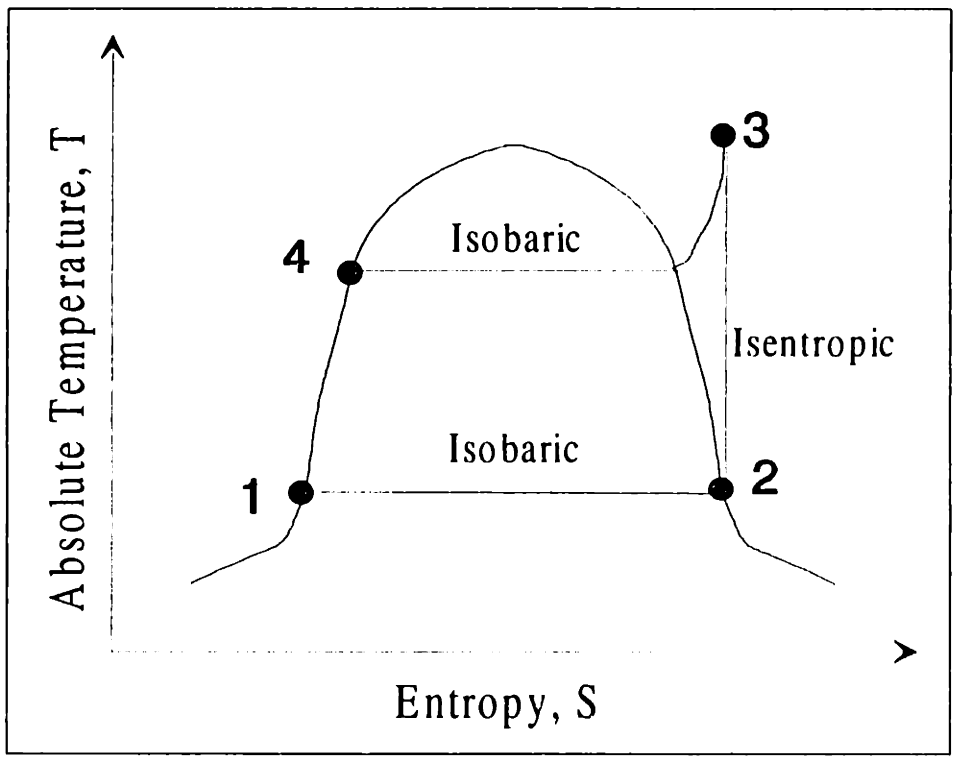

Figure 6.6: Once-Through Vapor-Compression Cooler Temperature-Entropy Diagram

$$w_{act} = \frac{w_{23}}{\eta}. \qquad (6\text{-}19)$$

Condenser heat rejected to the environment, q_{34}, between states three and four is

$$q_{34} = h_4 - h_3, \qquad (6\text{-}20)$$

and the ideal COP of the system is

$$COP = \frac{h_2 - h_1}{h_3 - h_2}. \qquad (6\text{-}21)$$

The total cooling load of the system, Q_{abs}, is

$$Q_{abs} = \dot{m} q_{12}, \qquad (6\text{-}22)$$

and the total compressor work, W_{23}, is

$$W_{23} = \dot{m}\, w_{23}. \qquad (6\text{-}23)$$

The total heat rejected, Qrej, is

$$Q_{rej} \geq \dot{m}\ (h_3 - h_4), \qquad (6\text{-}24)$$

where the value of Q_{rej} can be larger than eq.(6-24), depending on the irreversibilities of the system.

The system is sized as a function of the Q_{abs}. Again, for this system, the conservative 80-W cooling load is assumed. The four states of the process are listed in Table 6.7. Table 6.8 lists the results of the analysis.

Table 6.7: Fully Defined States for Once-Through Vapor-Compression Cooler

Point	State	T(°C)	P(Pa)	quality	h(kJ/kg)	s(kJ/kg-°K)	v(m^3/kg)
1	Sat. Liquid	100	$101x10^3$	0	418	1.3	0.00104
2	Sat. Vapor	100	$101x10^3$	1	2675	7.36	1.68
3	Super-Heated Vapor	437	$1.58x10^6$	1	3334	7.36	0.204
4	Sat. Liquid	200	$1.58x10^6$	0	851	2.33	0.00116

Table 6.8: Once-Through Vapor-Compression Cooler Results

Q_{abs}(W)	80
W (W)	23
Q_{rej}(W)	87
COP	3.5
Mass Flowrate (kg/s)	3.5×10^{-5} kg/s

6.6: Brayton Cycle Cooling

Refrigeration provided by the Brayton cycle, run in reverse, is commonly used in aircraft and represents the only gas cycle used in commercial systems. The cycle consists of two isobaric heat exchangers, an isentropic compressor, and an isentropic expander (see Figure 6.7). The Brayton cycle is less efficient than the vapor compression cycle given the same hot and cold reservoir temperatures. This increased inefficiency is caused by the isobaric versus the isothermal heat transfer in vapor-compression coolers. Brayton cycle coolers also require greater flowrates than those of the vapor-compression cooler for the same refrigeration load (Karlekar, 1983, pp.400-405).

The refrigerant of choice for the downhole Brayton cycle is helium. Bennett's investigation shows that helium displays higher heat transfer rates and lower pressure drops and required compression ratios relative to several other refrigerants (1988. pp.30-37). The following section develops a Brayton cycle cooler as a function of downhole parameters with helium as the working gas.

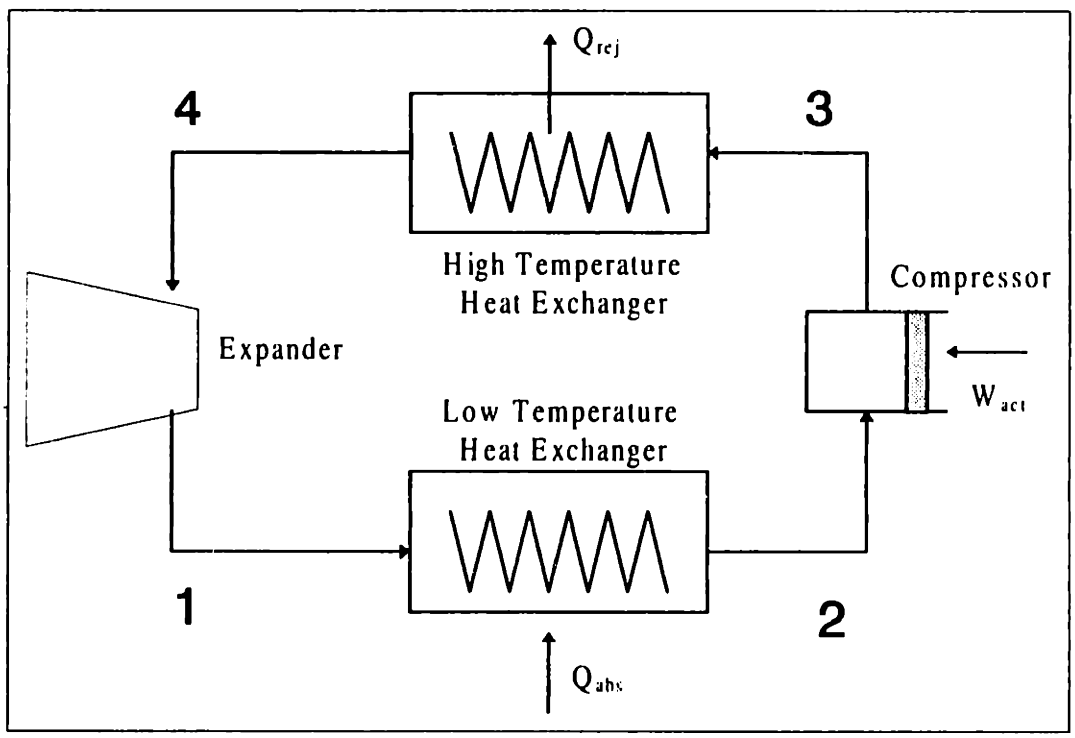

Figure 6.7: Brayton Cycle Cooler Components (Bennett, 1991, p.26)

6.6.1: Brayton Cycle Theory

The theory, assumptions, and terminology used for this analysis follow that of Bennett (see also Appendix F)(1991, pp.25-37). Figure 6.8 displays the temperature-entropy diagram for the Brayton cycle. The following assumptions are used to simplify the analysis: reversible processes, constant specific heats, and perfect gas behavior.

The working fluid absorbs heat in the low temperature heat exchanger during a constant pressure process at P_{low} and causes the temperature to rise. The heat absorbed in the refrigerant per unit mass of fluid is

$$q_{12} = h_2 - h_1 = c_p(T_2 - T_1) \; . \qquad (6\text{-}25)$$

The gas temperature at state two is slightly below the cooling load temperature. The refrigerant is then compressed from state two to state three. The process occurs fast enough to be considered adiabatic and assumed insentropic. The temperature of the compressor is

$$T_3 = T_2\left(\frac{P_3}{P_2}\right)^{\frac{\gamma-1}{\gamma}} , \qquad (6\text{-}26)$$

where

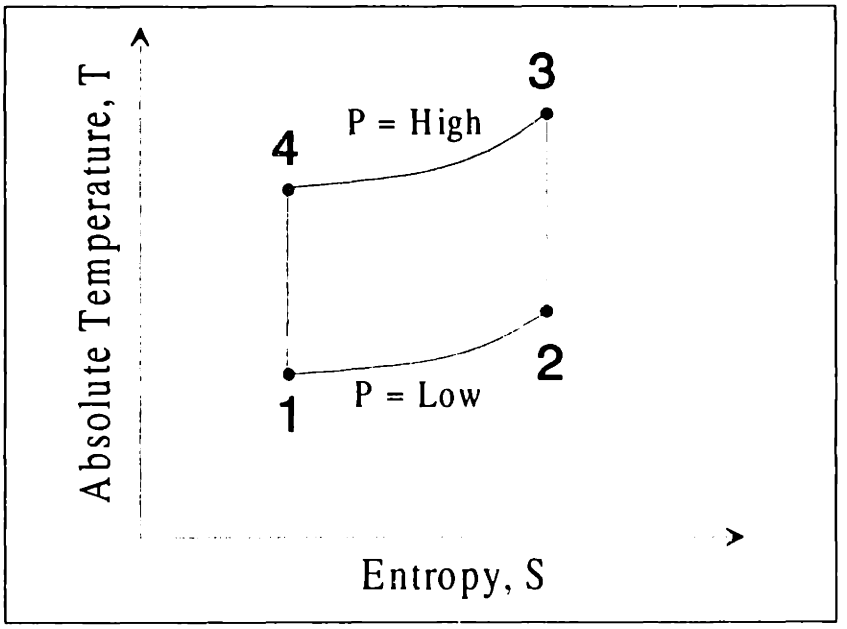

Figure 6.8: Brayton Cycle Cooler Temperature-Entropy Diagram (Bennett, 1991, p.26)

$$\gamma = \frac{c_p}{c_v}. \tag{6-27}$$

The ideal work per unit mass of the fluid in the compressor is

$$w_{23} = h_3 - h_2 = c_p(T_3 - T_2). \tag{6-28}$$

The gas is then cooled at the constant high pressure value until its temperature almost equals that of the hot reservoir. This relationship is given by

$$q_{34} = h_3 - h_4 = c_p(T_3 - T_4) \quad . \tag{6-29}$$

Between states four and one, an isentropic expansion occurs in a turbine. The temperature at the exit is

$$T_1 = T_4\left(\frac{P_1}{P_4}\right)^{\frac{\gamma-1}{\gamma}} . \tag{6-30}$$

It is possible to extract work from the turbine. The value of the extracted work per unit mass is

$$w_{41} = h_4 - h_1 = c_p(T_4 - T_1). \tag{6-31}$$

The work from eq.(6-31) is not available if an expansion valve is used in place of the turbine.

The COP of the system with the turbine component is

$$COP_t = \frac{q_{12}}{w_{23} - w_{41}} = \frac{T_2 - T_1}{(T_3 - T_2) - (T_4 - T_1)}. \tag{6-32}$$

The COP of the system with an expansion valve in place of the turbine is

$$COP_v = \frac{q_{12}}{w_{23}} = \frac{T_2 - T_1}{T_3 - T_2}. \tag{6-33}$$

The sizing of the unit is derived from the mass flowrate of refrigerant, $\dot{m}$. The mass flowrate is found via the required heat absorption or refrigeration load by

$$Q_{abs} = \dot{m} q_{12}. \tag{6-34}$$

Thus, the work required for the compressor is

$$W_{in} = \dot{m} w_{23} \quad . \tag{6-35}$$

Because of inefficiencies due to nonideal behavior such as pressure drops, heat transfers, etc., the actual work required is

$$W_{act} = \dot{m}\left[w_{23} - w_{41}\right] = \dot{m}\left[\frac{h_3 - h_2}{\eta_{comp}} - \eta_{turb}\left(h_4 - h_1\right)\right], \tag{6-36}$$

where η_{comp} and η_{turb} represent the efficiencies of the compressor and turbine. The heat rejected to the hot reservoir is then

$$Q_{rej} = Q_{abs} + W_{act} \, . \tag{6-37}$$

A preliminary analysis is conducted using helium as the refrigerant in the downhole environment. Table 6.9 lists the four states, temperatures, and pressures for the reverse Brayton cycle assuming a compression ratio of three. Table 6.11 lists the refrigerator results using helium (see Appendix F).

Table 6.9: Brayton Cycle States (c_p=5.23 kJ/kg-°K, γ=1.67)

State	T (°C)	P (atm)
1	31	1
2	125	1
3	345	3
4	200	3

Table 6.10: Brayton Cycle Refrigerator Results

Q_{abs}(W)	80
COP_t	1.84
COP_v	0.43
W_t(W)	43
W_v (W)	186
Heat Exchanger Length (m)	~1
Mass Flowrate (kg/s)	1.6×10^{-4}

6.7: Joule-Thompson Cycle Cooling

The Joule-Thompson cycle is very similar to the Brayton cycle except for the expansion device. The Joule-Thompson cycle uses a throttling valve in the place of a turbine expander. The major components of this system include a gas compressor, high temperature heat exchanger, low temperature heat exchanger, and throttling valve (see Figure 6.9).

6.7.2: Joule-Thompson Theory

The theory, assumptions, and terminology used for this analysis follow that of Bennett (see Appendix G) (Bennett, 1991, pp.59-63). The following assumptions are used in the preliminary analysis: reversible processes except for the throttling valve and compressible gas behavior described by a compressibility factor. The theory is the same as the Brayton cycle except for the expansion (isenthalpic) process.

In real gases, the derivative of the temperature with respect to pressure is nonzero. The ratio is known as the Joule-Thompson coefficient, μ, given by

$$\mu = \left(\frac{\partial T}{\partial p}\right)_h . \qquad (6\text{-}38)$$

This ratio is positive for pressure drops that result in temperature drops and negative for pressure drops that result in temperature increases. Figure 6.10 shows plots of constant enthalpy lines for a gas on temperature and pressure axes. The dotted line represents the locus of points, inversion curve, where the ratio is equal to zero. Expansions that occur to the left and right of the curve produce temperature drops and increases, respectively.

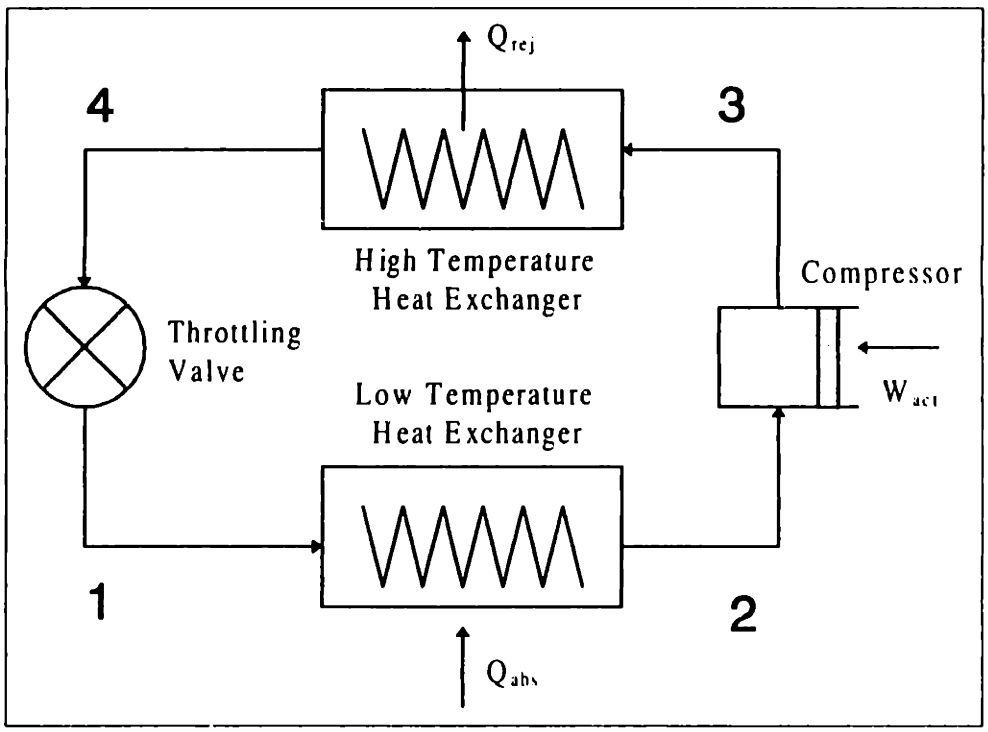

Figure 6.9: Joule-Thompson Cycle Cooler Components
(Bennett, 1988, p.26)

A relation for the Joule-Thompson coefficient is derived from the differential for enthalpy, dh, as

$$dh = c_p dT + \left[v - T\left(\frac{\partial\, v}{\partial\, T}\right)_p \right] dp\,, \qquad (6\text{-}39)$$

where v is the specific volume. Because of the isenthalpic throttling process, the ratio of temperature and pressure differentials becomes

$$\left(\frac{dT}{dp}\right)_h = \frac{1}{c_p}\left[T\left(\frac{dv}{dT}\right)_p - v \right]. \qquad (6\text{-}40)$$

For a gas that obeys

$$pv = ZRT\,, \qquad (6\text{-}41)$$

where R is the gas constant and Z is the compressibility coefficient, the entire differential is represented as

$$pdv + vdp = ZRdT + RTdZ\,. \qquad (6\text{-}42)$$

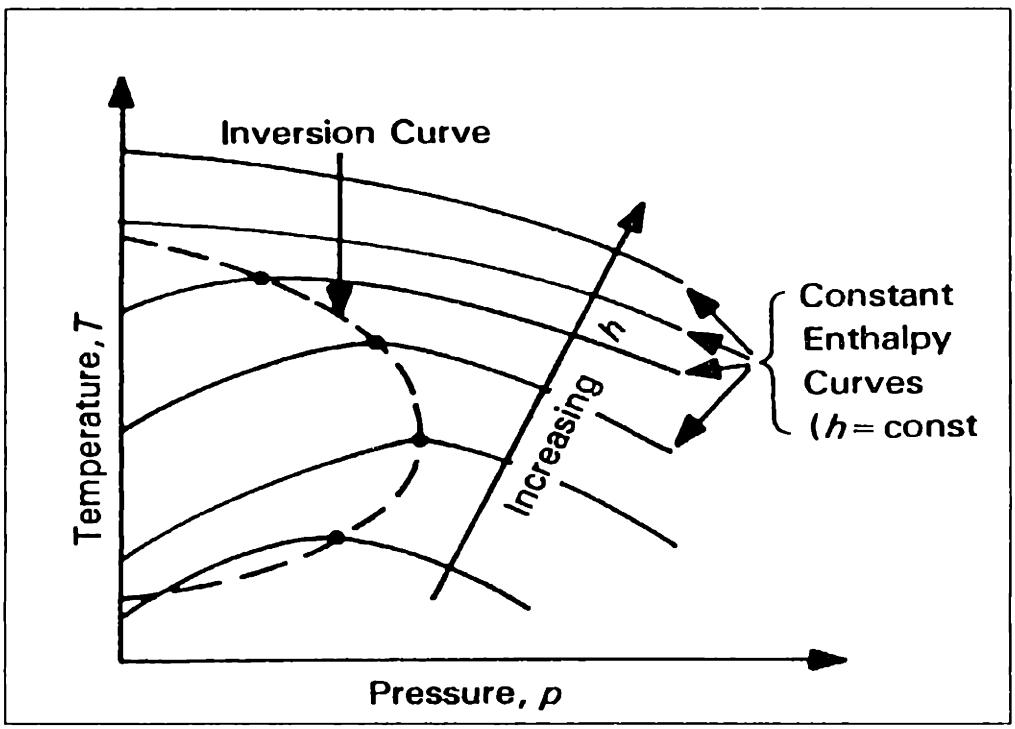

Figure 6.10: Constant Enthalpy Lines (Bennett, 1988, p.39)

Eq.(6-42) can then be rearranged to solve for the derivative of volume with respect to temperature, assuming constant pressure and is given as

$$\left(\frac{dv}{dT}\right)_p = \frac{ZR}{p} + \left(\frac{RT}{p}\right)\left(\frac{dZ}{dT}\right). \qquad (6\text{-}43)$$

Eq.(6-43) substituted into eq.(6-40) while using the equation of state and definition of the Joule-Thompson coefficient yields

$$\mu = \frac{1}{c_p}\frac{RT^2}{p}\frac{dZ}{dT}. \qquad (6\text{-}44)$$

Plots of the compressibility coefficient can be used to determine the sign of the Joule-Thompson coefficient without very much more property data on a given gas. Figure 6.11 displays a plot of the inversion curve on reduced coordinates of pressure and temperature. Points lying inside the curve have positive coefficients and can be used in conjunction with a gas expansion to generate reduced temperatures.

Applying Figure 6.11 to the oil-exploration downhole environment would necessitate a critical temperature, T_{crit}, of

$$\frac{T_h}{5} < T_{crit} < \frac{T_c}{0.5} \qquad (6\text{-}45)$$

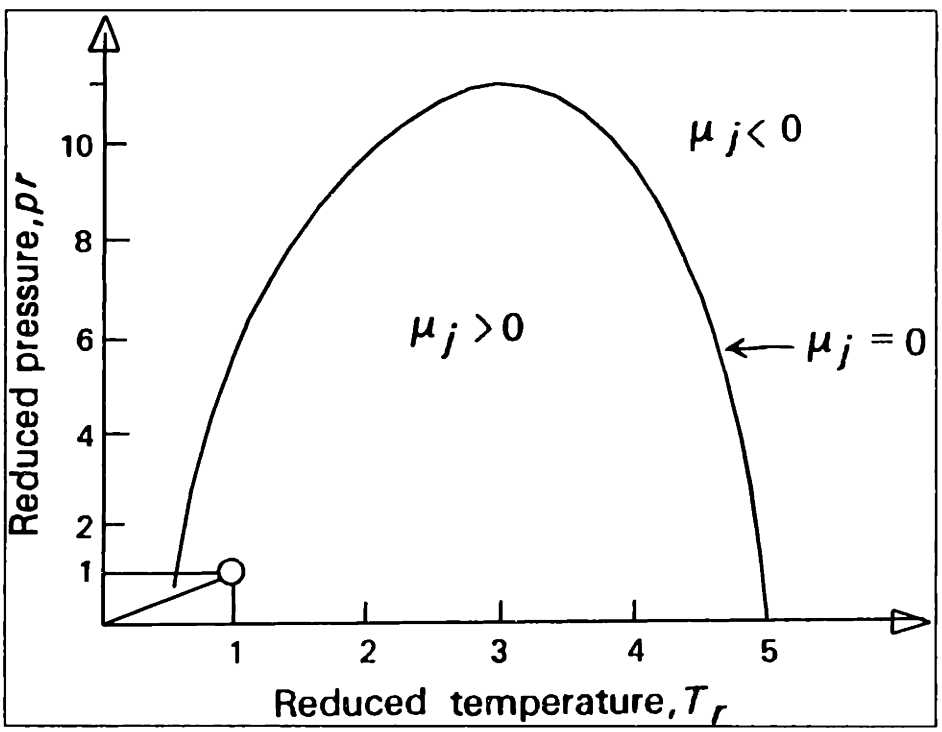

Figure 6.11: Inversion Curve (Bennett, 1988, p.39)

or

$$-178\ °C < T_{crit} < 523\ °C. \qquad (6\text{-}46)$$

From Figure 6.11 it also becomes apparent that the pressure from which the expansion takes place should follow

$$0.5 < P_r < 11. \qquad (6\text{-}47)$$

From eq.(6-44) it is seen that the gases with the greatest R/c_p and dZ/dT values will provide the greatest temperature drops and cooling. Of the refrigerants listed by Bennett (1991), carbon dioxide is the best suited for the downhole cooling system with a realistic maximum compression ratio of four (Griffith, 1995). Table 6.11 lists the states of the cycle along with their respective compressibility coefficients. The remaining state properties are found with the same equations developed in the Brayton cycle analysis (see Appendix F). Table 6.12 lists the overall refrigerator results (see Appendix G).

Table 6.11: Joule-Thompson Cycle States (Gyftopoulos, 1991, p.354)

State	T (°C)	P (Pa)	Z
1	31.2	7.39×10^6	~0.2
2	125	7.39×10^6	---
3	228	29.6×10^6	---
4	200	29.6×10^6	~0.85

Table 6.12: Joule-Thompson Cycle Results

Q_{abs} (W)	80
COP	0.91
W (W)	88
Heat Exchanger Length (m)	~5
Mass Flowrate (kg/s)	10×10^{-4}

Chapter 7: Performance Matrix and Method Selection

The various downhole systems are ranked as functions of performance, size, design complexity, and maintenance. Relative scores between one and ten are listed in several categories for which actual number values are unavailable. Each of the above-mentioned categories is directly related to cost. Consequently, cost is excluded as an individual category. The once-through vapor-compression cooler is chosen as the technique of choice for a downhole system. It displays good performance in terms of COP when compared to the active systems, as well as in terms of added flask length when compared to the passive systems. The system also ranks the lowest in maintenance and design complexity when compared to the systems not eliminated. In the following sections, the scoring and ranking are further discussed as functions of each category. The final section describes the once-through vapor-compression cooler in more detail including a downhole schematic.

This section contains relative scoring methods made without the actual numerical values. In industrial design, decisions many times must be made on this type of relative grading using logic and engineering experience. This is especially apparent when producing new products that must perform in new environments such as those in the oil-exploration industry.

7.1: Performance

The performance of the systems is perhaps the most critical parameter. With an 80-W cooling load and a 250-W conservative power estimate, the COP of the system is mandated to be 0.32 or greater. Recall from Section 6.1, the ideal or Carnot COP of the downhole system is 5.3. Figure 7.1 displays the COP's of the different active cooling systems. The vapor-compression coolers rank highest in this category with ideal COP's in the 3.5 to 4.3 range. However, the thermoelectric cooler is, for the most part, eliminated because of its ideal COP of only 0.5. Also, one must consider irreversibilities in the various active cooling systems that are certain to lower the actual COP values. For instance, both the thermoelectric and vapor-compression coolers in practice, under downhole conditions, produce COP's at approximately one-half their ideal values (United States I, 1977, p.31) (ITI, 1992). Consequently, for a conservative estimate, it will be assumed that the actual COP's of the various systems are equal to one-half their ideal values. Thus, both the thermoelectric cooler and the Brayton cycle cooler with the expansion valve can be eliminated from consideration in a downhole environment.

Since they require no input power, the passive systems in theory, display infinite COP's for a limited time. Therefore, their performance is better measured as a function of the added flask length necessary to remain downhole 10 hours in a 200°C borehole. The flask length increases result from the heat sink volumes required for each system and are discussed in Section 7.4.

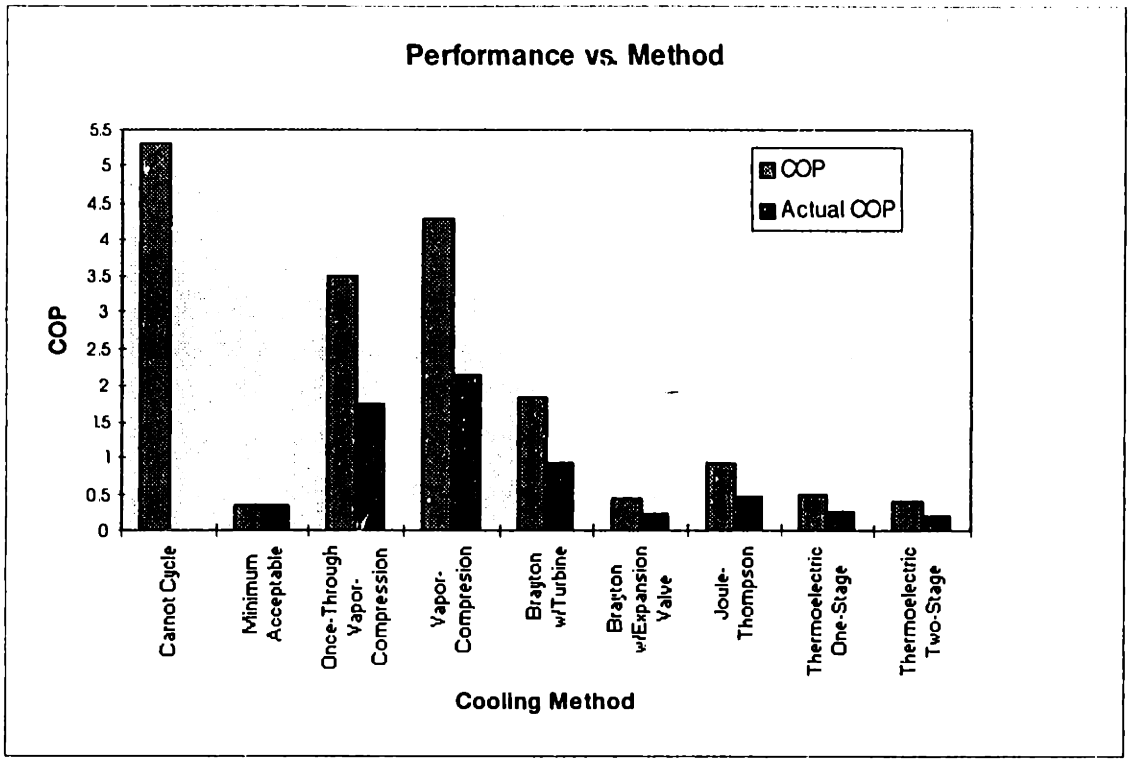

Figure 7.1: Performance vs. Cooling Methods

7.2: Design Complexity

The design complexity category is a relative scoring of the different systems and is plotted in Figure 7.2. The scores range from one to ten where the lower scores pertain to existing or easily utilized technology, and the higher scores represent nonexistent or complex components. Design complexity for each can also be related to development times and their corresponding costs. The lower scores would be more likely to cost less and require shorter development times. Both passive systems are relatively simple designs with no moving parts and are scored as one. The once-through vapor-compression cooler encompasses three components. The dynamic component for steam compression is not a completely new technology, even on the small geometric scale necessary in wireline tools (see Chapter 8). Likewise, small heat exchangers are not considered an insurmountable design obstacle when one considers heat pipes, fins, etc. Thus, the once-through vapor-compression system is scored with a three. The vapor-compression cycle cooler is slightly more complex with the addition of the throttling valve and the neccesity of a cyclic lubricant. This system is scored with a five. The Joule-Thompson cycle necessitates gas pressures much higher than those in the steam systems and is also composed of four components. This system is rated with a seven. The Brayton cycle cooler represents even greater complexity than the Joule-Thompson method, for it contains two dynamic components. The Brayton cycle cooler is scored with an eight. Lastly, the thermoelectric systems are simple in concept but do not exist in practice for downhole conditions. The system is also scored with a seven.

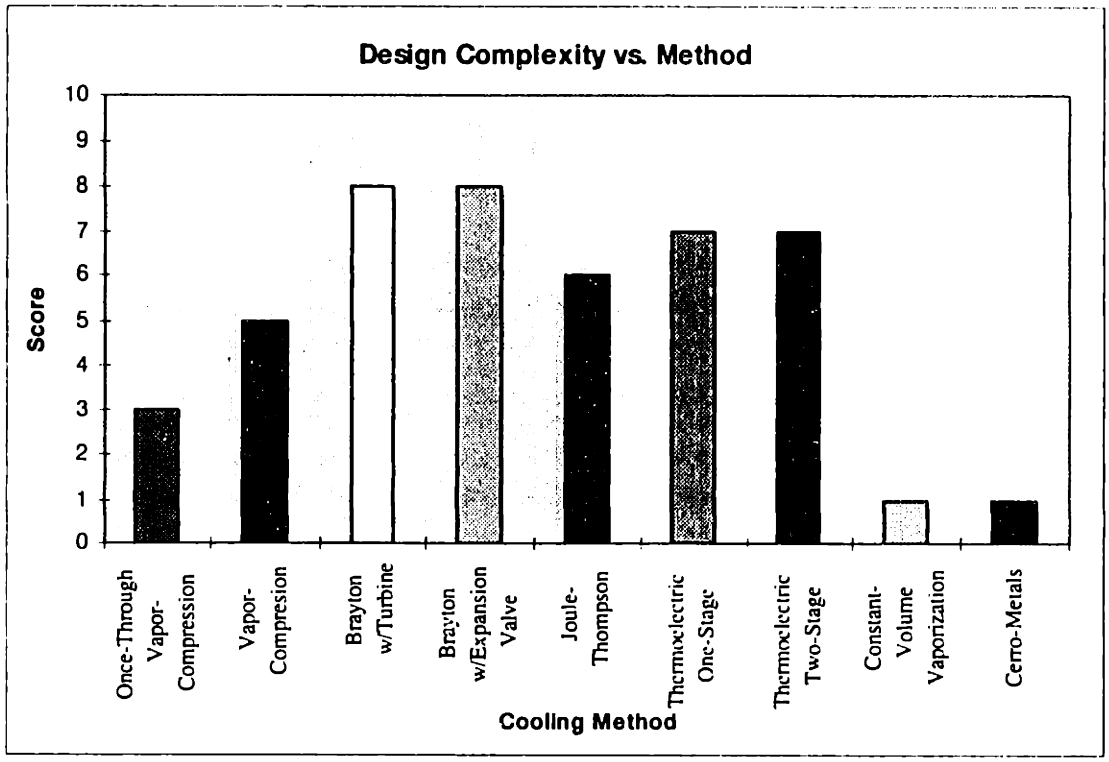

Figure 7.2: Design Complexity vs. Cooling Methods

7.3: Maintenance

The maintenance category is also a relative scoring of the different systems and is displayed in Figure 7.3. The scores range from one to ten where the lower scores pertain to little or no maintenance and the higher scores represent maintenance-intensive systems. Maintenance includes changing o-rings, filling and gas-charging tanks, restoring lubricant volumes, etc. The passive systems, by definition, are low maintenance and are scored with a one. Likewise, the thermoelectric coolers have no moving parts and receive a score of one as well. Because of the open-loop characteristic of the once-through vapor-compression cooler, the system only needs to be filled at atmospheric conditions before going downhole and emptied after retrieval uphole. Thus, a score of three is assigned to the once-through vapor-compression cooler. The remaining three cyclic systems would require slightly more maintenance due to their cyclic nature. This is especially apparent when one considers the necessity of a circulating lubricant moving with the working fluid. In addition, several of the systems must be charged to given pressures above atmospheric before going downhole. These systems are scored with a six.

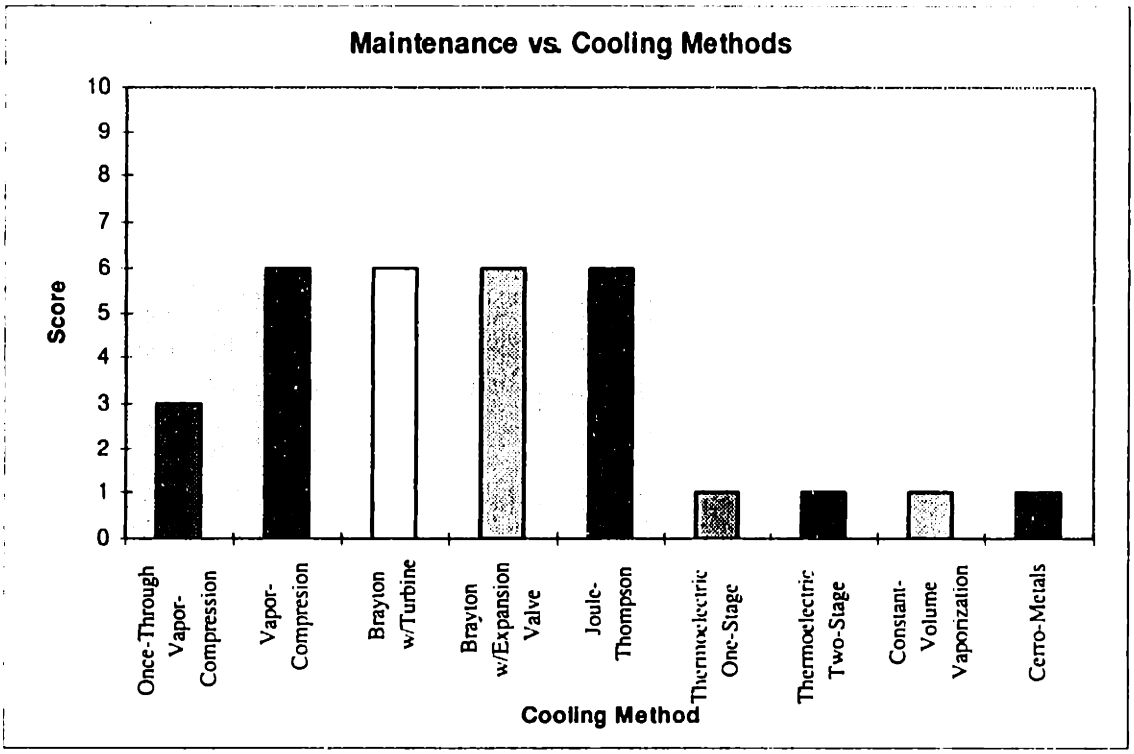

Figure 7.3: Maintenance vs. Cooling Methods

7.4: Size and Increased Flask Length

Size is also a critical design consideration both inside and outside a flask. The investigator assumes all the systems can be miniaturized to meet the diametric constraint. With knowledge of the heat transfer coefficients between the borehole and the outside the tool (see Chapter 4), the hot heat exchangers are also sized. The hot heat exchangers for all the cyclic systems are approximately 1m (see Chapter 6). In the passive systems, as well as the once-through vapor-compression cooler, a better indication of size is the added internal flask length required for the 10-hour downhole residence time in a 200°C borehole (see Chapter 5). Both the constant pressure vaporization and Cerro-metal systems produce lengths in excess of 2m within a flask. For the same downhole residence time, the once-through vapor-compression system produces an increase of only 0.3m. The average internal or payload flask length, in field locations throughout the world, is under 2m (Followay 1995). Since the flasks are very expensive items at roughly $20 thousand each, this investigator cannot mandate all new designs. Consequently, the two passive systems are not considered viable cooling schemes for the downhole residence time of ten or more hours in wireline tools.

7.5: Optimal Method

A schematic of the once-through vapor-compression cooler in its simplest form is shown in Figure 7.4. The system includes three major components: the cold heat exchanger (evaporator)/lower tank, compressor, and hot heat exchanger (condenser)/upper tank. The first component encompasses a lower tank of stored water in

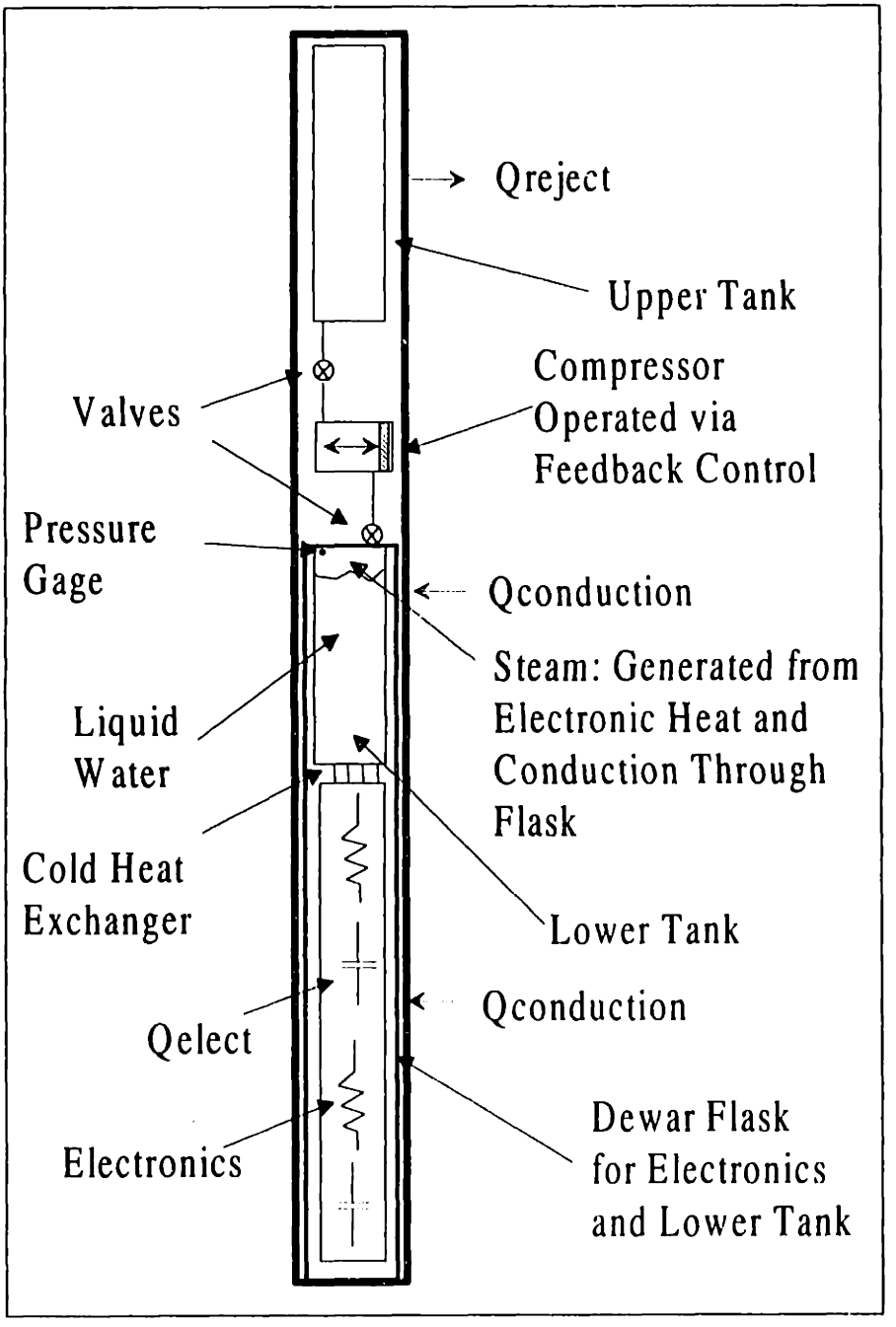

Figure 7.4: Optimal Method: Once-Through Vapor-Compression Cooler Schematic

thermal contact with a cold heat exchanger from the electronics, and is all stored within a Dewar flask. This system allows the heat, from conduction into the flask and electronic component dissipation, to be transferred to the tank of water. Consequently, the water begins to vaporize. The second major component is the compressor. The compressor maintains the lower tank at the specified atmospheric pressure value. It accomplishes this task by pulling the vaporized water or steam out of the lower tank and transporting it into the upper tank or hot heat exchanger, outside the Dewar flask. Thus, the compressor must attain pressures greater or equal to the saturation pressure of water at the given borehole temperature, along with the flowrates of steam produced by the total cooling load. For instance, the worst-case-scenario of a 200°C borehole requires compressor outlet pressures equal to or greater than 15.5×10^{5}Pa and a flowrate equal to 3.5×10^{-5}kg/s at the 80-W cooling load (see Section 6.5). The last component is simply a tank to which the compressed steam is transported and allowed to condense at borehole temperatures. The volume of the upper tank must be sized at least 1.16 times larger than the lower tank due to the increased specific volume of saturated water at 200°C over that at 100°C. Additionally, with knowledge of worst-case heat transfer coefficients in the downhole system (see Chapter 4), the upper tank must be made thermally conductive towards the borehole. Heat transfer of the cooling load and compressor work must be accomplished with as small a temperature difference as possible over that of the borehole. Each of the components is discussed in further detail in the following chapters.

Chapter 8: Once-Through Vapor-Compression Cooler: Design and Operation Specifications

8.1: General Description and Specifications

An overall description of the method is found in Sections 5.1, 6.5, and 7.5. Three major subsystems are combined to form the cooler. The subsystems are the compressor, the cold heat exchanger, and the hot heat exchanger. In addition to the three subsystems previously discussed, a sample wireline electronics chassis including heat-dissipating electronics must be made. The sample electronics would allow full-scale testing of the prototype system.

When designing for the downhole environment, usually both size and cost are minimized. Space is at a premium in downhole tools, and when available, the smallest components are used. Likewise, cost is minimized by designing with parts as standard and common as possible. Less expensive materials are also used in tools to minimize cost. However, these considerations are only important when the downhole tool works properly. In other words, a properly functioning tool is a necessity. This chapter explains in detail the required specifications of the various subsystems of the once-through vapor-compression cooler.

8.2: Compressor

8.2.1: Flowrate and Compression Ratio

The flowrate of the compressor is a direct function of the cooling load required of the system. From As shown in Chapters 2 and 3, the cooling load is specified at 80W. The 80-W cooling load is composed of 50W from the electronics and 30W from conduction from the borehole to the electronics chassis through the flask. From eq.(6-23) the mass flowrate of the cooler is specified as 3.5×10^{-5}kg/s. From the mass flowrate the volumetric flowrate, Q, is determined by

$$Q = \dot{m} v_2 \qquad (8\text{-}1)$$

where v_2 is the specific volume of the saturated vapor at 100°C. The volume flowrate is then 5.88×10^{-5}m^3/s or 58.8cc/s.

The inlet and outlet pressures of the compressor are predetermined by the states of the system. The inlet pressure to the compressor is equal to the saturation pressure of the water at 100°C. The saturation pressure of water at 100°C is 1.01×10^5Pa. The outlet pressure of the compressor must be equal to or exceed the saturation pressure of water at 200°C which is 1.55×10^6Pa. The required outlet pressure in excess of 1.55×10^6Pa is determined by the effectiveness of the hot heat exchanger. For instance, the hot heat

exchanger requires a finite temperature difference between itself and the borehole, which is at 200°C, to conduct the heat away from the tool. Therefore, outlet pressure must be equal to the saturation pressure of water at the temperature required in the hot heat exchanger. Section 8.4 discusses this issue in greater detail. A 3°C to 5°C temperature difference is designed for the hot heat exchanger. Consequently, the outlet pressure of the compressor at a maximum must equal 1.72×10^6Pa. The compression ratio of the compressor is equal to outlet pressure divided by inlet pressure. Table 8.1 lists the flowrate and pressure requirements of the downhole compressor.

Table 8.1: Compressor Flowrate and Pressure Requirements

Inlet Pressure(Pa)	1.01×10^5
Outlet Pressure(Pa)	1.72×10^6
Compression Ratio	17
Mass Flowrate (kg/s)	3.5×10^{-5}
Inlet Volumetric Flowrate (m^3/s)	5.88×10^{-5}

8.2.2: Compressor Size

The compressor designs must adhere to the overall design constraints described in Chapter 2. The design must fit into the common 0.0921m outer diameter constraint. In addition to this constraint, the ends of the compressor must be joined to the rest of the tool. Thus, the 1.38×10^8Pa o-ring grooves common to the 0.0921m outer diameter tool joints must also be used. With this in mind, the maximum outer diameter of the compressor assembly at either end must not exceed 0.0770m. The length of the compressor, like all the subsystems, is to be minimized. Table 8.2 lists the compressor size specifications.

Table 8.2: Compressor Size Specifications

Body Outer Diameter (m)	0.0921
End Outer Diameter (m)	0.0770
Length (m)	Minimized

8.2.3: Compressor Type

The compressor of choice for the size, pressures, and flowrates required of a downhole system is a positive-displacement, single-acting, reciprocating compressor (see Figure 8.1). Table 8.3 describes the operation constraints of the various compressor types. The compressors most commonly used up to pressures of 2.07×10^6Pa and at low power are reciprocating types (Avallone, 1978, p.14.33). Reciprocating compressors compress gas by reducing a volume that has been captured in a cylinder (see Figure 8.2). Compression occurs during a positive displacement of a piston within a cylinder. At the end of the stroke, the compressed gas exits via a discharge valve. The suction occurs upon returning the piston to its starting position where the volume of the compression chamber is largest (Pichot, 1986, p.70). These types of designs are common in both small air

compressors with outlet pressures up to $1.55x10^6$Pa and automobile air-conditioning compressors up to $2.07x10^6$Pa.

Both multi-staging and inter-cooling are recommended for increased efficiency in reciprocating compressors with outlet pressures in excess of $5.5x10^5$Pa and compression ratios greater than four (Avallone, 1978, p.14.33). However, because of the small packaging-size available and the extreme operation environment of oil-exploration tools, designs are kept as simple as possible. Therefore, the designs with fewer parts and less complexity leave the least opportunity for downhole failures. Inter-cooling and multi-staging the compressor would add design complexity in an already small package. The historic attempts at a similar design proved ineffective. Multi-staging and inter-cooling the steam compressor added inefficiencies due to the increased number of piston seals, tubing paths, and valves (United State, 1977 and 1979). With these considerations in mind, a single-stage compressor should be designed for the specified flowrate and with a compression ratio of 17.

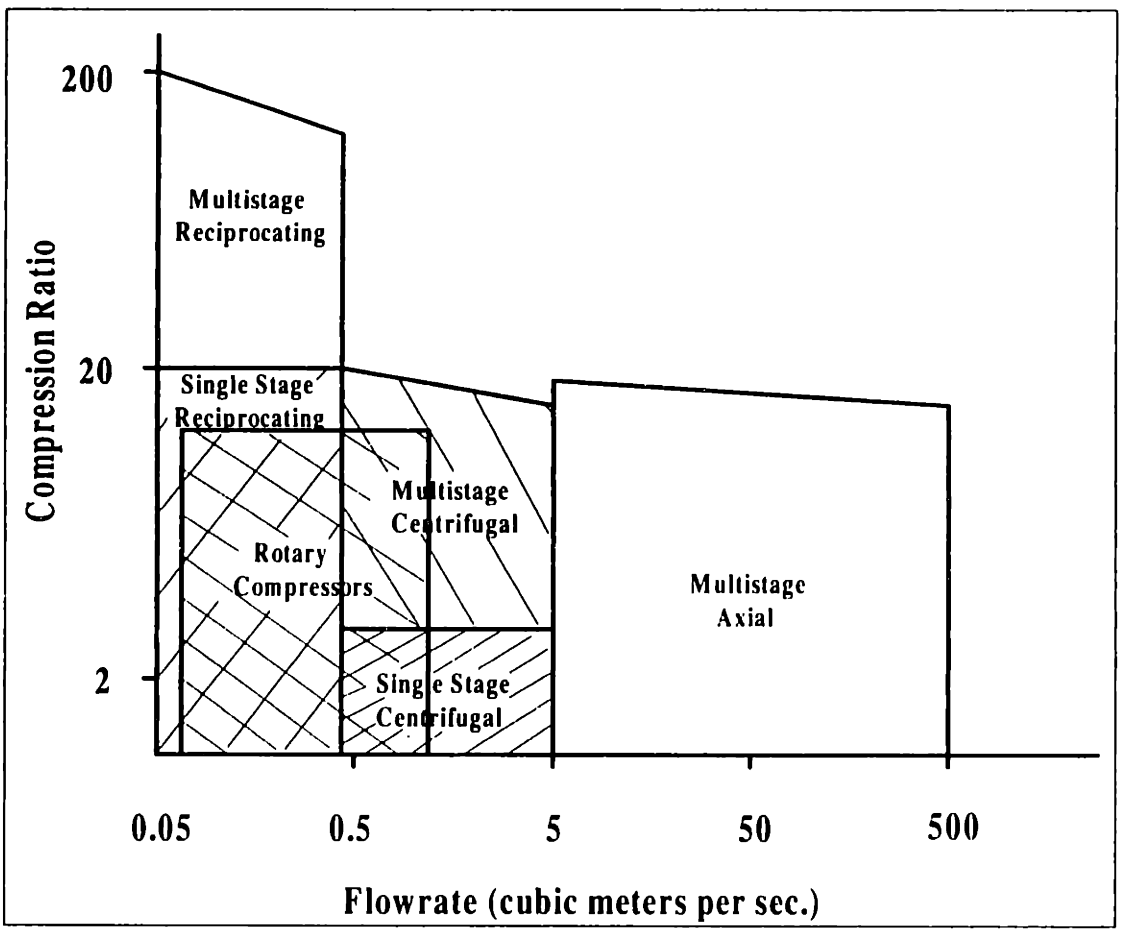

Figure 8.1: Typical Application Ranges of Compressor Types (Brown, 1986, p.3)

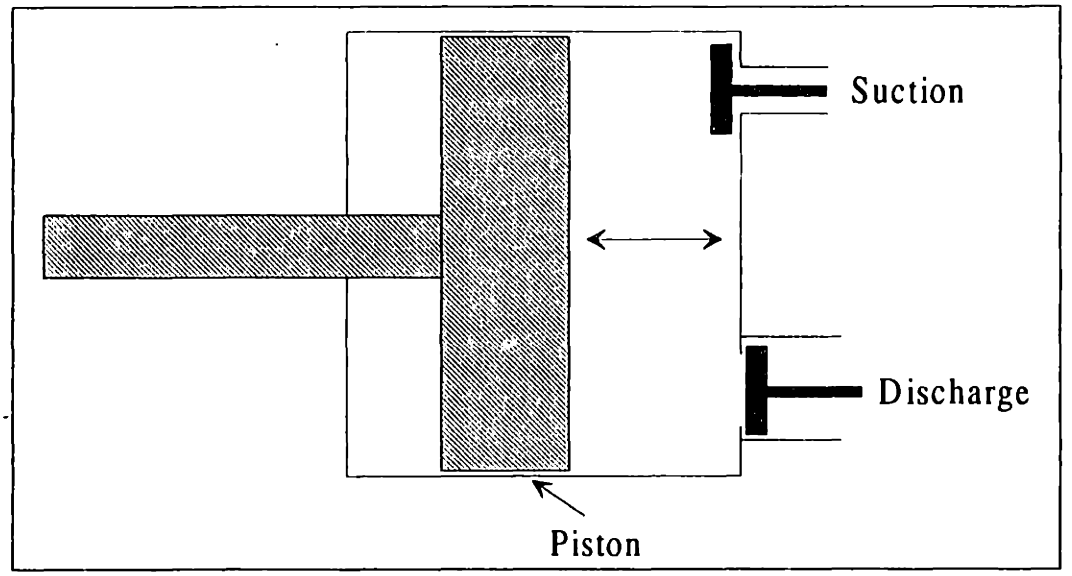

Figure 8.2: Operating Principle of Reciprocating Compressors
(Pichot, 1986, p.71)

Table 8.3: Compressor Types and Operation Characteristics (Pichot 1986)

	Applicable Pressure Range (10^5Pa)	Flowrate (m^3/s)	Comments
I. Positive Displacement			-Intermittent Flow
A. Reciprocating	1 - 2000	up to 0.5	-Most Versatile and Efficient
B. Rotary			
1. Blowers	1 - 2	0.05 - 8	-Low Pressure Only
2. Sliding Vane	2 - 15	0.01 - 3	-High Oil Consumption - Max. Press. Diff./Stage = $5x10^5$Pa - Max. of 3 Stages
3. Screw-Type	1 - 100	0.05 - 5	-Very Efficient -Fragile and Sensitive to Contaminants -Max. Press. Diff./Stage = $20x10^5$Pa
II. Turbo			-Continuous Flow -Suited for Large Flows
A. Centrifugal	1 - 400	0.25 - 20	-Max. Comp. Ratio = 12
B. Mixed Flow	1 - 400	0.25 - 100	-Same as Centrifugal and Axial
C. Axial	1 - 400	2 - 100	-Max. Comp. Ratio/Stage = 1.3 -Max. Comp. Ratio = 20

Single-stage compression devices are commonly used today at the small scales and temperature necessary of a downhole compressor. Small internal combustion and diesel engines used in remote-control airplanes display compression ratios from 8-20 when compressing combustion vapors (Higley, 1992, p.13). These motors are also packaged in volumes easily inserted in the 0.0921m diameters of downhole wireline tools. A 40-size remote-control airplane engine has a compression chamber volume of approximately $6.6 \times 10^{-6} m^3$ and operates at temperatures around 200°C (Fox, 1996). This compression chamber volume would necessitate approximately 600 strokes per minute or revolutions per minute in a downhole drive system for the steam flowrate of $5.88 \times 10^{-5} m^3/s$.

8.2.4: Compressor Efficiency: Mechanical and Volumetric

Mechanical efficiency for the positive-displacement single-acting compressor is to be maximized. For the 80-W cooling load, 250W of power is available. For an isentropic compression, the power required for the compressor is 23W (see Section 6.5). However, in real designs the compressor efficiency is always below unity. To maximize efficiency, both friction and pressure drops are minimized.

The two main locations of mechanical friction are the piston seals and rotary seals within the compressor assembly. Piston seals isolate the compression chamber from the compressor internals. Two types of seals are commonly used in small-geometry compression designs: piston rings and lapped. Piston rings are thin rings that are placed into grooves cut into the piston. The piston rings fill the clearance between piston and cylinder and, with the addition of lubricant, maintain the seal during the compression process (Pichot, 1986, p.78). The lapped design is characterized by a very tight tolerance between piston and cylinder and relies on the lubricant film between them for sealing during the compression process (Rice, 1993, p.17). Furthermore, to maintain the seal in the lapped design, the materials must expand and contract with temperature at approximately the same amount (Higley, 1992, p.14). Lubrication in both designs also serves to reduce friction, reduce wear, and distribute local heating over a larger area. Additives in lubricant also contain properties useful to the system as a function of the working fluid (e.g., rust inhibitors, etc.). Rotary seals surround the drive shaft and isolate the compressor internals from the environment.

Pressure drops within the compressor occur in valves and flow passages. To minimize pressure drops, flow restrictions are minimized. This is done in passages by increasing the cross-sectional area and allowing the fluid to more easily flow. In the same way, restrictions are also minimized in the valves. When using check valves in the compressors, their cracking pressures are also kept to a minimum value. By reducing the cracking or opening pressure of the check valve, less pressure is required above the ideal upper pressure limit in each stroke.

Volumetric efficiency for the single-acting positive-displacement compressor is to be maximized. Volumetric efficiency, η_v, is defined as (Avallone, 1978, p.14.33)

$$\eta_v = \frac{\text{actual delivery at intake conditions}}{\text{compressor displacement}} \quad . \qquad (8\text{-}2)$$

The cost of low volumetric efficiencies is reduced flowrates. Reduced flowrates would then necessitate a larger compressor given the same drive system. When designing in a small, limited geometry such as the wireline tool, a larger compressor would be less than optimal. To maximize volumetric efficiency, residual or dead volume should be minimized within the compression chamber. Residual volume is composed of the volumes in suction and discharge valves, clearance between the piston and the head of the compression chamber at the top of the piston stroke, and the equivalent volume of other dead spaces (Pichot, 1986, p.70).

8.2.5: Piston/Cylinder Materials

Material selection is crucial when designing for steam service in the pressure and temperature ranges necessary for the compressor. The compression chamber must survive steam service at pressures up to 1.58×10^6Pa and temperatures in excess of 200°C. Wear and friction behavior are also important for a reliable, long-lasting design. For material compatibility of the miniature steam compressor, one must look no farther than the steam engine. Steam engines encounter very similar pressures and temperatures as those required by the steam compressor. A material compatibility chart for pressurized, dynamic steam engine service versus wear performance is given in Figure 8.3.

RATING
E = Excellent
G = Good
P = Poor
B = Bad

	Aluminum	Brass, free machining	Bronze and Cast Brass	Cast Iron	Nickel Iron	Drill Rod (tool steel)	Nylon	Oilite (regular)	Oilite (super)	Steel SAE 1020	Steel SAE 1040	Steel SAE 4140 H.T.	Stainless Steel	Teflon
Aluminum	B													
Brass, free machining	B	B												
Bronze and Cast Brass	B	B	B											
Cast Iron	E	E	E	E										
Nickel Iron	E	E	E	E	E									
Drill Rod (tool steel)	E	E	E	E	E	E								
Nylon	G	G	G	E	E	E	B							
Oilite (regular)	P	P	P	E	E	E	G	B						
Oilite (super)	P	P	P	E	E	E	G	B	B					
Steel SAE 1020	P	P	G	E	E	E	G	G	G	B				
Steel SAE 1040	P	P	G	E	E	E	G	G	G	B	B			
Steel SAE 4140 H.T.	G	G	E	E	E	E	G	E	E	P	P	G		
Stainless Steel	P	P	P	E	E	E	G	G	G	B	B	G	B	
Teflon	G	G	G	E	E	E	E	G	G	G	G	E	G	B

Figure 8.3: Steam Service Material vs. Wear Performance
(Nelson, 1974, p.18)

8.3: Cold Heat Exchanger, Lower Tank, and Sample Electronics

8.3.1: Lower Tank

The lower tank must contain an ample supply of water for downhole residence times up to 10 hours in both a horizontal and vertical tool position. The mass of water, m, necessary for a 10-hour downhole residence time, t, of cooling is determined by

$$m = \frac{Q_{abs} t}{h_{sf}} \quad . \qquad (8\text{-}3)$$

With eq.(8-3) the mass of water is found equal to 1.28kg. The volume of the tank, V, is then found with the result of eq.(8-3) and the specific volume of saturated liquid water at 100°C or state one as

$$V = v_1 m \, . \qquad (8\text{-}4)$$

Eq.(8-4) results in a volume of $1.33 \times 10^{-3} m^3$.

The size of the lower tank is further constrained by the internal diameter of the flask. In operation, the tank must be inserted within the flask which has a maximum internal diameter of 0.076m. To avoid tolerance interference, the maximum diameter of the lower tank is limited to 0.0699m. In practice, however, the tank must accommodate through-wiring, but the constraint is relaxed for this prototype. The tank will, for all practical purposes, encounter no absolute pressure differences or wellbore fluids. Thus, its wall thickness should be sized to fit common, available stock tubing. An inexpensive material that does not suffer corrosion when put in contact with water, should be chosen for the lower tank. Galvanic corrosion between mating pieces should also be avoided by choosing the proper materials. Likewise, any threaded pairs should not exhibit galling. Length of the lower tank is then determined by dividing the volume found in eq.(8-4) by the cross-sectional area determined with the inner diameter of the stock tubing. For symmetry, the flow exit from the lower tank is chosen at the center of the uphole end of the cross-sectional area of the tank. In the case of a horizontally-positioned tool, only half the volume can be occupied by liquid to avoid the compressor taking in liquid. Therefore, the length should be increased by a factor of two for the same downhole residence time of 10 hours. Table 8.4 lists the lower tank specifications.

Table 8.4: Lower Tank Specifications

Volume (m^3)	1.33×10^{-3}
Outer Diameter (m)	0.06985
Inner Diameter (m)	Common Stock Available
Length (m)	(Water Volume/Cross-Sectional Area)x2
Material	-Inexpensive -Low Galling and Low Galvanic Corrosion -No Corrosion w/Water

8.3.2: Cold Heat Exchanger and Sample Electronics Chassis

Both the sample electronics chassis and the cold heat exchanger must adhere to various design and performance specifications. Both components are situated within the flask volume. Therefore, the same diameter constraints as the lower tank must also be applied to the cold heat exchanger and sample electronics chassis. The cold heat exchanger combined with the sample electronics chassis must also accommodate the internal flask minus the length of the lower tank. The sample electronics chassis should mimic the resistors, transformers, etc. behavior commonly used in wireline tools. The 50-W electronic heat dissipation is assumed to be evenly distributed along the length of the chassis. The cold heat exchanger must conduct the 50-W electronic heat load plus any other heat conducted through the walls of the flask from the electronics to the water in the lower tank. A maximum temperature difference of 25°C between the water at 100°C and the hottest part of the electronics chassis is allowed. The cross-sectional area of the cold heat exchanger should also be minimized to allow through-wiring within the tool. Maintenance requirements must be kept at a minimum, for the area must be easily accessible. With this in mind, free-flowing circulating heat transfer fluids are not to be used in the cold heat exchanger design (Followay, 1995). Table 8.5 lists the cold heat exchanger and sample electronics chassis specifications.

Table 8.5: Cold Heat Exchanger and Sample Electronics Chassis Specifications

Size: Both Systems	
Outer Diameter	Same as Lower Tank
Length	Accommodate Lower Flask Length Minus Lower Tank Length
Cross-Sectional Area	Minimize for Through Wiring
Sample Electronics Chassis	
Heat Dissipation (W)	50
Heat Distribution	Even Distribution Along Length
Cold Heat Exchanger	
Conduction Load (W)	50 from Electronics plus Heat Conducted Through Walls of the Dewar to Electronics Chassis
Allowable Temperature Difference (°C) between Tank and Electronics	25
Maintenance Requirements	Minimize

8.4: Upper Tank/Hot Heat Exchanger

The hot heat exchanger and upper tank assembly perform two major tasks. The upper tank must receive and hold fluid exiting the compressor. The hot heat exchanger must reject the absorbed heat from within the flask, plus the compressor work added to the steam, to the borehole at 200°C. In the simplest system, the two components are combined. In other words, if the surface area of the upper tank is large and thermal

resistance through the walls of the tank is low, it could act as the hot heat exchanger. For the prototype design, the simple combined upper tank/hot heat exchanger system should be used. Table 8.6 lists the upper tank/hot heat exchanger specifications.

8.4.1: Upper Tank/Hot Heat Exchanger Heat Rejection Specification

The hot heat exchanger must reject enough heat to the borehole so that the super-heated vapor exiting from the compressor can condense to its liquid form at the water saturation pressure at 200°C. The worst-case heat load from within the flask is equal to 50W of electronic heat plus 30W of conducted heat through the flask walls from the borehole at 200°C (see Section 2.3). Assuming an isentropic compression within the compressor and the flowrates required to absorb 80W from within the flask, eq.(6-24) produces a hot heat exchanger rejection load equal to 87W (see Section 6.5).

8.4.2: Hot Heat Exchanger and Upper Tank Size and Material

The hot heat exchanger must be sized to safely contain the entire volume of saturated liquid water at its end state and reject the heat load described above to the borehole with a small temperature differential across the inner wall of the upper tank and the borehole. Since the upper tank is outside the flask, its maximum diameter can reach 0.0921m. In practice, the entire diameter could not be utilized by the upper tank/hot heat exchanger system. The space would be shared with through-wiring, downhole sensors, and actuators. For the prototype, this constraint is relaxed and the entire cross-sectional area will be encompassed by the upper tank/hot heat exchanger system. The minimum inner volume of the tank must accommodate the entire mass of liquid water at the 200°C saturation state. This volume is found as the product of the water mass and the specific volume at state four and equals $0.00148 m^3$.

The exposed surface area should be maximized to provide the lowest thermal resistance between the assembly and borehole, and the thickness of the tank should also be minimized to reduce thermal resistance between the inside and outside of the tank. A goal temperature difference of 3°C-5°C between the inner tank and borehole is chosen. A further constraint on the minimum thickness is the $1.38 \times 10^8 Pa$ pressure of the borehole. The stress in the tank should at worst-case conditions never approach the yield point. The upper tank system should also follow the same material specifications as the lower tank plus be made of downhole-compatible materials. Downhole-compatible materials are able to resist the corrosive downhole environment and temperature while maintaining sufficient strength. A few examples of downhole-compatible materials are AISI 630 17-4PH, K-500 Monel, Beryllium-Copper, and Titanium Beta-C.

With the outer diameter, thickness, minimum volume, inner wall to borehole temperature gradient, and material of the upper tank specified, its length can be calculated. With the borehole film coefficient, h, of $100 W/m^2\text{-}°C$ (see Chapter 4), and the assumption that the entire internal surface area of the tank is isothermal at T_i, the minimum length can

be found using a heat transfer analysis through a cylinder with a convective boundary layer (Lienhard, 1987, pp.56-58). The equation for minimum length, l, is

$$l = \frac{Q\left[\frac{1}{2\pi h r_o} + \frac{\ln\left(\frac{r_o}{r_i}\right)}{2\pi k}\right]}{T_i - T_H}, \qquad (8\text{-}5)$$

where Q is the total heat rejected by the hot heat exchanger, r_o and r_i are the outer and inner radii of the tank, respectively, k is the thermal conductivity of the tank material, and T_H is the borehole temperature. If this length does not accommodate the liquid volume of $0.00148 m^3$ then it must be increased to meet the specified volume. Table 8.6 summarizes the upper tank/hot heat exchanger specifications.

Table 8.6: Upper Tank/Hot Heat Exchanger Specifications

Heat Rejection (W)	87
Minimum Volume (m^3)	0.00148
Outer Diameter (m)	0.0921
Outer Surface Pressure Rating (Pa)	1.38×10^8
Material	Same as Lower Tank Specifications plus Downhole Compatibility
Length	Sized to the Maximum of Either: 1) Minimum Volume 2) Eq.(8-5)

Chapter 9: Prototype Design and Testing

9.1: Design Method

The goal for the downhole active cooler prototype was to, ultimately, prove downhole feasibility in a wireline tool. If properly designed, the sealed system would not be affected by borehole pressure. Thus, it was not necessary to build the system to meet the downhole pressure specifications between the subcomponents, such as the compressor, upper and lower tanks, etc. The prototype was tested in an oven with a film coefficient on the same order-of-magnitude as those calculated for boreholes (see Section 9.3). Likewise, the control electronics of the system were not miniaturized to fit into the tool itself. The electronics design necessary to control the cooler would be trivial in practice compared to those of the standard tool functions (Jaroska, 1995). Consequently, the active cooler prototype was controlled by electronics external to the tool. For proof-of-concept for the downhole cooler, the entire system was designed and tested at the geometry constraints and operation parameters of a downhole wireline tool in an oven at 200°C.

The added expenses of designing and building the system to meet downhole borehole pressure and internal control electronics were avoided in the prototype. Environmental seals, through-wiring passages, and flowline passages connecting the subsystems were avoided by not exposing the tool to downhole pressures. As a result, expensive gun-drilling operations were not necessary and the subsystems could be joined without high-pressure joints. The subsystems were connected with stainless steel SwageLoc fittings and 0.00635m outer diameter by 0.00089m thickness stainless steel tubing. In addition to the pressure expenses, the expense of electrical engineering design, debug, and construction times were avoided by using uphole control systems.

9.2: Final Prototype Design

The overall assembly is plotted in Figure 9.1 and includes the sample electronics, lower tank/cold heat exchanger, compressor, lubrication system, and upper tank/hot heat exchanger assemblies (see Appendix N). The entire prototype system excluding flask is approximately 2.4m long. All sections except for the downhole motor (see Section 9.2.7) also meet the outer diameter constraints of Chapter 2. The following sections describe the design of the prototype and employ British units (inches) in the drawings and assemblies in place of SI units. This is done according to industrial and machine shop conventions. The assembly drawings are included in the text with references to part drawings and company part numbers. Both the part drawings and product specifications when applicable are given in Appendix K.

Although not downhole compatible, aluminum pieces were used in the prototype. Aluminum was used in the tubes of the lower and upper tanks, and the compressor valve

head piece. In practice, the last two pieces listed should not be made of aluminum in a downhole design. Their use in the prototype was for reasons of cost and material availability. Since the prototype was for uphole testing only, their use does not affect the mechanical performance of the prototype. Additionally, in the hot heat exchanger, the film coefficient of the borehole does not need to be adjusted to account for the difference in thermal conductivity between aluminum and downhole-compatible materials, such as stainless steel (see Appendix I).

9.2.1: Sample Electronics

The sample electronics chassis was developed by Dipti Nevrekar as an MIT Bachelor of Science thesis (1996). Her work was performed as a supplement to the current investigation, and some parts of the cold heat exchanger were developed as well. The assembly drawing for the sample electronics chassis is shown in Figure 9.2. The detailed drawings are given in Nevrekar's thesis (1996). The diameter and lengths of the chassis are 0.0699m and 0.438m, respectively. The chassis structure is made of aluminum. Three kapton strip heaters are mounted on a punch board that spans the aluminum structure. The heaters each have a resistance of 15.68ohms and when connected in parallel have a total resistance, R_t, of 6.4ohms at a temperature of 100°C.

The sample electronics are powered by a Hewlett Packard #6443B DC power supply. The voltage, v_{heat}, required to produce an electronic heat dissipation, P_{heat}, is equal to

$$v_{heat} = \sqrt{P_{heat} R_t} \; . \qquad (9\text{-}1)$$

Electronics heat dissipation values between 0W and 50W are available with the given power supply.

9.2.2: Cold Heat Exchanger and Lower Tank System

Figures 9.3 and 9.4 display the cold heat exchanger and cold heat exchanger/lower tank assemblies. The cold heat exchanger, except for the aluminum mating piece, was also developed in the thesis of Nevrekar (1996), after investigating several alternatives. The details of the cold heat exchanger system can be found in that study. Two, 0.457m by 0.0165m by 0.00660m, Noren Products flat TPhcBS heat pipes are mounted on an aluminum holder that is then placed on a thin, high thermally conductive pad (Berquist Co. Sil Pad 400) on top of the kapton strip heaters. The heat pipes transfer the heat from the electronics to the water in the lower tank through an aluminum mating piece. The air gaps between the heat pipes, aluminum holder, and aluminum mating piece are eliminated by filling them with high thermally conductive Dow Corning 340 heat sink compound.

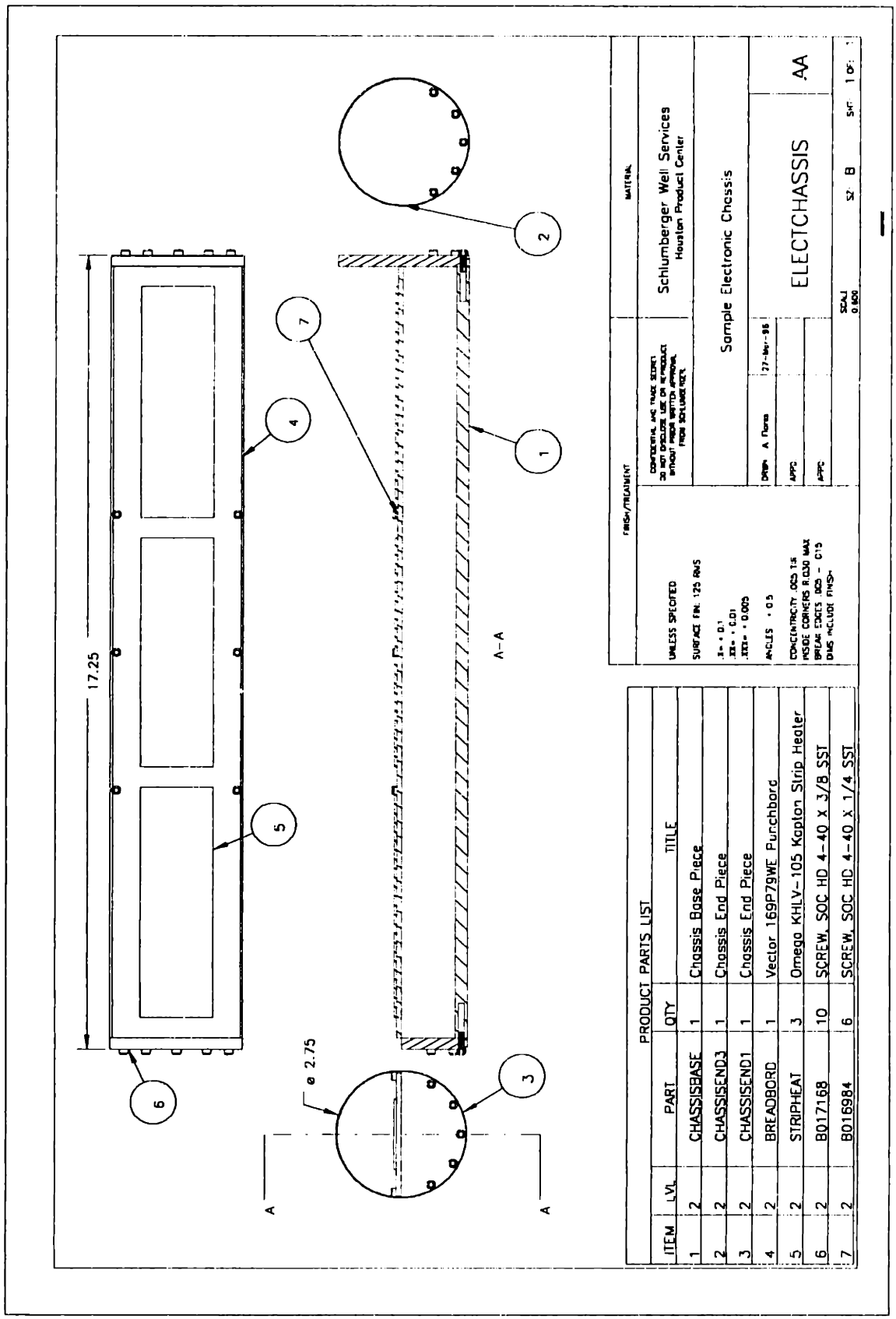

Figure 9.2: Sample Electronics Chassis Assembly

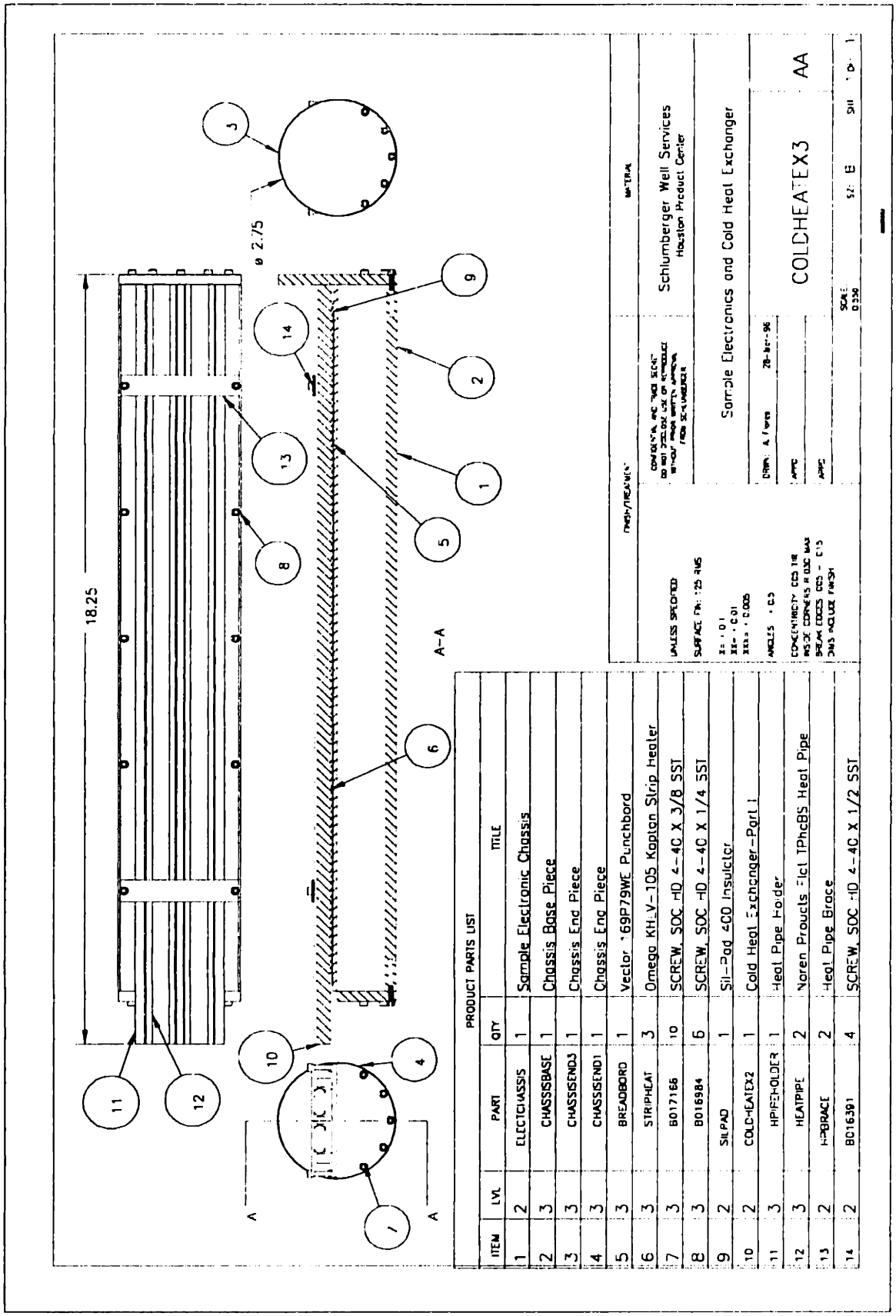

Figure 9.3: Cold Heat Exchanger Assembly

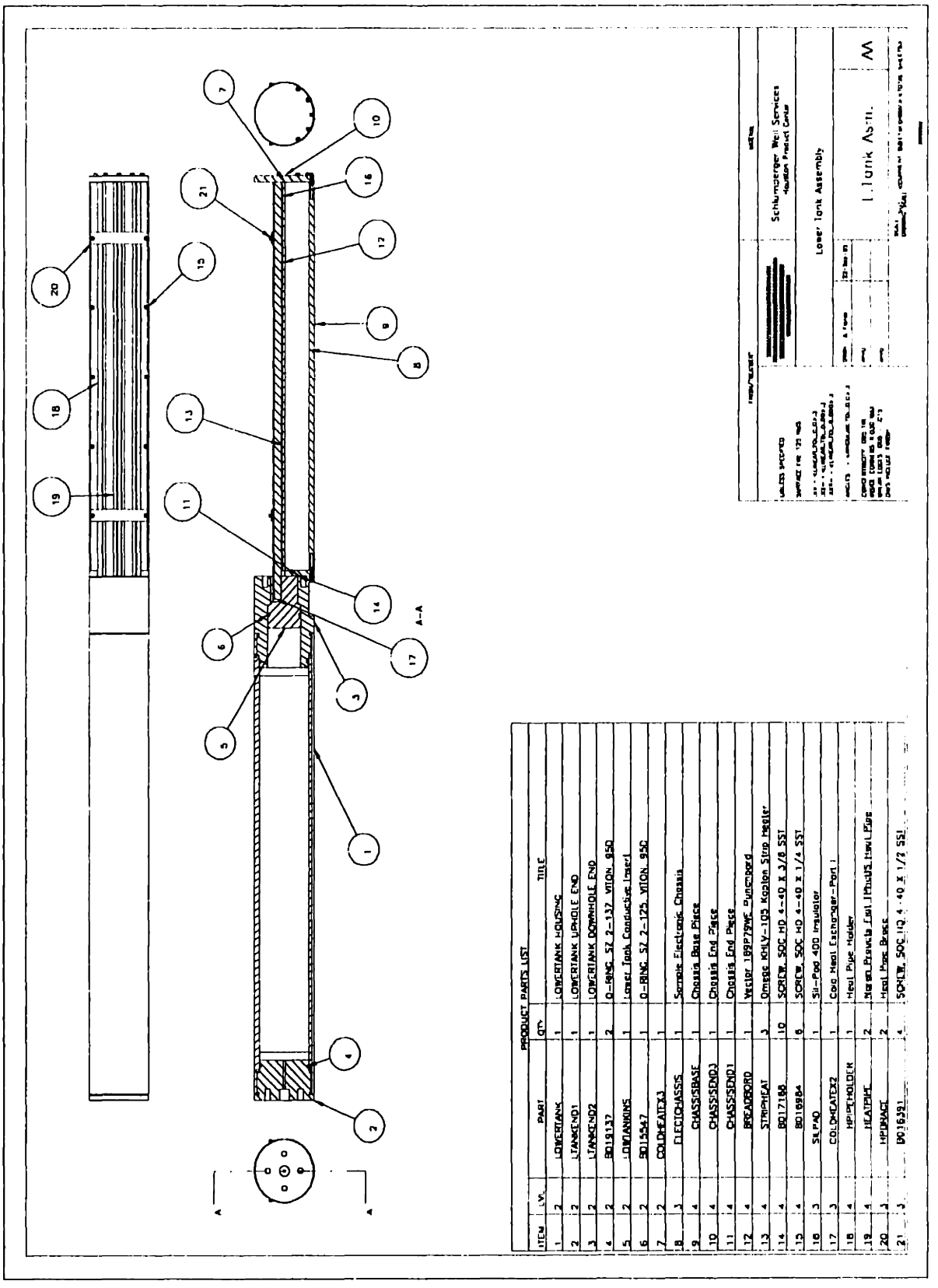

Figure 9.4: Cold Heat Exchanger/Lower Tank Assembly

The lower tank is sized to fit into the flask and carry 1kg of water. The volume of the lower tank is approximately $0.001m^3$. However, when the system is laid in the horizontal position with the exit of the tank in the center of the cross-section, the effective volume of the tank is halved. Thus, only 0.5kg of water can be carried in the lower tank in horizontal tests.

9.2.3: Dewar Flask

The flask used in the tests is a UDFH-KA Dewar flask manufactured by National-K-Works. The flask properties and diameter dimension schemes are detailed in Chapter 3. The flask has a total length of 2.36m and a payload or insulated length of 1.71m. The ends of the flask are insulated with Teflon shavings.

9.2.4: Compressor

Figure 9.6 displays the compressor assembly. The compression chamber piston, cylinder, and connecting rod are made as internal parts of a Fox Manufacturing Co. 40-size engine, and their assembly part number is 24080 (see Figure 9.5). The piston/cylinder seal is a lapped design with the piston made of mehanite and the cylinder made of 12L14 steel. The parts are manufactured to last for approximately 126 million strokes at a temperature of 232°C (Fox, 1996). That equates to a downhole time of approximately 1000 hours at compressor shaft speeds of 2000 rpm.

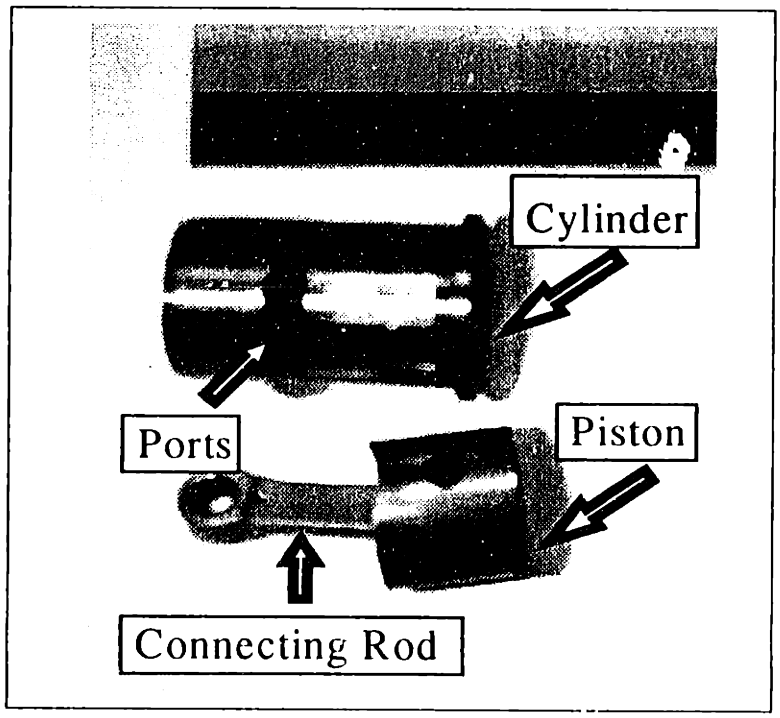

Figure 9.5: Fox Piston, Cylinder, and Connecting Rod

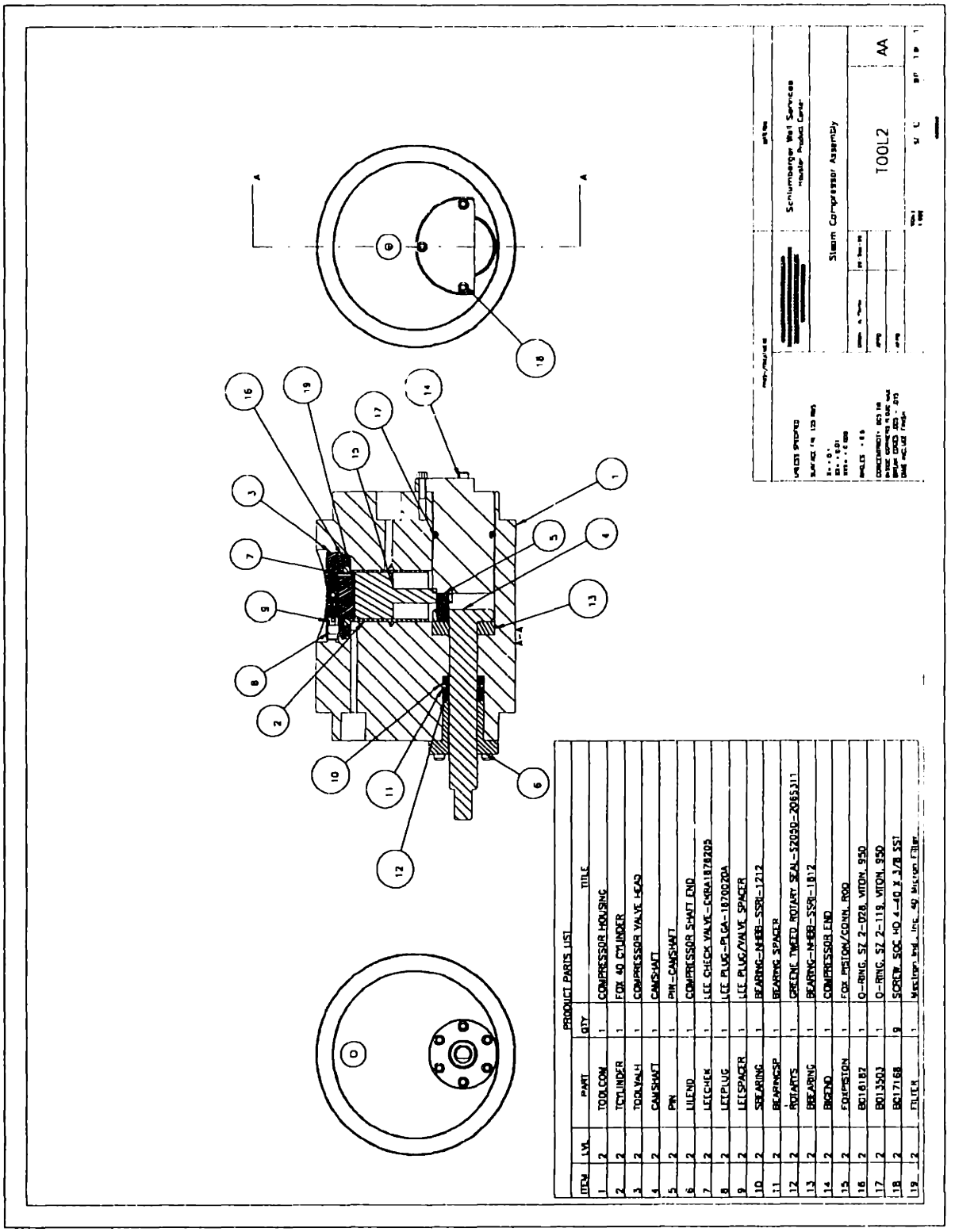

Figure 9.6: Compressor Assembly

The intake porting of the compressor also mimics the design of a small internal combustion engine. The intake port is located at the bottom of the piston stroke. As the piston travels downward, a small vacuum is created in the compression chamber. When the bottom port is then exposed as the piston crosses its surface, the steam is sucked into the compression chamber volume. On the upward path of the piston, the port is sealed by the circumferential area of the piston and lubricant (see Appendix H). This design is also similar to the porting of small air compressors. In this porting configuration, an intake valve is eliminated, along with its design complexities and inefficiencies.

A miniature Lee Co. check valve is used as the exhaust valve in the compressor. The check valve displays a nominal cracking pressure of 34.5×10^3Pa. These check valves are rugged, reliable, all metal designs that are commonly used in the oil exploration industry. The valve is hard-mounted in the compressor head piece. A small 40-μm Mectron Industries, Inc. filter is placed in front of the valve on the compression chamber side inlet hole. The filter kept contaminants from entering and plugging the valve, especially during the "break-in" period of the seal.

The drive system of the compressor consists of the crankshaft, connecting rod, bearings, and a rotary seal. The rotary seal isolates the crankcase from the external pressure of the environment. A Greene-Tweed steam-service rotary seal is used in the design. Two different, but standard-sized ball bearings are used in the drive system, and the crankshaft dimensions are copied from those in the standard Fox 40-size engine. For compatibility with the rotary seal, a hardness of 45-55Rc is specified for the crankshaft. As mentioned earlier, the piston connecting rod is taken directly from the Fox 40-size engine.

9.2.5: Lubricant System

Figure 9.7 displays the lubricant system. A lubricant is maintained under pressure and compensated by two springs in series. A three-way, normally-closed, high-temperature Lee Co. solenoid valve is periodically opened and closed, allowing lubricant to travel into the compressor intake line through a Lee Co. Visco-Jet restrictor. From the intake line, the lubricant travels into the compression chamber and maintains the high pressure seal. Some lubricant also "blows-by" the seal and serves to lubricate the crankcase internals similar to a four-stroke model airplane engine (Higley, 1992, p.9). Appendix H explains the programmable open and close rates of the solenoid valve. The programmable controller is a Cole Palmer System IV controller. The power supply for the solenoid valve is a Systron Donner #TL-8-30V power supply. During the system tests, pressure on the lubricant side is maintained by the user at approximately 2.07×10^6Pa. A hydraulic line is connected to the lower line on the lubricator end that contains the solenoid valve. Lubricant is periodically pumped into the reservoir with an Enerpac #P-141 hydraulic pump from outside the oven to maintain reservoir pressure. The reservoir pressure is measured by a Bourns 0-600psig pressure gage. In practice, a screw-drive system could maintain the reservoir pressure autonomously.

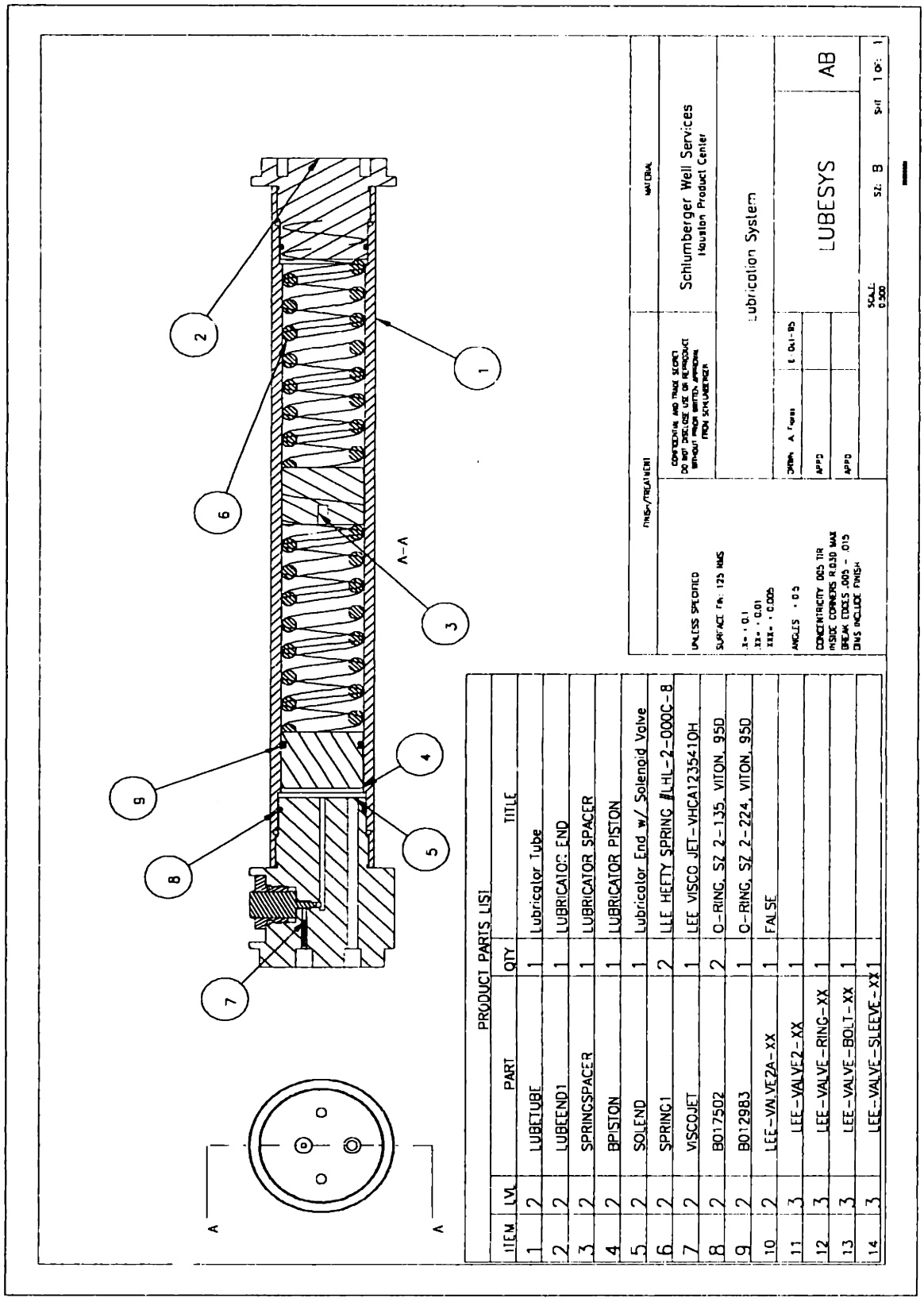

Figure 9.7: Lubricant System Assembly

The lubricant used in the final tests was Dow Corning-200, 500cSt Silicone Oil. A model of the piston/cylinder seal displayed the need for a viscosity of approximately 50cSt at the operating temperature and shaft speeds of the compressor (see Appendix H).

9.2.6: Hot Heat Exchanger/Upper Tank

The hot heat exchanger/upper tank assembly is plotted in Figure 9.8. The assembly serves to both store the high pressure steam and conduct heat from the steam to the borehole through its walls. Appendix I describes the temperature required within the tank to conduct a given condenser heat flux to a 200°C borehole with a specified convection film coefficient. As mentioned above, the tank was made of aluminum which is not compatible with the downhole environment. However, the aluminum housing made no difference from a heat transfer standpoint in the design. In other words, the limiting resistance to thermal conduction is the borehole film coefficient, not the material of the upper tank (see Appendix I). The temperature difference required for the aluminum housing is only 0.3°C less than that required for the downhole-compatible stainless steel housing.

9.2.7: Motor

The original downhole motor assembly is plotted in Figure 9.9. The assembly has an outer diameter of approximately 0.102m which is larger than the diameter constraint stated in Chapter 2. The 2/3HP high-temperature downhole motor displayed in the assembly is commonly used in Schlumberger wireline tools. The development of a new motor to fit the geometry constraints does not represent a serious design challenge (see Appendix L) (Jaroska, 1995). However, due to long lead times in excess of three months, as well as high development costs, a new downhole-compatible motor was not purchased for the uphole prototype.

The entire motor/compressor assembly is displayed in Figure 9.10. The two shafts are joined by a Boston Gear #JS75B telescoping universal joint. After several hours of high temperature use, the downhole motor shaft broke. It is believed unsupported side loads caused a fatigue fracture in the shaft. At that point, the tests were run with a large room temperature motor located outside the oven.

A Dayton direct-current motor was used to drive the compressor in place of the downhole assembly. Again, the Boston Gear telescoping universal joint joined the two rotating shafts. Appendix J further explains the motor system and calibration. Figure 9.11 shows the Dayton motor in its operation position outside the oven.

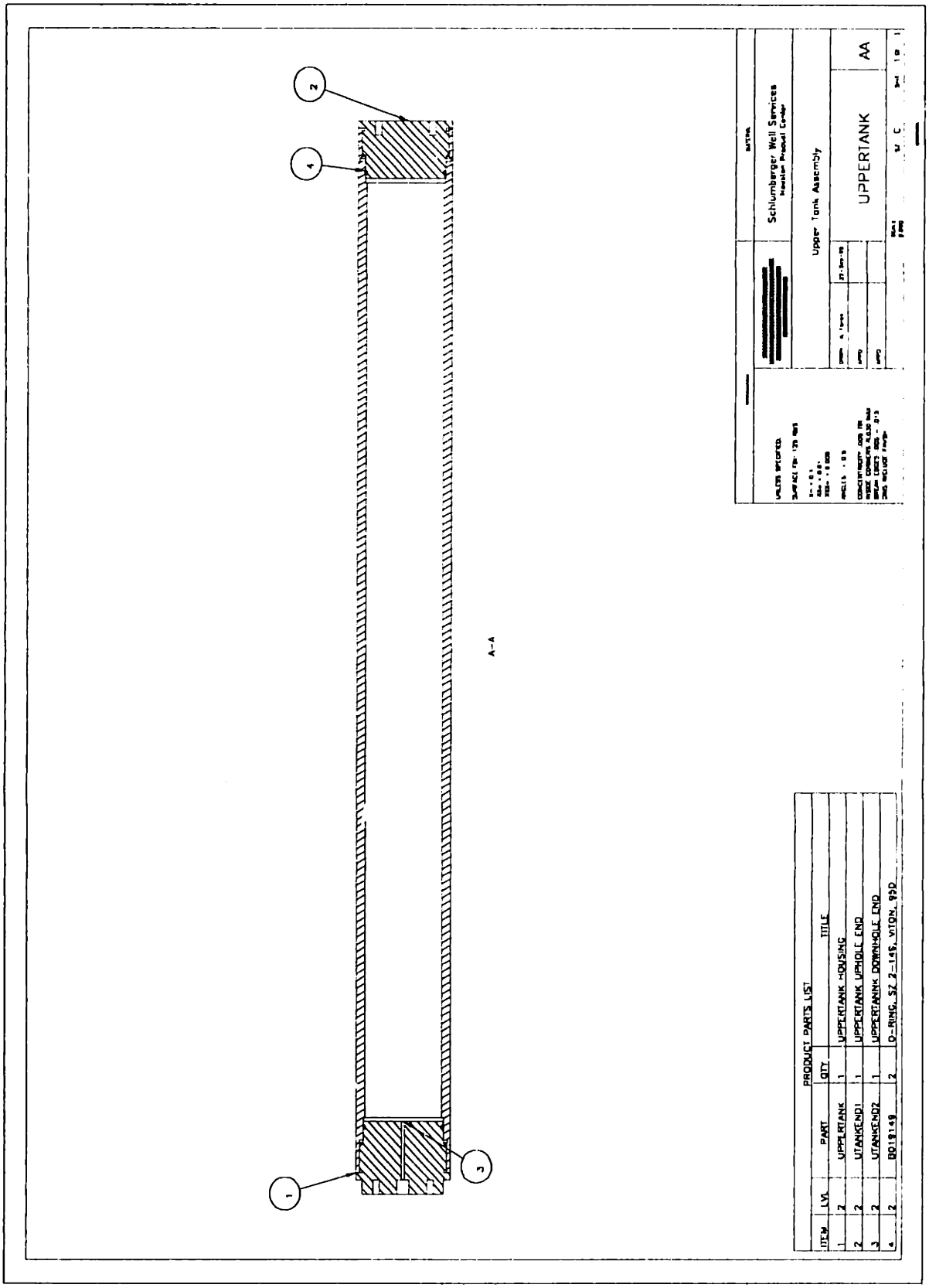

Figure 9.8: Hot Heat Exchanger/Upper Tank Assembly

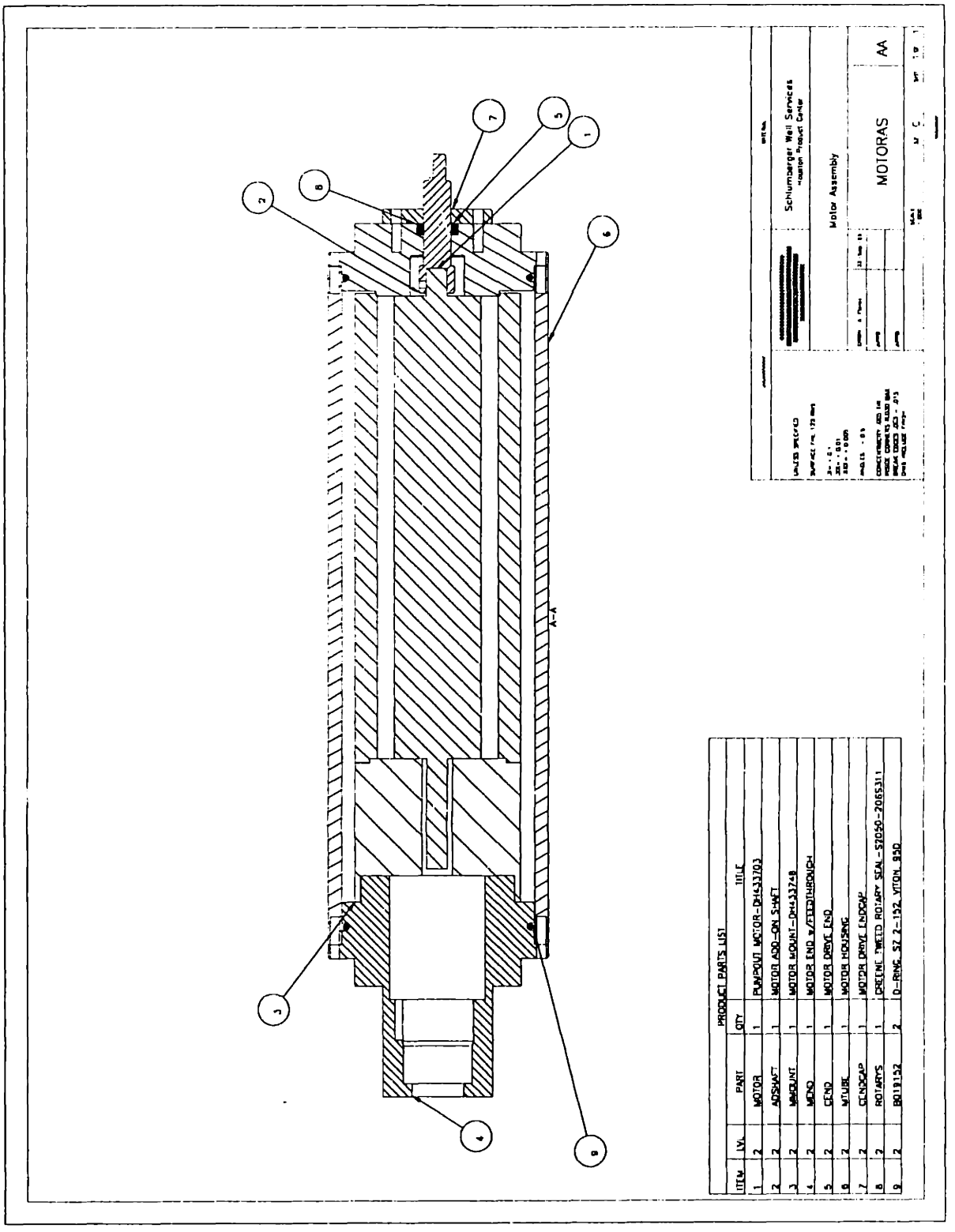

Figure 9.9: Downhole Motor Assembly

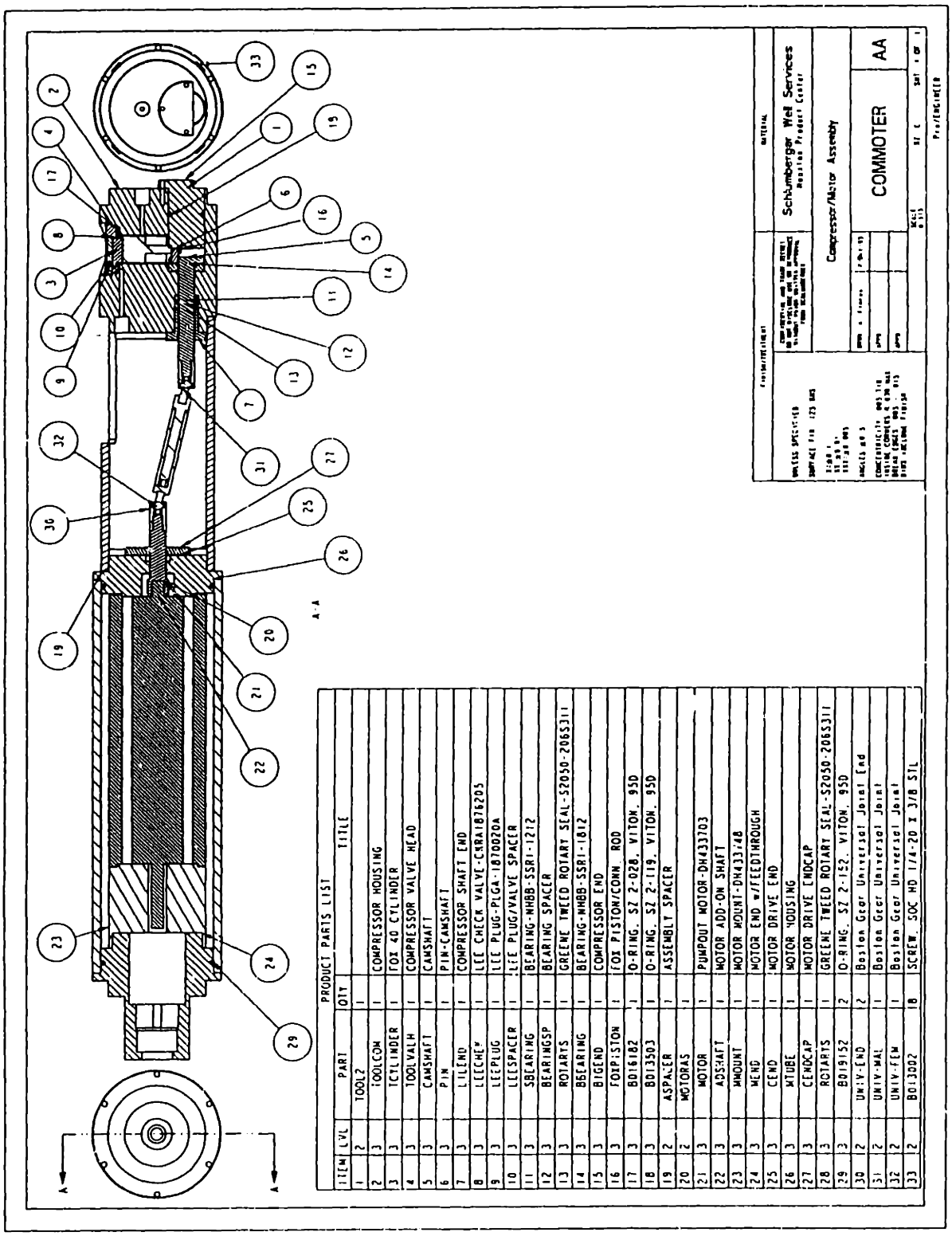

Figure 9.10: Motor/Compressor Assembly

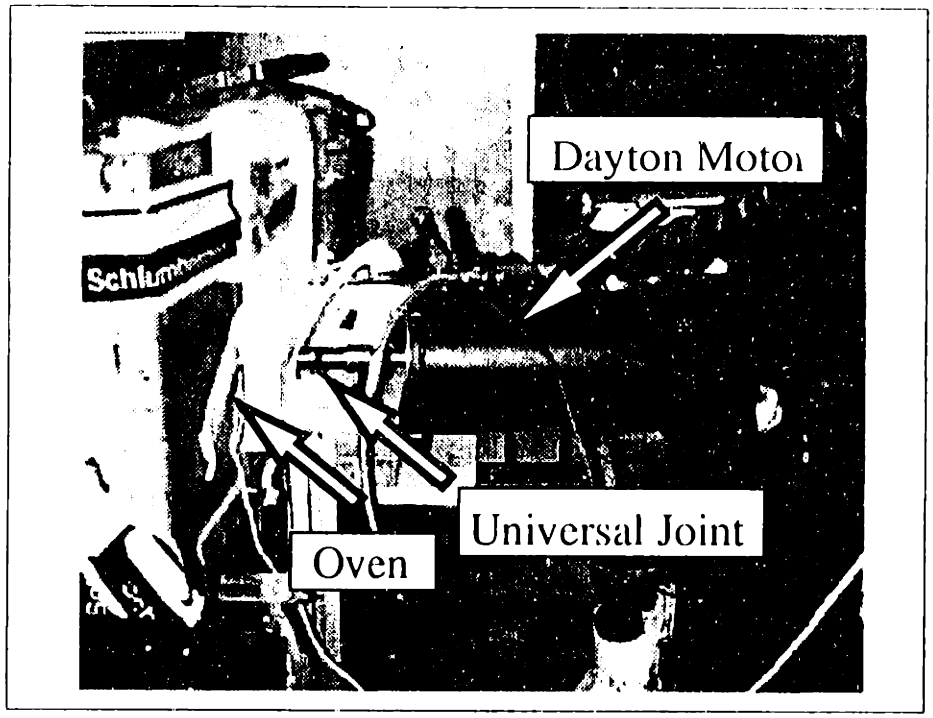

Figure 9.11: Uphole Motor

9.3: System Testing

A schematic of the overall testing system for the uphole prototype is shown in Figure 9.12. The assembly from Figure 9.1 had to be parted lengthwise into two pieces and laid horizontal to fit in the test oven (see Figures 9.12-9.15). The following sections explain, in detail, the testing and data acquisition systems used for the feasibility of the uphole prototype.

9.3.1: Testing Method

The first step was to bring the tool and flask up to steady state temperature both internally and externally. Temperatures of the tool and external flask housing were brought up to 200°C by setting the oven thermostat to the 200°C mark. Inside the flask, its internal housing, lower tank (half-filled with distilled water), and the cold heat exchanger system were heated by the power inputted into the sample electronics. During this period, the tubing exit from the lower tank was open to atmospheric pressure outside the oven. The internal components were heated until steam was generated from the water within the lower tank. At that time, with the desired sample electronics heat flux, the temperatures along the sample electronics were recorded by thermocouples mounted along the length of the heat pipes at distances from the end of the lower tank equal to 0.0444m, 0.216m, and 0.0349m (see Figure 9.15). The tubing exit from the lower tank was then closed, diverting the steam to the inlet of the compressor.

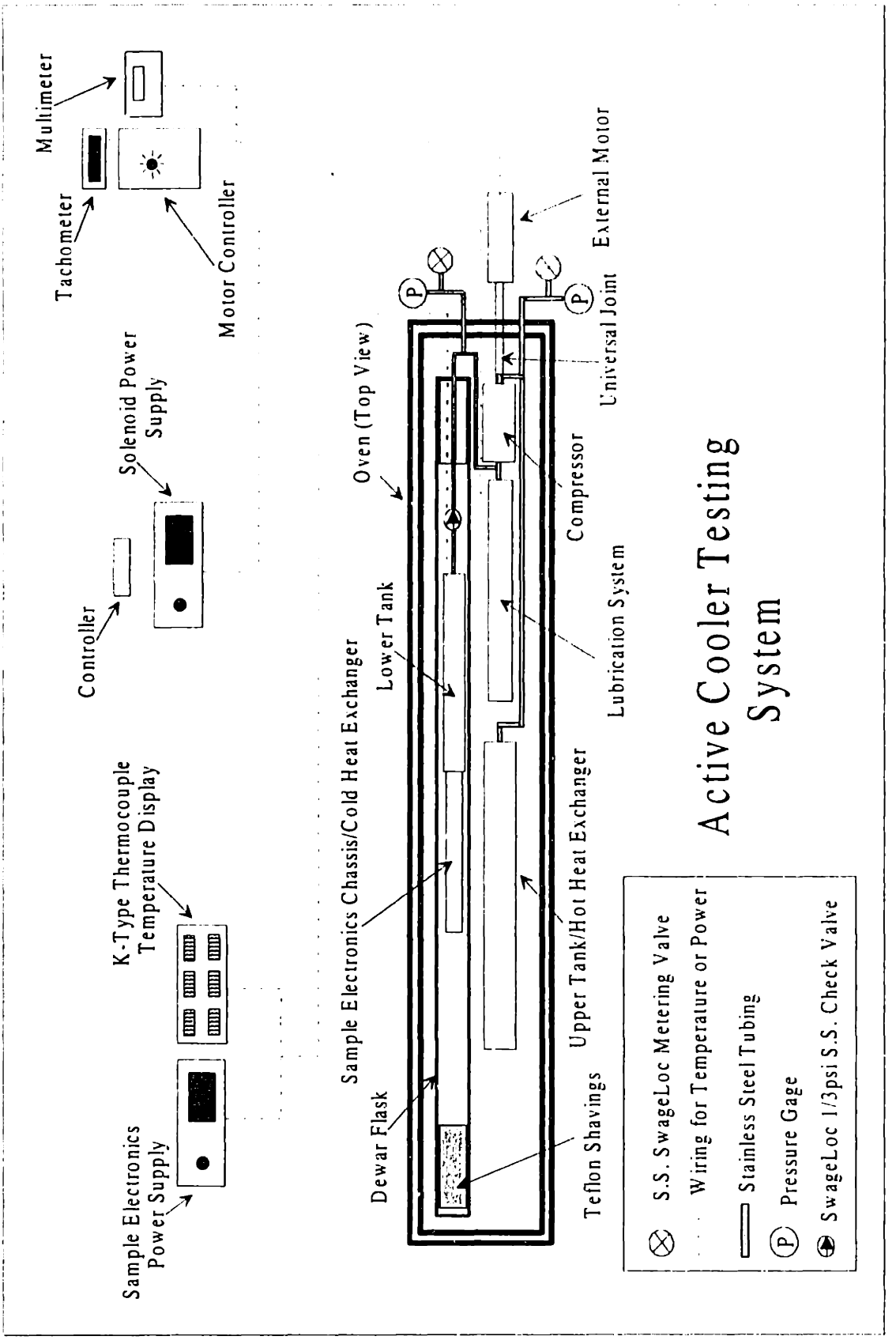

Figure 9.12: Active Cooler Testing System

Once the entire system was brought to temperature and the sample electronics were dissipating the correct heat flux, the active cooler was started and data was recorded. First, the lubrication system was started. A specified flowrate of lubricant was injected into the inlet line of the compressor. Immediately following this, the compressor was started by turning on the external motor. The motor speed was adjusted by the operator until the pressure in the lower tank was slightly below zero gage pressure. The pressures in the lower tank and upper tank, temperatures in the cold heat exchanger, and shaft speed and input current to the motor were all recorded at 2-minute to 3-minute intervals for the duration of the test. Meanwhile, the operator continued to maintain the pressure in the lubricant system by periodically injecting more lubricant into its reservoir.

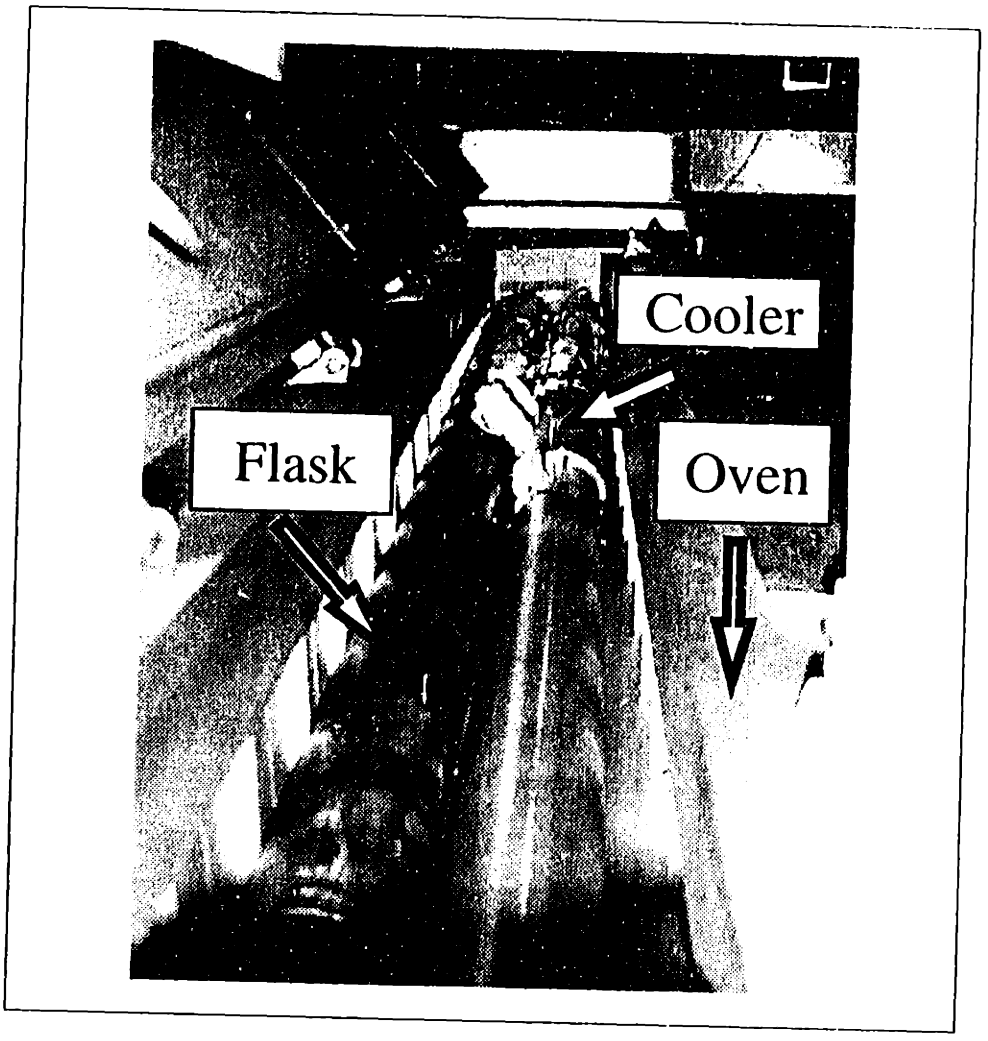

Figure 9.13: Active Cooler Tests Layout in Oven

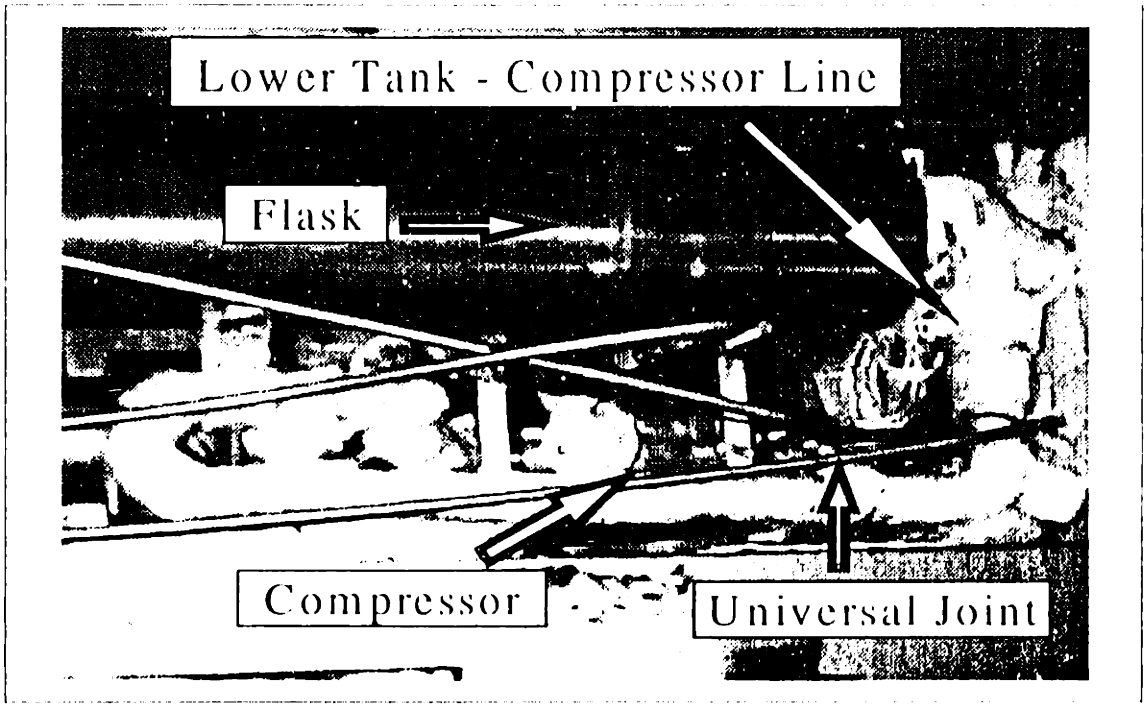

Figure 9.14: Compressor Test Drive System in Oven (Top View)

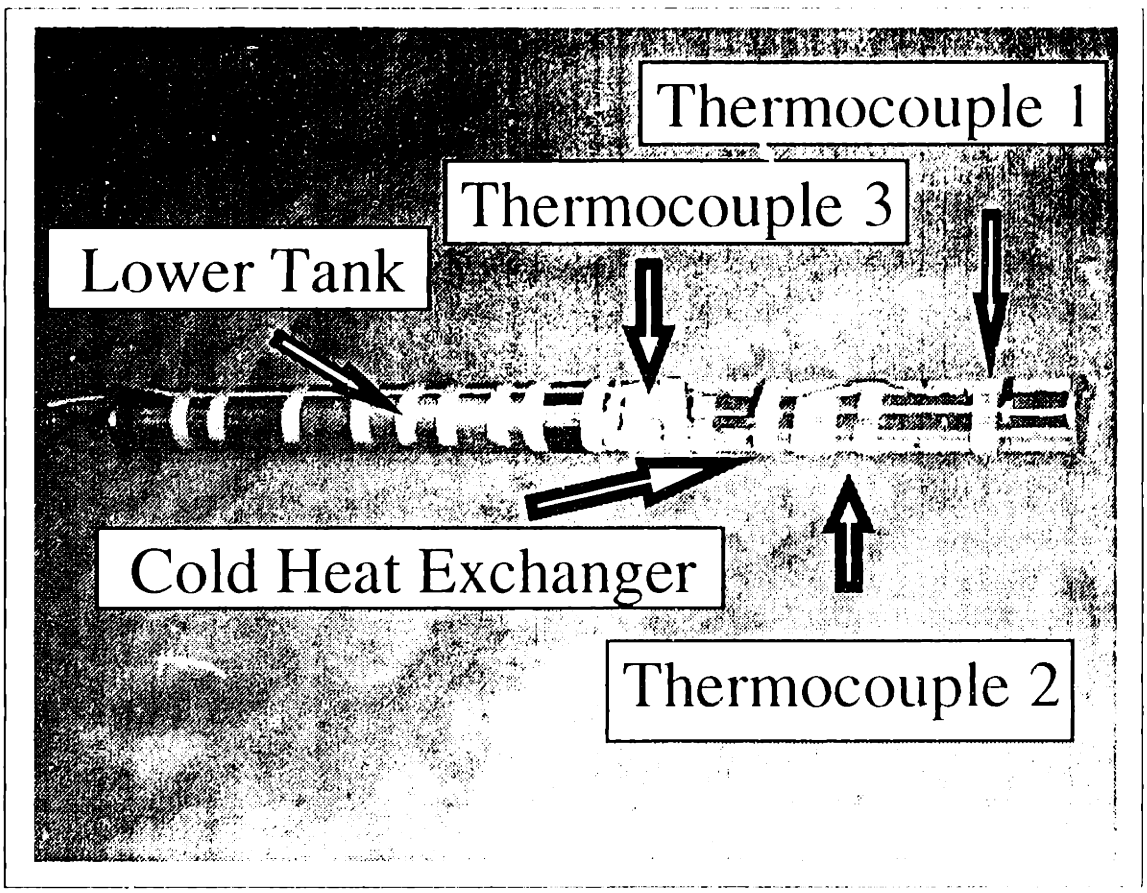

Figure 9.15: Lower Tank/Cold Heat Exchanger with Thermocouples

9.3.2: Testing and Acquisition Systems

The oven used in the tests was a Depatch Industries #PTC-1-27 model. The maximum temperature of the oven was 260°C. The payload size of the oven was 2.44m by 0.203m by 0.152m. It contained a thermostat control system in which a temperature could be set and maintained up to its maximum temperature. The convective heat transfer coefficient in the oven was calculated to be 34W/m^2-°C (see Appendix I).

During the tests both pressure and temperature were measured. Temperatures were measured with K-type thermocouples and displayed on Omega Engineering 4000 Series heater controllers. In addition to the sample electronics, thermocouples were placed on the lower tube exiting the lower tank, the external housing of the flask, and the compressor valve head piece. In the thermocouple scheme of the sample electronics, thermocouples were taped to the top of the heatpipes at the specified distances given in the previous section. This was the method utilized in the cold heat exchanger investigation of Nevrekar (1996). Although not directly on the electronics, this method theoretically produces temperature readings to within 0.5°C of the actual sample electronics temperatures (Nevrekar, 1996, p.37). The oven temperature was measured by its internal thermometer. Pressure in the upper tank was measured by a McDaniel Controls, Inc. model #AB50301 0-1000psig liquid-filled pressure gage. The pressure in the lower tank was measured by two gages. One gage contained a vacuum reading and was a Marshal Town 30-0mm Hg, 0-250psig pressure gage. The other lower tank gage was a Marshal Town 0-15 inches of water, 0-3.5 kPa pressure gage.

Input power to the motor was inferred from its input current and shaft speed. The instruments used in the process, as well as the power calibration tables of the motor are explained in Appendix J.

9.4: Compressor Characterization Tests

To determine the volumetric efficiency and flowrate of the compressor, its behavior was fully characterized. Zero-pressure-differential compressor flowrate tests were run, as well as steam flowrate tests at full operating conditions within the oven.

With no compression ratio from inlet to outlet the flowrate versus shaft speed was recorded for the compressor. Air at room temperature was used as the transport fluid. The flowrate of the air was recorded with an Omega Engineering, Inc. Series FL-110 rotameter. This flowrate equaled the volumetric flowrate displaced by the piston stroke, Q_{stroke}, at different shaft speeds.

For the steam flowrate tests, the steam mass rates versus sample electronic heat fluxes were first determined. These tests were executed by setting the sample electronics heat flux equal to a given value within the flask while the entire external system was at the oven temperature of 200°C. The steam was allowed to exit the oven system from within the lower tank assembly located within the flask into a water-filled graduated cylinder outside the oven at atmospheric pressure and room temperature. After a period of time, the increased volume of water in the cylinder was measured and converted to an increased mass value. The increased mass value was divided by the time the system was allowed run. Thus, the steam flowrate associated with a given sample electronics heat flux within a flask at the downhole high temperature specification was determined. It was found in practice that only a negligible amount of heat flux was conducted through the flask walls from the environment at 200°C and into the lower tank. Therefore, the steam mass flowrate, $\dot{m}$, generated by the sample electronic heat flux, Q, equaled

$$\dot{m} = \frac{Q}{h_{jf}}, \qquad (9\text{-}2)$$

where h_{jf} is the latent heat of vaporization of water at 100°C and atmospheric pressure.

At full temperature and pressure operation, the volumetric inlet flowrate of the compressor, Q_{inlet}, could then be directly related to the heat flux from the sample electronics. This was accomplished by multiplying the specific volume of state two of the process by the result of eq.(9-2). This required, however, that the compressor could maintain the lower tank at 0 gage pressure at the specified shaft speed.

Finally, with the data from the previously described tests, the volumetric efficiency of the compressor could be determined. The volumetric efficiency of a compressor, η_v, is defined as the volume flowrate displaced by the piston stroke divided by the inlet flowrate of the compressor, Q_{inlet}, (see eq.(8-2)) at a given shaft speed or

$$\eta_v = \frac{Q_{inlet}}{Q_{stroke}} . \qquad (9\text{-}3)$$

Chapter 10: Active Cooler Results and Discussion

10.1: Overall System Results and Comments

Figure 10.1 plots the results versus time of the active cooler tests at a temperature of 200°C and a sample electronics heat flux of 30W. The tests were run with a piston/cylinder seal that had already been "broken in" by two hours of previous operation. The final test was run for approximately two hours. After steady-state temperatures and pressures showed no variance in this period, continued testing offered no further utility, and the tests were concluded. Life testing was not deemed critical for the feasibility prototype, since many changes are recommended for the next iteration which would alter its behavior. Table 10.1 summarizes the results of the once-through vapor-compression cooler tests.

10.2: Cooling Load

The maximum cooling load or sample electronics heat flux for the system is limited to 30W at compressor shaft speeds of 1500rpm. This limit became apparent after several tests at higher heat fluxes were unsuccessfully attempted. The 30-W limit differed from the 50W design specification due to the addition of the filter screen in the compression chamber. After several of the miniature check valves were plugged, the 40-μm filter was added in front of the valve. However, by doing this, the residual or dead volume in the compression chamber was significantly increased, resulting in a decreased volumetric efficiency. Another interesting characteristic was the independence of flowrate versus shaft speed in the range of 1250rpm-2250rpm at the pressure ratio of the steam tests. The power also remained roughly constant in that shaft speed range as well. This investigator believes the inlet flow port may cause a flow restriction, and the restriction allows only a limited steam flow into the compression chamber while it is opened by the movement of the piston.

10.3: Pressures and Temperatures

Pressure was measured in both the upper and lower tanks during the system tests. The absolute pressure in the lower tank was maintained at 1.01×10^5Pa for the duration of the test. The pressure in the lower tank at the onset of the test was approximately 1.03×10^5Pa but quickly dropped to its steady-state value after the compressor was started. The pressure in the upper tank quickly rose as super-heated steam vapor was added to its interior. The steady-state absolute pressure of the upper tank equaled 16.9×10^5Pa.

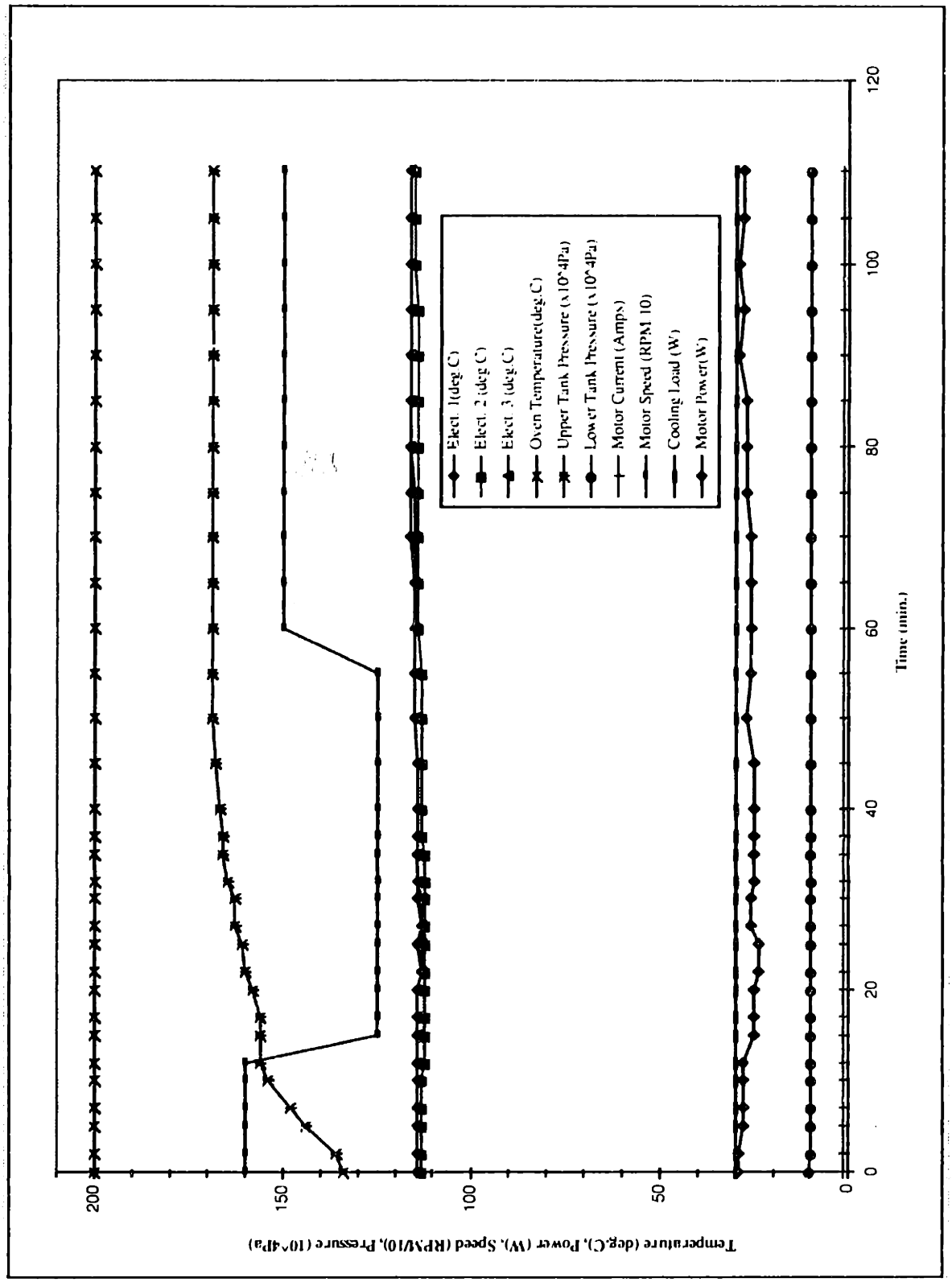

Figure 10.1: Once-Through Vapor-Compression Cooler Test Results

The steady-state pressure in the upper tank corresponded to a saturation temperature in the tank equal to 204°C. This temperature falls in the design specification range for the hot heat exchanger of 3°C-5°C above the borehole temperature (see Section 8.4.2). The factor of three between the total rejection heat flux specified of 87W and the actual heat rejection rate of 33W is offset by the heat transfer coefficient of 34W/m^2-°C in the oven versus that of the borehole at 100W/m^2-°C.

As described in Chapter 9, the tests were run in the horizontal tool position representing a worst-case-scenario for the cold heat exchanger. However, the thermocouples showed no temperature gradient across the length of the heat pipes. At 50W of electronic heat, the thermocouples displayed an average temperature of 122°C. The 30-W heat load produced an average heat pipe temperature of 114°C. Thus, the aluminum mating piece displayed the high thermal resistance and required the large temperature differences between the heat pipes and the water in the lower tank at 100°C. Although this system could be improved (see Chapter 11), it still operated below the targeted 125°C temperature for the electronics.

Temperature was also measured on the outside of the compressor valve head piece. This temperature at steady-state operation of the cooler was roughly 225°C.

10.4: Power and Coefficient of Performance

For the 30-W cooling load of the refrigeration system, approximately 29W of input power was required into the motor. Consequently, the COP of the system equaled approximately one. From the input power and eq.(6-19), the mechanical efficiency was found for the system at 0.3 or 30% of the isentropic case. The efficiency of the motor was not separately accounted for in this analysis. The Dayton motor, used for the tests, operates at efficiencies of 85% and higher at the speeds and loads used by the compressor (Jaroska, 1995). Since conservative results were sought, the inefficiencies added by the motor are lumped into those from friction and flow restrictions. Friction from the rotary seal and piston/cylinder seal caused a power loss of 18W at 1500rpm. The power required to move steam past the check valve cracking pressure and restriction equaled 5W at 1500rpm. Thus, the power required for the steam compression process only, was equal to approximately 6W. The 6-W compression power is on the same order-of-magnitude as the 9W estimated by the isentropic process at the given mass flowrate of the system. In reality, however, the actual compression power must be larger than the ideal isentropic case. This investigator believes that the friction power measurements were slightly over estimated and their measurement errors stacked to produce the low 6-W power value for compression.

10.5: Volumetric Efficiency

To determine the volumetric efficiency of the compressor, the piston displacement flowrate and the volumetric flowrate of steam at operating conditions were found. The

piston displacement flowrate versus shaft speed is plotted in Figure 10.2. At a shaft speed of 1500rpm the displacement flowrate is equal to $4.5x10^{-5}m^3/s$. An electronic heat flux of 30W within a flask in a 200°C oven produced a steam mass flowrate of $1.33x10^{-5}kg/s$. This mass flowrate corresponded to an inlet volume flowrate to the compressor equal to $2.23x10^{-5}m^3/s$. With equation(9-3) the volumetric efficiency for the compressor was found equal to 0.5 or 50% of that in the perfect system.

Table 10.1: Once-Through Vapor-Compression Cooler Test Results

Parameter	Test Result
Electronics Cooling Load (W)	30
Motor's Input Power (W)	29
COP	1
Lower Tank Pressure (Pa)	$1.01x10^5$
Upper Tank Pressure (Pa)	$16.9x10^5$
Upper Tank Temperature (°C)	204
Hottest Electronics' Temperature (°C)@ 50W	122
Hottest Electronics' Temperature (°C)@ 30W	114
Inlet Mass Flowrate (kg/s)	$2.23x10^{-5}$
Volumetric Efficiency (%)	50

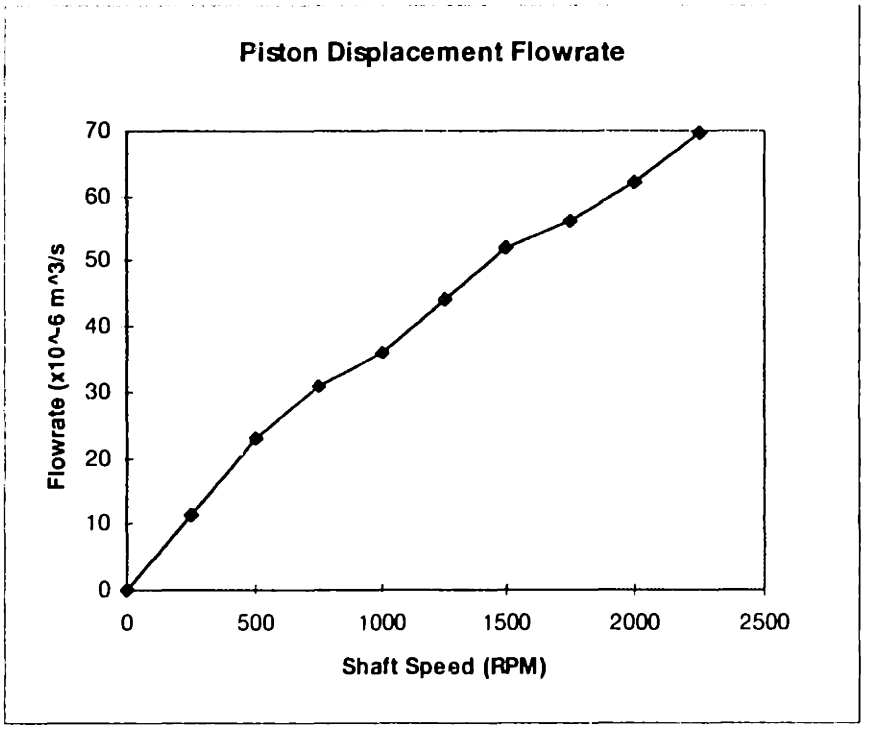

Figure 10.2: Piston Displacement Flowrate versus Shaft Speed

Chapter 11: Conclusions and Recommendations

11.1: Summary and Significance

The present investigation both revealed and proved the feasibility of the optimal cooling method for the electronics chassis of wireline tools in the downhole oil-exploration environment. The once-through vapor compression cooler displayed the best performance, lowest design complexity, lowest cost, and lowest maintenance of all the other cooling methods while still maintaining the small geometry required in downhole tools. Additionally, a full-scale prototype was successfully built and tested at downhole temperature. The cooler was able to absorb 30W of heat from the electronics of the tool while their temperature was kept at 114°C within a Dewar flask. The heat load was then rejected to the high temperature downhole environment at 200°C. The coefficient of performance of the refrigerator equaled approximately one.

The results of the present study offer a viable solution to the ever-increasing problem of designing for high temperatures in the oil-exploration environment. Designers now have a choice between designing a "cold" section for high temperature-sensitive electronics and using an active cooler, or finding electronics that work up to the 200°C mark. However, the availability of high temperature components is continuing to decrease and will eventually cause a shift in the behavior of designers toward the "cold" method. Additionally, the method developed in this study is not limited to wireline tools. Measurement-While-Drilling (MWD) tools, as well as Logging-While-Drilling (LWD) tools could also use the once-through vapor-compression cooling method for the same purposes as the wireline tool. The only differences required would be a slightly different geometry and longer downhole residence times. Both of those issues do not represent large design challenges. For instance, the downhole residence times could easily be increased by increasing the volume of the lower tank.

With an active cooler system, new performance enhancing capabilities are possible for the downhole tools. For instance, downhole computer processing is conceivable when temperatures are kept below 125°C in the electronics sections. Also, new sensors such as downhole cameras, recorders, etc. are also feasible with the "cold" electronics sections provided by the active cooler. These new performance enhancements would offer a competitive advantage to the company offering them in their exploration tools.

The next step towards developing a downhole cooler should improve on the existing design. Section 11.3 describes the recommended improvements by subsystem for the next prototype.

11.2: Goals Versus Results

Table 11.1 lists the design and operation constraints versus the results of the active cooler prototype.

Table 11.1: Design and Operation Constraints vs. Results

Parameter	Constraint Value	Prototype Result	Comment
Borehole Pressures	1.01×10^5 - 1.38×10^8 Pa	Not Accounted for in Uphole Prototype (See Chapter 9)	Next Prototype
Borehole Temperature	200°C	Successfully Tested to 200 °C in an Oven	Success
Film Coefficient of Borehole - function(Tool Speed, Borehole Fluids, Wellbore Diameters)	$100 W/m^2$-°C	Successfully Tested in an Oven with a Film Coefficient equal to $34 W/m^2$-°C	Success
Vibrations and Shocks	(see Chapter 2)	Not Tested, however, no new downhole components used in design.	Attainable
Power	250W-500W	30W required for 30W cooling load COP~1	Success
Diameter	0.0921m	0.0921m	Success
Weight and Length	Minimized	Length = 2.44m w/o Flask Weight < 50kg w/o Flask	Success
Electronics Temperature	< 125°C	114°C for 30W cooling load 122°C for 50W cooling load	Success
Total Refrigeration Load	~80W	30W	Next Prototype
Conduction through Flask	~30W	~1W	--
Electronic Heat Generated	50W	30W	Next Prototype
Downhole Residence Time	10 hours	5 hours available for Horizontal Tests, easily increased. Longest tests ~2 hours	Attainable
Complexity	Minimized	Simple Design and Operation	Success
Maintenance	Minimized	Low	Success
Unit Price	~$10,000	Prototype Parts ~$7000 Downhole Motor~$5000	Slightly Over

All of the environmental constraints for the cooler were met or considered feasible. For cost reasons, the uphole prototype design did not account for the high pressures of the downhole environment (see Chapter 9). However, a high pressure design would offer no new feasibility or design challenges. The 200°C temperature specification was successfully met in the prototype, as well as the heat transfer coefficient specification required by a downhole fluid environment. Although the prototype was not tested for downhole vibrations and shocks, the current design contains no assemblies or parts that are not already being used in downhole wireline tools (e.g., pumps, motors, valves, etc.). Thus, the shocks and vibrations should not represent a limiting constraint.

The majority of the performance and design constraints were also met by the prototype. The input power required for the cooling loads fell well below the threshold originally put forth. Furthermore, if one assumes a conservative COP of one, the 80-W cooling load would require and 80-W input power. The diameter constraints were successfully met with the exception of the motor assembly. Downhole motors at the required size do exist, but the cost and lead times associated with obtaining one did not fit into the schedule of this investigation. Weight and length were kept to a minimum at approximately 50kg and 2.5m respectively. The cold heat exchanger successfully rejected heats loads up to 50W in a 200°C oven from the electronics with their temperatures remaining below 125°C. Due to a compressor volumetric efficiency of approximately 50%, however, the prototype was only able to carry a total heat load from the electronics of 30W instead of the design goal of 50W. In the horizontal tests, the cooling time for an 80-W total heat load at 200°C was approximately 5 hours. The longest feasibility tests lasted approximately 2 hours. However, to increase downhole residence time the designer would simply have to increase the length of the lower tank. The design complexity was minimized resulting in a very simple design and operation procedure. The user only needed to empty the upper tank, and fill both the lower tank and lubricant reservoir before testing. Maintenance was also minimized. The entire system was tested for a total period of over 24 hours at high temperature in which none of the pieces were replaced except the piston/cylinder assembly. The costs of the prototype approximately met the goal stated in Chapter 2.

11.3: Detailed Recommendations by Subsystem

Before an actual downhole cooler can be used in a Schlumberger wireline tool, several issues must addressed. The next generation prototype should be a full-scale, pressure-compatible, self-contained and controlled version, capable of at least ten hours of downhole residence time. The following sections describe the major issues and recommendations for future work on downhole active cooler.

11.3.1: Cold Heat Exchanger/Lower Tank Assembly

Heat pipes represent the optimal method of heat transfer in a downhole tool, but the current cold heat exchanger design should be further optimized. To decrease surface contact resistance to heat transfer, either the electronics, lower tank, or both assemblies should be directly potted to their heat pipes. Silver soldering is a technique that has proved successful in other downhole designs. The geometry of the heat pipes should also be experimented with to find the optimal configuration. In practice, for instance, the active cooling system would have to be modular enough to accommodate different chassis lengths for different tools. Thus, it would be necessary to design the chassis conductive enough so that the heat pipes of the lower tank could be joined to it and transfer the heat load. A chassis made of aluminum with internal heat pipes will most likely be the optimal solution. The mating between lower tank heat pipes and chassis heat pipes could occur via a high thermally conductive fluid encased joint (see Figure 11.1).

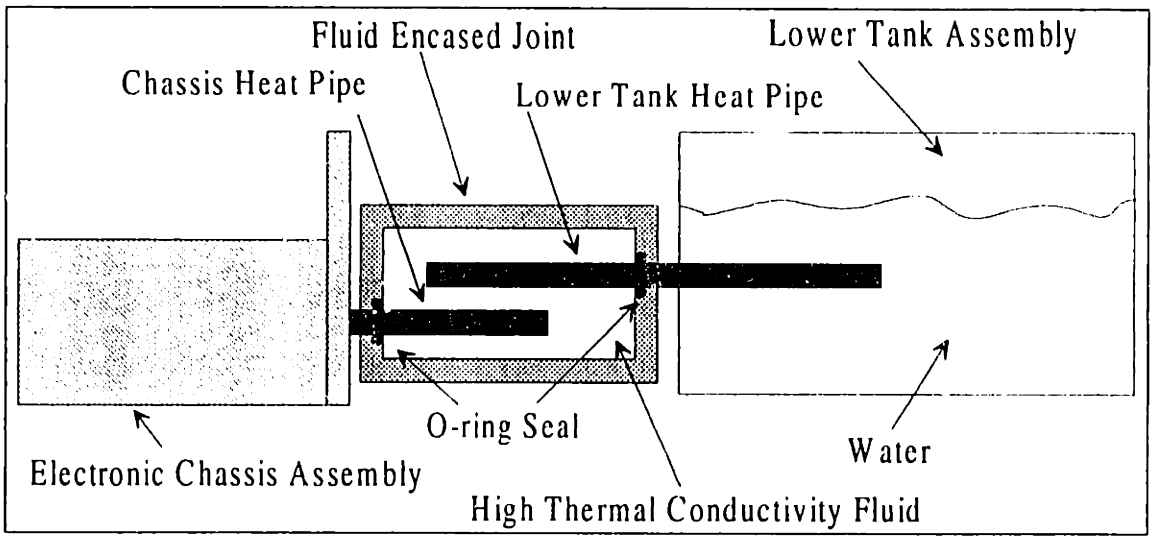

Figure 11.1: High Thermal Conductivity Heat Pipe Joint

The lower tank must also be modified for use in an actual tool. In practice, both power and data paths must run throughout the length of the flask. Therefore, it would be necessary to design wire feed-throughs along or through the length of the lower tank. The feed-throughs would connect the electronics within the flask to their power source or to the components and sensors that they are controlling.

11.3.2: Hot Heat Exchanger/Upper Tank Assembly

Like the lower tank assembly, the upper tank assembly must also pass power and data throughout its length. Wire feed-throughs would have to be designed along the outside of the upper tank assembly. Therefore, the upper tank cannot fill the entire cross-section of the tool.

The hot heat exchanger assembly used in this investigation could be improved significantly. The surface area should be maximized to increase conductivity to the borehole. However, traditional refrigeration fin heat exchangers would be plugged by borehole muds and cannot be used. A heat exchanger design shown in Figure 11.2 would be a much more effective design. Calculations for this type of system are detailed in Appendix E. From the outlet of the compressor, the super-heated steam should be forced through small diameter tubing that is exposed to the borehole fluid. Order-of-magnitude calculations produce lengths of approximately 1m-2m for heat exchangers of this type when conducting the heat load from the cooler to the borehole (see Appendix E). The volume of the upper tank should only be sized to accommodate the volume of saturated water from the lower tank at the hot borehole temperature.

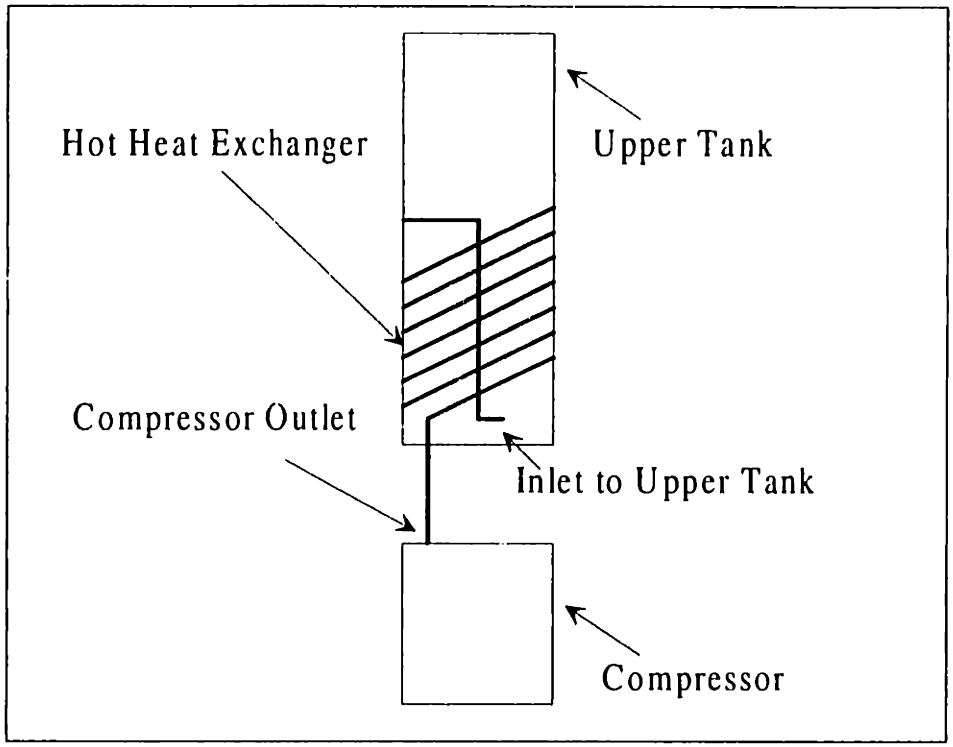

Figure 11.2: Recommended Hot Heat Exchanger Schematic

11.3.3: Lubrication Assembly

The lubrication assembly would also have to be modified. The lubricant should contain properties conducive for steam service, in addition to the viscosities mandated by the piston/cylinder seal. In other words, properties such as rust inhibitors and water absorption that are commonly found in steam cylinder oils should be mixed into the lubricant for the system. Dow Corning-200, 500cSt silicone oil was used where Mobil steam cylinder oils failed only because of its high viscosity of 50cSt at 200°C. The optimal lubricant would be a higher viscosity steam cylinder oil. The springs used in the lubricant assembly displayed linear force displacement curves. This resulted in lubricant reservoir pressures changing as the volume of the lubricant changed. Pressure had to periodically be adjusted by the user by adding more lubricant. A constant pressure reservoir could be attained by either custom-made constant force springs or a screw-drive system. The constant force springs would need a stroke that could accommodate the lubricant volume required for a specified downhole residence time. The screw-drive system could maintain a constant piston force on the lubricant with the use of a pressure feedback/motor system (see Figure 11.3).

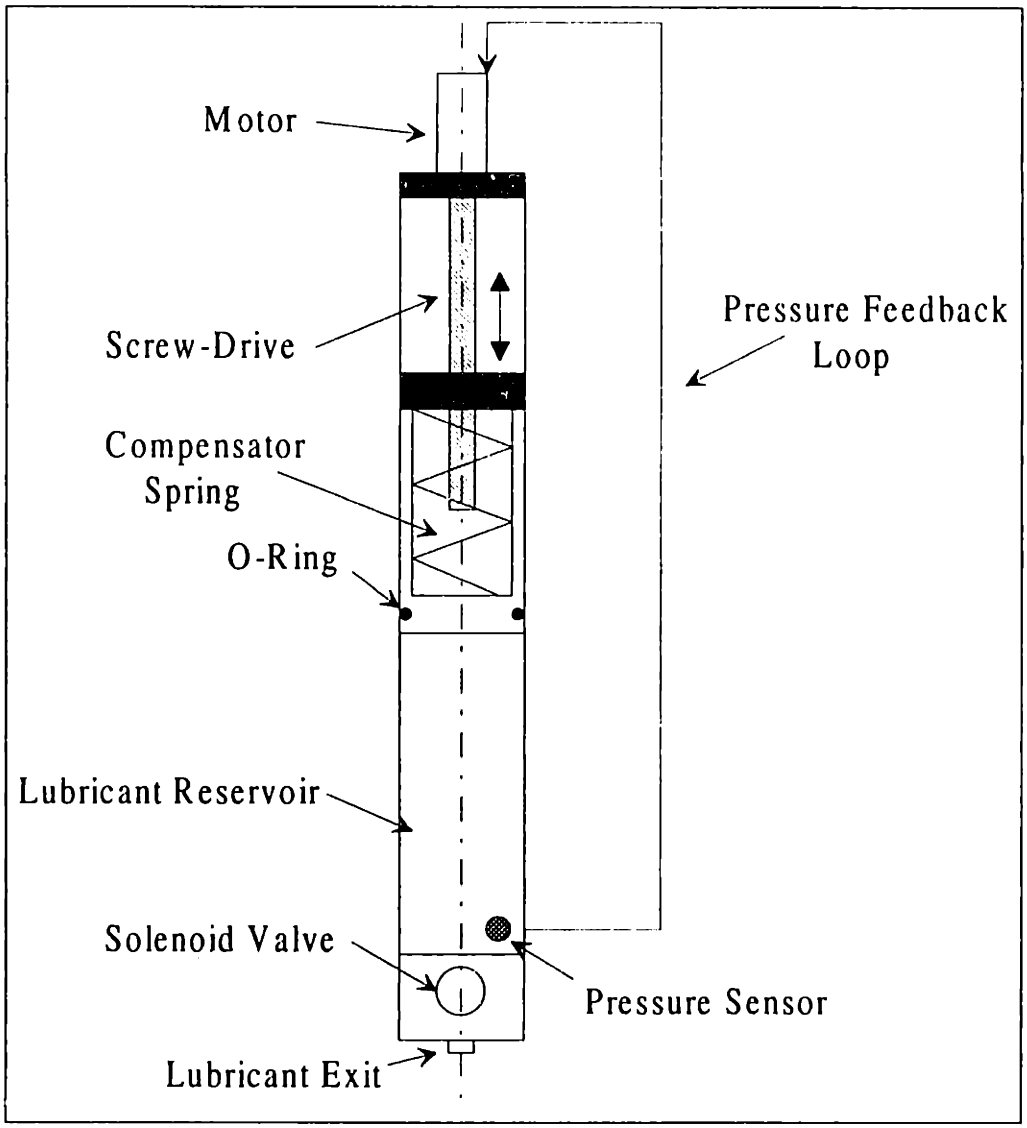

Figure 11.3: Screw-Drive Lubrication System

11.3.4: Compressor

Volumetric efficiency of the compressor must be increased. This would be accomplished by decreasing the dead volume in the compression chamber. The majority of the dead volume exists in the discharge valve and the filter. Historically, the Lee Company has been quite responsive to modifying standard designs for custom applications. With this in mind, the investigator would recommend combining the filter inside the miniature valve and decreasing any extra internal valve volume.

The crankcase of the compressor should also be slightly modified. The bearings used around the shaft should be the self-sealed type. Thus, the bearings would not have to

rely on "blow-by" lubrication from the compression chamber. Likewise, the "blow-by" behavior and flowrate should be characterized as a function of time at worst-case loading conditions and tool position. The crankcase volume would then have to be sized equal to the volume of "blow-by" lubricant for a specified downhole residence time. This would avoid the crankcase volume filling with lubricant and seizing.

The outer surface area of the compressor should also be increased to allow more conduction to the borehole and lower temperature operation. In this investigation, the temperature outside the valve head piece of the compressor measured approximately 225°C. This temperature could be significantly reduced by the above method. The reduction in temperature would provide an environment more conducive to longer seal lives throughout the compressor.

Different compression chamber seals should be examined. Although the lapped piston/cylinder seal proved adequate for the feasibility studies, experiments comparing lapped to piston ring seals as a function of frictional losses, wear, cost, and operating life should be executed. Different piston ring materials should also be tested as a function of the above criteria. Piston rings made of chrome or cast iron may provide a good starting point. For piston ring designs, however, the intake porting in the cylinder must be rectangular not rounded as used in the present study.

The apparent flowrate limit in the 1250rpm-2000 rpm shaft speed range of the compressor must also be further investigated. The investigator believes the intake porting between the flow inlet and the compression chamber may be sized too small. Thus, fluid restrictions, given a set pressure gradient created by the compression chamber vacuum, are not allowing lubricant and steam to flow faster than $2.23 \times 10^{-5} m^3/s$. Increasing the cross-sectional areas of the porting passages should be attempted, as the first possible solution.

Once the flowrate limit is solved, the compressor size should be further miniaturized. The decrease in volume flowrate per stroke could be countered by running the compressor at faster shaft speeds. The miniaturization of the compressor would facilitate packaging in a variety of other oil-exploration tools including the MWD and LWD types.

11.3.5: Motor

A downhole compatible motor should be purchased and incorporated into the downhole design. The motor must be efficient enough at downhole temperature and compressor loads so as not to exceed the available 200-W power limit. This translates to at least a 40% efficient motor assuming a total cooling load of 80W and a cooler COP of one. The Astro Instrument Corporation is one reliable source for downhole motors with efficiencies up to 80% at downhole temperature (see Appendix L).

11.3.6: Control Circuitry

The control circuitry must also be designed and built for the downhole cooler. If the behavior of the system was well established, only a lower tank pressure or temperature sensor feedback control system with the motor drive of the compressor would be required. A sensitive pressure gage located in the lower tank could be linked to the compressor drive system. The shaft speed would be increased or decreased to maintain the pressure in the lower tank within a bandwidth around the atmospheric value of 1.01×10^5Pa. Downhole pressure gages with accuracies of +/-3500Pa are commonplace in the oil-exploration industry and do not represent a design challenge. The system may also be controlled with the temperature reading of the fluid in the lower tank. The least expensive, working alternative should be utilized in the final design.

Appendices

Appendix A: Dewar Flask Analysis

A.1 Temperature Rise of Dewar / Tool System (w/ Electronic Heat Generation)

When placed into a hot wellbore, heat is conducted into the electronic chassis through the walls of the Dewar flask causing its internal temperature to rise. For an upper-bound estimate, the environment surrounding the flask is assumed to be at 200°C. To create a worst-case-scenario, the temperature at the exterior wall, T_H, is taken to be 200°C. In the actual system the skin temperature would be less than or equal to 200°C as a function of convection interactions between the outer surface of the flask, borehole fluid, and tool speed. For this analysis, the tool internals and inner housing were assumed to be a lumped mass at the same temperature. The end effects are also neglected and the flask and its internals are assumed to be homogeneous throughout their length. In Chapter 3, Figure 3.2 displays the dimensioning scheme of the flask, and Table 3.1 gives its the size and properties.

Initially at time, t, equal to 0 sec., the temperature of the interior of the flask and the inner housing was assumed to be at the same temperature T_i equal to 25°C. At $t > 0$ sec., the temperature of the interior and the housing increases. The internal energy, E , of the lumped mass is given by

$$mc_pT = E, \qquad \text{(A-1)}$$

where m is the mass, c_p is the specific heat, and T is the instantaneous temperature. Differentiating eq.(A-1) with respect to time gives

$$mc_p \frac{dT}{dt} = \frac{dE}{dt}, \qquad \text{(A-2)}$$

where

$$\frac{dE}{dt} = Q. \qquad \text{(A-3)}$$

The quantity Q is the energy, E, per unit time or heat flux transferred into the lumped mass through the flask's walls and electronic heat, Q_{gen}, and is given by

$$Q = \frac{T_H - T}{\sum R} + Q_{gen}, \qquad \text{(A-4)}$$

where $\sum R$ is the sum of the effective thermal resistance of the layers of steel and insulation surrounding the housing and interior.

Therefore,

$$mc_p \frac{dT}{dt} = \frac{T_H - T}{\sum R} + Q_{gen}. \qquad \text{(A-5)}$$

For a cylindrical object, the effective resistance is

$$R_{eff} = \frac{\ln\left(\frac{r_{out}}{r_{in}}\right)}{2\pi\, k L}, \qquad \text{(A-6)}$$

where r_{out} and r_{in} are the external and internal radii, respectively, k is the thermal conductivity of the material, and L is the length of the section of interest (Inropera, 1990, p.98). The thermal resistances for the steel and insulation are given by

$$R_{st} = \frac{\ln\left(\frac{r_4}{r_3}\right)}{2\pi\, k_{st} L} \qquad \text{and} \qquad R_{ins} = \frac{\ln\left(\frac{r_3}{r_2}\right)}{2\pi\, k_{ins} L}. \qquad \text{(A-7)}$$

The total effective resistance is found by combining the two expressions in eq.(A-7):

$$\sum R = R_{st} + R_{ins}. \qquad \text{(A-8)}$$

Knowing Q_{gen} is positive and the intial temperature of the lumped mass, eq.(A-5) produces a positive heat transfer rate. The value $\frac{dT}{dt}$ is therefore positive, indicating that the flask internals are being heated. Introducing

$$\Theta = T_H - T + Q_{gen} \sum R \qquad \text{(A-9)}$$

where

$$\frac{d\Theta}{dt} = -\frac{dT}{dt} \qquad \text{(A-10)}$$

and substituting eq.(A-9) and eq.(A-10) into eq.(A-5) and rearranging yields

$$\frac{d\Theta}{\Theta} = -\frac{1}{mc_p \sum R} dt \quad . \qquad \text{(A-11)}$$

Integrating eq.(A-11) from the initial conditions at which T = T_i and t = 0, to some later time gives

$$\ln\left(\frac{\Theta}{\Theta_i}\right) = -\frac{t}{mc_p \sum R} \quad . \qquad \text{(A-12)}$$

Eq. (A-12) can then be rearranged to equal

$$\frac{\Theta}{\Theta_i} = e^{-\frac{t}{mc_p \sum R}} . \qquad \text{(A-13)}$$

Using the relationship

$$m = \rho V , \qquad \text{(A-14)}$$

where ρ is density and V is volume, it is assumed the flask internals (electronics, etc.) and the its inner steel housing are a lumped mass where the product mc_p is the effective internal energy equal to

$$mc_p = \left(\rho\, Vc_p\right)_{int} + \left(\rho\, Vc_p\right)_{in.hous} . \qquad \text{(A-15)}$$

Combining the above equations yields an explicit formula for the internal temperature of the flask as a function of time of

$$T(t) = \left(T_i - T_H - q_{gen} \sum R\right) e^{-\frac{t}{\left[\left(\rho\, Vc_p\right)_{int} + \left(\rho\, Vc_p\right)_{in.hous}\right] \sum R}} + T_H + Q_{gen} \sum R . \qquad \text{(A-16)}$$

Appendix B: Bingham Plastic Flow Analysis:

(Reprinted with Permission of Dr. Julian Pop of Schlumberger Wireline Services)
(Pop, 1982)

Model Schematic and Assumptions:

Consider the steady, laminar flow of an incompressible Bingham Fluid between concentric cylinders where the inner cylinder moves with a constant velocity, V_t relative to a stationary outer cylinder (wellbore) of radius r_H (see Figure B.1).

The velocity profile of the fluid is assumed to have the form

$$v_r = 0,\ v_\theta = 0,\ v_z = v(r) \qquad \text{(B-1)}$$

With respect to a staitonary cylindrical polar coordinate system the z-axis of which coincides with the axis of the moving cylinder. Oldroyd has extended the simple definition of Bingham materials given above to the 3 -D case (Oldroyd, 1947) (see also Fredrickson, 1958). If $\underset{\sim}{T}$, denotes the stress tensor, and $\underset{\sim}{S}$ the extra stress tensor then

$$\underset{\sim}{S} = \underset{\sim}{T} + p\underset{\sim}{1} = (\mu + \frac{\tau_o}{\sqrt{II}})\underset{\sim}{A} \text{ if } tr(\underset{\sim}{S}^2) > \tau_o \qquad \text{(B-2)}$$

and

$$\underset{\sim}{A} = 0 \text{ if } tr(\underset{\sim}{S}^2) \le \tau_o^2 \qquad \text{(B-3)}$$

where p is the fluid pressure,

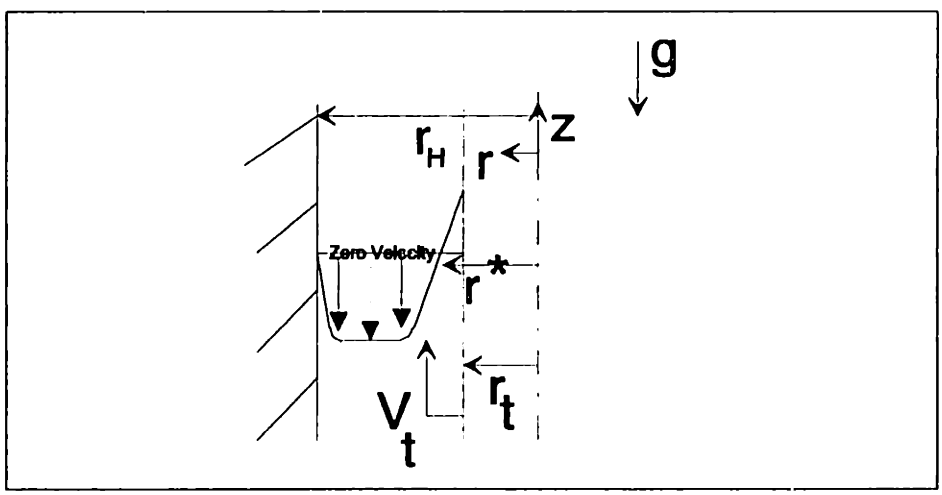

Figure B.1

$$\underset{\sim}{A} = grad\, \underset{\sim}{v} + grad^T\, \underset{\sim}{v} \qquad \text{(B-4)}$$

is twice the symmetric part of the velocity gradient, $\underset{\sim}{v}$ is the velocity of a fluid particle,

$$II = .5\ \mathrm{tr}(\underset{\sim}{A}^2), \qquad \text{(B-5)}$$

and

$$\mathrm{tr}(\underset{\sim}{A}) = \sum_{i=1}^{3} A_{ii}. \qquad \text{(B-6)}$$

Using the above velocity profile we see that

$$\mathrm{tr}\left(\underset{\sim}{A}^2\right) = \left(\frac{dv}{dr}(r)\right)^2 = \left(v'(r)\right)^2. \qquad \text{(B-7)}$$

The stress tensors then become

$$T<rr> = T<\theta\theta> = T<zz> = -P$$

$$T<rz> = \mu\, v'(r) + Y\, \mathrm{sgn}(v'(r)) \text{ if } T^2 <rz> \ > \ \tau_o^{\,2} \qquad \text{(B-8)}$$

$$T<rz> \leq \tau_o \text{ if } \quad v'(r) = 0,$$

where

$$\mathrm{sgn}(x) = \begin{cases} 1 \text{ if } x > 0 \\ 0 \text{ if } x = 0 \\ -1 \text{ if } x < 0 \end{cases}. \qquad \text{(B-9)}$$

Since $\underset{\sim}{v}$ has the form $\underset{\sim}{v} = v(r)\underset{\sim}{e}_3$ where $\underset{\sim}{e}_3$ is the unit vector in the z-direction, for any constitutive equation of the form

$$\underset{\sim}{T} = -p\,\underset{\sim}{1} + f(\underset{\sim}{A})\,\underset{\sim}{A}, \qquad \text{(B-10)}$$

the non-trivial equations of motion reduce to

$$p = p(z). \qquad \text{(B-11)}$$

In other words, pressure is a function of z only. Thus,

$$\frac{1}{r}\frac{d}{dr}(rT<rz>)-\frac{dp}{dz}-\rho g=0 \qquad \text{(B-12)}$$

If one lets the potential φ be defined by

$$\varphi(z) = p(z) + \rho g z, \qquad \text{(B-13)}$$

then (B-12) becomes

$$\frac{1}{r}\frac{d}{dr}(rT<rz>)=\frac{d\varphi}{dz}=const. \qquad \text{(B-14)}$$

since T<rz> is a function of r alone and φ is a function of z alone. Thus a first integrand of the equation of motion can can be written as

$$rT<rz>=\frac{r^2}{2}\frac{d\varphi}{dz}+\bar{\alpha} \qquad \text{(B-15)}$$

where $\bar{\alpha}$ is a constant of integration.

Boundary Conditions

The obvious boundary conditions to be utilized in this analysis are

$$v(r_o) = 0 \qquad \text{(B-16)}$$

and

$$v(r_i) = V_i. \qquad \text{(B-17)}$$

However, since we assume the total volume flux in the annulus equal to that displace by the tool, there must exist an r (say r=r*) such that

$$r_i < r^* < r_H \qquad \text{(B-18)}$$

and

$$v(r^*) = 0. \qquad \text{(B-19)}$$

Moreover, from the continuity of T<rz>, for some

$$r_i > r^{**} > r^*, \qquad \text{(B-20)}$$

$$T<rz>(r^{**}) = 0. \qquad \text{(B-21)}$$

Consequently, (B-15) can be written in the form

$$T < rz > (r) = \frac{1}{2}\frac{d\varphi}{dz}\left(r - \frac{r**^2}{r}\right). \qquad \text{(B-22)}$$

The following non-dimensional parameters will be introduced:

$$\xi = \frac{r}{r_H}, \qquad \text{(B-23)}$$

$$\xi* = \frac{r*}{r_H} \qquad \text{(B-24)}$$

$$\alpha^2 = \frac{r**^2}{r_H^2} \qquad \text{(B-25)}$$

$$\tau = \frac{T < rz >}{\tau_o}, \qquad \text{(B-26)}$$

$$H = \frac{r_H \dfrac{d\varphi}{dz}}{2\tau_o}, \qquad \text{(B-27)}$$

$$\upsilon = \frac{\mu\nu}{r_H\tau_o}, \qquad \text{(B-28)}$$

and,

$$k = \frac{r_i}{r_H}. \qquad \text{(B-29)}$$

Then (B-22) can be written as

$$\tau = H\left(\frac{\xi^2 - \alpha^2}{\xi}\right) \qquad \text{(B-30)}$$

and for the Bingham fluid

$$\nu' + \mathrm{sgn}(\nu') = H\left(\xi - \frac{\alpha^2}{\xi}\right) \qquad \text{(B-31)}$$

if

$$\tau^2 > 1, \tag{B-32}$$

and

$$v' = 0 \tag{B-33}$$

if

$$\tau^2 \leq 1. \tag{B-34}$$

To determine the values of ξ (and alternatively r) for which the fluid is in plug flow, we seek the roots of the equation

$$H^2\left(\frac{\xi^2 - \alpha^2}{\xi}\right)^2 = 1, \tag{B-35}$$

ie.

$$\xi^4 - \left(2\alpha^2 + \frac{1}{H^2}\right)\xi^2 + \alpha^4 = 0. \tag{B-36}$$

Since (B-36) is a quadratic in ξ^2, its roots have the form

$$(\xi_+, \xi_-, -\xi_-, -\xi_+), \ \xi_+ \geq \xi_- > 0 \tag{B-37}$$

provided that they exist. We are interested in those roots such that

$$0 < k \leq \xi_- \leq \xi_+ \leq 1 \tag{B-38}$$

since negative values of ξ are incompatible with both the geometric configuration of the problem and the requirement that the velocity change sign at some radial position r*.

From (B-36) it follows that

$$\xi_+^2 + \xi_-^2 = 2\alpha^2 + \frac{1}{H^2}, \tag{B-39}$$

and

$$\xi_+^2 \xi_-^2 = \alpha^4. \tag{B-40}$$

Likewise,

$$\xi_+ - \xi_- = \frac{1}{H} \tag{B-41}$$

and

$$\xi_+ \xi_- = \alpha^2 \quad . \tag{B-42}$$

The interpretation of ξ_+ and ξ_- is shown schematically in Figure B.2.

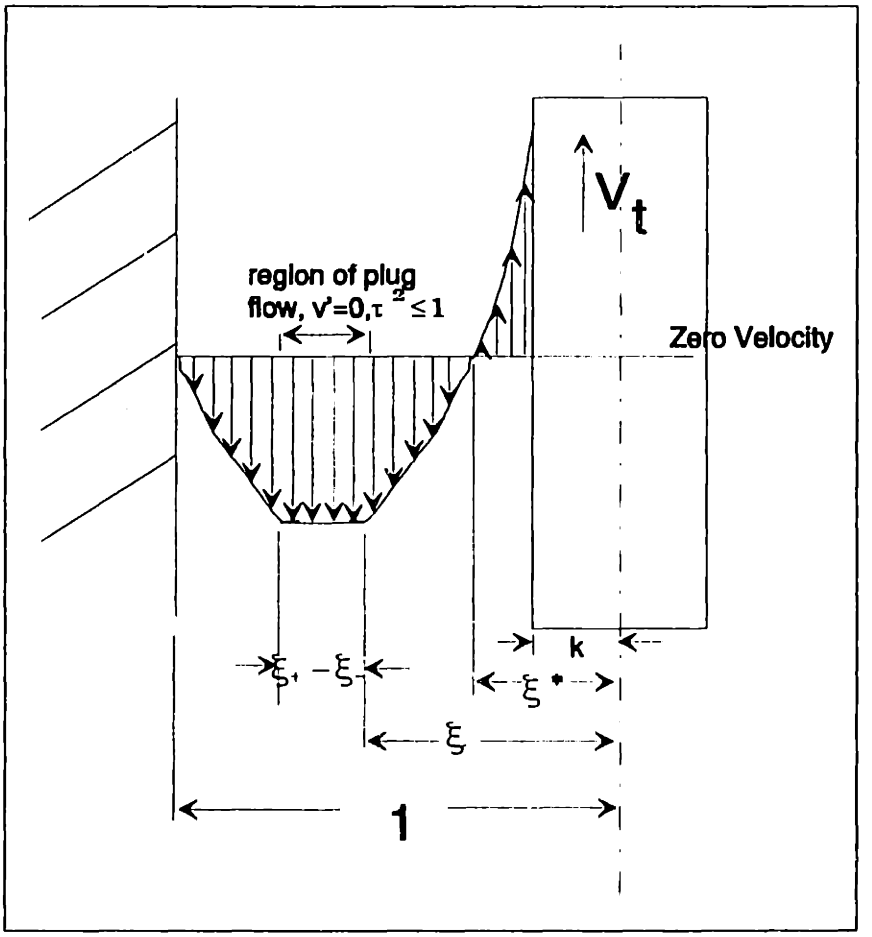

Figure B.2: Nondimensional Schematic

Determination of Velocity Profile

In the region $k \le \xi \le \xi_-$,

$$\nu' - 1 = H\left(\xi - \frac{\alpha^2}{\xi}\right). \qquad \text{(B-43)}$$

On integrating we obtain

$$\nu(\xi) - \xi = \frac{H}{2}\xi^2 - H\alpha^2 \ln(\xi) + a. \qquad \text{(B-44)}$$

Using the first boundary condition and defining

$$W = \nu(k) = \frac{\mu V_t}{r_H \tau_w}, \qquad \text{(B-45)}$$

an expression for the constant of integration can be found as

$$a = W - k - \frac{H}{2}k^2 + H\alpha^2 \ln(k). \qquad \text{(B-46)}$$

Substituting this expression into that for $\nu(\xi)$ gives

$$\nu(\xi) = W + (\xi - k) + \frac{H}{2}(\xi^2 - k^2) - H\alpha^2 \ln\left(\frac{\xi}{k}\right). \qquad \text{(B-47)}$$

Since $\nu(\xi^*)=0$, (B-47) can be used to solve for ξ^* once H has been specified.

In the region $1 \ge \xi \ge \xi_+$,

$$\nu' + 1 = H\left(\xi - \frac{\alpha^2}{\xi}\right) \qquad \text{(B-48)}$$

from which it follows that

$$\nu(\xi) + \xi = \frac{H}{2}\xi^2 - H\alpha^2 \ln(\xi) + b \qquad \text{(B-49)}$$

where b is a constant of integration. The boundary condition at the wall can be used to solve for b given as

$$b = 1 - \frac{H}{2}, \qquad \text{(B-50)}$$

and therefore for $1 \ge \xi \ge \xi_+$,

$$v(\xi) = (1-\xi) - \frac{H}{2}(1-\xi^2) - H\alpha^2 \ln(\xi). \qquad \text{(B-51)}$$

In particular,

$$v(\xi_-) = W + (\xi_- - k) + \frac{H}{2}(\xi_-^2 - k^2) - H\alpha^2 \ln\left(\frac{\xi_-}{k}\right) \qquad \text{(B-52)}$$

and

$$v(\xi_+) = (1-\xi_+) - \frac{H}{2}(1-\xi_+^2) - H\alpha^2 \ln(\xi_+). \qquad \text{(B-53)}$$

But, by the continuity of the velocity profile

$$v(\xi_-) = v(\xi_+) \qquad \text{(B-54)}$$

or

$$v(\xi_+) - v(\xi_-) = 0 \qquad \text{(B-55)}$$

which yields

$$W - 1 + (\xi_+ - \xi_-) - k + \frac{H}{2}(1-k^2) + \frac{H}{2}(\xi_-^2 - \xi_+^2) - H\alpha^2 \ln\left(\frac{\xi_-}{\xi_+ k}\right) = 0. \qquad \text{(B-56)}$$

By the use of (B-41) and (B-42), ξ_- and α_2 can be eliminated in (B-56) to yield an expression relating H and ξ_+:

$$W - 1 - k + \left(2\xi_+ - \frac{1}{H}\right) + \frac{H}{2}(1-k^2) + \frac{H}{2}\left\{\left(\xi_+ - \frac{1}{H}\right)^2 - \xi_+^2\right\} -$$
$$H\xi_+\left(\xi_+ - \frac{1}{H}\right)\ln\left(\frac{\xi_+ - \frac{1}{H}}{\xi_+ k}\right) = 0 \qquad \text{(B-57)}$$

Following the convention of Fredrickson and Bird (1947) we define

$$T = \frac{1}{H} \qquad \text{(B-58)}$$

and rewrite (B-57) as

$$2WT = (T+k)^2 - 1 + 2T(1-\xi_+) + 2\xi_+(\xi_+ - T)\ln\left(\frac{\xi_+ - T}{\xi_+ k}\right). \qquad \text{(B-59)}$$

Equation (B-59) represents one equation for the determination of T and ξ_+. Another relation between T and ξ_+ can be obtained by considering the resultant volumetric discharge through any annular cross-section.

Flow Rate Condition:

The rate of fluid flow across any section of the annulus is given by

$$\varphi = 2\pi \int_{r_t}^{r_H} v(r) r dr \qquad \text{(B-60)}$$

i.e.

$$\varphi = 2\pi r_H^2 \int_{r_t}^{r_H} v(r)\left(\frac{r}{r_H}\right) d\left(\frac{r}{r_H}\right) \qquad \text{(B-61)}$$

which can be further simplified to

$$\varphi = \left(\frac{2\pi r_H^3 \tau_o}{\mu}\right) \int_k^1 v(\xi)\xi \, d\xi. \qquad \text{(B-62)}$$

The integral in (A4-62) can be written as

$$\int_k^1 v(\xi)\xi \, d\xi = \int_k^{\xi_-} v(\xi)\xi \, d\xi + \frac{v(\xi_+)}{2}(\xi_+^2 - \xi_-^2) + \int_{\xi_+}^1 v(\xi)\xi \, d\xi. \qquad \text{(B-63)}$$

On substituting the appropriate expressions for $v(\xi)$ in (B-63), carrying out the indicated integrations and using the equations for $v(\xi_-)$ and $v(\xi_+)$ together with (B-41), (B-42), and (B-59), we find after considerable algebra that

$$\varphi = \frac{\pi r_H^4 \frac{d\varphi}{dz}}{8\mu}\left\{4TWk^2 - 2(\xi_+ - T)\xi_+(1-k^2) - \frac{4}{3}T(1+k^3) + (1-k^4) + (2\xi_+ - T^3)\frac{T}{3}\right\} \qquad \text{(B-64)}$$

The lifting of the tool causes a volumetric flux in the annulus equal to

$$\varphi = -\pi r_t^2 V_t \ . \qquad \text{(B-65)}$$

Using (B-64) and (B-65) a second relation between T and ξ_+ is given by

$$\frac{T}{3}(2\xi_+ - T)^3 - \frac{4}{3}T(1+k^3) + 1 - k^4 - 2(\xi_+ - T)\xi_+(1-k^2) = 0. \qquad \text{(B-66)}$$

To complete the solution of the original problem there remains only to solve (B-59) and (B-66) for T and ξ_+ once W and k have been specified.

Concerning the range of values that the parameters k, ξ_+, and T can take on, clearly

$$0 < k \le \xi_- \le \xi_+ < 1. \qquad \text{(B-67)}$$

It follows from (A4-41) that

$$T \le 1\text{-}k. \qquad \text{(B-68)}$$

Solutions of Equations (B-59) and (B-66): Work Curves

Equations (B-59) and (B-66) represent a system of two non-linear simultaneous equations for the determination of T and ξ_+ once W and k have been specified. Since the primary objective of this exercise is the determination of the pressure drop (alternatively T), it would be convenient to have a representation of T in terms of the given values of W and k; i.e. eliminate ξ_+. Clearly this is not easily carried out.

The procedure for determining the relationship between T, W, and k used here is very simple:

(I) Choose T and calculate ξ_+ from equation (B-66) for various values of k.

(II) Using the chosen values of T and k and the value of ξ_+ determined in (I), calculate W from (B-59).

In this manner, curves of W versus k for constant values of T were generated. The results are depicted in Figures B.3-B.5.

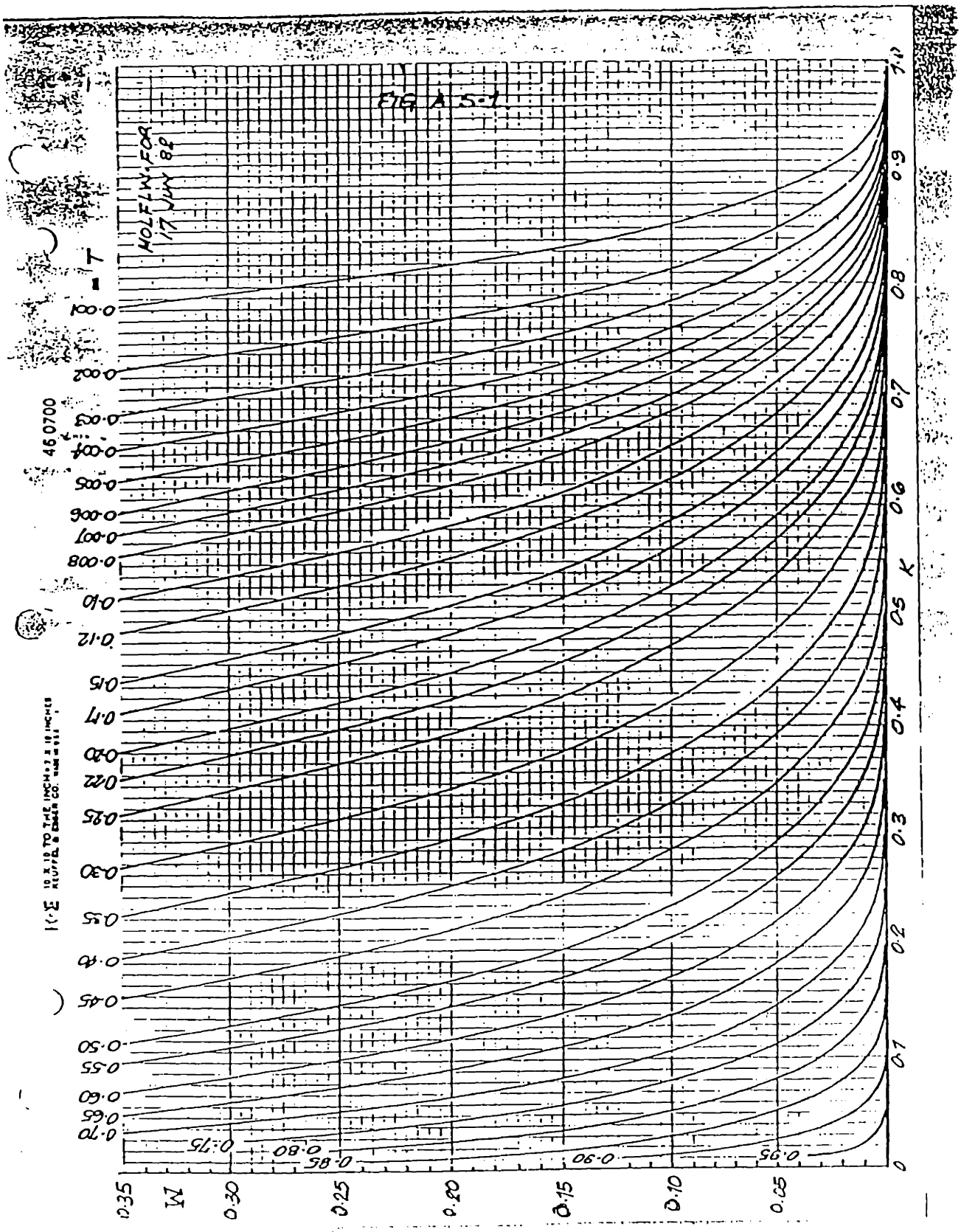

Figure B.3: Work Curves #1

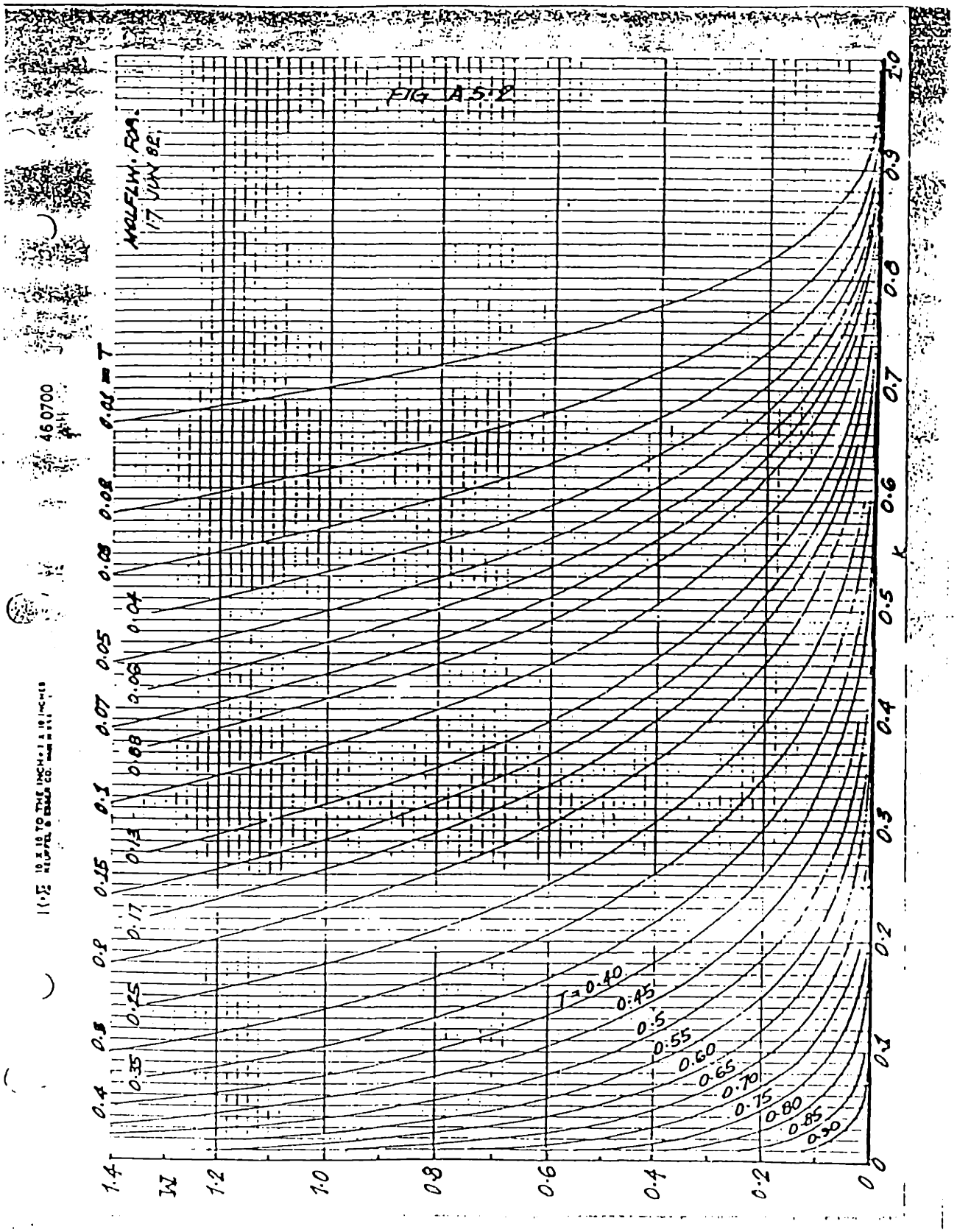

Figure B.4: Work Curves #2

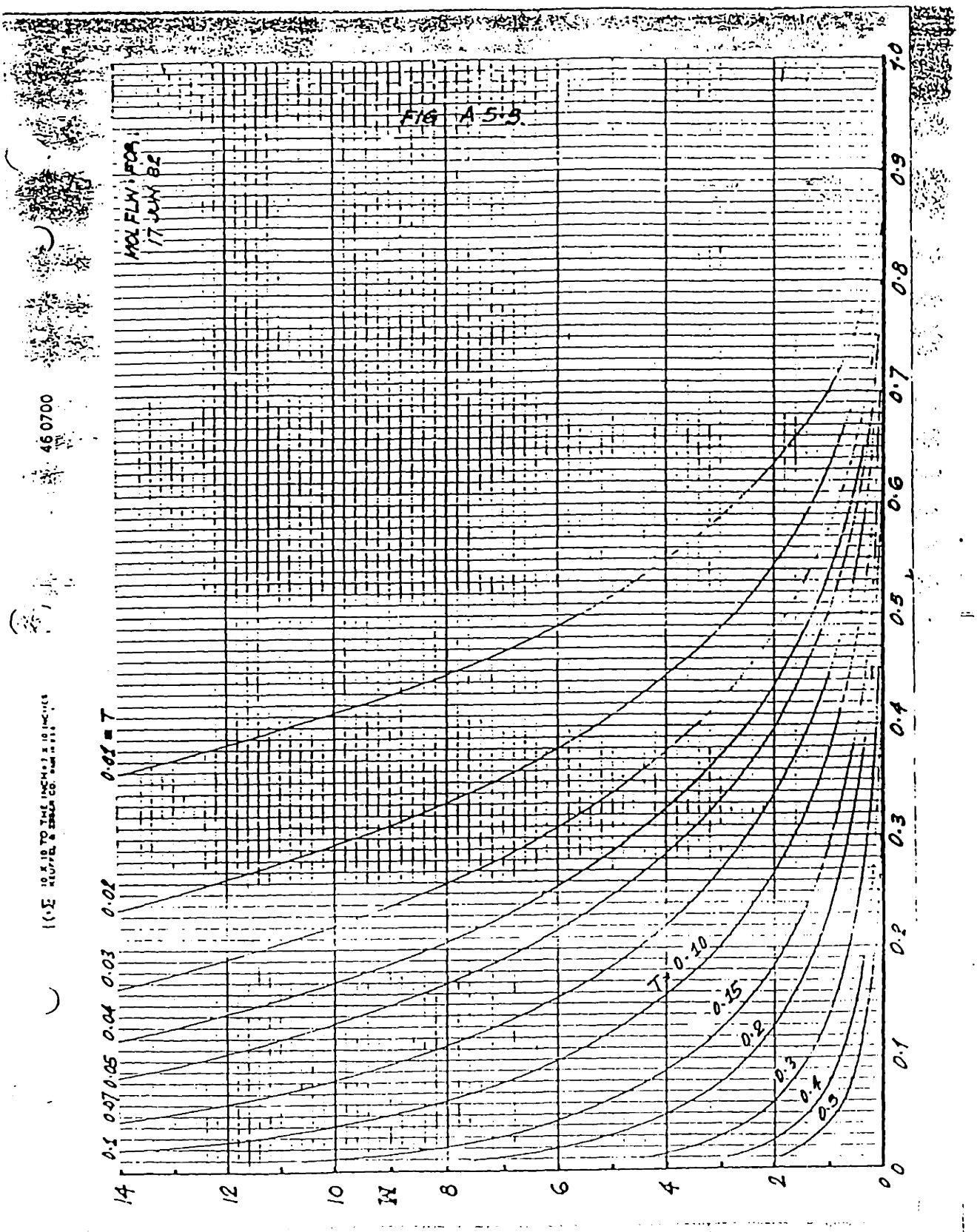

Figure B.5: Work Curves #3

Appendix C: Heat Transfer Analysis

In the following analysis, the overall heat transfer coefficients for the three non-zero flow sections (plug and laminar) between the tool and borehole are developed (see Figure 4.2). The three heat transfer coefficients are then normalized to a total heat transfer coefficient for the outside area of the tool.

Consider a thermal boundary layer δ_T formed between parallel plates with one side heated to a constant wall temperature T_w and moving with a steady velocity V_t and a steady flow of fluid between the plates with velocity profile u(y). The growth of the boundary layer with distance is formulated with an integral approach and the assumptions in Table C.1.

Table C.1: Heat Transfer Analysis Assumptions

a) Fully Developed Velocity Profile
b) Temperature of Fluid outside Boundary Layer equal to T∞
c) Temperature of Tool Wall equal to a constant, T_w from x = 0 to x = L
d) Length of Tool equal to L
e) Thermal Boundary Layer << than gap between plates or r_H-r_t and starts at x = 0.
f) Constant Fluid Properties

Figure C.1 displays the integral thermal boundary layer. Conservation of energy

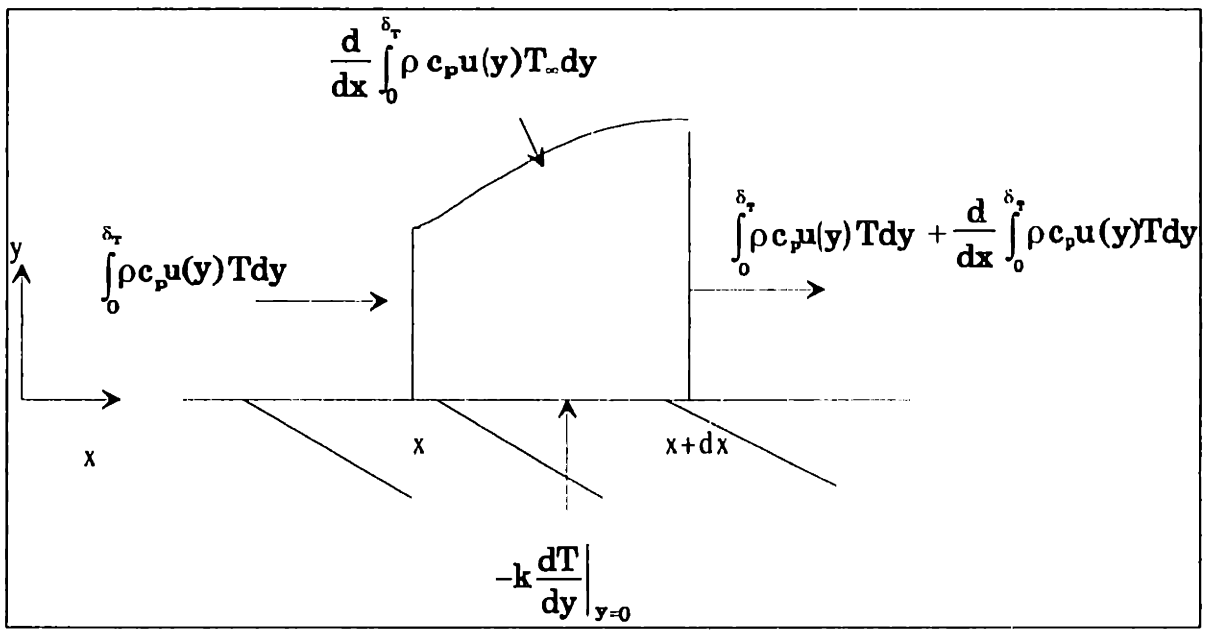

Figure C.1: Thermal Boundary Layer Integral Approach

and mass within a dx length of boundary layer results in

$$\frac{d}{dx}\int_0^{\delta_T} \rho\, u(y)(T_\infty - T)dy = k\frac{dT}{dy}\Big|_{y=0} \quad . \qquad \text{(C-1)}$$

Substituting

$$\theta = \frac{T - T_W}{T_\infty - T_W} \qquad \text{(C-2)}$$

and

$$\eta = \frac{y}{\delta_T} \qquad \text{(C-3)}$$

into eq.(C-1) the following equation gives

$$\rho\, c_p V_t \frac{d\delta_T}{dx}\int_0^1 \frac{u(y)}{V_t}(1-\theta)d\eta = \frac{k}{\delta_T}\frac{d\theta}{d\eta}\Big|_{\eta=0} . \qquad \text{(C-4)}$$

The boundary conditions for eq.(C-4) are written as

$$\theta\ (\eta = 0) = 0,$$

$$\theta\ (\eta = 1) = 1, \qquad \text{(C-5)}$$

and

$$\frac{d\theta}{d\eta}(\eta = 1) = 0.$$

As stated in the assumptions, a linear temperature profile is assumed in the thermal boundary layer causing

$$\theta = \eta, \qquad \text{(C-6)}$$

and

$$\frac{d\theta}{d\eta}\Big|_{\eta=0} = 1 . \qquad \text{(C-7)}$$

Equation (C-4) is then simplified to

$$\rho c_p V_t \frac{d\delta_T}{dx} \int_0^1 \frac{u(y)}{V_t}(1-\eta)d\eta = \frac{k}{\delta_T} \quad . \qquad \text{(C-8)}$$

Plug Flow

In the plug flow analysis, the fluid velocity was found to be a constant. Thus, eq.(C-8) changes to

$$\rho c_p u \frac{d\delta_T}{dx} \int_0^1 (1-\eta)d\eta = \frac{k}{\delta_T} \quad . \qquad \text{(C-9)}$$

Integrating eq.(C-9) and using the definition of thermal diffusivity results in

$$\delta_T d\delta_T = \frac{2\alpha}{u} dx . \qquad \text{(C-10)}$$

Equation (C-10) is then integrated knowing

$$\delta_T(x=0) = 0 \qquad \text{(C-11)}$$

to produce

$$\delta_T = \left(\frac{4\alpha x}{u}\right)^{\frac{1}{2}} . \qquad \text{(C-12)}$$

The heat transfer coefficient with x is derived from

$$h(x) = \frac{-k\left.\frac{dT}{dy}\right|_{y=0}}{T_w - T_\infty} \qquad \text{(C-13)}$$

and can be further simplified to

$$h(x) = \frac{k}{\delta_T} \qquad \text{(C-14)}$$

or

$$h(x) = k\left(\frac{4\alpha x}{u}\right)^{-\frac{1}{2}} . \qquad \text{(C-15)}$$

The overall heat transfer coefficient for a given length is

$$h_L = \frac{1}{L}\int_0^L h(x) \ , \qquad \text{(C-16)}$$

resulting in

$$h_L = \left(\frac{uk^2}{\alpha L}\right)^{\frac{1}{2}} \qquad \text{(C-17)}$$

for the plug flow model where the velocity in terms of the thermal boundary layer reference frame is equal to

$$u = \frac{V_t(2r_H - r_t)}{2(r_H - r_t)}. \qquad \text{(C-18)}$$

Remember, however, that the previous velocity profile was developed for the three non-zero flow sections. Consequently, the overall heat transfer coefficient must be normalized to the exposed outside area of the tool. The new overall heat transfer coefficient for plug flow is expressed as

$$h_{L_{slug}}' = \frac{3}{4}\left(\frac{V_t(2r_H - r_t)}{2(r_H - r_t)}\frac{k^2}{\alpha L}\right)^{\frac{1}{2}}. \qquad \text{(C-18)}$$

Laminar Flow

The velocity profiles for the laminar flow case are not constant and must be accounted for in the integration of eq.(C-8). The velocities of the four sections with respect to a moving tool reference are

$$u_I = 0,$$

$$u_{II\&III} = -\frac{6V_t r_H}{5(r_H - r_t)^3}\left[y^2 - (r_H - r_t)y\right] + \frac{V_t y}{(r_H - r_t)}, \tag{C-19}$$

and

$$u_{IV} = -\frac{6V_t r_H}{5(r_H - r_t)^3}\left[y^2 - 2(r_H - r_t)y\right] + \frac{V_t y}{2(r_H - r_t)}.$$

Letting

$$\delta = r_H - r_t, \tag{C-20}$$

eq.(C-19) becomes

$$u_I = 0,$$

$$u_{II\&III} = -\frac{6V_t r_H}{5\delta^3}\left(y^2 - \delta\, y\right) + \frac{V_t y}{\delta}, \tag{C-21}$$

and

$$u_{IV} = -\frac{6V_t r_H}{5\delta^3}\left(y^2 - 2\delta\, y\right) + \frac{V_t y}{2\delta}.$$

Plugging the $u_{II\&III}$ velocity profiles into eq.(C-8) and going through the same procedures as in the plug flow section produces the following expression relating the thermal boundary layer with x:

$$\left(-\frac{3r_H}{40}\frac{\delta_T}{\delta} + \frac{2r_H}{15} + \frac{2\delta}{18}\right)\frac{\delta_T^3}{\delta^2} = \frac{\alpha}{V_t}x. \tag{C-22}$$

Remembering that the thermal boundary layer is assumed to be much less than r_H and δ, changes eq.(C-22) to

$$\left(\frac{2r_H}{15} + \frac{2\delta}{18}\right)\frac{\delta_T^3}{\delta^2} = \frac{\alpha}{V_t}x \tag{C-23}$$

which is rearranged to

$$\delta_T = \left[\frac{45(r_H - r_t)^2}{(11r_H - 5r_t)}\frac{\alpha}{V_t}\right]^{\frac{1}{3}} x^{\frac{1}{3}}. \qquad \text{(C-24)}$$

The overall heat transfer coefficient is derived for sections II and III with eq.(C-16) and eq.(C-24) as

$$h_{L,II\&III} = \frac{3}{2}k\left[\frac{(11r_H - 5r_t)V_t}{45(r_H - r_t)^2 \alpha L}\right]^{\frac{1}{3}}. \qquad \text{(C-25)}$$

The previous process is used to develop the overall heat transfer coefficient for section IV with the result of

$$h_{L,IV} = \frac{3}{2}k\left[\frac{(29r_H - 5r_t)V_t}{90(r_H - r_t)^2 \alpha L}\right]^{\frac{1}{3}}. \qquad \text{(C-26)}$$

Remember, however, that the previous velocity profile was developed for the three non-zero flow sections. Consequently, the overall heat transfer coefficient must be normalized to the exposed outside area of the tool. The new overall heat transfer coefficient for laminar flow is expressed as

$$h_{L,laminar} = \frac{3}{4}k\left[\frac{(11r_H - 5r_t)V_t}{45(r_H - r_t)^2 \alpha L}\right]^{\frac{1}{3}} + \frac{3}{8}k\left[\frac{(29r_H - 5r_t)V_t}{90(r_H - r_t)^2 \alpha L}\right]^{\frac{1}{3}}. \qquad \text{(C-27)}$$

Appendix D: Thermoelectric Cooling

D.1: Summary

To determine the most feasible methods of cooling for downhole electronics, several cooling systems must be evaluated. The systems must be explored with regards to the specifications determined in the previous sections (i.e., geometry, hot & cold reservoir temperatures, required time, etc.). The system to be evaluated is thermoelectric cooling.

Thermoelectric cooling employs the Peltier effect. In 1934 Jean Peltier found that if one passed an electric current across two dissimilar metals, a heating or cooling flux would occur between the two metals. The direction of the flux would depend on the direction in which the current was passed. Advantages of thermoelectric cooling include size, no moving parts, and simple implementation. The greatest disadvantage is the very low efficiencies at which the coolers operate, especially at higher temperatures. The effectiveness of the cooling or heating between the two metals depends on several properties. These properties are often lumped into a Figure-of-Merit, Z (1/°K), given by

$$Z = \frac{\alpha^2}{RK} \qquad \text{(D-1)}$$

where α (V/K) is the Seebeck coefficient, R (Ω) is the electrical resistance, and K (W/°K) is a thermal conductivity value for the cooler (Goldsmid, 1964, pp.5-11).

D.2: Theory

Note: The following formulation closely follows that of Bennett (1991, pp. 64-74).

In a thermoelectric cooling device (see Figure D.1), the cooling or heating is a result of the change in average kinetic energy of a current carrier as it crosses a junction. The #1 branch represents an n-type semiconductor doped with excess negative charges and #2 branch a p-type semiconductor doped with excess positive charges. They are connected electrically in series by a link that is assumed to have no electrical resistance at the cold junction and to a voltage source at the hot junction. They are also thermally in parallel between the cold junction at temperature T_c and the hot junction at temperature T_h. Assuming the device is insulated, there is no lateral heat transfer between n and p type semiconductor branches. The branches are assumed of constant cross section but not necessarily the same cross section or length. Lastly, it is assumed that there are no thermal contact resistances between either reservoir and the connecting bus bar. An energy balance on both arms at the cold junction sums the Peltier cooling minus the Joule heating and thermal conduction. The Peltier cooling in each branch is

$$Q_{P1} = -\alpha_1 T_c I \qquad \text{(D-2)}$$

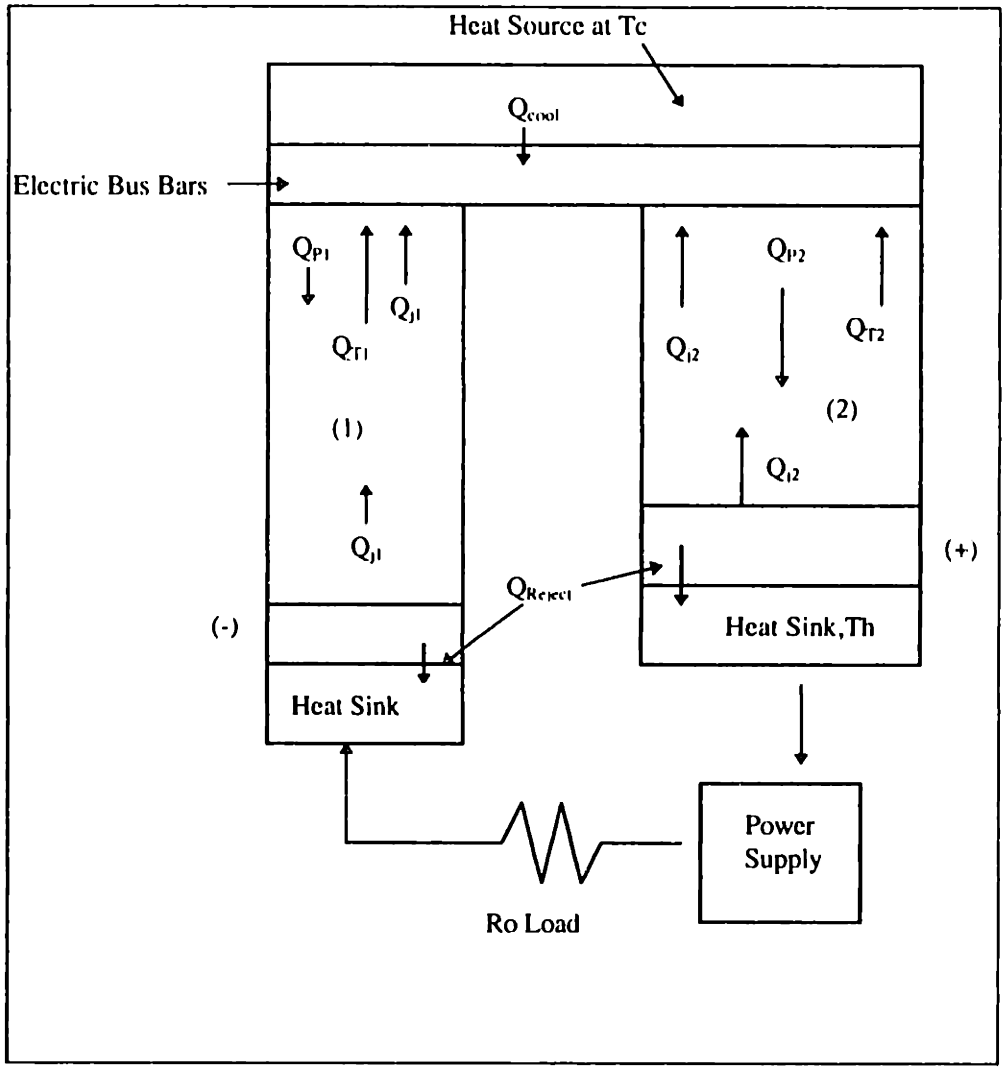

Figure 6a.1: Single Stage Thermoelectric Refrigerator(Goldsmid, 1964, p. 6)

and

$$Q_{P2} = \alpha_2 T_c I \qquad \text{(D-3)}$$

where Q_{P1} and Q_{P2} are the heat fluxes from the cool reservoir to the hot reservoir due to the Peltier effect, and the α's are the respective Seebeck coefficients of the two semiconductor materials. The summed heat flux of eq.(D-2) and eq.(D-3) is reduced by both Joule heating and thermal conductivity between the two reservoirs via the semiconductors. Only one half the total Joule heating input for each branch is attributed to the cold reservoir because it is continually produced and distributed between reservoirs. The Joule heat input flux, Q_j, and thermal conduction flux, Q, at the cold reservoir are

$$Q_{j1} = \frac{I^2 l_1 \rho_1}{2A_1} \text{ and } \quad Q_{j2} = \frac{I^2 l_1 \rho_2}{2A_2}, \qquad \text{(D-4), (D-5)}$$

$$Q_1 = \frac{-k_1 A_1 (T_h - T_c)}{l_1} \quad \text{and} \quad Q_2 = \frac{-k_2 A_2 (T_h - T_c)}{l_2}, \qquad \text{(D-6), (D-7)}$$

where, I's are currents, l's are the lengths, A's are the areas, k's are the thermal conductivities, ρ's are the electrical resistivities in Ω-m, and T's are the corresponding absolute temperatures of the two junctions. Combining eq.(D-3) through eq.(D-7) in a heat balance results in a cooling of Q_{abs} equal to

$$Q_{abs} = IT_c(\alpha_2 - \alpha_1) - (\tfrac{I^2 R}{2}) - K\Delta T, \qquad \text{(D-8)}$$

where

$$K = \frac{k_1 A_1}{l_1} + \frac{k_2 A_2}{l_2}, \qquad \text{(D-9)}$$

$$R = \frac{l_1 \rho_1}{A_1} + \frac{l_2 \rho_2}{A_2}, \qquad \text{(D-10)}$$

and

$$\Delta T = T_h - T_c. \qquad \text{(D-11)}$$

Minimum voltage and power requirements to run a refrigerator are equal to the voltage necessary to overcome the IR drop plus the Seebeck emf, and the power from the product of voltage and current:

$$V = (\alpha_2 - \alpha_1)\Delta T + IR \qquad \text{(D-12)}$$

$$P \text{ or } W = IV = I(\alpha_2 - \alpha_1)\Delta T + I^2 R. \qquad \text{(D-13)}$$

The COP is the ratio of the cooling flux given by eq.(D-8) divided by the total power of the refrigerator:

$$COP = \frac{IT_c(\alpha_2 - \alpha_1) - \frac{I^2 R}{2} - K\Delta T}{(\alpha_2 - \alpha_1)I\Delta T + I^2 R}. \qquad \text{(D-14)}$$

D.3: Theory Applied to Optimum Designs

There are several ways to both size a thermoelectric cooling unit and determine its relative performance or efficiency. Probably the simplest method is to maximize the COP of the cooler at given operating conditions by finding the optimal geometry (Goldsmid, 1964). Given maximum current available, reservoir temperatures, and semiconductor properties, the theoretical maximum COP is determined. The optimal geometry results in the product of the eq.(D-9) and eq.(D-10) being at a minimum, therefore

$$RK_{min} = \left[(k_1 \rho_1)^{\frac{1}{2}} + (k_2 \rho_2)^{\frac{1}{2}} \right]^2 . \qquad \text{(D-15)}$$

With eq.(D-15) a maximum COP can be determined by

$$COP_{max} = \frac{T_c \left[(1 + ZT_m)^{\frac{1}{2}} - \left(\frac{T_h}{T_c} \right) \right]}{(T_h - T_c) \left[(1 + ZT_m)^{\frac{1}{2}} + 1 \right]} \qquad \text{(D-16)}$$

where the median temperature, T_m (°K), is given by:

$$T_m = \frac{T_h + T_c}{2} . \qquad \text{(D-17)}$$

The input current required is given by

$$I = \frac{(\alpha_2 - \alpha_1)\Delta T}{R \left[(1 + ZT_m)^{\frac{1}{2}} - 1 \right]} . \qquad \text{(D-18)}$$

The work or power requirement is derived via

$$W = Q_{abs} COP_{max} \qquad . \qquad \text{(D-19)}$$

Resistance of the cooler pair is found by rearranging eq.(D-18) and assuming an I_{max} value. Since the individual couples work in parallel, their individual power consumptions are found with eq.(D-13). Finally, the total number of couples, N, is found by dividing eq.(D-13) by eq.(D-19).

D.4: Single-Stage Cooler

From the Figures-of-Merit versus temperature curves, it becomes apparent that the Bismuth Telluride pairs (Bi_2Te_3) perform the best at median temperatures between 125°C and 225°C (see Figure 6.2). With the properties of the Bismuth Telluride pairs, a theoretical COP_{max} is derived. Average properties for the semiconductor pairs are found as functions of temperature (Goldsmid, 1964). Table D.1 lists the parameters and analysis results of the single-stage cooler.

Table D.1: Single-Stage Thermoelectric Cooler Parameters

T_h (°K)	473
T_c (°K)	400
T_m(°K)	436
Z_{max} (°K^{-1}) (Bennett, 1988, p.84)	~1.96 x 10^{-3}
α_{tot} (μV°K^{-1})	383.7
$\lvert\alpha_1/\alpha_2\rvert$	0.608
RK_{min}(V^2°K^{-1})	7.5 x 10^{-5}
COP_{max}	0.39
Q_{abs}(W)	80
W (W)	205
R (ohms)(Assuming I_{max}= 20 amps)	3.9 x 10^{-3}
Wi (W)	2.1
N	100

Therefore, the COP is equal to approximately 10 % of Carnot efficiency.

D.5: Multiple-Stage Cooler

Due to the allowed geometry, a multistage cooler consisting of two layers of thermoelectrics may be possible. The first stage must absorb the 80-W cooling load, Q_{abs}, and the second or outer stage must absorb both Q_{abs} and the power W_1 of the first stage. For the same reasons chosen in the single-stage cooler, both pairs are Bismuth Telluride. The first stage will cool from 125°C to 190°C and the second stage will cool from 190°C to 200°C. Table D.2 lists the properties and results of the analyses of both stages. Therefore, the COP represents approximately 13 % of the Carnot efficiency

Table D.2: Two-Stage Thermoelectric Cooler Parameters

	First Stage	Second Stage	Total System
T_h (°K)	463	473	473
T_c (°K)	400	463	400
T_m(°K)	432	468	----
Z_{max} (°K^{-1}) (Bennett 1988)	~2.3 x 10^{-3}	~1.6 x 10^{-3}	----
α_{tot} (μV°K^{-1})	400	340	----
$\lvert\alpha_1/\alpha_2\rvert$	0.82	0.89	----
RK_{min}(V^2°K^{-1})	6.95 x 10^{-5}	7.1 x 10^{-5}	----
COP_{max}	0.67	6.0	0.50
Q_{abs}(W)	80	200	80
W (W)	120	33	153
R (ohms)(Assuming I_{max}= 20 amps)	3.07 x 10^{-3}	5.3 x 10^{-4}	----
Wi (W)	1.7	0.279	----
N	69	118	----

Appendix E: Vapor-Compression Cycle

E.1: Summary

In an effort to determine the most feasible methods of cooling for downhole electronics, several cooling systems must be evaluated. The systems must be explored with regards to the specifications determined in the previous sections (i.e., geometry, hot & cold reservoir temperatures, required time, etc.). In this section the vapor-compression cooler is examined.

A vapor-compression cycle with a refrigerant fluid, run in reverse provides the conventional refrigeration seen in most homes and automobiles (Karlekar, 1983, p.237). The basic vapor-compression cycle consists of two isobaric heat exchange processes, an isentropic compression, and an isenthalpic expansion device. In their simplest forms these four processes translate to an evaporator heat exchanger, a condensing heat exchanger, a compressor, and an expansion valve (see Figure 6.3).

E.2: Theory

Note: The following formulation follows that of Bennett (1991, pp.31-35)

A vapor compression cooler T-s diagram is given in Figure 6.4. The theory is derived on a per-unit-mass flowing through the cycle, $\dot{m}$, basis. The heat absorbed from the source, q_{12}, is

$$q_{12} = h_2 - h_1, \qquad \text{(E-1)}$$

where the h_i's represent the specific enthalpies of the different states. The compression process between states two and three raises the vapor to a superheated condition isentropically. The work required for this process, w_{23}, is

$$w_{23} = h_3 - h_2. \qquad \text{(E-2)}$$

Irreversibilities in the system cause the real value of work, w_{act}, in eq.(E-2) to increase. This inefficiency is accounted for by the compressor efficiency value, η, and is expressed by

$$w_{act} = \frac{w_{23}}{\eta}. \qquad \text{(E-3)}$$

Condenser heat rejected to the environment, q_{34}, between states three and four is

$$q_{34} = h_4 - h_3. \qquad \text{(E-4)}$$

From state four to one the refrigerant expands isenthalpically resulting in an ideal COP of

$$COP = \frac{h_2 - h_1}{h_3 - h_2} . \qquad \text{(E-5)}$$

The total cooling capacity of the cycle, Q_{abs}, is

$$Q_{abs} = \dot{m} q_{12} \quad , \qquad \text{(E-6)}$$

and the total compressor work, W_{23}, is

$$W_{23} = \dot{m} w_{23}. \qquad \text{(E-7)}$$

From an energy balance for the system, the total heat rejected, Q_{rej} (W), becomes

$$Q_{rej} \geq Q_{12} + W_{23}, \qquad \text{(E-8)}$$

where the actual value of Q_{rej} is larger than eq.(E-9) due to irreversibilities in the cycle and its components.

E.3: Theory Applied to Downhole Conditions

A preliminary analysis was conducted using water as the refrigerant in a downhole environment similar to Bennett (1991). It was assumed that saturated vapor exited at state two and saturated liquid at state four. The components were sized to allow a Q_{abs} equal to 80W. The evaporator temperature is assumed to be at 125°C. With these assumptions and those made in Section E.2, tables can be constructed for the necessary states of the cycle with water (see Tables E.1 and E.2).

The mass flowrate is derived through an iteration knowing that state two is a saturated vapor, state one has the same pressure as state two (i.e., a wet vapor), and the Q_{abs} specification.

Table E.1: Fully Defined States for Vapor-Compression Cycle with Water

Point	State	T(°C)	P(Pa)	quality	h(kJ/kg)	s(kJ/kg-°K)	v(m^3/kg)
1	Wet Vapor	125	$232x10^3$	0.149	851	2.40	0.00125
2	Sat. Vapor	125	$232x10^3$	1	2713.5	7.0775	0.7706
3	Super-Heated Vapor	351	$1.58x10^6$	1	3148	7.0775	0.177
4	Sat. Liquid	200	$1.58x10^6$	0	851	2.33	0.00116

Table E.2: Vapor-Compression Refrigerator Results

Q_{abs}(W)	80
COP	4.29
W (W)	18.7
Mass Flowrate (kg/s)	4.3×10^{-5}

E.4: Heat Exchanger Sizing

A logical constraint of the various cycles are the required heat exchanger sizes. It is necessary that the heat exchangers in the coolers be on the order of 1m as opposed to 100m. Additionally, it is argued that the internal heat exchanger or evaporator can be varied to fit the size of the downhole constraints by using convection fans, heat pipes, etc. However, the outside heat exchanger or condenser can be modified only slightly. The designer must rely on the film coefficient from the borehole for heat transfer to a simple piping configuration. Consequently, the outside heat exchanger or condenser must be sized to determine system feasibility.

For simplicity, assume the geometry described by the following section. A tube of length L is extended vertically in the tool and exposed to the flow in the wellbore. The overall heat transfer coefficient between the temperature of the internal fluid, T, and the temperature of the wellbore fluid, T_H , can found by summing the collective resistances and normalizing with respect to the inside tube area. The summation is given by

$$\sum R = R_1 + R_2 + R_3 \quad . \qquad \text{(E-9)}$$

The resistance from the internal flow, R_1, is given by

$$R_1 = \frac{1}{h\pi D_i L} \qquad \text{(E-10)}$$

where h is the internal heat transfer coefficient and D_i is the internal diameter of the tool. The resistance of the tube material and thickness, R_2, is given by

$$R_2 = \frac{ln\left(\frac{D_o}{D_i}\right)}{2\pi kL} \qquad \text{(E-11)}$$

where D_o is the outside tube diameter and k is the thermal conductivity of the tube material. The resistance of the external flow, R_3, is given by

$$R_3 = \frac{1}{h_H \pi D_o L} \qquad \text{(E-12)}$$

where h_H is the heat transfer coefficient from the external flow to the tube's perimeter. The cumulative heat transfer coefficient, U_{tot}, with respect to the inside of the tube then becomes

$$U_{tot} = \frac{1}{\frac{1}{h} + \frac{1}{h_H}\left(\frac{D_i}{D_o}\right) + \frac{D_i \ln\left(\frac{D_o}{D_i}\right)}{2k}} \quad . \qquad \text{(E-13)}$$

The third term in the denominator can be made sufficiently small as to be deemed neglible by choosing a high conductivity material for the tube.

Equations can now be developed to relate the temperature of the internal flow to a given length of pipe. Using a fluid parcel analysis one derives

$$\dot{m} c_p \frac{\partial T}{\partial x} = U(T - T_H)\pi D_i \, . \qquad \text{(E-14)}$$

With an initial temperature of the fluid at zero length, T_o, the differential equation can be solved, resulting in

$$T(x) = (T_o - T_H)e^{-\frac{UD_i\pi}{\dot{m}c_p}x} + T_H \, . \qquad \text{(E-15)}$$

With eq.(E-15), one can find the length at which the fluid temperature equals that of state four. The h_H value is given from the external flow and heat transfer and heat transfer analysis (see Appendix C). The worst-case-scenario for a moving tool in oil would give a value of h_H equal to approximately 100W/m^2-°C. To find h for the internal flow one must first determine if the flow is laminar or turbulent.

In practice, one must begin by finding fluid properties at the given temperatures, pressures, etc. Estimates can be found in handbooks, steam tables, etc. Then the type of flow must be determined to find the corresponding Nusselt, Nu, numbers for the heat transfer considerations. In our low mass flowrate case, the internal flow is estimated to be laminar and the Nu number is approximated as a constant equal to four. For a worst case scenario, the h is derived from the vapor properties at state three as opposed to the liquid properties at state four. The thermal properties of state three are listed in Table E.3 along with some assumed heat exchanger tubing dimensions.

Table E.3: Heat Exchanger Parameters for Vapor-Compression Cycle (Thermophysical Properties, 1979)

State Three	
μ (N-s/m^2)	~20 x 10^{-6}
k (W/m-°C)	~0.05
c_p (J/kg-°K)	~3500
Geometry	
D_i (m)	0.0032
D_o (m)	0.0064
Re	~850
T_o (°C)	351
T_H (°C)	200

With the values from Table E.3 and the previously described theory, an internal heat transfer coefficient can be derived along with the overall heat exchanger length. Table E.4 lists the heat exchanger results.

Table E.4: Vapor-Compression Cycle Heat Exchanger Results

h (W/m^2-°C)	~60
U (W/m^2-°C)	~46
L (m)	~1

Appendix F: Brayton Cycle

F.1: Summary

In an effort to determine the most feasible methods of cooling for downhole electronics, several cooling systems must be evaluated. The systems must be explored with regards to the downhole specifications determined in previous sections (i.e., geometry, hot and cold reservoir temperatures, required time, etc.). In this section the reverse Brayton cooling cycle is examined.

Refrigeration provided by the Brayton cycle, run in reverse, is commonly used in aircraft and represents the only gas cycle used in commercial systems. The cycle consists of two isobaric heat exchangers, an isentropic compressor, and an isentropic expander (see Figure 6.7) (Karlekar, 1983, pp.400-405).

F.2: Theory

Note: The following formulation follows that of Bennett (1991, pp.25-37)

Figure 6.8 displays the T-s diagram for the Brayton cycle. The following assumptions are used to simplify the analysis: reversible processes, constant specific heats, and perfect gas behavior.

The working fluid, or gas refrigerant, absorbs heat in the low-temperature heat exchanger during a constant pressure process at P_{low} and causes the temperature to rise. The heat absorbed in the refrigerant per unit mass of fluid is

$$q_{12} = h_2 - h_1 = c_p\left(T_2 - T_1\right) . \qquad \text{(F-1)}$$

The gas temperature at state two is slightly below the cooling load temperature. The refrigerant is then compressed from state two to state three. The process occurs fast enough to be considered adiabatic and assumed insentropic. The temperature of the compressor is

$$T_3 = T_2\left(\frac{P_3}{P_2}\right)^{\frac{\gamma-1}{\gamma}} \qquad \text{(F-2)}$$

where

$$\gamma = \frac{c_p}{c_v} . \qquad \text{(F-3)}$$

The ideal work per unit mass of the fluid in the compressor is

$$w_{23} = h_3 - h_2 = c_p(T_3 - T_2). \qquad \text{(F-4)}$$

The gas is then cooled at the constant high pressure value until its temperature almost equals that of the hot reservoir. This relationship is given by

$$q_{34} = h_3 - h_4 = c_p(T_3 - T_4) \quad . \qquad \text{(F-5)}$$

Between state four and state one, an isentropic expansion occurs in a turbine. The temperature at the exit is given by

$$T_1 = T_4\left(\frac{P_1}{P_4}\right)^{\frac{\gamma-1}{\gamma}} . \qquad \text{(F-6)}$$

Work can potentially be extracted from the turbine and is given on a per unit mass basis as

$$w_{41} = h_4 - h_1 = c_p(T_4 - T_1). \qquad \text{(F-7)}$$

The work from eq.(F-7) is not available if an expansion valve is used in its place.

The COP of the system with the turbine component is

$$COP_t = \frac{q_{12}}{w_{23} - w_{41}} = \frac{T_2 - T_1}{(T_3 - T_2) - (T_4 - T_1)} \quad . \qquad \text{(F-8)}$$

The COP of the system with an expansion valve in place of the turbine is

$$COP_v = \frac{q_{12}}{w_{23}} = \frac{T_2 - T_1}{T_3 - T_2} . \qquad \text{(F-9)}$$

The sizing of the unit is derived from the mass flowrate of refrigerant, $\dot{m}$. The mass flowrate is determined with the heat absorption or refrigeration load required by

$$Q_{abs} = \dot{m} q_{12} . \qquad \text{(F-10)}$$

Thus, the work required for the compressor is

$$W_{in} = \dot{m} w_{23} \quad . \qquad \text{(F-11)}$$

Because of inefficiencies due to nonideal behavior such as pressure drops, heat transfers, etc., the actual work required is

$$W_{act} = \dot{m}\left[w_{23} - w_{41}\right] = \dot{m}\left[\frac{h_3 - h_2}{\eta_{comp}} - \eta_{turb}\left(h_4 - h_1\right)\right], \qquad \text{(F-12)}$$

where η_{comp} and η_{turb} represent the efficiencies of the compressor and turbine. The heat rejected to the hot reservoir is given by

$$Q_{rej} = Q_{abs} + W_{act}. \qquad \text{(F-13)}$$

F.3: Theory Applied to Downhole Conditions

The refrigerant of choice for the downhole Brayton cycle is helium. Bennett's thesis showed that helium displays higher heat transfer rates and lower pressure drops and required ratios relative to several other refrigerants (Bennett, 1991 p.54). Table F.1 lists the temperatures and pressures of the four states for the reverse Brayton cycle assuming a compression ratio of three. Table F.2 lists the refrigerator results using helium.

Table F.1: Brayton Cycle State (using c_p=5.23 kJ/kg-°K, γ=1.67)

State	T (°C)	P (Pa)
1	31	1.01×10^5
2	125	1.01×10^5
3	345	3.03×10^5
4	200	3.03×10^5

Table F.2: Refrigerator Results

Q_{abs}(W)	80
COP_t	1.84
COP_v	0.43
W_t(W)	43
W_v (W)	186
Mass Flowrate (kg/s)	1.6×10^{-4}

F.4: Heat Exchanger Sizing

A logical constraint of the various cycles are the required heat exchanger sizes. It is necessary that the heat exchangers in the coolers be on the order of 1m, as opposed to 100m. Additionally, it can be argued that the internal heat exchanger can be varied to fit the size of the downhole constraints by using convection fans, heat pipes, etc. However, the outside heat exchanger can be modified only slightly. The designer must rely on the film coefficient from the borehole for heat transfer to a simple piping configuration. Consequently, the outside heat exchanger must be sized to determine system feasibility.

For simplicity assume the geometry described in the following. A tube of length L is extended vertically in the tool and exposed to the flow in the wellbore. The overall heat transfer coefficient between the temperature of the internal fluid, T ,and the temperature of the wellbore fluid, T_H , is found by summing the collective resistances and normalizing with respect to the inside tube area. The summation is given by

$$\sum R = R_1 + R_2 + R_3 \quad . \tag{F-14}$$

The resistance from the internal flow, R_1, is given by

$$R_1 = \frac{1}{h\pi D_i L} \tag{F-15}$$

where h is the internal heat transfer coefficient, D_i is the internal diameter of the tool, and L is the length of the tube. The resistance of the tube material and thickness, R_2, and is given by

$$R_2 = \frac{ln\left(\frac{D_o}{D_i}\right)}{2\pi kL} \tag{F-16}$$

where D_o is the outside tube diameter and k is the thermal conductivity of the tube material. The resistance of the external flow, R_3, is given by

$$R_3 = \frac{1}{h_H \pi D_o L} \tag{F-17}$$

where h_H is the heat transfer coefficient from the external flow to the tube's perimeter. The cumulative heat transfer coefficient, U_{tot}, with respect to the inside of the tube then becomes

$$U_{tot} = \frac{1}{\frac{1}{h} + \frac{1}{h_H}\left(\frac{D_i}{D_o}\right) + \frac{D_i\, ln\left(\frac{D_o}{D_i}\right)}{2k}} \tag{F-18}$$

The third term in the denominator can be made sufficiently small as to be deemed negligible by choosing a high conductivity material for the tube. Equations can now be developed to relate the temperature of the internal flow to a given length of pipe. Using a fluid parcel analysis one derives

$$\dot{m} c_p \frac{\partial T}{\partial x} = U(T - T_H)\pi D_i \quad . \tag{F-19}$$

With an initial temperature of the fluid at zero length, T_o, the differential equation can be solved, resulting in

$$T(x) = (T_o - T_H)e^{-\frac{UD_i\pi}{\dot{m}c_p}x} + T_H . \qquad \text{(F-20)}$$

With eq.(F-20), one can find the length at which the fluid temperature equals that of state 4. The h_H value is given from the external flow and heat transfer and heat transfer analysis (see Appendix C). The worst case scenario for a moving tool in oil would give a value of h_H equal to approximately 100W/m^2-°C. To find h for the internal flow, one must first determine if the flow is laminar or turbulent.

In practice, one must begin by finding fluid properties at the given temperatures, pressures, etc. Estimates can be found in handbooks, steam tables, etc. Then the type of flow must be determined to find the corresponding Nu numbers for heat transfer considerations. In our low mass flowrate case, the internal flow is estimated to be laminar and the Nu is a constant assumed to equal four. The average thermal properties are listed in Table F.3 along with some assumed heat exchanger tubing dimensions.

Table F.3 Heat Exchanger Parameters (Thermophysical Properties, 1979)

Properties	
μ (Ns/m^2)	~30x10^{-6}
k (W/m-°C)	~0.225
c_p(J/kg-°C)	~5230
ρ_{avg}(kg/m^3)	~0.26
Geometry	
D_i (m)	0.0254
D_o (m)	0.0381
Re	~300
T_o (°C)	345
T_H (°C)	200

With the values of Table F.3 and the previously described theory, an internal heat transfer coefficient can be derived along with the overall heat exchanger length. Table F.4 lists the heat exchanger results.

Table F.4: Heat Exchanger Results

h (W/m^2-°C)	~35
U (W/m^2-°C)	~30
L (m)	~1

Appendix G: Joule-Thompson Cycle

G.1: Summary

In an effort to determine the most feasible methods of cooling for downhole electronics, several cooling systems must be evaluated. The systems must be explored with regards to the downhole specifications determined in previous sections (i.e., geometry, hot reservoir and cold reservoir temperatures, required time, etc.). In this section the Joule-Thompson cycle is examined.

The Joule-Thompson cycle is very similar to the Brayton cycle with the exception of the expansion device. The Joule-Thompson cycle uses a throttling valve in the place of a turbine expander. The major components of this system include a gas compressor, high temperature heat exchanger, low temperature heat exchanger, and throttling valve (see Figure 6.9).

G.2: Theory

Note: The following formulation follows that of Bennett (1991, pp.59-63)

The following assumptions are used in the preliminary analysis: reversible processes with the exception of the throttling valve and compressible gas behavior described by a compressibility factor. The theory is the same as Brayton Cycle except for the expansion (isenthalpic).

In real gases, the derivative of the temperature with respect to pressure is nonzero. The ratio is known as the Joule-Thompson coefficient, μ, given by

$$\mu = \left(\frac{\partial T}{\partial p}\right)_h . \qquad \text{(G-1)}$$

This ratio is positive for pressure drops that produce temperature drops and negative for pressure drops that result in temperature increases. Figure 6.10 shows plots of constant enthalpy lines for a gas on temperature and pressure axes, and the dotted line represents the locus of points, inversion curve, where the ratio is equal to zero. Expansions that occur to the left and right of the inversion curve produce temperature drops and increases respectively.

A relation for the Joule-Thompson coefficient is derived from the differential for enthalpy, dh, as

$$dh = c_p dT + \left[v - T\left(\frac{\partial v}{\partial T}\right)_p \right] dp , \qquad \text{(G-2)}$$

where v is the specific volume. Because of the isenthalpic throttling process, the ratio of temperature and pressure differentials becomes

$$\left(\frac{dT}{dp}\right)_h = \frac{1}{c_p}\left[T\left(\frac{dv}{dT}\right)_p - v\right]. \qquad \text{(G-3)}$$

For a gas that obeys the law

$$pv = ZRT, \qquad \text{(G-4)}$$

where R is the gas constant and Z is the compressibility coefficient, the entire differential is represented as

$$pdv + vdp = ZRdT + RTdZ. \qquad \text{(G-5)}$$

Eq.(G-5) can then be rearranged to solve for the derivative of volume with respect to temperature assuming constant pressure and is given as

$$\left(\frac{dv}{dT}\right)_p = \frac{ZR}{p} + \left(\frac{RT}{p}\right)\left(\frac{dZ}{dT}\right). \qquad \text{(G-6)}$$

Eq.(G-6) substituted into eq.(G-3) while using the equation of state and definition of the Joule-Thompson coefficient yields

$$\mu = \frac{1}{c_p}\frac{RT^2}{p}\frac{dZ}{dT}. \qquad \text{(G-7)}$$

Plots of the compressibility coefficient can be used to determine the sign of the Joule-Thompson coefficient without very much more property data on a given gas. Figure 6.11 displays a plot of the inversion line on reduced coordinates of pressure and temperature. Points lying inside the curve have positive coefficients and can be used in conjunction with a gas expansion to provide reduced temperatures.

Applying Figure 6.11 to our application would necessitate a critical temperature, T_{crit}, of

$$\frac{T_h}{5} < T_{crit} < \frac{T_c}{0.5} \qquad \text{(G-8)}$$

or

$$-178°C < T_{crit} < 523°C. \qquad \text{(G-9)}$$

From Figure 6.11 it also becomes obvious that the pressure from which the expansion takes place should follow

$$0.5 < P_r < 11. \qquad \text{(G-10)}$$

G.3: Theory Applied to Downhole Conditions

From eq.(G-7) it is apparent that the gases with the greatest R/c_p and dZ/dT values will provide the greatest temperature drops and cooling. Of the refrigerants listed by Bennett (1991), carbon dioxide is the best suited for the downhole cooling system with a realistic maximum compression ratio of four (Griffith, 1995). Table G.1 lists the properties of CO_2. The Joule-Thompson coefficient from eq.(G-7) is derived using the following

$$\mu = \frac{1}{c_p}\frac{RT_{av}^{\,2}}{p_{av}}\left(\frac{Z_1 - Z_4}{T_1 - T_4}\right), \qquad \text{(G-11)}$$

where p_{av} and T_{av} represent the average pressure and temperature between states four and one. The temperature drop between states four and one is then estimated by

$$T_1 - T_4 = \mu\,(p_1 - p_4). \qquad \text{(G-12)}$$

State one is assumed to be at p_c and T_c , and T_4 is set equal to the borehole temperature. P_4 is then iterated to a value such that the temperature difference from eq.(G-12) is equal to that assumed in eq.(G-11). Table G.2 lists the states of the cycle along with the compressibility coefficient. The remaining state properties are found with the same equations developed in the Brayton cycle analysis (see Appendix 6c). Table G.3 lists the overall refrigerator results.

Table G.1: CO_2 Properties (Karlekar, 1983, pp. 195, 434, 576)

R (kJ/kg-°K)	0.18892
c_p (kJ/kg-°K)	~0.8418
T_c (°C)	31
P_c (Pa)	7.39×10^6
μ(°K/Pa)	$\sim 7.0 \times 10^6$
γ	~1.2

Table G.2: Joule-Thompson Cycle States (Gyftopoulos, 1991, p.354)

State	T (°C)	P (Pa)	Z
1	31.2	7.39×10^6	~0.2
2	125	7.39×10^6	---
3	228	29.6×10^6	---
4	200	29.6×10^6	~0.85

Table G.3: Joule-Thompson Refrigerator Results

Q_{abs} (W)	80
COP	0.91
W (W)	88
Mass Flowrate (kg/s)	$10x10^{-4}$

G.4: Heat Exchanger Sizing

Like the previous systems, the hot heat exchanger must be sized for feasibility. The analysis from the Brayton cycle will also be used here (see Appendix F). Table G.4 lists the average gas properties between states three and four as well as the assumed geometry of the system. Table G.5 lists the results of the analysis.

Table G.4: Heat Exchanger Parameters (Pitts, 1977, pp.304-305)

Properties	
μ (Ns/m^2)	$\sim 34x10^{-6}$
k (W/m-°K)	~0.06
c_p(J/kg-°K)	~841
ρ_{avg}(kg/m^3)	~38
Geometry	
D_i (m)	0.0254
D_o (m)	0.0381
Re	~1350
T_o (°C)	228
T_H (°C)	200

Table G.5: Heat Exchanger Results

h (W/m^2-°K)	~9
U (W/m^2-°K)	~9
L (m)	~5

Appendix H: Lubrication

H.1: Lapped Piston/Cylinder Lubrication Analysis

The first series of compressor tests were characterized by a certain "nonideal" behavior. The compressor worked, as designed, for periods of one to two hours, but at a given point in time the compressor discontinued maintaining the lapped piston/cylinder seal. Consequently, steam was no longer transported from the lower tank into the upper tank, and the pressure in the lower tank rapidly increased. This increase also caused the temperature in the lower tank and sample electronics to increase and the overall failure of the system.

In their original application, the lapped piston/cylinder seals are run through a "break-in" process. The lapped seal comes from the factory with almost no clearance between piston and cylinder. This condition results in a large amount of friction when the motor is run. The "break-in" process entails running the motor for approximately one hour and results in a larger running clearance between the piston and cylinder with significantly less friction. It became apparent that the one to two hours of useful operating time of the steam compressor equaled the "break-in" time of the lapped seal. The piston/cylinder clearance after the "break-in" process was consistent from test to test. The lubricant used in the steam compressor was Mobil Super Steam Cylinder Oil and displays a viscosity of approximately 5cSt at 200°C. With these considerations in mind, the compression chamber was modeled.

Figure H.1 describes the model's geometry. Table H.1 lists the model assumptions.

Table H.1: Compression Chamber Model Assumptions

1) Air in the compression chamber
2) Air is an ideal gas
3) Isentropic compression
4) When pressure in the chamber equals high pressure, P_H, the piston is stopped
5) Constant fluid properties
6) System at 200°C
7) Pressure gradient in the clearance region is constant and equal to P_H minus the inlet pressure, P_L, over the exposed seal length
8) Laminar flow of lubricant in the clearance between the piston and cylinder with no slip conditions at stationary wall and piston.
9) The volume of the lubricant in the clearance divided by the volumetric flux, Q, of the lubricant in the clearance due to the pressure gradient is the characteristic time of the seal.
10) The characteristic time of the seal must be less than the speed of one revolution of the piston crankshaft for a proper seal.

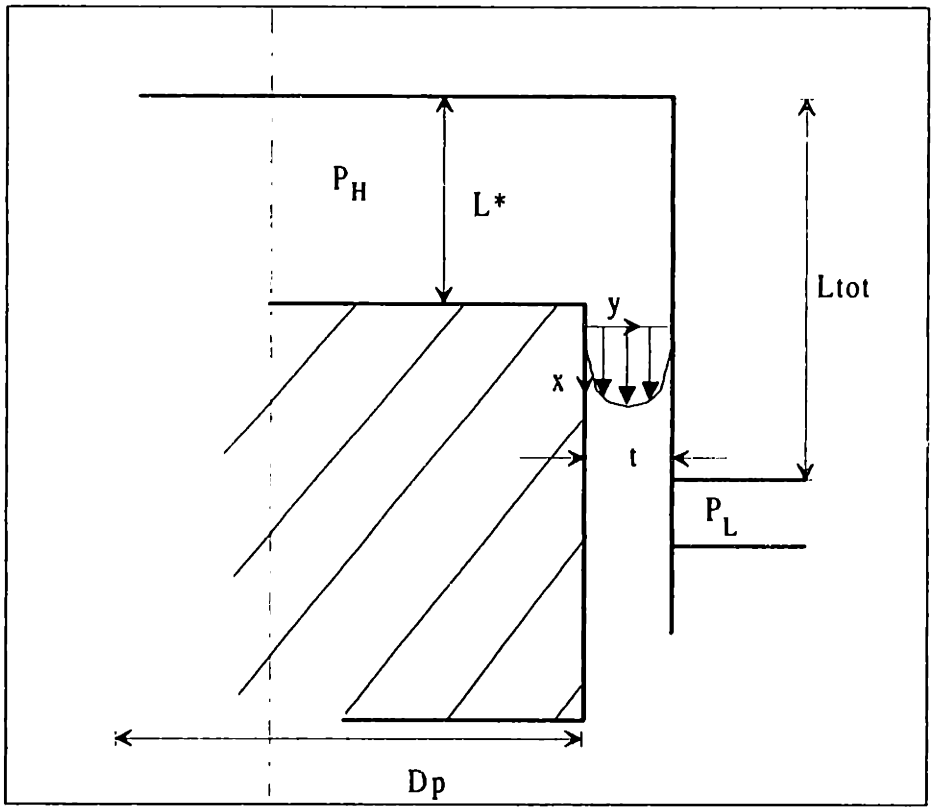

Figure H.1: Model Geometry

With assumptions one through three, and knowledge of the compression chamber geometry, several parameters can be defined. The total length of the piston stroke, l_{tot}, is determined by

$$l_{tot} = \frac{V_{total}}{A_{piston}} \quad , \qquad \text{(H-1)}$$

where V_{total} is the volume of the compression chamber and A_p is the area of the piston's face which is found with the piston diameter, D_p, with

$$A_p = \frac{\pi D_p^{\,2}}{4} \, . \qquad \text{(H-2)}$$

An isentropic compression process produces a volume value in the compression chamber, V*, for the high pressure, P_H, equal to

$$V^* = \frac{\rho_o V_{total} R T_{in} \left(\frac{P_H}{P_L} \right)^{\frac{R}{c_p}}}{P_H}, \qquad \text{(H-3)}$$

where ρ_o is the inlet air density, R is the gas constant for air, T_{in} is the inlet temperature of the air, and c_p is the specific heat of the air at constant pressure. The length of the piston/cylinder clearance, filled with lubricant, L_{lub}, at the high pressure is equal to

$$L_{lub} = L_{total} - L^*, \qquad \text{(H-4)}$$

where L* is equal to

$$L^* = \frac{V^*}{A_p}. \qquad \text{(H-5)}$$

From eq.(H-4) and the clearance thickness after "break-in", t, the volume of the lubricant in the clearance, V_{lub}, can be derived with

$$V_{lub} = \pi L_{lub} t D_p. \qquad \text{(H-6)}$$

A 1-D laminar flow analysis in the clearance with the assumptions from Table H.1 results in

$$Q = -\frac{\pi D_p}{12\mu} \frac{\partial P}{\partial x} t^3, \qquad \text{(H-7)}$$

where

$$\frac{\partial P}{\partial x} = -\frac{P_H - P_L}{L_{Lub}}. \qquad \text{(H-8)}$$

Combining eq.(H-6), eq.(H-7), and eq.(H-8) gives a value of the time required to drain the lubricant film, t_{drain}, as

$$t_{drain} = \frac{V_{lub}}{Q}. \qquad \text{(H-9)}$$

The time per stroke or time per revolution, t_{stroke}, is derived as

$$t_{stroke} = \Omega_{shaft}^{-1}, \qquad \text{(H-10)}$$

where Ω_{shaft} is the revolutions per second that the compressor shaft is spinning. Table H.2 lists air properties, lubricant properties, and compression chamber dimensions. Table H.3 lists the resulting time constants associated with various values of lubricant kinematic viscosities and motor shaft speeds.

Table H.2: Model Variable Values

Variable	Value
R (J/kg-°K)	287
c_p(J/kg-°K)	1010
P_H/P_L	15
P_L(Pa)	1.01×10^5
V_{total} (m^3)	1.96×10^{-6}
D_p(m)	0.0213
t (m) after break-in	5.08×10^{-6}
ρ_{lub}(kg/m^3)	900

Table H.3: Time Constant Results

Variable	Result
t_{drain} (s)(ν_{lub}=3cSt)	0.019
t_{drain} (s)(ν_{lub}=4cSt)	0.026
t_{drain} (s)(ν_{lub}=5cSt)	0.032
t_{drain} (s)(ν_{lub}=50cSt)	0.0032
t_{stroke}(Ω_{shaft}=2000rpm)	0.030
t_{stroke}(Ω_{shaft}=20000rpm)	0.0030

The results show that when the shaft is rotating at 2000rpm and Mobil Super Steam Cylinder Oil is being used, the lubricant time constants are approximately equal to the time per stroke in the system at 0.03 seconds. The same oil viscosity works well in model airplane engines at the same temperatures because the engines are rotating ten times faster. Thus, the stroke time is equal to 0.003 seconds instead of 0.03 seconds. The cooling system worked well in the "break-in" period of the lapped piston/cylinder seal because the clearance between the two sliding pieces was nil. To solve the seal problem after "break-in" and at a shaft speed of 2000rpm, it is necessary to increase the kinematic viscosity of the lubricant by a factor of ten to 50cSt at 200°C.

H.2: Lubrication Flowrate

The lubrication flowrate was empirically determined. The pressure in the lubrication system was maintained at approximately 20.7×10^5Pa. A solenoid valve was then opened at specified intervals and the lubricant was allowed to flow past a restrictor and into the compressor intake line. The solenoid displayed an opening lag time of 0.040

seconds. In other words, if the solenoid was opened for 0.1 seconds electronically, the actual open time would be 0.060 seconds. The optimal lubricant flowrate for the lapped piston/cylinder seal was found to be approximately $1.0x10^{-8}m^3/s$. This value was found by injecting different flowrates into the compressor while compressing air at a 15 time compression ratio at room temperature and finding the flowrate at which pressure was stabilized at an inlet air flowrate of approximately $1.0x10^{-4}m^3/s$.

The programmable ratio per second of solenoid open time over total time was found with the flow equations through the restrictor. The Lee Co. visco jet restrictor has a lohm rate of 41,000. A lohm is defined such that a one lohm restriction will permit a flow of 378 liters per minute of water with a pressure drop of 172kPa at a temperature of 27°C (Lee, 1989, p.M-30). Given the pressure difference, H, in kPa between the inlet and exit of the restrictor, the lohm rate, L, specific gravity, S, and the viscosity of the lubricant, the flowrate can be found. The equation for the flowrate in m^3/s is

$$I = 0.00048\frac{V}{L}\sqrt{\frac{H}{S}}, \qquad \text{(H-11)}$$

where V is a viscosity factor for the lubricant at the operating conditions of the compressor (Lee 1989, pp. M-11-M-32). The lubricant flowrate, Q_{lub}, of the system ignoring acceleration effects would then be

$$Q_{lub} = I\frac{t_{open} - t_{lag}}{t_{total}}, \qquad \text{(H-12)}$$

where t_{open} is the open time of the solenoid valve from the programmer per iteration, t_{lag} is the solenoid valve lag time, and t_{total} is the total operating time per iteration. Table H.4 lists the values and result of eq.(H-11) and eq.(H-12). Thus, if the programmer opens the valve for 0.1 seconds every 3 seconds at the specified pressure difference, the lubricant flowrate will approximately equal the goal flowrate of $1.0x10^{-8}m^3/s$.

Table H.4: Flowrate Parameters and Results

Variable	Value or Result
V	1
L (lohms)	41,000
S	850
H (kPa)	2069
I (m^3/s)	$5.8x10^{-7}$
t_{open}(s)	0.1
t_{lag}(s)	0.040
t_{total}(s)	3.0
Q_{lub}(m^3/s)	$1.2x10^{-8}$

Appendix I: Hot Heat Exchanger Analysis

I.1: Model

Figure I.1 shows a simplified schematic of the hot heat exchanger. Super-heated steam enters the upper tank from the compressor where it condenses to a saturated liquid at the compressor outlet pressure. The steam condenses as heat is transferred from within the tank to the borehole. The rate at which energy is transferred from within the upper tank to the borehole is the condensing heat flux, Q_{rej}. The temperature within the tank is assumed uniform and constant. Conduction through the ends of the upper tank is also ignored. Given the material properties and dimensions of the upper tank, the states and mass flowrate in the cooling system, and the borehole heat transfer coefficient, it is desired to find the temperature in the upper tank required to conduct the condensing heat flux to the borehole.

From eq.(6-24) the heat flux rejected to the borehole, Q_{rej}, is

$$Q_{rej} = \dot{m}(h_3 - h_4), \qquad \text{(I-1)}$$

where $\dot{m}$ is the steam's mass flowrate, and the h's represent the enthalpies of states three and four. Combining eq.(F-16) and eq.(F-17) from the heat exchanger analysis of Appendix F produces the heat flux versus temperature relationship given by

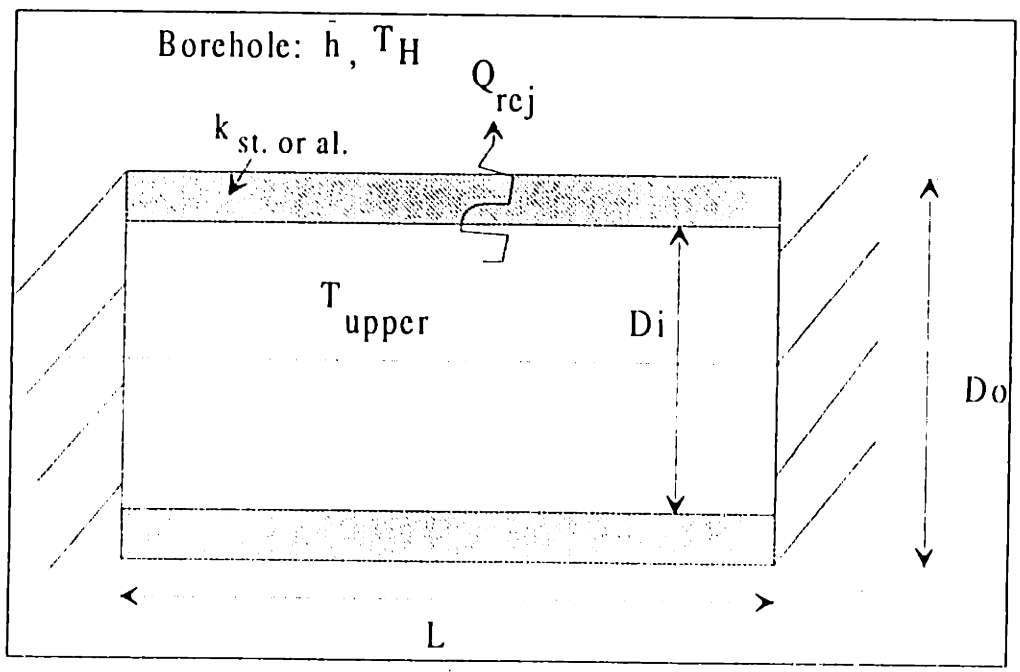

Figure I.1: Hot Heat Exchanger Model Schematic

$$Q_{rej} = \frac{T_{upper} - T_H}{\frac{\ln\left(\frac{Do}{Di}\right)}{2\pi k_{st,al} L} + \frac{1}{\bar{h}\pi DoL}}, \qquad \text{(I-2)}$$

where the variables are defined in Figure I.1. Equation (I-2) can be rearranged to solve for the internal temperature of the upper tank with

$$T_{upper} = Q_{rej}\left[\frac{\ln\left(\frac{Do}{Di}\right)}{2\pi k_{st,al} L} + \frac{1}{\bar{h}\pi DoL}\right] + T_H \; . \qquad \text{(I-3)}$$

Table I.1 lists the variable values for the current system. Table I.2 lists the T_{upper} values required for both the aluminum, al., and stainless steel, st., housings.

Table I.1: Variable Values

Variable	Value
T_H(°C)	200
h_3(kJ/kg)	3334
h_4(kJ/kg)	851
k_{st}(W/m-°C)	13.7
k_{al}(W/m-°C)	200
Do(m)	0.0921
Di(m)	0.0730
L(m)	0.826
$\dot{m}$ (kg/s)	$3.5\text{x}10^{-5}$
$\bar{h}$ (W/m^2-°C)	100

Table I.2: Temperature Results

Variable	Result
T_{upper} for Aluminum (°C)	203.7
T_{upper} for Stainless Steel (°C)	203.9

I.2: Oven Heat Transfer Coefficient

The final tests were performed in an oven at 200°C. Internal to the oven, fans circulate hot air for the purpose of uniform heating. The equivalent heat transfer coefficient of the air in the oven on the surface of the upper tank was required to prove downhole compatibility. In other words, the heat transfer coefficient should be equal to or less than those witnessed in boreholes. The cooling tests were run with a steam mass flowrate equal to $1.3\text{x}10^{-5}$ kg/s resulting in a Q_{rej} value of 33W (see eq.(I-1)). With these

values a T_{upper} of 204°C was required to conduct the heat from within the upper tank through the aluminum housing and into the oven. Rearranging eq.(I-3) and solving for the heat transfer coefficient produces a value for $\bar{h}$ equal to 34W/m^2-°C. This value is approximately one-third of the estimated borehole heat transfer coefficient. Thus, in terms of heat transfer, the oven tests are a conservative but true representation of the borehole environment.

Appendix J: Motor-Power Calibration

To accurately measure input power to the 1/2-HP Dayton DC motor/controller system as a function of current and shaft speed only, it must be calibrated as a function of these parameters. The calibrations were performed with the motor/controller system, dynamometer, current meter, and voltage meter (see Figure J.1). Table J.1 lists the manufacturers and part numbers of the devices. A range of torque values were applied to the motor shaft at speeds of 1250, 1500, 1750, 2000, and 2250rpm. Both current and rms. voltages were measured from the motor controller to the motor. It should be noted that voltage from the controller is a function of the motor current. From the measurements the motor current at specified speeds can be related to the input power of the motor by looking at Table J.2 directly, or linearly interpolating between the test current and speed values. The dynamometer torque values, although consistent, were not accurate. Thus, the motor efficiency at different loads and speeds should not be inferred from the tables.

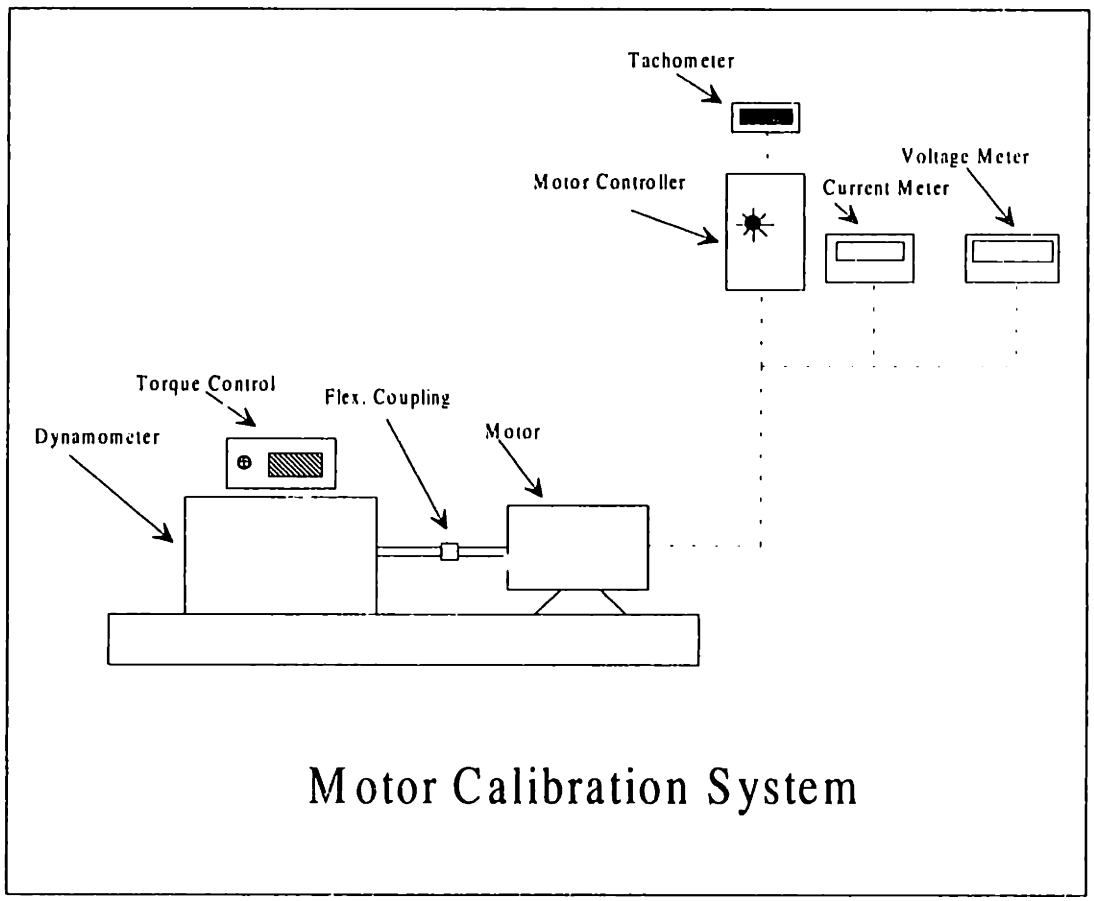

Figure J.1: Motor Power Calibration System

Table J.1: Motor Calibration Components

Device	Description
Motor	1/2 HP Dayton-Permanent Magnet DC Motor #2M168C
Motor Controller	Dayton-DC Speed Controller #47829B
Tachometer	Dart Control Inc., Programmable Tachometer #DM4004
Current Meter	Fluke 77 Series II Multimeter
Voltage Meter	Hewlett Packard Multimeter #34401A
Dynamometer	Magtrol Inc., #HD-700-6 up to 425 in.-oz. Dynamometer
Torque Adjust	Magtrol Inc., #4636
Dynamometer Readout Display	Magtrol Inc., #4618

Table J.2: Motor System Input Power Calibration Table

Speed = 1250 RPM or 131 rad/s			
Approximate Torque (N-m)	Current (Amps)	Voltage (v)	Input Power (W)
0	0.86	19.5	16.8
0.035	0.94	20.5	19.3
0.071	1.04	22	22.9
0.11	1.15	23.4	26.9
0.14	1.24	24.6	30.5
0.18	1.34	25.9	34.7
0.21	1.45	27.2	39.4
0.25	1.5	27.8	41.7
0.28	1.59	28.9	46
Speed = 1500 RPM or 157 rad/s			
Approximate Torque (N-m)	Current (Amps)	Voltage(v)	Input Power (W)
0	0.89	19.8	17.6
0.035	0.98	21	20.6
0.071	1.07	22.3	23.9
0.11	1.17	23.6	27.6
0.14	1.27	24.8	31.5
0.18	1.37	26.1	35.8
0.21	1.47	27.3	40.1
0.25	1.53	28	42.8
0.28	1.62	28.9	46.8
Speed = 1750 RPM or 183 rad/s			

Approximate Torque (N-m)	Current (Amps)	Voltage(v)	Input Power (W)
0	0.9	19.9	17.91
0.035	1	21.2	21.2
0.071	1.08	22.3	24.084
0.11	1.2	23.8	28.56
0.14	1.3	25	32.5
0.18	1.39	26	36.14
0.21	1.49	27	40.23
0.25	1.56	27.8	43.368
0.28	1.65	28.9	47.685
Speed = 2000 RPM or 209 rad/s			
Approximate Torque (N-m)	Current (Amps)	Voltage(v)	Input Power (W)
0	0.93	19.9	18.507
0.035	1.03	21.1	21.733
0.071	1.11	22.1	24.531
0.11	1.2	23.3	27.96
0.14	1.29	24.3	31.347
0.18	1.38	25.1	34.638
0.21	1.48	26.1	38.628
0.25	1.56	27.1	42.276
0.28	1.65	27.8	45.87
Speed = 2250 RPM or 236 rad/s			
Approximate Torque (N-m)	Current (Amps)	Voltage(v)	Input Power (W)
0	0.96	19.4	18.624
0.035	1.05	20.5	21.525
0.071	1.12	21.4	23.968
0.11	1.2	22.2	26.64
0.14	1.29	23.1	29.799
0.18	1.36	23.9	32.504
0.21	1.46	24.7	36.062
0.25	1.53	25.5	39.015
0.28	1.63	26.2	42.706

Appendix K: Part Drawings

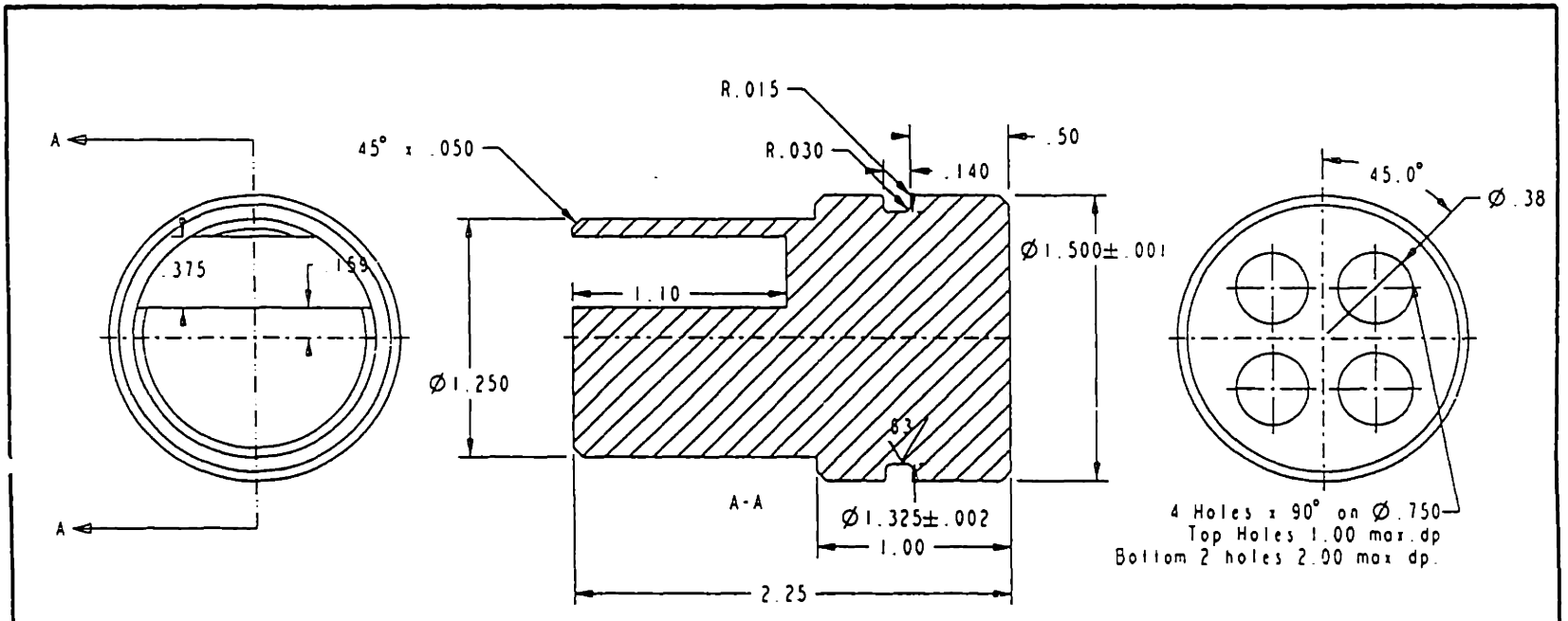

FINISH/TREATMENT		MATERIAL Aluminum
UNLESS SPECIFIED: SURFACE FIN: 125 RMS X=±0.1 XX=±0.01 XXX=±0.005 ANGLES ±0.5 CONCENTRICITY .005 TIR INSIDE CORNERS R.030 MAX BREAK EDGES .005 - .015 DIMS INCLUDE FINISH	CONFIDENTIAL AND TRADE SECRET DO NOT DISCLOSE USE OR REPRODUCE WITHOUT PRIOR WRITTEN APPROVAL FROM SCHLUMBERGER	Schlumberger Well Services Houston Product Center
	Lower Tank Insert Piece	
	DRWN A Flores 28-Mar-96	LOWTANKINS AA
	APPD	
	APPD	
	SCALE 2.000 SZ D SHT 1 OF 1	

Pro/ENGINEER

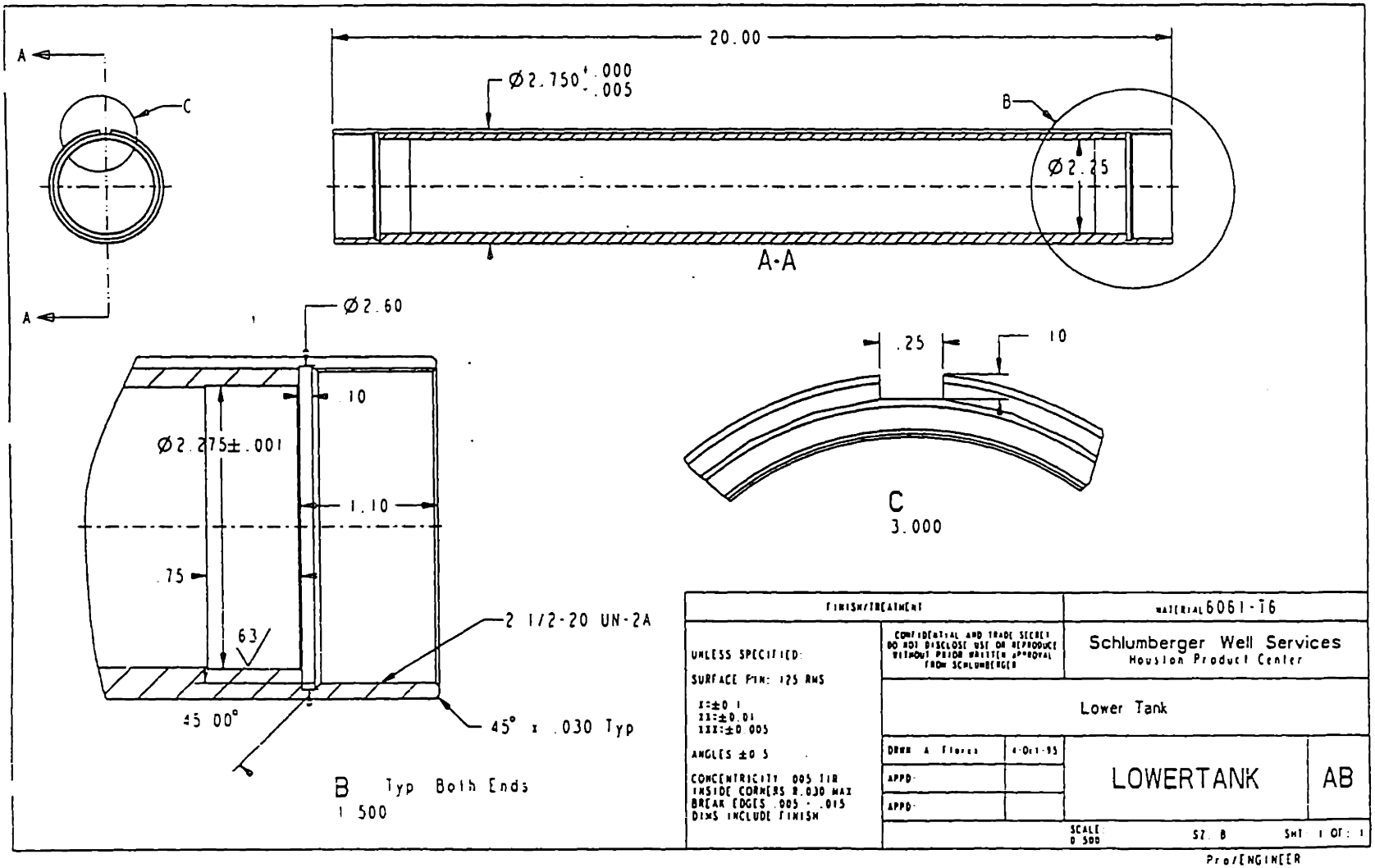
A
A
C
20.00
Ø2.750 +.000 -.005
B
Ø2.25
A-A
Ø2.60
.10
Ø2.275±.001
1.10
.75
63
2 1/2-20 UN-2A
45 00°
45° x .030 Typ
B Typ Both Ends
1 500
.25
.10
C
3.000
FINISH/TREATMENT
MATERIAL 6061-T6
UNLESS SPECIFIED:
SURFACE FIN: 125 RMS
X=±0.1
XX=±0.01
XXX=±0.005
ANGLES ±0.5
CONCENTRICITY .005 TIR
INSIDE CORNERS R.030 MAX
BREAK EDGES .005 - .015
DIMS INCLUDE FINISH
CONFIDENTIAL AND TRADE SECRET DO NOT DISCLOSE NOT OR REPRODUCE WITHOUT PRIOR WRITTEN APPROVAL FROM SCHLUMBERGER
Schlumberger Well Services
Houston Product Center
Lower Tank
DRWN A Flores
4-Oct-95
APPD
APPD
LOWERTANK
AB
SCALE: 0.500
SZ B
SHT 1 OF 1
Pro/ENGINEER

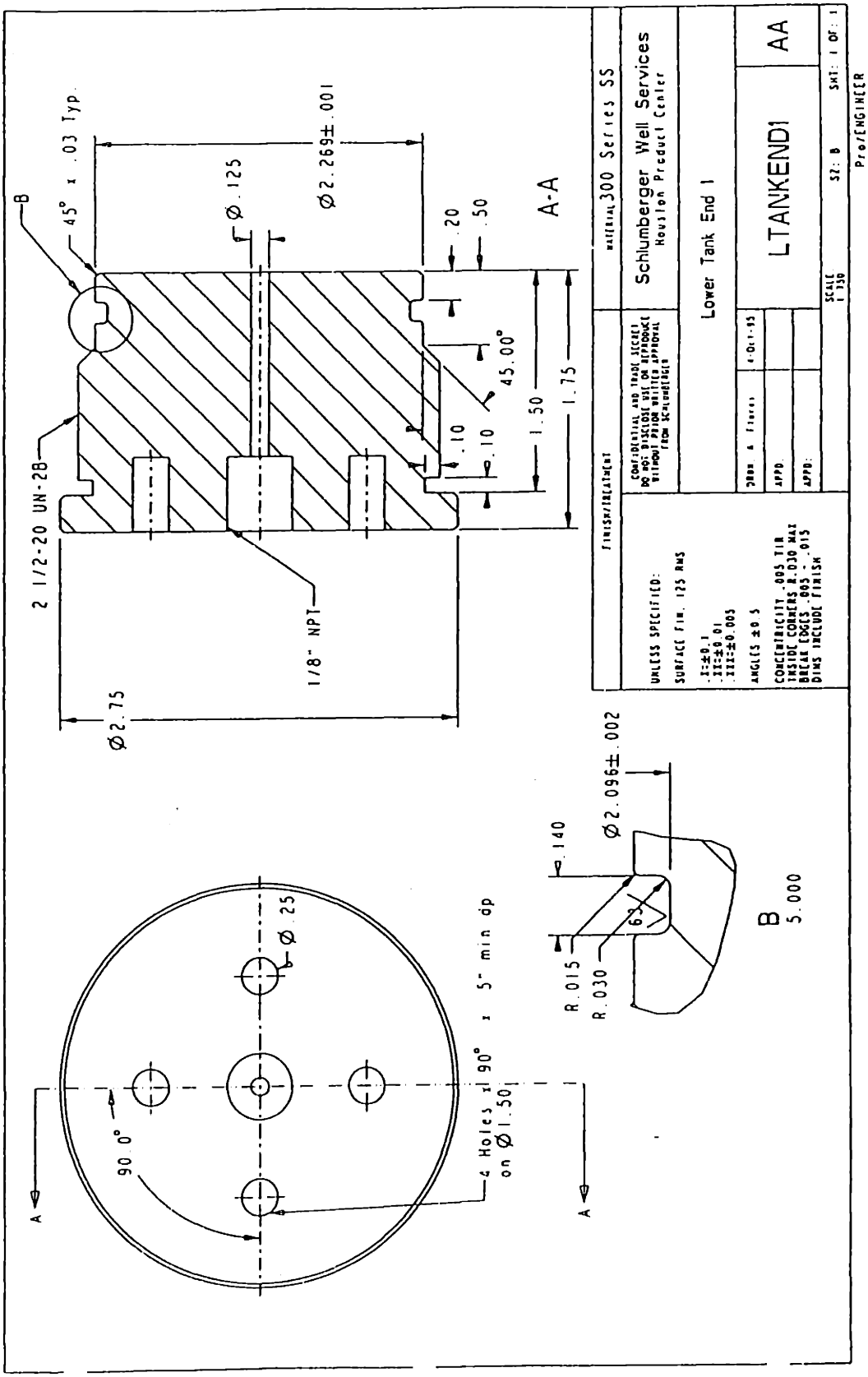
B
45° x .03 Typ
2 1/2-20 UN-2B
1/8" NPT
Ø2.75
Ø.125
Ø2.269±.001
.20
.50
45.00°
.10
.10
1.50
1.75
A-A
Ø2.096±.002
.140
R.015
R.030
60°
B
5.000
A
A
90 0°
Ø .25
4 Holes at 90° x 5" min dp
on Ø1.50
MATERIAL 300 Series SS
Schlumberger Well Services
Houston Product Center
Lower Tank End 1
LTANKEND1
AA
SCALE 1:10
SIZE: B
SHT: 1 OF: 1
Pro/ENGINEER

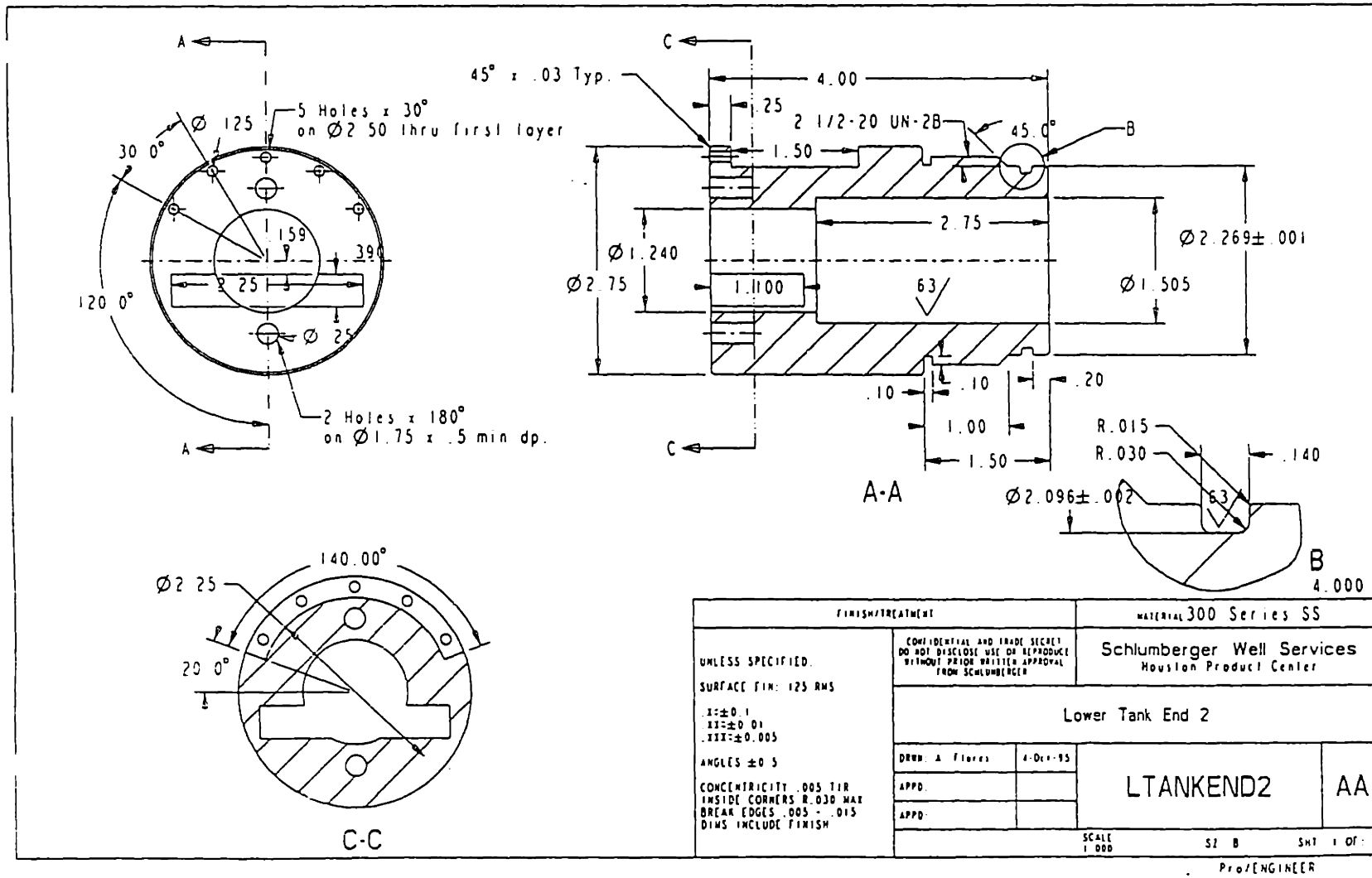

FINISH/TREATMENT		MATERIAL 300 Series SS
UNLESS SPECIFIED. SURFACE FIN: 125 RMS .X=±0.1 .XX=±0.01 .XXX=±0.005 ANGLES ±0 5 CONCENTRICITY .005 TIR INSIDE CORNERS R.030 MAX BREAK EDGES .005 - .015 DIMS INCLUDE FINISH	CONFIDENTIAL AND TRADE SECRET DO NOT DISCLOSE USE OR REPRODUCE WITHOUT PRIOR WRITTEN APPROVAL FROM SCHLUMBERGER	Schlumberger Well Services Houston Product Center
		Lower Tank End 2
	DRWN. A Flores 4-Dec-95 APPD. APPD.	LTANKEND2 AA
		SCALE 1.000 SZ B SHT 1 OF 1

Pro/ENGINEER

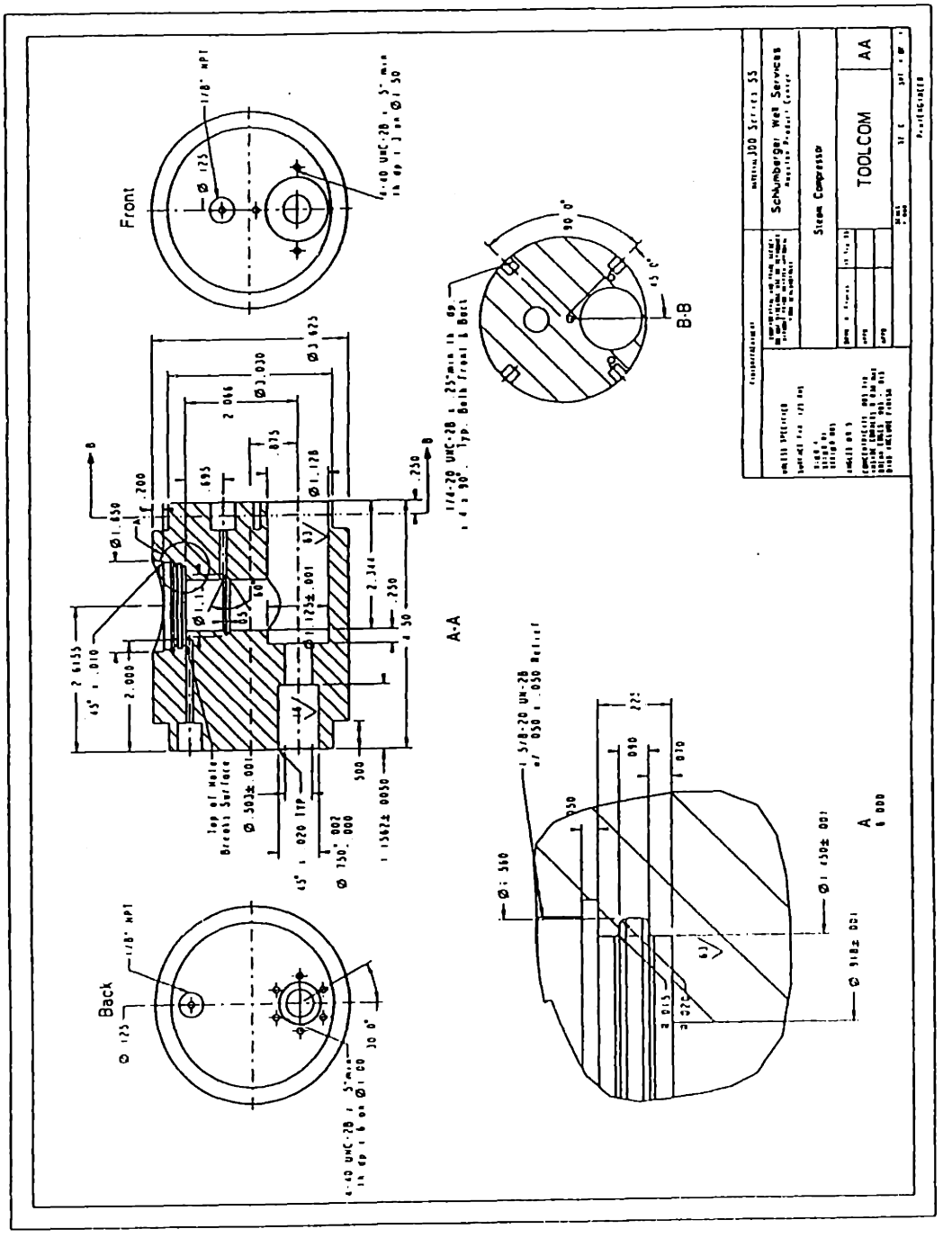
Front
Back
A-A
B-B
A
Schlumberger Well Services
Steam Compressor
TOOLCOM
AA

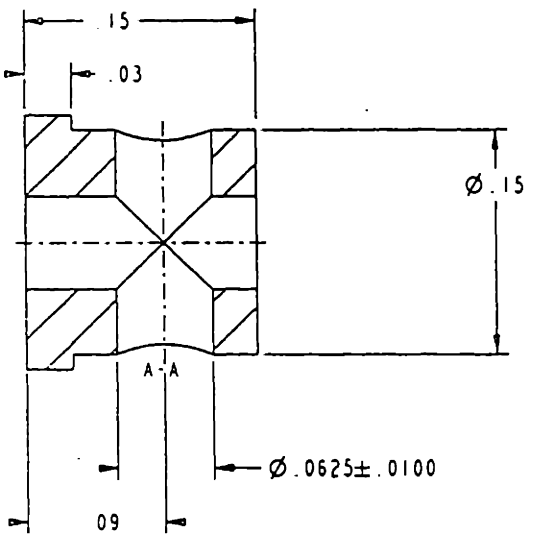

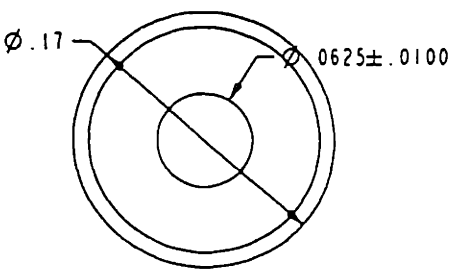

FINISH/TREATMENT		MATERIAL 6061-T6
UNLESS SPECIFIED: SURFACE FIN: 125 RMS .X=±0.1 .XX=±0.01 .XXX=±0.005 ANGLES ±0.5 CONCENTRICITY .005 TIR INSIDE CORNERS R.030 MAX BREAK EDGES .005 - .015 DIMS INCLUDE FINISH	CONFIDENTIAL AND TRADE SECRET DO NOT DISCLOSE USE OR REPRODUCE WITHOUT PRIOR WRITTEN APPROVAL FROM SCHLUMBERGER	Schlumberger Well Services Houston Product Center
		Lee Spacer
	DRWN: A. Flores 19-Sep-95 APPD: APPD:	LEESPACER AA
	SCALE: 15.000 SZ: B	SHT: 1 OF: 1

Pro/ENGINEER

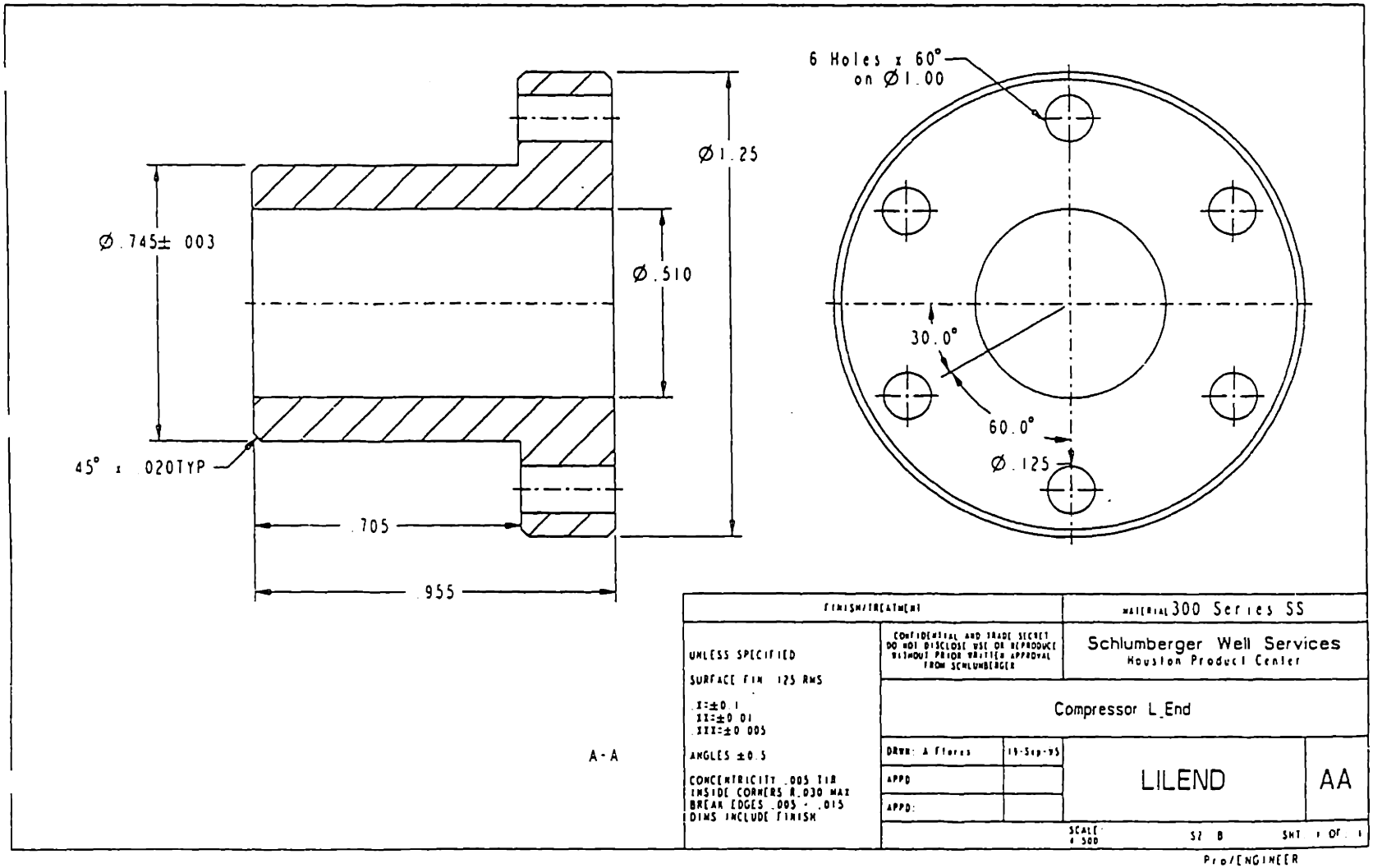
6 Holes x 60°
on Ø1.00
Ø1.25
Ø.745± 003
Ø.510
30.0°
60.0°
Ø.125
45° x .020TYP
.705
.955
A-A
FINISH/TREATMENT
UNLESS SPECIFIED
SURFACE FIN 125 RMS
X=±0.1
XX=±0.01
XXX=±0.005
ANGLES ±0.5
CONCENTRICITY .005 TIR
INSIDE CORNERS R.030 MAX
BREAK EDGES .005 - .015
DIMS INCLUDE FINISH
MATERIAL 300 Series SS
CONFIDENTIAL AND TRADE SECRET
DO NOT DISCLOSE USE OR REPRODUCE
WITHOUT PRIOR WRITTEN APPROVAL
FROM SCHLUMBERGER
Schlumberger Well Services
Houston Product Center
Compressor L_End
DRWN: A Flores
19-Sep-95
APPD
APPD:
LILEND
AA
SCALE: 1.500
SZ B
SHT 1 OF 1
Pro/ENGINEER

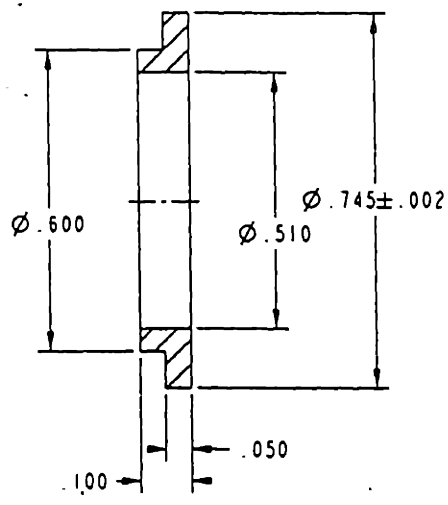

A-A

FINISH/TREATMENT		MATERIAL 300 Series SS
UNLESS SPECIFIED: SURFACE FIN: 125 RMS .X=±0.1 .XX=±0.01 .XXX=±0.005 ANGLES ±0.5 CONCENTRICITY .005 TIR INSIDE CORNERS R.030 MAX BREAK EDGES .005 - .015 DIMS INCLUDE FINISH	CONFIDENTIAL AND TRADE SECRET DO NOT DISCLOSE USE OR REPRODUCE WITHOUT PRIOR WRITTEN APPROVAL FROM SCHLUMBERGER	Schlumberger Well Services Houston Product Center
		Seal Spacer
	DRWN: A. Flores 20-Sep-95	BEARINGSP AA
	APPD:	
	APPD:	
	SCALE 5.000 SZ B SHT 1 OF 1	

Pro/ENGINEER

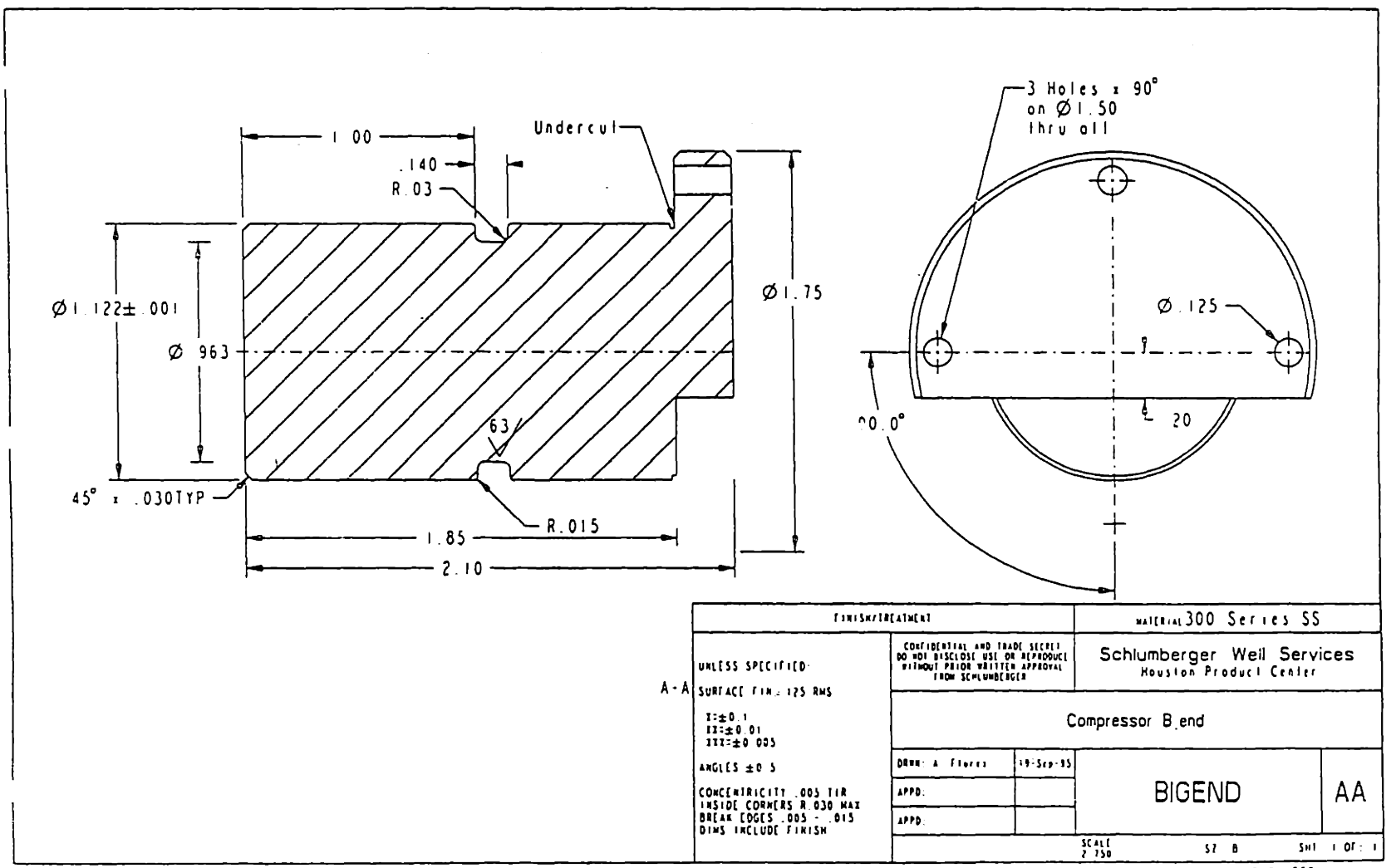

FINISH/TREATMENT		MATERIAL 300 Series SS
UNLESS SPECIFIED SURFACE FIN. 125 RMS X=±0.1 XX=±0.01 XXX=±0.005 ANGLES ±0.5 CONCENTRICITY .005 TIR INSIDE CORNERS R.030 MAX BREAK EDGES .005 - .015 DIMS INCLUDE FINISH	CONFIDENTIAL AND TRADE SECRET DO NOT DISCLOSE USE OR REPRODUCE WITHOUT PRIOR WRITTEN APPROVAL FROM SCHLUMBERGER	Schlumberger Well Services Houston Product Center
A-A	Compressor B.end	
	DRWN: A. Flores 19-Sep-95	BIGEND AA
	APPD:	
	APPD:	
	SCALE 2.750 SZ B SHT 1 OF 1	

Pro/ENGINEER

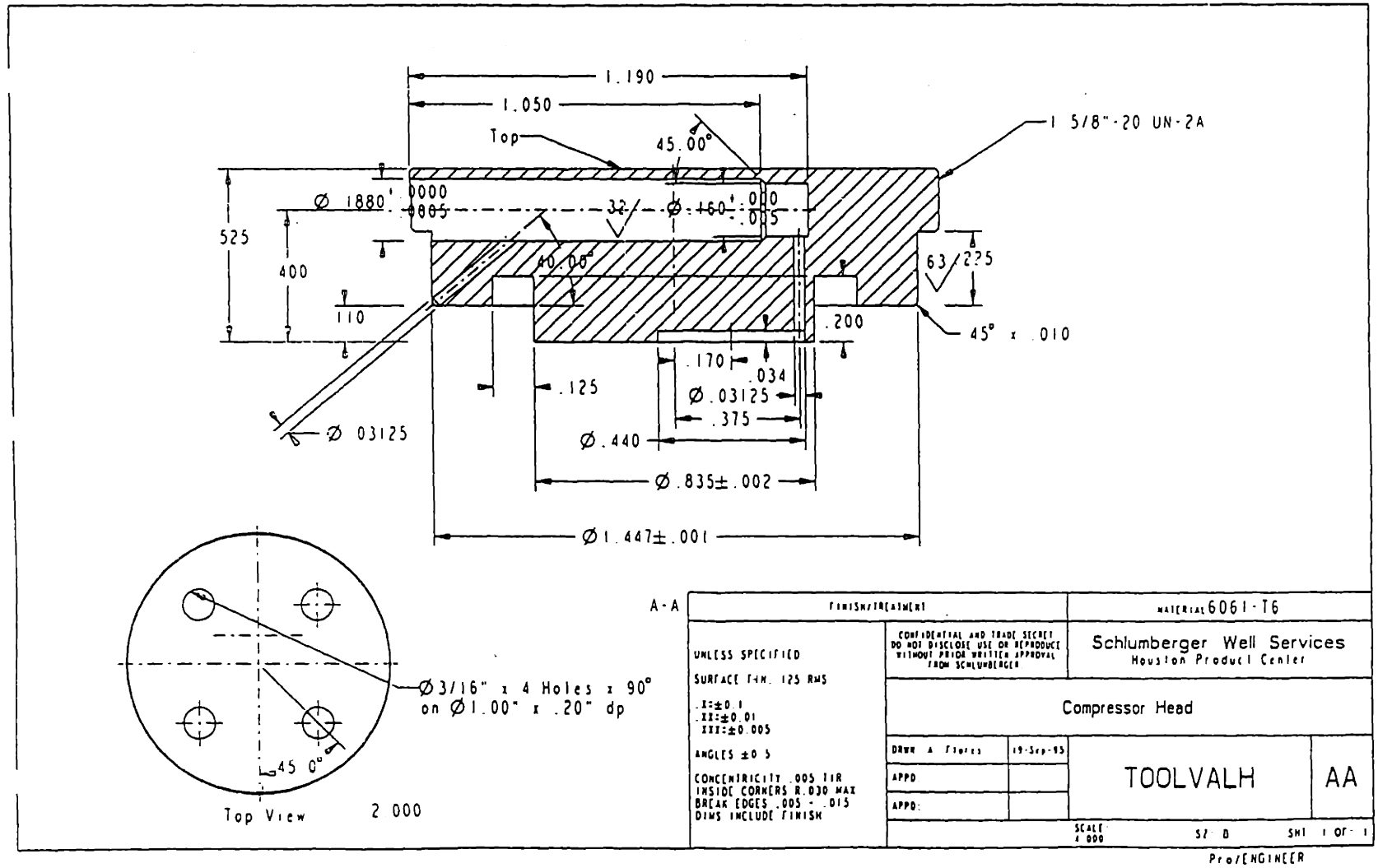
1.190
1.050
Top
45.00°
1 5/8"-20 UN-2A
Ø 1880
525
400
110
40.00°
63/
.200
45° x .010
.170
.034
.125
Ø .03125
.375
Ø .03125
Ø .440
Ø .835±.002
Ø1.447±.001
A-A
Ø3/16" x 4 Holes x 90°
on Ø1.00" x .20" dp
45.0°
Top View
2.000
FINISH/MATERIAL
MATERIAL 6061-T6
UNLESS SPECIFIED
SURFACE FIN. 125 RMS
.X=±0.1
.XX=±0.01
.XXX=±0.005
ANGLES ±0.5
CONCENTRICITY .005 TIR
INSIDE CORNERS R.030 MAX
BREAK EDGES .005 - .015
DIMS INCLUDE FINISH
CONFIDENTIAL AND TRADE SECRET
DO NOT DISCLOSE USE OR REPRODUCE
WITHOUT PRIOR WRITTEN APPROVAL
FROM SCHLUMBERGER
Schlumberger Well Services
Houston Product Center
Compressor Head
DRWN A Flores
19-Sep-95
APPD
APPD
TOOLVALH
AA
SCALE
1.000
SZ B
SHT 1 OF 1
Pro/ENGINEER

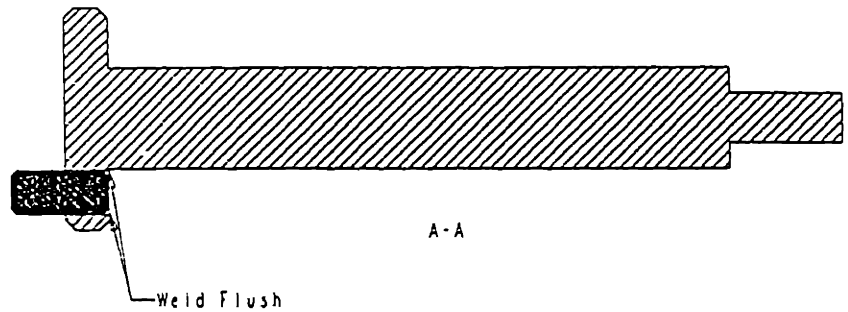

FINISH/TREATMENT		MATERIAL
UNLESS SPECIFIED: SURFACE FIN: 125 RMS .X=±0.1 .XX=±0.01 .XXX=±0.005 ANGLES ±0.5 CONCENTRICITY .005 TIR INSIDE CORNERS R.030 MAX BREAK EDGES .005 - .015 DIMS INCLUDE FINISH	CONFIDENTIAL AND TRADE SECRET DO NOT DISCLOSE USE OR REPRODUCE WITHOUT PRIOR WRITTEN APPROVAL FROM SCHLUMBERGER	Schlumberger Well Services Houston Product Center
		Cam -Shaft
	DRWN: A. Flores 7-Sep-95	CAM AA
	APPD:	
	APPD:	
	SCALE: 2.000 SZ: B SHT: 1 OF: 1	

Pro/ENGINEER

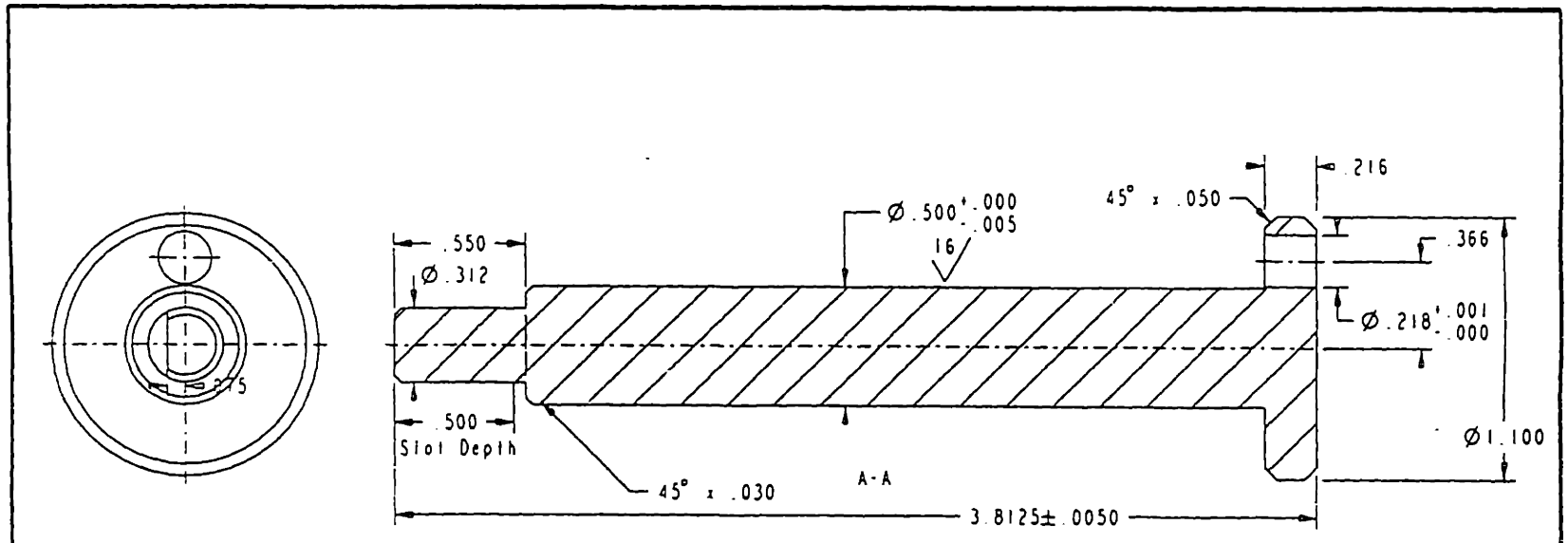

FINISH/TREATMENT		MATERIAL 4340 Rc 45-55
UNLESS SPECIFIED SURFACE FIN 125 RMS X=±0.1 XX=±0.01 XXX=±0.005 ANGLES ±0.5 CONCENTRICITY .005 TIR INSIDE CORNERS R.030 MAX BREAK EDGES .005 - .015 DIMS INCLUDE FINISH	CONFIDENTIAL AND TRADE SECRET DO NOT DISCLOSE USE OR REPRODUCE WITHOUT PRIOR WRITTEN APPROVAL FROM SCHLUMBERGER	Schlumberger Well Services Houston Product Center
		Cam Shaft
	DRWN A Flores 6-Sep-95	CAMSHAFT AA
	APPD	
	APPD	
	SCALE 2.500 SZ B	SHT 1 OF 1

Pro/ENGINEER

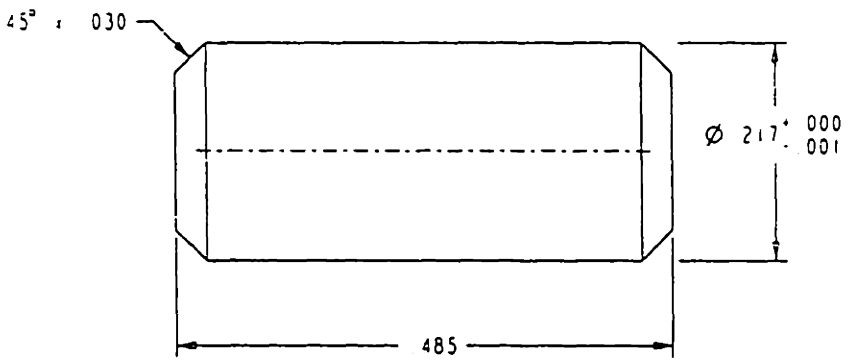

FINISH/TREATMENT		MATERIAL: AISI 630 COND H-1025
UNLESS SPECIFIED SURFACE FIN 125 RMS X: ±0.1 XX: ±0.01 XXX: ±0.005 ANGLES ±0.5 CONCENTRICITY .005 TIR INSIDE CORNERS R .030 MAX BREAK EDGES .005 - .015 DIMS INCLUDE FINISH	CONFIDENTIAL AND TRADE SECRET DO NOT DISCLOSE, USE OR REPRODUCE WITHOUT PRIOR WRITTEN APPROVAL FROM SCHLUMBERGER	Schlumberger Well Services Houston Product Center
		Pin
	DRWN A. Flores 6 Sep 95	PIN AA
	APPD	
	APPD	
	SCALE 10.000 SZ B	SHT 1 OF 1

PROPRIETARY

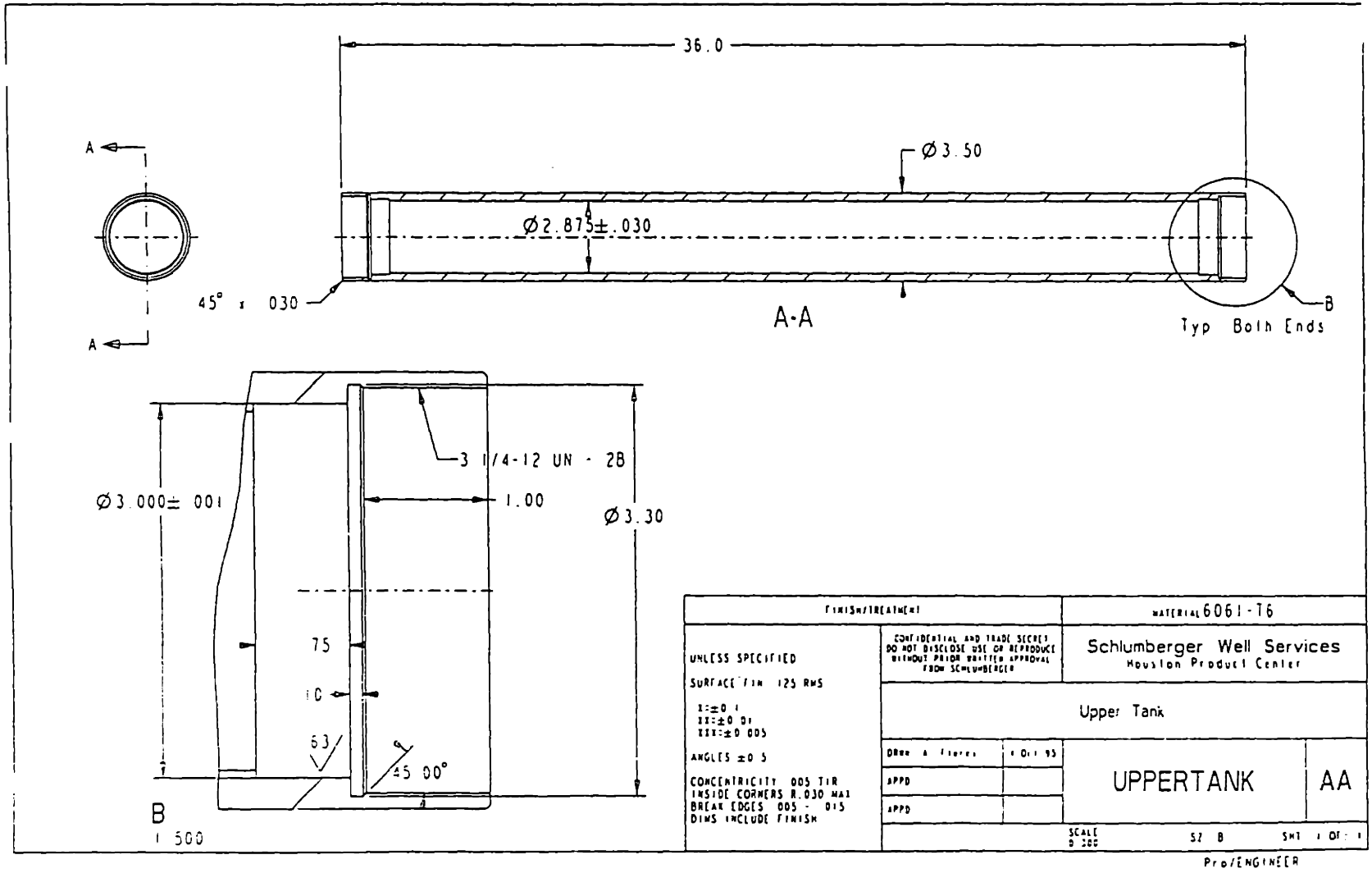
36.0
Ø3.50
Ø2.875±.030
45° x .030
A-A
Typ Both Ends
A
A
B
3 1/4-12 UN - 2B
Ø3.000± .001
1.00
Ø3.30
75
10
63
45.00°
B
1.500
FINISH/TREATMENT
MATERIAL 6061-T6
UNLESS SPECIFIED
SURFACE FIN 125 RMS
X=±0.1
XX=±0.01
XXX=±0.005
ANGLES ±0.5
CONCENTRICITY .005 TIR
INSIDE CORNERS R.030 MAX
BREAK EDGES .005 - .015
DIMS INCLUDE FINISH
CONFIDENTIAL AND TRADE SECRET
DO NOT DISCLOSE USE OR REPRODUCE
WITHOUT PRIOR WRITTEN APPROVAL
FROM SCHLUMBERGER
Schlumberger Well Services
Houston Product Center
Upper Tank
DRWN A Flores
4 Oct 93
APPD
APPD
UPPERTANK
AA
SCALE
0.100
SZ B
SHT 1 OF 1
Pro/ENGINEER

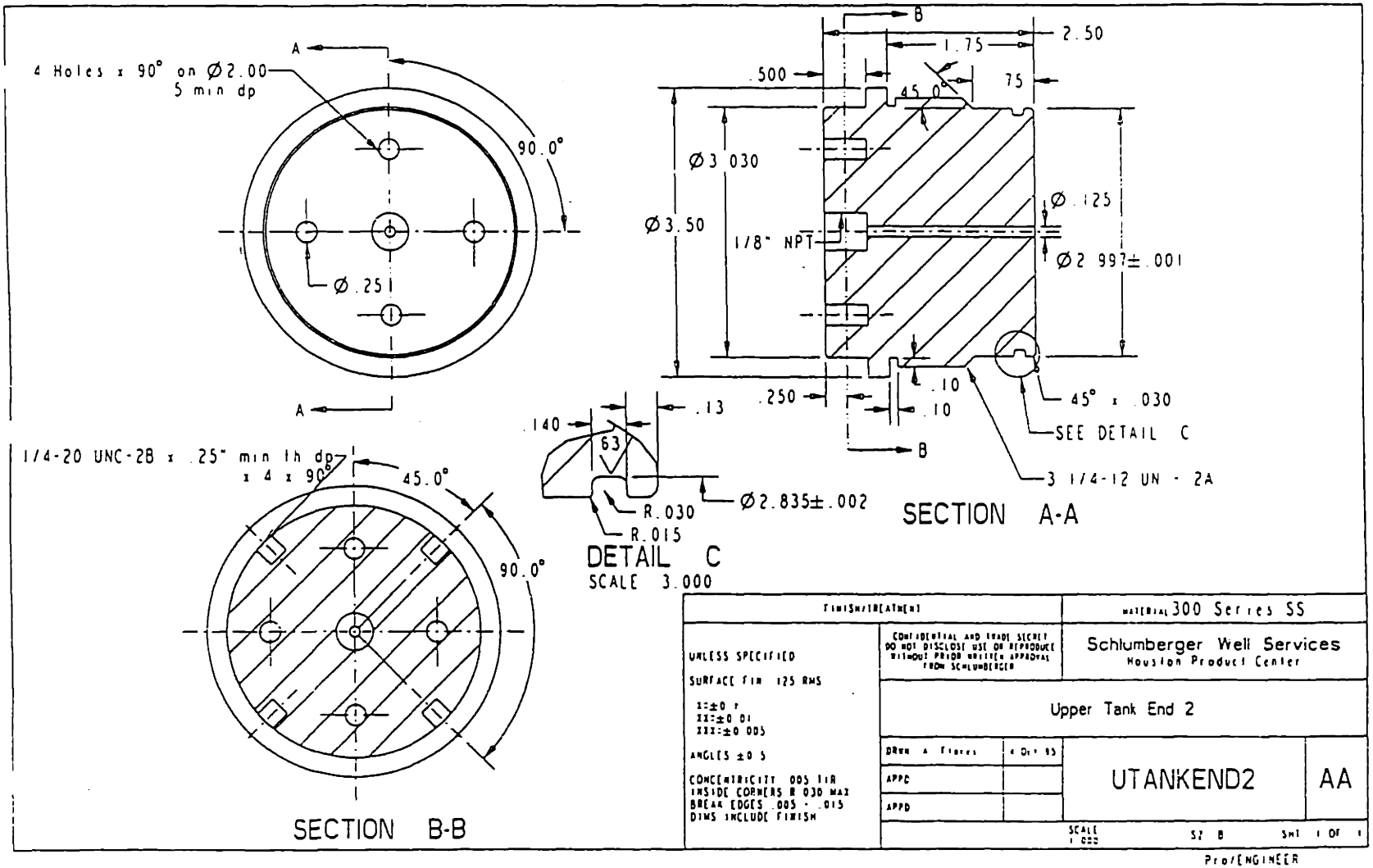
4 Holes x 90° on Ø2.00
5 min dp
A
90.0°
Ø.25
A
1/4-20 UNC-2B x .25" min th dp
x 4 x 90°
45.0°
90.0°
SECTION B-B
B
2.50
1.75
.500
.75
45.0°
Ø3.030
Ø3.50
1/8" NPT
Ø.125
Ø2.997±.001
.10
.250
.10
45° x .030
SEE DETAIL C
3 1/4-12 UN - 2A
B
SECTION A-A
.140
.13
63
R.030
R.015
Ø2.835±.002
DETAIL C
SCALE 3.000
FINISH/TREATMENT
MATERIAL 300 Series SS
UNLESS SPECIFIED
SURFACE FIN 125 RMS
X=±0.1
XX=±0.01
XXX=±0.005
ANGLES ±0.5
CONCENTRICITY .005 TIR
INSIDE CORNERS R.030 MAX
BREAK EDGES .005 - .015
DIMS INCLUDE FINISH
CONFIDENTIAL AND TRADE SECRET
DO NOT DISCLOSE USE OR REPRODUCE
WITHOUT PRIOR WRITTEN APPROVAL
FROM SCHLUMBERGER
Schlumberger Well Services
Houston Product Center
Upper Tank End 2
DRWN A Flores 4 Oct 95
APPD
APPD
UTANKEND2
AA
SCALE 1.000
SZ B
SHT 1 OF 1
Pro/ENGINEER

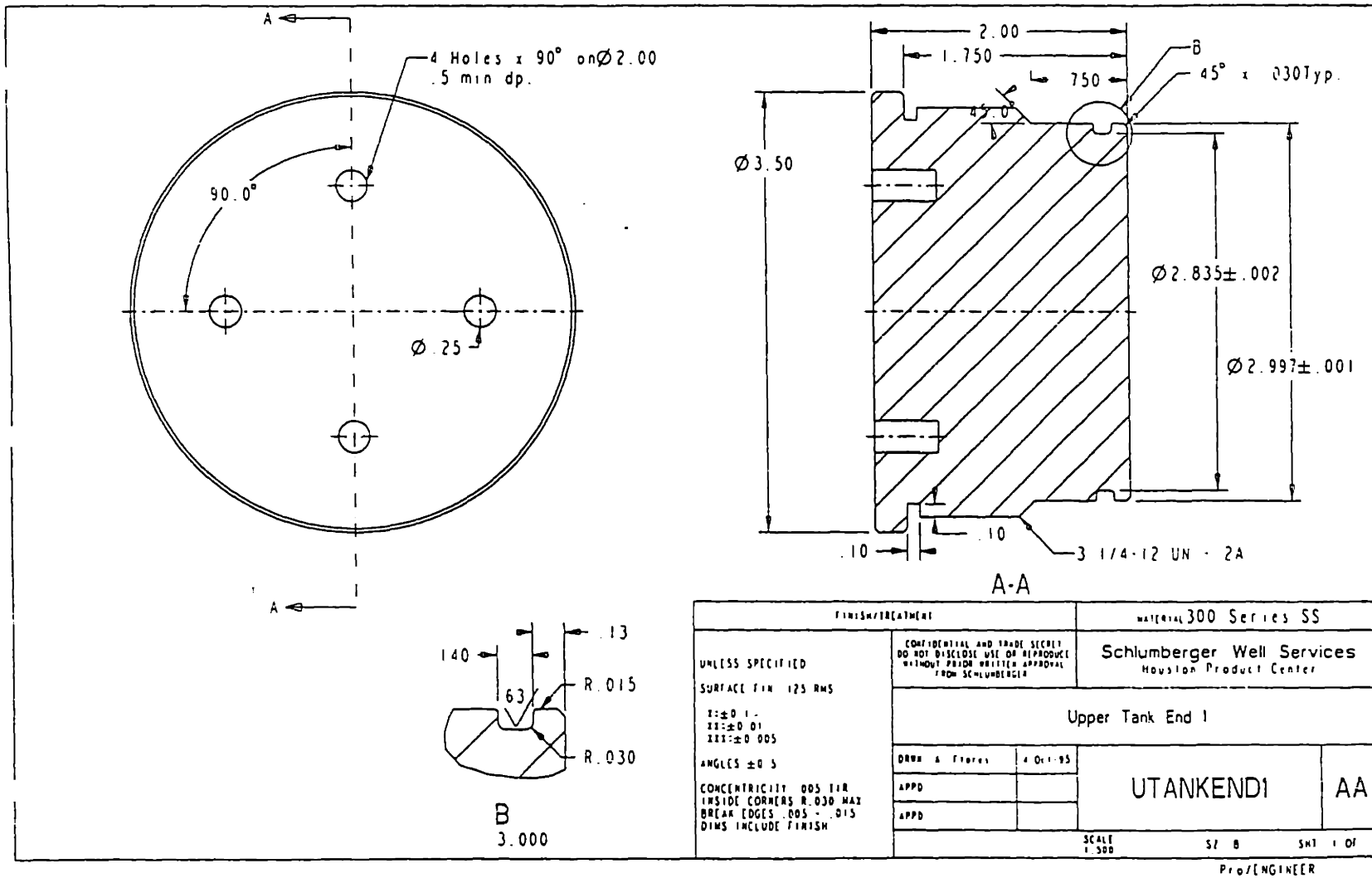
A
4 Holes x 90° on Ø2.00
.5 min dp.
90.0°
Ø .25
A
2.00
1.750
.750
45.0°
B
45° x .030 Typ.
Ø3.50
Ø2.835±.002
Ø2.997±.001
.10
.10
3 1/4-12 UN - 2A
A-A
.13
140
63
R.015
R.030
B
3.000
FINISH/TREATMENT
MATERIAL 300 Series SS
UNLESS SPECIFIED
SURFACE FIN 125 RMS
X:±0.1
XX:±0.01
XXX:±0.005
ANGLES ±0.5
CONCENTRICITY .005 TIR
INSIDE CORNERS R.030 MAX
BREAK EDGES .005 - .015
DIMS INCLUDE FINISH
CONFIDENTIAL AND TRADE SECRET
DO NOT DISCLOSE USE OR REPRODUCE
WITHOUT PRIOR WRITTEN APPROVAL
FROM SCHLUMBERGER
Schlumberger Well Services
Houston Product Center
Upper Tank End 1
DRWN A Flores
4 Oct-95
APPD
APPD
UTANKEND1
AA
SCALE 1.500
SZ B
SHT 1 OF 1
Pro/ENGINEER

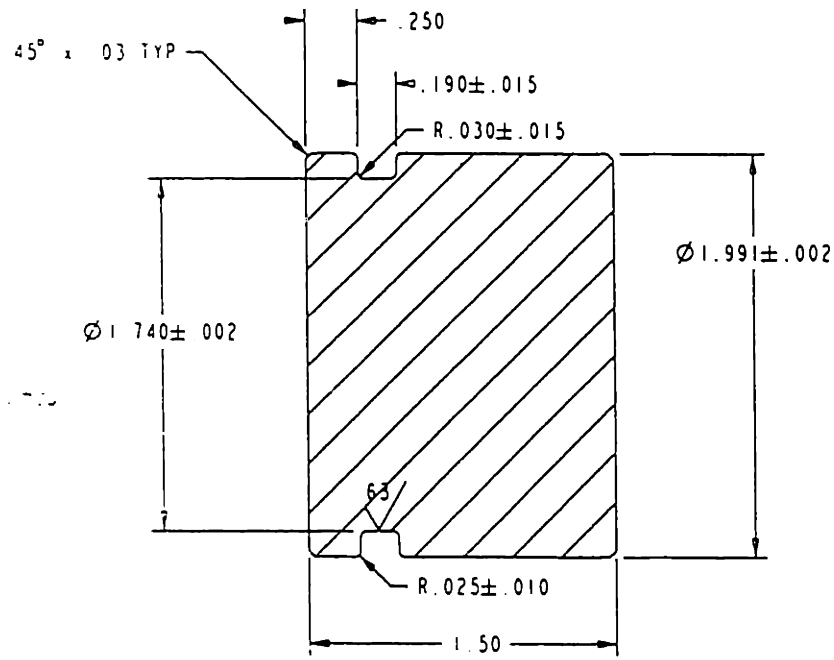

A-A

FINISH/TREATMENT		MATERIAL 6061-16
UNLESS SPECIFIED: SURFACE FIN 125 RMS .X=±0.1 .XX=±0.01 .XXX=±0.005 ANGLES ±0.5 CONCENTRICITY .005 TIR INSIDE CORNERS R.030 MAX BREAK EDGES .005 - .015 DIMS INCLUDE FINISH	CONFIDENTIAL AND TRADE SECRET DO NOT DISCLOSE USE OR REPRODUCE WITHOUT PRIOR WRITTEN APPROVAL FROM SCHLUMBERGER	Schlumberger Well Services Houston Product Center
		Bottom Piston
	DRWN: A. Flores 30-Aug-95	BPISTON AA
	APPD:	
	APPD:	
	SCALE: 2.000 SZ: B	SHT: 1 OF: 1

PROJ ENGINEER

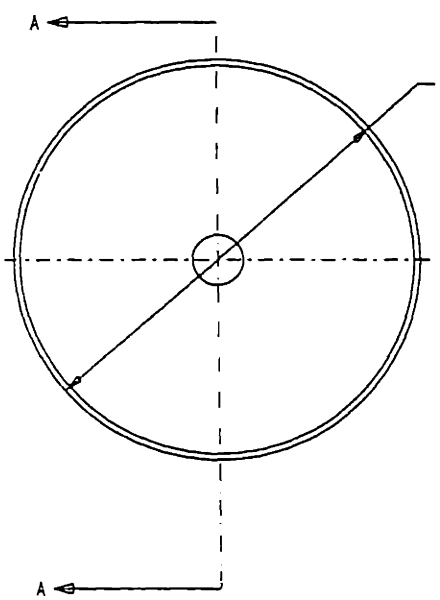

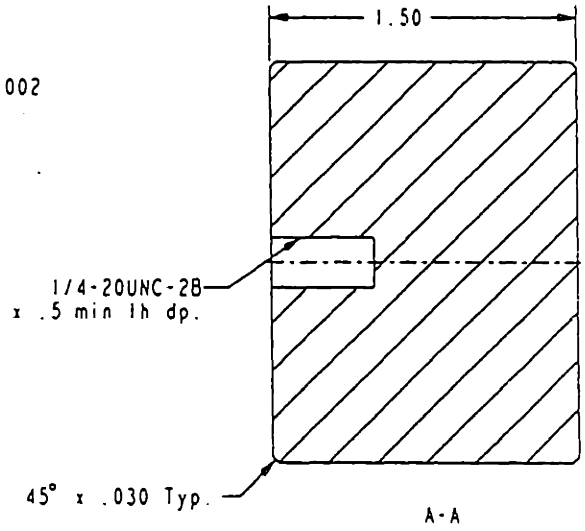

FINISH/TREATMENT		MATERIAL 6061-T6
UNLESS SPECIFIED: SURFACE FIN: 125 RMS .X=±0.1 .XX=±0.01 .XXX=±0.005 ANGLES ±0.5 CONCENTRICITY .005 TIR INSIDE CORNERS R.030 MAX BREAK EDGES .005 - .015 DIMS INCLUDE FINISH	CONFIDENTIAL AND TRADE SECRET DO NOT DISCLOSE USE OR REPRODUCE WITHOUT PRIOR WRITTEN APPROVAL FROM SCHLUMBERGER	Schlumberger Well Services Houston Product Center
		Spring Spacer
	DRWN: A. Flores 5-Oct-95	SPRINGSPACER AA
	APPD:	
	APPD:	
	SCALE: 2.000 SZ: B SHT: 1 OF: 1	

Pro/ENGINEER

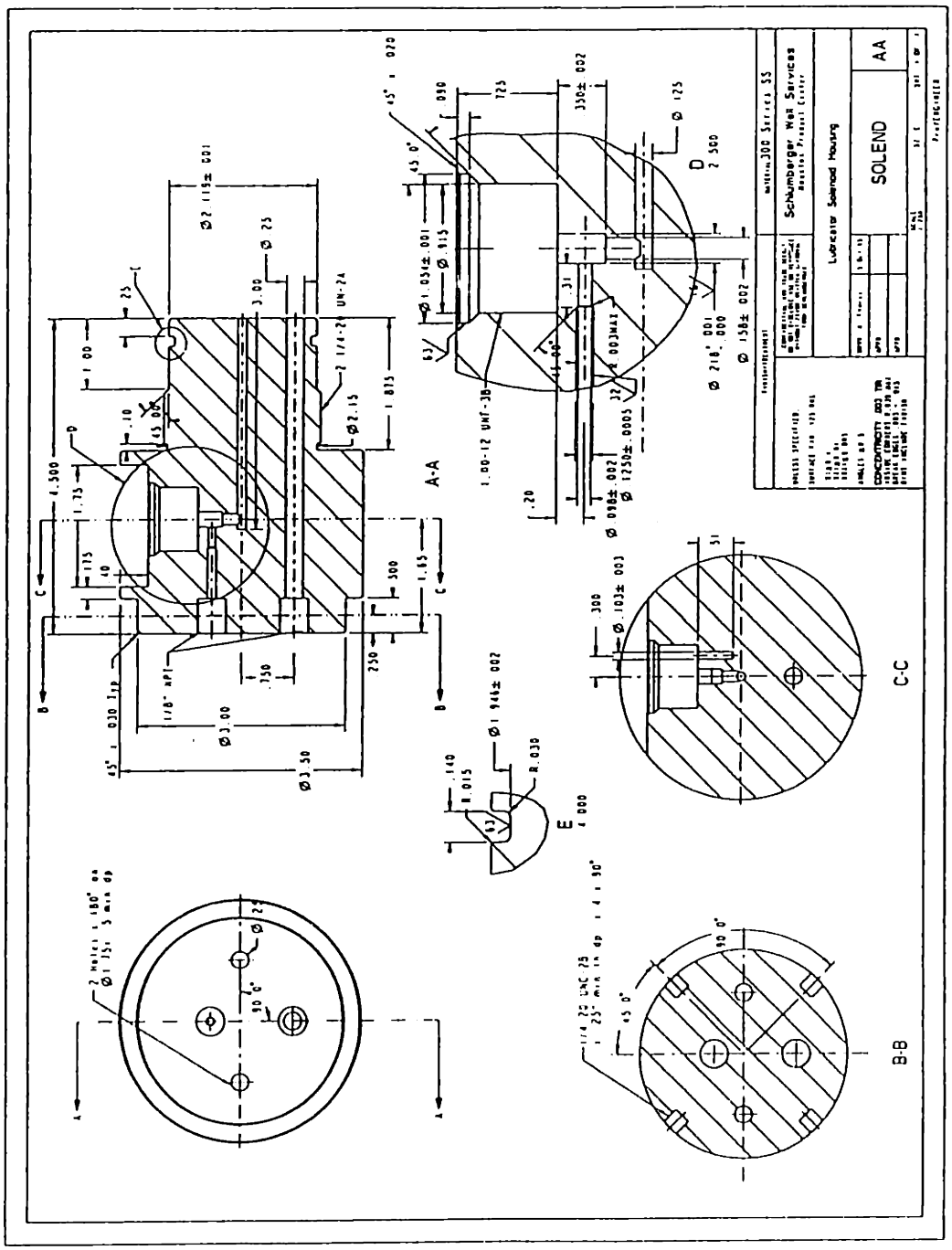
A-A
B-B
C-C
D
E
SOLEND
AA
Schlumberger Well Services
Lubricator Solenoid Housing

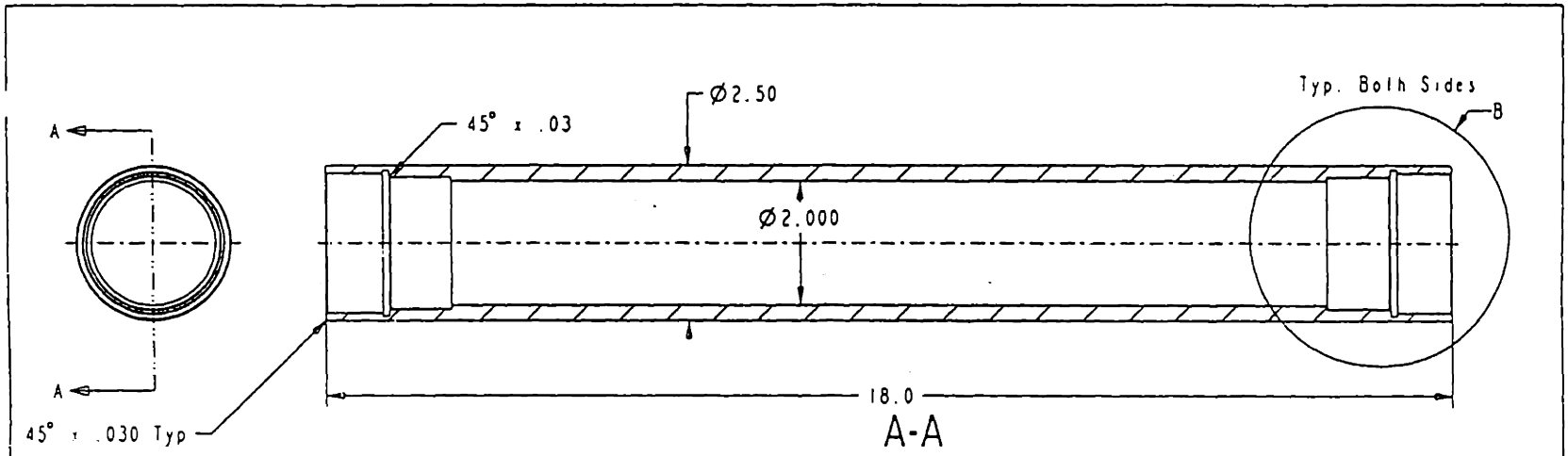

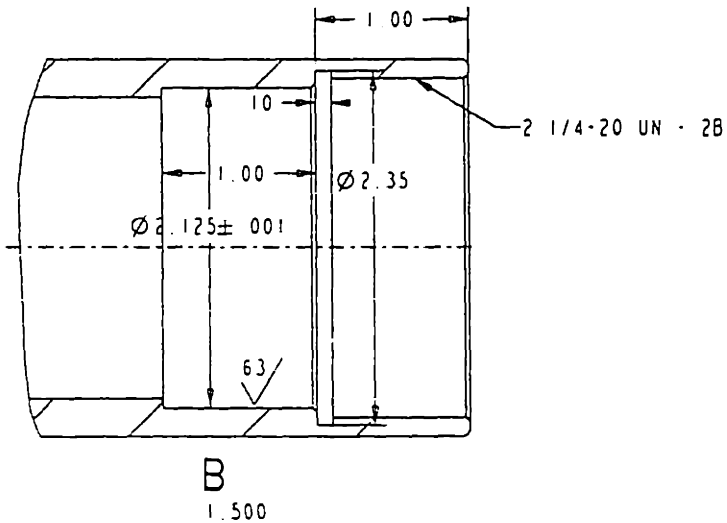

FINISH/TREATMENT		MATERIAL 6061-T6
UNLESS SPECIFIED: SURFACE FIN: 125 RMS X=±0.1 XX=±0.01 .XXX=±0.005 ANGLES ±0.5 CONCENTRICITY .005 TIR INSIDE CORNERS R.030 MAX BREAK EDGES .005 - .015 DIMS INCLUDE FINISH	CONFIDENTIAL AND TRADE SECRET DO NOT DISCLOSE USE OR REPRODUCE WITHOUT PRIOR WRITTEN APPROVAL FROM SCHLUMBERGER	Schlumberger Well Services Houston Product Center
		Lubrication Tube
	DRWN: A Flores 5-Oct-95 APPD: APPD:	LUBETUBE AA
	SCALE 0.650 SZ: B	SHT: 1 OF: 1

Pro/ENGINEER

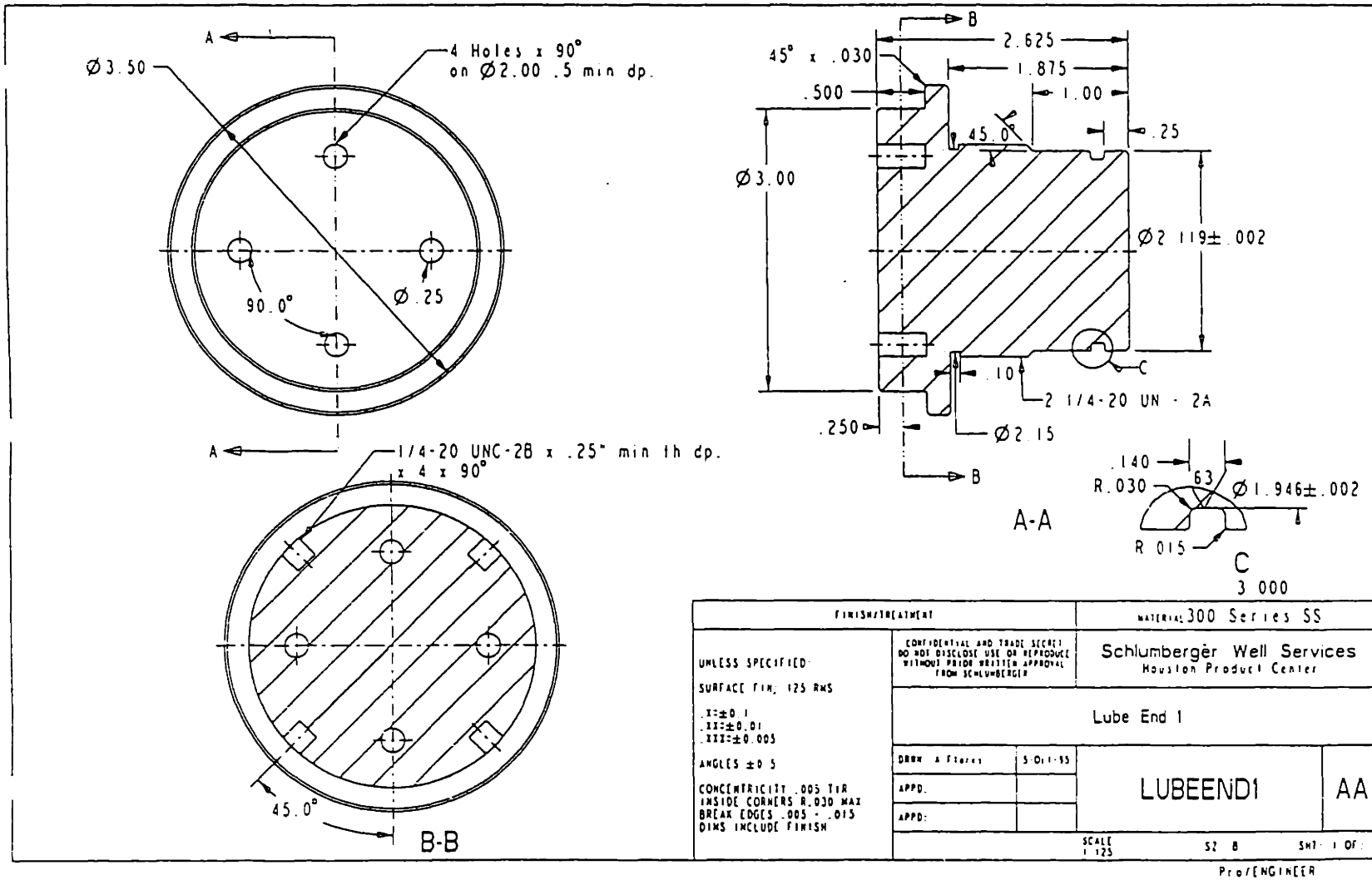

FINISH/TREATMENT		MATERIAL 300 Series SS
UNLESS SPECIFIED SURFACE FIN. 125 RMS .X=±0.1 .XX=±0.01 .XXX=±0.005 ANGLES ±0.5 CONCENTRICITY .005 TIR INSIDE CORNERS R.030 MAX BREAK EDGES .005 - .015 DIMS INCLUDE FINISH	CONFIDENTIAL AND TRADE SECRET DO NOT DISCLOSE USE OR REPRODUCE WITHOUT PRIOR WRITTEN APPROVAL FROM SCHLUMBERGER	Schlumbergèr Well Services Houston Product Center
		Lube End 1
	DRWN A Flores 5-Oct-95	LUBEEND1 AA
	APPD.	
	APPD:	
	SCALE 1:125 SZ B	SHT 1 OF 1

Pro/ENGINEER

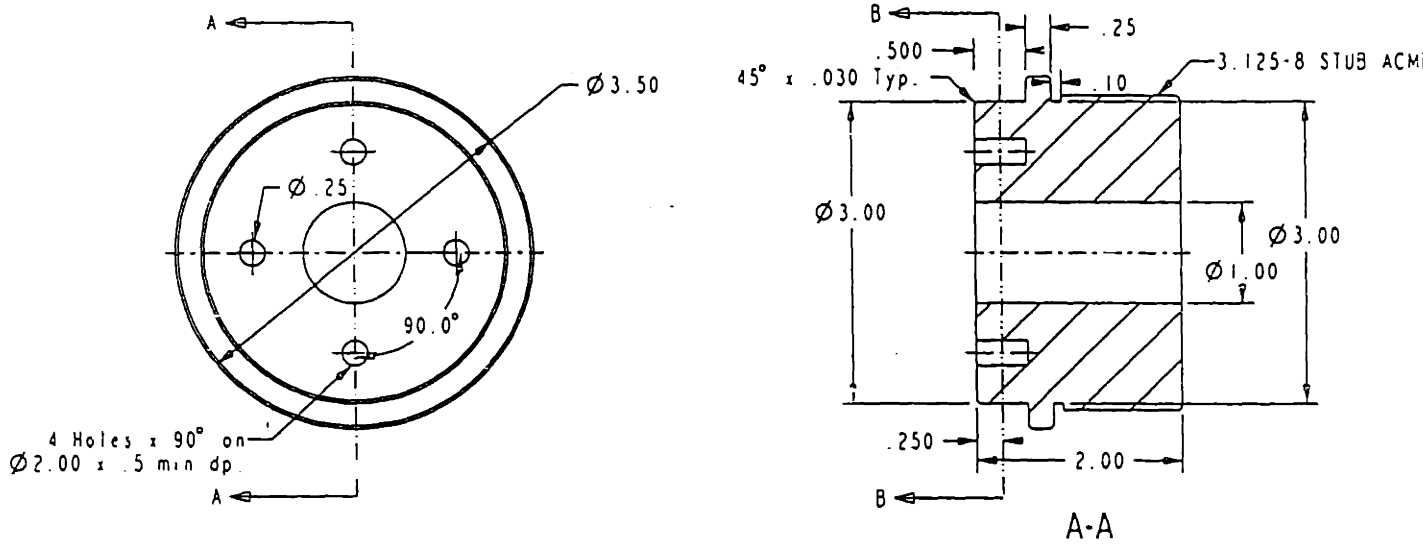

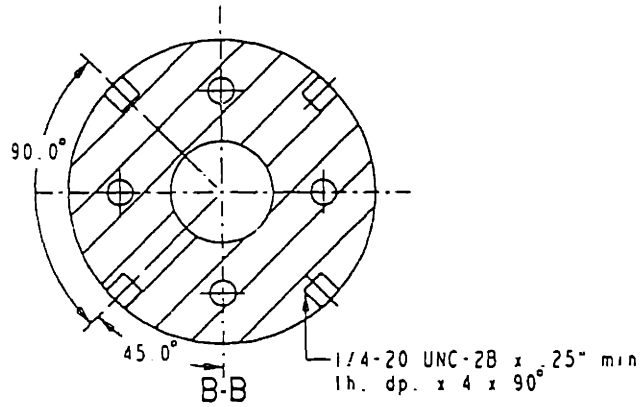

FINISH/TREATMENT		MATERIAL 6061-T6
UNLESS SPECIFIED: SURFACE FIN: 125 RMS .X=±0.1 .XX=±0.01 .XXX=±0.005 ANGLES ±0.5 CONCENTRICITY .005 TIR INSIDE CORNERS R.030 MAX BREAK EDGES .005 - .015 DIMS INCLUDE FINISH	CONFIDENTIAL AND TRADE SECRET DO NOT DISCLOSE USE OR REPRODUCE WITHOUT PRIOR WRITTEN APPROVAL FROM SCHLUMBERGER	Schlumberger Well Services Houston Product Center
		Lube End 2
	DRWN: A Flores 5-Oct-95	LUBEEND2 AA
	APPD:	
	APPD:	
	SCALE 1.000	SZ B SHT: 1 OF: 1

Pro/ENGINEER

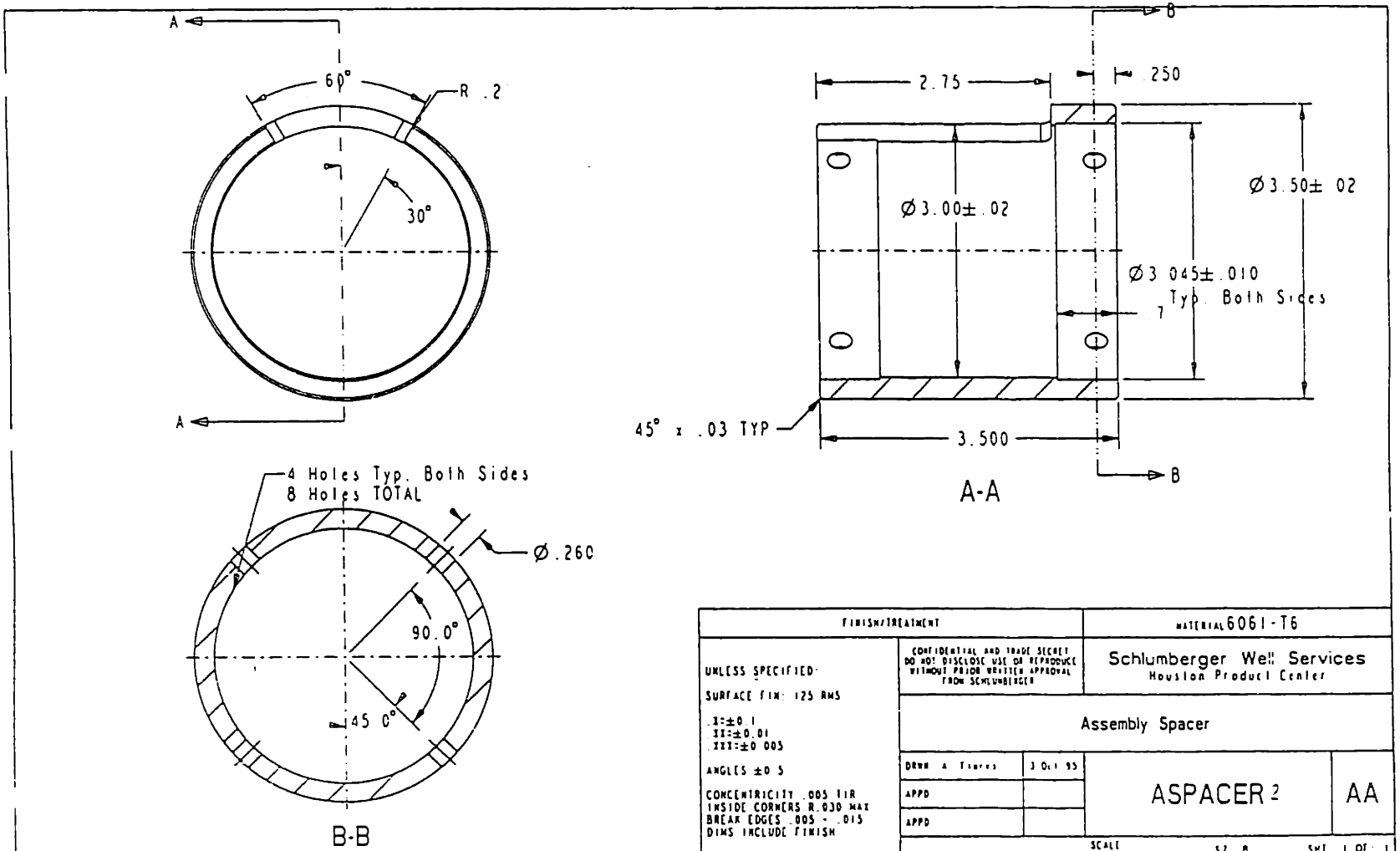
A
60°
R .2
30°
A
B
2.75
.250
Ø3.00± .02
Ø3.50± 02
Ø3 045± .010
Typ. Both Sides
.7
45° x .03 TYP
3.500
B
A-A
4 Holes Typ. Both Sides
8 Holes TOTAL
Ø.260
90.0°
45.0°
B-B
FINISH/TREATMENT
UNLESS SPECIFIED:
SURFACE FIN: 125 RMS
.X=±0.1
.XX=±0.01
.XXX=±0.005
ANGLES ±0.5
CONCENTRICITY .005 TIR
INSIDE CORNERS R.030 MAX
BREAK EDGES .005 - .015
DIMS INCLUDE FINISH
CONFIDENTIAL AND TRADE SECRET
DO NOT DISCLOSE USE OR REPRODUCE
WITHOUT PRIOR WRITTEN APPROVAL
FROM SCHLUMBERGER
MATERIAL 6061-T6
Schlumberger Well Services
Houston Product Center
Assembly Spacer
DRWN A Flores
3 Oct 95
APPD
APPD
ASPACER 2
AA
SCALE
: 000
SZ B
SHT 1 OF 1
Pro/ENGINEER

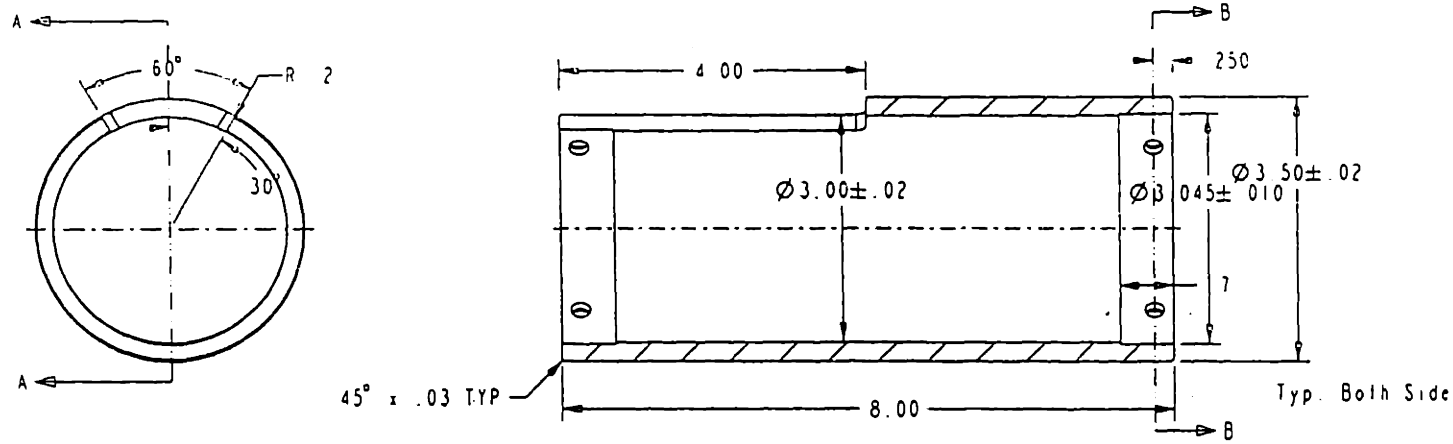

A-A

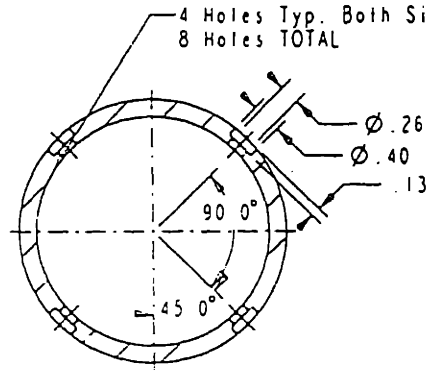

B-B

FINISH/TREATMENT		MATERIAL 6061-T6
UNLESS SPECIFIED SURFACE FIN 125 RMS X: ±0.1 XX: ±0.01 XXX: ±0.005 ANGLES ±0.5 CONCENTRICITY .005 TIR INSIDE CORNERS R.030 MAX BREAK EDGES .005 - .015 DIMS INCLUDE FINISH	CONFIDENTIAL AND TRADE SECRET DO NOT DISCLOSE USE OR REPRODUCE WITHOUT PRIOR WRITTEN APPROVAL FROM SCHLUMBERGER	Schlumberger Well Services Houston Product Center
		Assembly Spacer
	DRWN A Flores 3 Oct 95	ASPACER AA
	APPD	
	APPD	
	SCALE 0.750	SZ D SHT 1 OF 1

Pro/ENGINEER

Appendix L: Downhole Motor

ASTRO INSTRUMENT CORPORATION
450 GOOLSBY BLVD., DEERFIELD, FL 33442-3019
(954) 698-6000 FAX (954) 698-6011

FAX TRANSMISSION			
To:	Schlumberger	Date:	2-27-96
Attn:	Aaron Flores	Our Ref:	ML B0029
Fax No:	1-713-275-4762	Your Ref:	—
From:	Peter Sinatra	Page 1 of 3	
Subject:	Proposal		

Aaron, Per your phone call yesterday, please find enclosed ASTRO proposal 6035-1 for your review and consideration.

Rom pricing for quantities of 10, 25, and 50 would be: #5600.00, #4200.00, and #3500.00. there would also be an NRE of #3000.00.

Shipment would be 16-18 weeks ARO.

Please call if there are any questions. Thank You.

cc: Borger Engineering
Ed Borger

NOTE: OTHER PINION AND MOUNTING CONFIGURATIONS AVAILABLE AS REQUIRED BY CUSTOMER

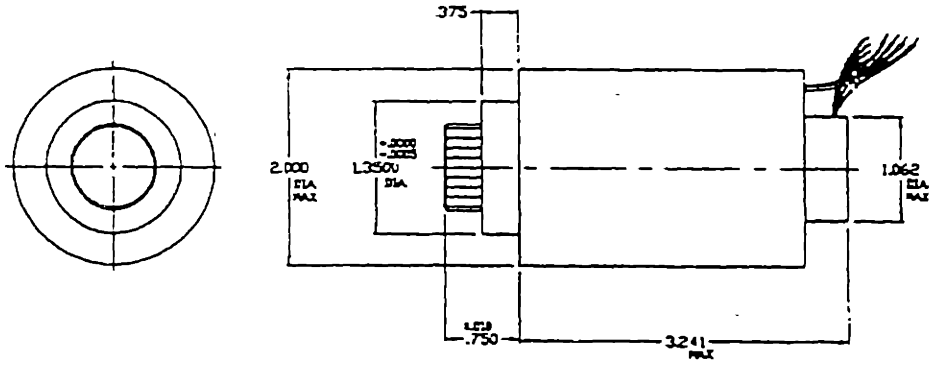

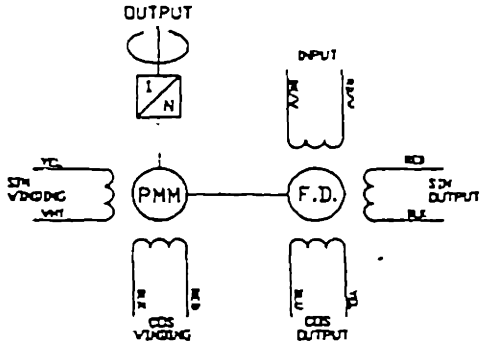

ROTATION CCW VIEWING SHAFT END

PINION DATA

No. OF TEETH	A/R
PITCH AT 20 DEGREE P.A.	
THEO. PITCH DIA.	
TESTING RADIUS	
OUTSIDE DIA. (REF.)	
INVOLUTE TOOTH FORM	
AGMA QUALITY No.	

MOTOR DATA

PERFORMANCE AT 25°C UNIT TEMP

EXCITATION (VAC)	50
POWER OUTPUT AT 2400 RPM (WATTS)	250
TORQUE OUTPUT AT 2400 RPM (Lb-In)	8.8

FIELD DIRECTOR DATA

PERFORMANCE AT 25°C UNIT TEMP

EXCITATION (VRMS)	10
FREQUENCY (KHz)	32
OUTPUT (VRMS)	10

ADDITONAL DATA

UNIT OPERATING TEMPERATURE RANGE -55 TO +225°C

UNIT CAPABLE OF OPERATION IMMERSED IN HYDRAULIC FLUID AT A PRESSURE OF 15,000 PSI

PROPOSAL No. 6035-1

CUSTOMER	SHLM SQL
CUSTOMER SPECIFICATION	ASTRO PROP
N.S.N.	

ASTRO INSTRUMENT CORPORATION

DOWN HOLE COMPRESSOR DRIVE

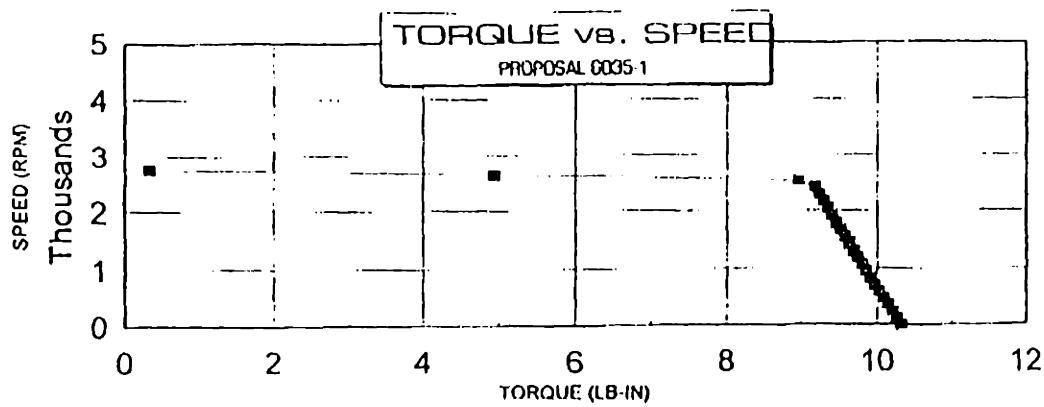

MOTOR TYPE:	32		GHD=	3.91	
INPUT VOLTAGE=	50	*VDC*	DCR=	0.295	*OHMS*
CURRENT LIMIT=	6.976	*ADC*	KT=	1.48	*LB-IN/AMP*
TEMPERATURE=	25	*°C*	KB=	0.02	*Vp/RPM*

OUTPUT SPEED (RPM)	INPUT VOLTAGE (Vpk)	INPUT CURRENT (Apk)	POWER FACTOR (DEG)	INPUT POWER (WATTS)	OUTPUT TORQUE (LB-IN)	OUTPUT POWER (WATTS)	POWER LOSS (WATTS)	EFF.
0	2.1	6.976	1.000	14.36	10.32	0.00	14.36	0.0%
120	4.3	6.976	0.992	29.90	10.26	14.58	15.33	48.7%
240	6.6	6.976	0.987	45.45	10.21	28.98	16.46	63.8%
360	8.9	6.976	0.984	60.99	10.15	43.23	17.76	70.9%
480	11.2	6.976	0.982	76.54	10.09	57.31	19.23	74.9%
600	13.5	6.976	0.981	92.08	10.03	71.23	20.85	77.4%
720	15.8	6.976	0.979	107.62	9.97	84.98	22.65	79.0%
840	18.0	6.976	0.979	123.17	9.92	98.57	24.60	80.0%
960	20.3	6.976	0.978	138.71	9.86	112.00	26.71	80.7%
1080	22.6	6.976	0.978	154.26	9.80	125.27	28.99	81.2%
1200	24.9	6.976	0.977	169.80	9.74	138.38	31.43	81.5%
1320	27.2	6.976	0.977	185.35	9.69	151.32	34.02	81.6%
1440	29.5	6.976	0.977	200.89	9.63	164.11	36.78	81.7%
1560	31.8	6.976	0.976	216.43	9.57	176.74	39.69	81.7%
1680	34.1	6.976	0.976	231.98	9.52	189.22	42.76	81.6%
1800	36.4	6.976	0.976	247.52	9.46	201.53	45.99	81.4%
1920	38.6	6.976	0.976	263.07	9.40	213.70	49.37	81.2%
2040	40.9	6.976	0.976	278.61	9.35	225.70	52.91	81.0%
2160	43.2	6.976	0.975	294.16	9.29	237.55	56.60	80.8%
2280	45.5	6.976	0.975	309.70	9.24	249.25	60.45	80.5%
2400	47.8	6.976	0.975	325.24	9.18	260.79	64.45	80.2%
2520	50.0	6.860	0.976	334.72	8.96	267.21	67.51	79.8%
2640	50.0	4.097	0.991	202.94	4.94	154.23	48.71	76.0%
2760	50.0	0.910	0.999	45.49	0.32	10.61	34.88	23.3%
2760	50.0	0.910	0.999	45.49	0.32	10.61	34.88	23.3%

02/26/96 BPMMGHD.WK4

Appendix M: Patent Application - Informal Style

Method and Apparatus for Actively Cooling Instrumentation in a High Temperature Environment

Field of the Invention

This invention relates to an apparatus and method for cooling instruments in an apparatus while operating that apparatus in high temperature environments. In particularly it relates to the use of a cooling agent to cool the tool electronics in a logging tool when the tool is exposed to earth formation temperatures and thereby preventing tool failure.

Background of the Invention

The environment encountered by downhole oil exploration tools can be very severe. Temperatures up to and in excess of 200°C and pressures up to 1.38×10^8Pa are not uncommon. Consequently, producers of oil exploration tools must design robust tools that can operationally sustain these harsh conditions for extended lengths of time. Perhaps the most challenging of all conditions to design electronics that can reliably operate in high temperature environments. Standard electronic components are usually rated to only 125°C. Thus, it becomes necessary to create or experimentally find electric components that can survive the high temperatures existing downhole. Since the components are constantly changing via new manufacturing techniques, updates, etc., this process of creating electronic components is expensive, time consuming, and never ending. In an effort to combat the high temperature requirement of electronics, the chassis or electronics compartments in downhole tools could be kept at or below 125°C.

Today, tools rated to 175°C are sometimes inserted into Dewar Flasks when exploring boreholes in excess of 175°C. Dewar Flasks act to insulate the tool electronics and to slow the heating of the electronic chassis similar to a large "thermal bottle". The flask is a passive system that extends the downhole residence time of the tools by approximately four to six hours. Often the downhole residence times required for exploration are much greater than those offered by the expensive Dewar Flask system.

The problem at hand points toward the need for an active cooling system that can maintain the electronic chassis below 125°C for extended lengths of time. Standard electronics could then be used without the need for the expensive high temperature components.

Active cooling systems already exist for a variety of applications such cooling food products, motor vehicles and buildings. These active cooling systems,

better known as air conditioners and refrigerators, can effectively operate for extended periods of time with little to no maintenance. A cooling system makes heat move, It takes heat from one location and moves it to another location. The location from which heat was removed obviously becomes colder. For example, a refrigerator takes heat out of the inside and moves it to the outside. The heat flows into the air and the inside, having lost heat, becomes colder.

Vapor compression active cooling systems work by evaporation. When a liquid turns into a vapor, it loses heat and becomes cooler. This change is because the molecules of vapor need energy to move and leave the liquid. This energy comes from the liquid; the molecules left behind have less energy and so as a result, the liquid is cooler.

For an active cooling system to work continuously, the same cooling agent (etc., Freon) must be repeatedly used for an indefinite period. These cooling systems have three basic patterns: the vapor-compression system, the gas-expansion system and the absorption system. The vapor-compression system is the most effective and is used more extensively than the other arrangements. The vapor-compression system consists of four main elements: an evaporator, a compressor, a condenser and an expansion device.

Referring to Figure 1, in the evaporator **1**, the cooling agent boils (evaporates) at a temperature sufficiently low to absorb heat from a space or medium that is being cooled. The boiling temperature is controlled by the pressure maintained in the evaporator, since the higher the pressure, the higher the boiling point. The compressor **2** removes the vapor as it is formed, at a rate sufficiently rapid to maintain the desired pressure. This vapor is then compressed and delivered to a condenser **3**. The condenser dissipates heat to circulating water or air. The condensed liquid cooling agent, now ready for use in the evaporator **1**, is then sharply reduced in pressure by passing through an expansion valve **4**. Here, the pressure and temperature of the cooling agent drop until they reach the evaporator pressure and temperature, thus allowing the cooling cycle to repeat.

During expansion some of the liquid of the cooling agent flashes into vapor so that a mixture of liquid and flash vapor enters the evaporator. In a cooling system, the low pressure in the evaporator is set by the cooling temperature which is to be maintained. The high pressure maintained in the condenser is determined ultimately by the available cooling medium (etc., the temperature of circulating water or the atmosphere air temperature. The process is one in which the cooling agent absorbs heat at a low temperature and then under the action of mechanical work, the cooling agent is compressed and raised to a sufficiently high temperature to permit the rejection of this heat. Mechanical work or energy supplied to the compressor as power is always required to raise the temperature of the system.

To further explain the cooling process, the four major components are examined in greater detail. The evaporator **1** is the part of the cooling system in which the cooling is actually produced. The liquid cooling agent and vapor from the expansion valve **4** are introduced into the evaporator. As the liquid vaporizes, it absorbs heat at low temperature and cools its surroundings or the medium in contact with it. Evaporators may be direct expansion (acting directly to cool a space or product) or they may operate as indirect-expansion units to cool a secondary medium, such as water or a brine which in turn is pumped to a more distant point of utilization. A domestic refrigerator, for example, is a direct-expansion unit in that its evaporator directly cools the air in the food compartment and also directly contacts the water trays used for making ice. Evaporators vary greatly in design, with those used for cooling air often made as continuous pipe coils, with fins mounted outside the pipes to give greater surface contact to the air being chilled. For cooling liquid, such as a brine water, the shell and tube arrangement is common. In this case, the brine passes through tubes surrounded by the boiling (evaporating) cooling agent, which is contained in a larger cylindrical shell. The brine tubes, in turn, are welded or rolled into tube sheets at the end of the shell to prevent leakage of the cooling agent from the shell or into the brine circuit.

The expansion valve **4** that feeds the evaporator must control the flow so that sufficient cooling agent flows into the evaporator for the cooling load but not in such excess that liquid passes over to the compressor, with the possibility of causing damage to it.

The compressor **2**, the key element of the system, can be powered by means such as electric motor, steam or internal combustion engine, or steam or gas turbine. Most compressors are of the reciprocating (piston) type and range from the fractional-horsepower size, such as those found in domestic refrigerators or in small air-conditioning units, to the large multi-cylinder units that serve large industrial systems. In these large multi-cylinder units, capacity can be controlled with automatic devices that prevent the in certain cylinders from closing. For example, in a six-cylinder unit, if the valves are held open on two of the cylinders to keep them inoperative, the capacity of the machine is reduced by one-third when operating at normal speed.

Centrifugal compressors are used for large refrigeration units. These compressors employ centrifugal impellers that rotate at high speed. Centrifugal compressors depend for their compression largely on the dynamic action of the gases themselves as they flow in the diffusion passages of the compressor. These compressors can be large centrifugal compressors made with a single impeller or with two to four or more impellers in series, to compress the gas through the range required. These compressors are used extensively for large air-conditioning installations and also for usage in the industrial field when gases are compressed for liquefaction or for transportation, such as in the natural-gas industry, and when air is compressed to produce liquid oxygen or nitrogen.

The condenser **3** of a vapor system must dissipate heat from the hot vapor it receives from the compressor and condense this vapor to liquid for reuse by the evaporator. Condensers either dissipate heat to the ambient atmosphere through externally finned surfaces or by a shell and tube arrangement in which the vapor delivers heat to a circulating fluid (etc., water) that passes through tubes contacting the cooling agent vapor. The temperature of the vapor is kept above that of the circulating water or air by compression to insure that heat is transferred to the coolant; thus, when the vapor is allowed to expand, its temperature drops well below that of the cooling agent.

Double-pipe condensers are also used. In such units, the cooling agent vapor and condensate pass in one direction through the annular space between the two tubes, while the water, flowing in the opposite direction through the central tube, performs the cooling function.

The air conditioning concept works on the principle of exchanging heat from a heated substance to a cold substance. In this principle, the temperature from a hot substance (such as a fluid) is transferred to a cold fluid. As the temperature of the hot fluid decreases, the temperature of the cold fluid increases. Heat exchangers are manufactured in many different designs and are used extensively in various industries. Heat exchangers are given different names when they serve a special purpose. Thus boilers, evaporators, superheaters, condensers and coolers may all be considered heat exchangers.

An example of a heat exchanger is illustrated in Figure 2a and explains the basic operation of a hat exchanger. This exchanger is constructed from two pipes **5** and **6** in a concentric arrangement. Inlet and exit ducts are provided for the two fluids. In the sketch, the cold fluid flows through the inner tube **7** and the warm fluid via inlet pipe **5** in the same direction through the annular space between the outer and the inner tube. This flow arrangement is called parallel flow. In it heat is transferred from the warm fluid through the wall of the inner tube (the so-called heating surface) to the cold fluid. The temperature in both fluids varies as shown in Figure 2b. In plot **9**, the temperature of the warm fluid decreases from $t_{\omega 1}$ to $t_{\omega 2}$. In plot **10**, the temperature of the cold fluid increases from t_{c1} to t_{c2}. The amount of heat Q that is transferred from one fluid to the other per unit of time, called heat flow, can be calculated from the following equation:

$$Q = mc\,(t_2 - t_1) \qquad (1)$$

This equation states that the heat flow Q(kW) can be obtained by multiplying the mass per unit of time of fluid m(kg/sec) by the specific heat c(KJ/kg-°C) of the fluid and by the temperature increase $t_2 - t_1$ (°C)of the fluid entrance to the exit of the heat exchanger. The specific heat is a property of the fluid involved and its current state. The amount of heat leaving the warm fluid must be the same as the amount of

heat received by the cold fluid. The mass flow and the temperature increase for the cold or the decrease for the warm fluid can therefore be entered into equation (1). The heat exchanger may have to be designed, for example, to increase the temperature of a prescribed mass per unit time m_c of cold fluid from t_{c1} to t_{c2}. Entering these value into equation (1) then determines the heat flux Q which has to be transferred in the heat exchanger. This value will be needed in the following discussion to calculate the heating surface of the exchanger.

The temperature difference Δt_1 between the fluids at the entrance of the heat exchanger decreases to the value Δt_2 at the exit, as illustrated in Figure 2a. A heat exchanger is operated in counterflow when the direction of one of the fluids is reversed. The counterflow arrangement has the advantage that the exit temperature t_{c1} of the colder fluid can be increased beyond the exit temperature t_{w2} of the warm fluid. In addition, a smaller surface area is required in counterflow than in parallel flow to transfer the same amount of heat. This is so because the mean temperature difference Δt_m in the counterflow heat exchanger, for a given heat flux and prescribed inlet temperatures, is higher than in the parallel-flow exchanger.

The heating surface of the heat exchanger can be obtained from the equation:

$$A = \frac{Q}{U\Delta t_m} \qquad (2)$$

The equation indicates that the required surface area A (m^2) is obtained by dividing the heat flux Q obtained with equation (1) by the overall heat transfer coefficient U and the mean temperature difference Δt_m(°C). Larger heat exchangers utilize a bundle of tubes through which one of the fluids flows. The tubes are enclosed in a shell with provisions for the other fluid to flow through the spaces between the tubes. Fluid flowing outside the tubes can be directed either in the same direction as or counter to the effective flow in the tube bundles. In the latter arrangement, parallel or counter flow can be approximated in the way shown in Figure 2a. In another arrangement, the cold fluid is distributed in such a manner that it flows in parallel through the tubes forming the heating surface and is then collected by a header. This arrangement creates a cross flow, as shown schematically in Figure 2a. In nuclear reactors, fuel rods may replace the tubes, and the cooling fluid flowing around the rods removes the heat generated by the fission process. In a similar way, rods containing electric resistance heaters may supply heat to the fluid passing through the exchanger between the rods.

As previously mentioned, there is a need for a downhole cooling system that can keep logging tool electronics cool in order to avoid tool failure from the extreme downhole temperatures. There have been attempts to apply the refrigeration concept to downhole tools. In 1977, Mechanics Research attempted to develop a system that incorporated a refrigeration technique for use in a geothermal

well. The system design was to be a closed system that would operate continuously, similar to the refrigerator cooling concept of Figure 1. However, the specific objective of the project was to develop a compressor for such a system. The project did not achieve its chief objectives. Therefore, a need still remains for a system that can actively cool instrumentation in a high temperature environment.

Summary of the Invention

In the present invention, an active cooling system allows constant low pressure vaporization of a tank of water while in thermal communication with the electronic chassis of downhole logging tool. The tool electronics and a lower tank of water are in thermal communication with one another via a cold heat exchanger. The heat from the electronics, as well as that from the hot borehole (up to approximately 200°C) causes the water in the lower tank to boil or vaporize into steam. As the water vaporizes, the steam is removed from the tank and compressed via a compressor to an upper tank. By removing the steam from the lower tank as it is generated, its pressure and resulting temperature can be regulated and thereby regulating the temperature of the electronics. For instance, the temperature of lower tank can be maintained at approximately 100°C if its internal pressure is kept at approximately 1.01×10^5Pa (14.7 psi). The vapor in the upper tank must be compressed to a pressure greater than the saturation pressure of the steam at the temperature of the borehole in order to empty the lower tank. A 200°C borehole would require a pressure of 1.55×10^6Pa (225 psi). Once the steam enters the upper tank, it is allowed to cool to the borehole temperature. Thus, the upper tank serves as the hot heat exchanger in the system. A control system between a lower tank pressure sensor and the compressor maintains a constant pressure vaporization in the lower tank. Once the lower tank is emptied of water, the system is spent and the tool must return to the surface and the tank refilled. Likewise, the upper tank must be emptied before the tool re-enters the borehole.

Three major subsystems are combined in the present invention as shown in Figure 3a. The subsystems are the compressor **11**, the cold heat exchanger (evaporator) **10** and the hot heat exchanger (condenser) **12**. In addition, a sample wireline electronics chassis including heat-dissipating electronics is implemented. A schematic of the present invention in its simplest form is shown in Figure 4. The evaporator **17** encompasses a lower tank of stored water **16** in thermal contact with a cold heat exchanger **18** from the electronics and is all within a Dewar flask **15**. This system allows the heat from conduction into the flask and electronic component dissipation, to be transferred to the tank of water. Consequently, the water begins to vaporize. The second major component is the compressor **23**. The compressor maintains the lower tank **17** at the specified atmospheric pressure value. It accomplishes this task by pulling the vaporized water or stream out of the lower tank and transporting it into the upper tank or hot heat exchanger **24**, outside the Dewar flask. Thus, the compressor must attain pressures greater or equal to the saturation pressure of water at a given borehole temperature, along with the

flowrates of stream produced by the total cooling load. For instance, the worst-case-scenario of a 200°C borehole requires compressor outlet pressures equal to or greater than 15.5×10^5Pa and a flowrate equal to 3.5×10^{-5}kg/s at the 80-W cooling load. The upper tank/hot heat exchanger **24** is simply a tank to which the compressed stream is transported and allowed to condense at borehole temperatures. The volume of the upper tank should be sized at least 1.16 times larger than the lower tank due to the increased specific volume of saturated water at 200°C over that at 100°C. Additionally, with knowledge of worst-case heat transfer coefficients in the downhole system, the upper tank must be made thermally conductive towards the borehole. Heat transfer of the cooling load and compressor work must be accomplished with as small a temperature as possible over that of the borehole.

Brief Description of the Drawings

Figure 1 is a schematic of the components of a refrigeration cooling concept.

Figure 2a is an isometric cross-sectional view of a parallel-flow heat exchanger.

Figure 2b is a graph of the changes in fluid temperatures that take place in the parallel heat exchanger.

Figure 3 is a diagram of the hybrid vapor compression once-through system of the present invention.

Figure 4 is a diagram of the active cooling system of the present invention.

Figure 5 is a diagram of a sample electronics chassis.

Figure 6 is a diagram of a cold heat exchanger.

Figure 7 is a diagram of the cold heat exchanger and lower tank assembly of the present invention.

Figure 8 is a diagram of a compressor assembly.

Figure 9 is a diagram of the lubrication assembly of the present invention.

Figure 10 is a diagram of the hot heat exchanger upper tank assembly of the present invention.

Figure 11 is a diagram of the compressor/motor assembly.

Detailed Description of the Invention

The overall assembly of the invention is shown in Figure 4 and includes the sample electronics **16**, lower tank/cold exchanger **19** (evaporator), compressor **23**, lubrication system, and upper tank/hot heat exchanger **24** (condenser) assemblies. The invention is described in the context of a designed and manufactured prototype of the invention. Although not downhole compatible, aluminum pieces were used in the prototype. Aluminum was used in the tubes of the lower and upper tanks, and the compressor valve head piece. In practice, the tubes of the upper tank and compressor valve head piece should not be made of aluminum in a downhole design.

Figure 5 shows the electronic chassis assembly containing the logging tool electronics. The detailed assembly drawings are given in Dipti Nevrekar's Thesis (Publication MIT 1996). The chassis has a base **30** made of aluminum. The diameter and lengths of the chassis are 0.0699m and 0.43m, respectively. End pieces **31** and **32** are connected to the chassis base **30** by screws **35**. End piece **31** is connected to a lower tank and is therefore smaller in length than end piece **32**. A breadboard **34** containing electronic components is attached to the chassis as shown. It is attached to the base via screws **36**. The breadboard contains the electronic components **37**. In the test structure, Kapton Strip heaters serve as the electronics. These heaters have a resistance of 15.68 ohms and when connected in parallel have a total resistance, R_t of 6.4 ohms at a temperature of 100°C. The sample electronics are powered by a Hewlett Packard #6443B DC power supply. The voltage, v_{heat}, required to produce an electronic heat dissipation, P_{heat}, is equal to:

$$v_{heat} = \sqrt{P_{heat} R_t} \qquad (3)$$

Electronics heat dissipation values between 0W and 50W are available with the given power supply.

Figure 6 shows the cold heat exchanger assembly. As shown, the electronic chassis **40** has a chassis base piece **30**, end pieces **31** and **32**, sample electronics **37** attached to a breadboard **34**. Also shown is a portion of a cold heat exchanger **41** adjacent the electronics **37**. Heat pipe holder **42** contains heat pipes **43**. The heat pipes **43** are mounted in the channels of the holder. A heat pipe brace **44** secures the pipes in the holder **42**. Screws **36** and **46** secure the heat exchanger and heat pipe brace.

In Figure 7, the heat exchanger prototype **39** has two 0.457m by 0.0165m by 0.00660m, Noren Products flat TPheBS heat pipes **43** mounted on an aluminum holder **42** that is placed on a thin, high thermal conductive pad (Berquist Co. Sil Pad 400) insulator **47** on top of the Kapton strip heaters **37**. The heat pipes transfer the heat from the electronics **37** to the water contained in the lower tank **50** through an aluminum mating piece **54**. The mating piece **54** is in contact with the heat pipes **43** through the heat exchanger portion **41**. A screw **56** attaches the heat exchanger to the lower tank. The air gaps between the heat pipes, aluminum holder and aluminum mating piece are eliminated by filling these gaps with a high thermally conductive Dow Corning 340 heat sink compound. An O-ring **55** provides a seal between the lower tank and the heat exchangers to prevent water flow to the electronics. Two other O-rings **53** and **53b** are located at the uphole end **51** and the downhole end **52** of the lower tank. The lower tank **50** is sized to fit into the flask and carry 1kg of water. The volume of the lower tank is approximately $0.001 m^3$. However, when the system is laid in the horizontal position with the exit of the tank in the center of the cross-section, the effective volume of

the tank is halved. Thus, only 0.5kg of water can be carried in the lower tank in horizontal tests.

The flask used in the present invention is a UDFH-KA Dewar flask manufactured by National K-Works. The flask properties and diameter dimension schemes are detailed in Chapter 3 of the inventor's dissertation entitled "Active Cooling for Electronics in a Wireline Oil-Exploration Tool" Massachusetts Institute of Technology, June 1996. The flask has a total length of 2.36m and a payload or insulated length of 1.71m. The ends of the flask are insulated with Teflon shavings.

Figure 8 displays the compressor assembly used in the active cooler. The compressor is composed of several mechanical parts. The outer housing **60** of the compressor contains two volumes: the compression chamber **61** and the crankshaft chamber **62**. In the compressor chamber is a piston **63**, piston rod **64**, piston cylinder **65** and valve head piece **66**. The piston cylinder guides the stroke of the piston. The piston/cylinder seal is a dynamic lapped design with the piston made of mehanite and the cylinder made of 12L14 steel. These parts were manufactured to last for approximately 126 million strokes at a temperature of 232°C. These specifications equal a downhole time of approximately 1000 hours at compressor shaft speeds of 2000rpm.

The intake port **67** is located at the bottom of the piston stroke and the exit port **68** is located at the top of the piston stroke. In operation, as the piston travels downward, a small vacuum is created in the compression chamber. The port **67** is exposed as the piston crosses its surface and steam is sucked into the compression chamber volume. On the upward stroke of the piston, the port **67** is sealed by the circumferential area of the piston and lubricant. The steam is compressed by the upward motion of the piston. This high pressure vapor exits via the compression valve head piece **66** and port **68**. A miniature Lee check valve **69** is placed in the valve head piece and serves as the exhaust valve in the compressor. The valve is hard-mounted in the compressor head piece. A miniature spacer **70** and Lee mechanical plug **71** keep the check valve **69** in a pressure-sealed position. To filter large particles from the vapor flow, a small 40 μm Mectron Industries, Inc. filter **73** is placed in front of the miniature check valve in the valve head piece on the chamber inlet side. The filter keeps contaminants from entering and plugging the valve, especially during the break-in period of the seal. In this design, an intake valve is eliminated, along with its design complexities and inefficiencies.

The valve head piece **66** utilizes a 95 durameter viton o-ring **72** to isolate the compression chamber volume from the environment. The piston stroke is controlled by the spinning of the crankshaft assembly. The crankshaft assembly is made from a crankshaft **75**, bearings **76** and **76b**, a rotary seal **77** and a pin welded **78** into the shaft. In operation, the crankshaft pin **78** is inserted in the piston rod **64**. When the crankshaft is rotated the piston **63** moves up and down. Two different, but standard-sized ball bearings **76** and **76b** guide the rotation of the crankshaft. A

Greene-Tweed steam-service rotary seal **77**, spacer **79** and bearings **76** are contained in the compressor assembly by an end piece **82** held in place by six socket head screws. The crankshaft is held inside the compressor by an end piece **80** which is held in place by three socket head screws. This end piece also utilizes a 95 durameter viton o-ring **84** for pressure isolation between the compressor internals and the environment. For compatibility with the rotary seal, a hardness of 45-55Rc is specified for the crankcase. As mentioned earlier, the piston connecting rod is taken directly from the Fox 40-size engine.

Figure 9 shows the lubricant system for the compressor. This system has a lubricator tube **85**, with a lubricator piece **86**. Lubricant in the tube is maintained under pressure and is compensated by two springs **87** in series. These springs **87** are separated by a spacer **88**. The springs are contained on one end by the end piece **89**. The end piece and lubricator piece utilize a 95 durameter viton o-ring **90** and **90b** for pressure isolation from the environment. The other end of the springs is contained by a piston **91**. The springs apply force to the piston which then applied pressure to a lubricant stored on the other side of the piston. The piston maintains the lubricant seal with a 95 durameter viton o-ring **90c**. A three-way normally-closed, high-temperature Lee Co. solenoid valve **93** is periodically opened and closed as a function of time, allowing lubricant to travel into the compressor intake line through a Lee Co. Visco-Jet restrictor **94**. The restrictor piece restricts the flow of lubricant to lower flowrates than that of the solenoid valve alone. Both the restrictor and valve pieces are located in the lubricator piece. From the intake line, the lubricant travels into the compression chamber of the compressor and maintains the dynamic lapped pressure seal. Some lubricant also "blows-by" the seal and serves to lubricate the crankcase internals. A hydraulic line is connected to the lower line on the lubricator piece that contains the solenoid valve and is used to fill the lubricant reservoir before operation. The lubricant inlet line is then plugged during operation.

Lubricant is periodically pumped into the reservoir under pressure. The reservoir pressure is measured by a pressure gage. In practice, a screw-drive system could maintain the reservoir pressure autonomously. The lubricant used in the final tests was Dow Corning-200, 500cSt Silicone oil. A model of the piston/cylinder seal displayed the need for a viscosity of approximately 50cSt at the operating temperature and shaft speeds of the compressor.

The motor assembly is used to spin the crankshaft of the compressor. The motor shaft is coupled to the crankshaft of the compressor by a telescoping universal joint. The motor assembly housing and compressor housing are connected by a spacer piece and held in place by eight socket head screws.

The hot heat exchanger/upper tank assembly is shown in Figure 10. The assembly comprises an upper tank **100**, uphole **101** and downhole ends **102** and O-rings **103** and **103b**, and serves to both store the high pressure steam and conduct

heat from the steam to the borehole through its walls. As mentioned above, the tank is made of aluminum which is not compatible with the downhole environment. However, the aluminum housing makes no difference from a heat transfer standpoint in the design. In other words, the limiting resistance to thermal conduction is the borehole film coefficient, not the material of the upper tank. The temperature difference required for the aluminum housing is only 0.3°C less than that required for the downhole-compatible stainless steel housing.

The original downhole motor/compressor assembly is shown in Figure 11. The motor assembly is a standard motor containing major parts such as a motor mount **110**, a motor end **111**, motor add-on shaft **112**, the pump out motor **113**, a motor housing **114** , a spacer **115**, which perform standard operations. A universal end **116** and female end **117** to connect the motor the compressor. A universal joint **118** connects the motor and compressor and provides the means by which the motor dries the compressor. The universal joint is connected to the compressor by a male end **119**. The assembly has an outer diameter of approximately 0.102m. The 2/3HP high-temperature downhole motor displayed in the assembly is a commonly used motor in wireline tools. The development of a new motor to fit the geometry constraints does not represent a serious design challenge. However, due to time and costs, a new downhole was not purchased for the uphole prototype.

The method and apparatus of the present invention provides a significant advantage over the prior art. The invention has been described in connection with the preferred embodiments. However, the invention is not limited thereto. Changes, variations and modifications to the basic design may be made without departing from the inventive concept in this invention. In addition, these changes, variations modifications would be obvious to those skilled in the art having the benefit of the foregoing teachings contained in this application. All such changes, variations and modifications are intended to be within the scope of the invention which is limited by the following claims.

We claim:

1. An apparatus for actively cooling instrumentation contained in a logging tool comprising:

a) a first container having a cooling agent therein, said container being located adjacent said instrumentation;

b) a heat exchanger in thermal communication with said first container and said instrumentation for transferring heat from said instrumentation to said cooling agent in said container;

c) a second container for receiving said heating cooling agent; and

d) a compressor in fluid communication said first container for pumping heating cooling agent from said first container and in fluid communication with said second container for pumping said heated cooling agent to said second container.

2. The apparatus of claim 1 wherein said first and second containers are lower and upper tanks respectively.

3. The apparatus of claim 2 wherein said lower tank is connected to said instrumentation via said heat exchanger.

4. The apparatus of claim 2 further comprising an insulated flask for containing said lower tank, said heat exchanger and said instrumentation.

5. The apparatus of claim 4 wherein said instrumentation is electronic circuits.

6. The apparatus of claim 1 wherein said cooling is water.

7. The apparatus of claim 6 further comprising a vapor control system to maintain a constant pressure vaporization of said cooling agent in said lower tank.

8. The apparatus of claim 7 further comprising a pressure controller to maintain pressure in said upper tank of steam which results from heating said cooling agent.

9. The apparatus of claim 8 wherein the pressure of said steam is measured by a pressure gage inside said lower tank.

10. An apparatus for actively cooling instrumentation contained in a logging tool comprising:

a) a means for containing a cooling agent, said means being located adjacent said instrumentation;

b) a means for transferring heat from said instrumentation to said cooling agent in said container means;

c) a second means for containing a cooling agent after said cooling agent has been heated and transferred from said first container means; and

d) a cooling agent transfer means in fluid communication with said first and second container means for transferring said heated cooling agent from said first container means to said second container means.

11. The apparatus of claim 10 further comprising an insulated means for containing said lower tank, said heat exchanger and said instrumentation.

12. The apparatus of claim 10 wherein said cooling agent transfer means comprises a compressor means and a vapor control means.

13. The apparatus of claim 12 wherein said control means is located such that said control means controls vapor entering said compressor means and vapor exiting said compressor means.

14. The apparatus of claim 10 further comprising a pressure sensing means for detecting pressure of cooling agent when said cooling is transformed form a liquid state to a vapor state.

15. A method of actively cooling instrumentation contained in a logging tool comprising the steps of:

a) transferring heat from said instrumentation to a cooling agent stored in a tank adjacent said electronics;

b) maintaining the temperature of said cooling agent at approximately the boiling point of said cooling agent; and

c) controlling the temperature of said instrumentation through the cooling agent such that the temperature of said instrumentation is the approximately the same as the temperature of said cooling agent.

16. The method of claim 15 wherein said temperature of said cooling agent is maintained by:

- allowing sufficient heat to transfer to said cooling such that said cooling agent begins to boil and vaporize;
- transferring the vaporized portion of said cooling agent out of said tank; and
- transferring said vaporized cooling agent into a condensing tank.

17. The method of claim 16 wherein the vaporized portion of said cooling agent is transferred from said tank by:

- pumping said vaporized cooling agent from said cooling agent tank; and
- regulating the flow rate of said vaporized agent from said cooling agent tank to maintain a desired vapor pressure.

18. The method of claim 17 wherein said vaporized cooling agent is maintained at a pressure of approximately 1.01×10^3Pa.

19. The method of claim 16 further comprising the step of condensing said vapor into liquid cooling agent.

Abstract of the Disclosure

An apparatus and method are disclosed for actively cooling instrumentation, in particular electronic circuits, in especially, high temperature environment. This apparatus has a tank containing a cooling agent, a heat exchanger to transfer heat from the instrumentation to the cooling agent, a compressor and a tank to hold cooling agent removed from the first tank. In this operation, the cooling agent tank is located in close proximity to the instrumentation. As the instruments generate heat, the heat is transferred through the heat exchanger to the cooling agent. The cooling agent boils and vaporizes from the heat and is pumped out of the tank by a compressor. As the cooling agent vaporizes and is pumped out of the tank, heat contained in the cooling agent is transferred out of the tank as well. The rate at which the vapor is pumped out of the tank controls the temperature of the cooling agent in the tank. The vapor is compressed under pressure and pumped to a storage tank where the vapor condenses back to a liquid.

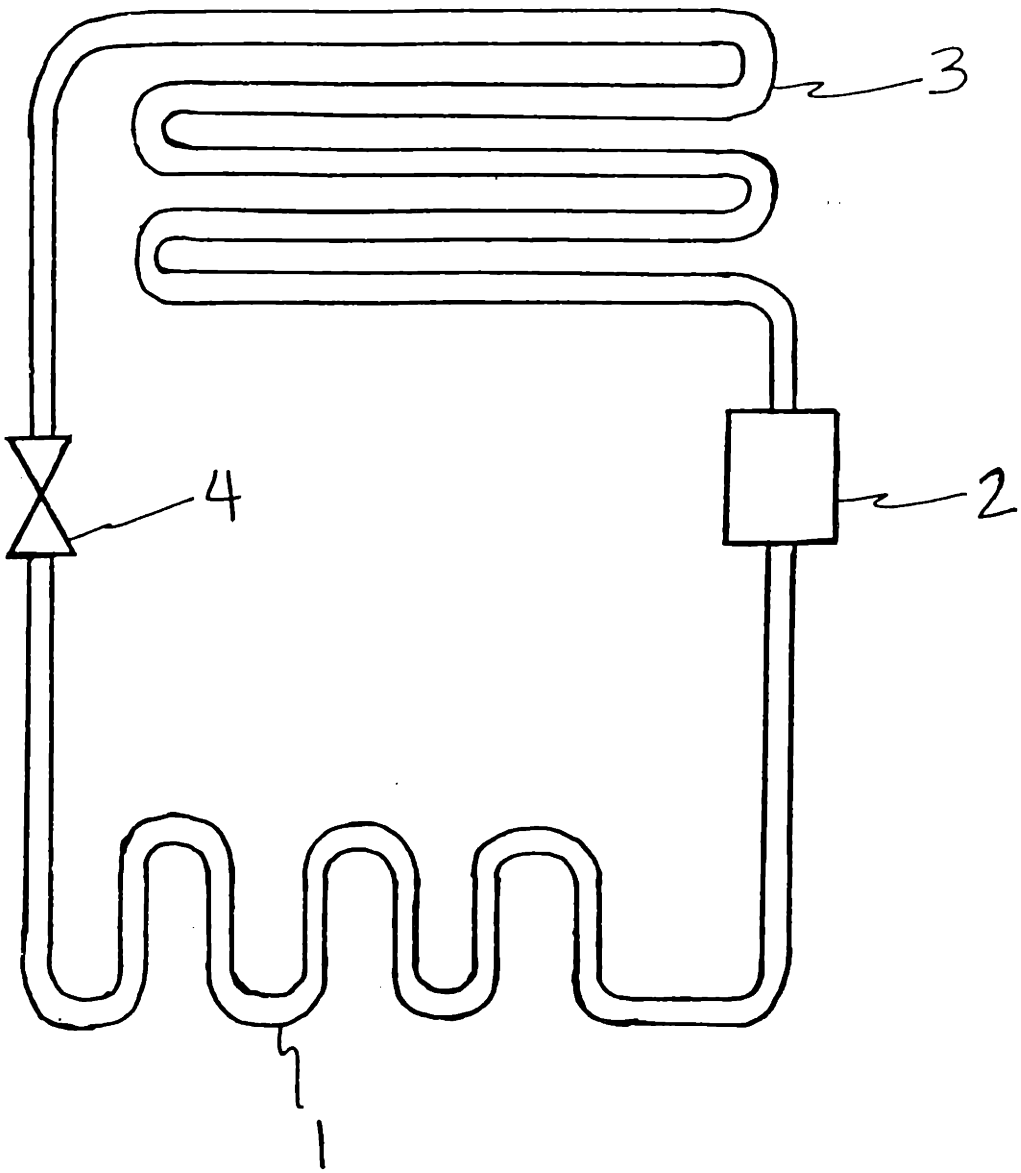

Figure 1

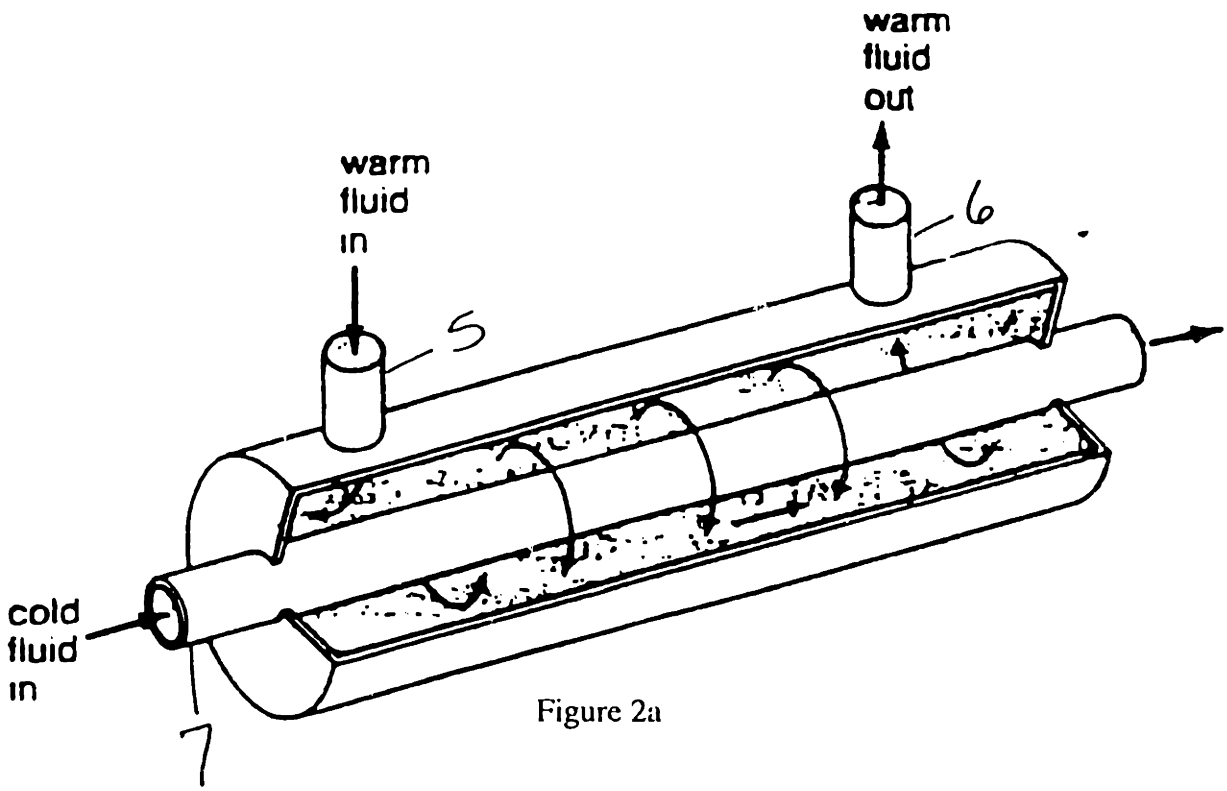

Figure 2a

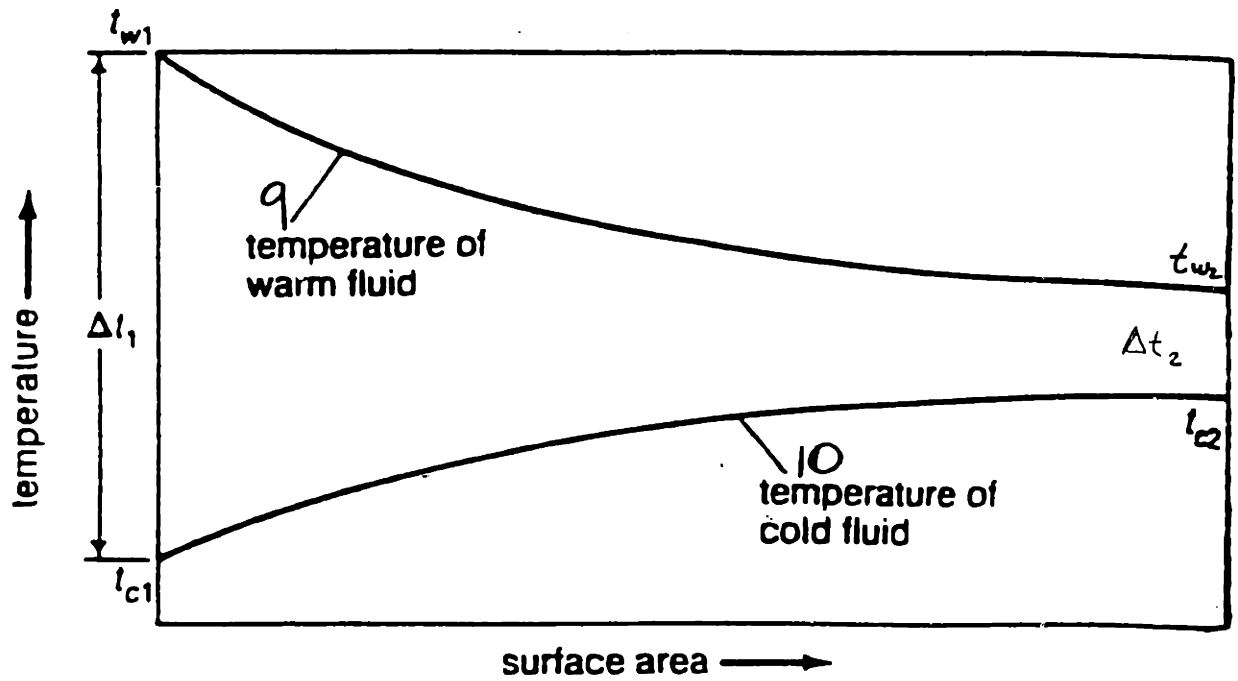

Figure 2b

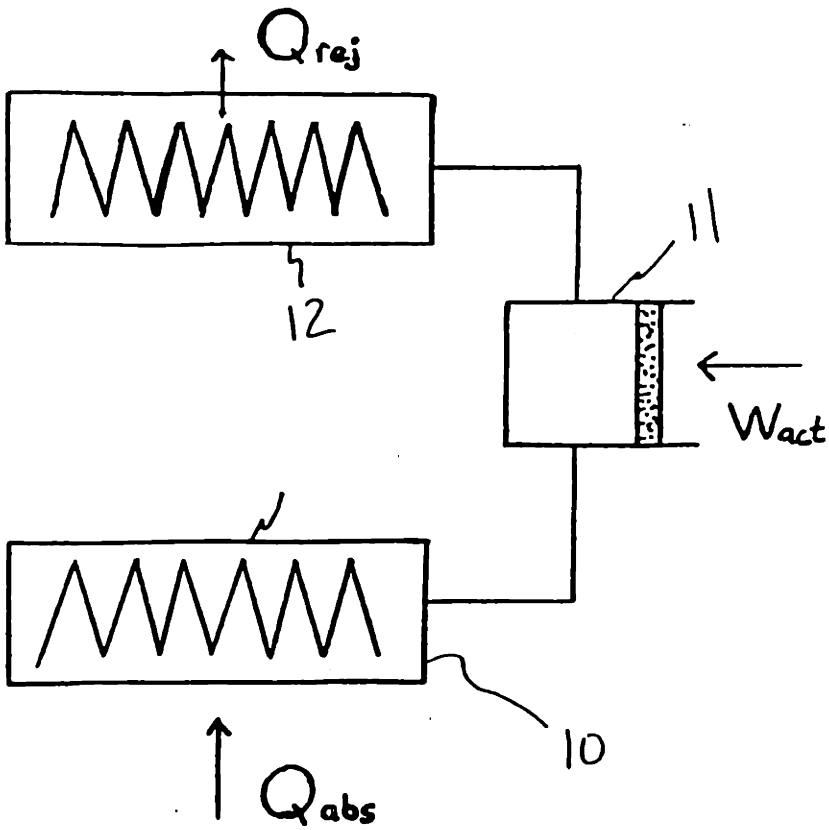

Figure 3

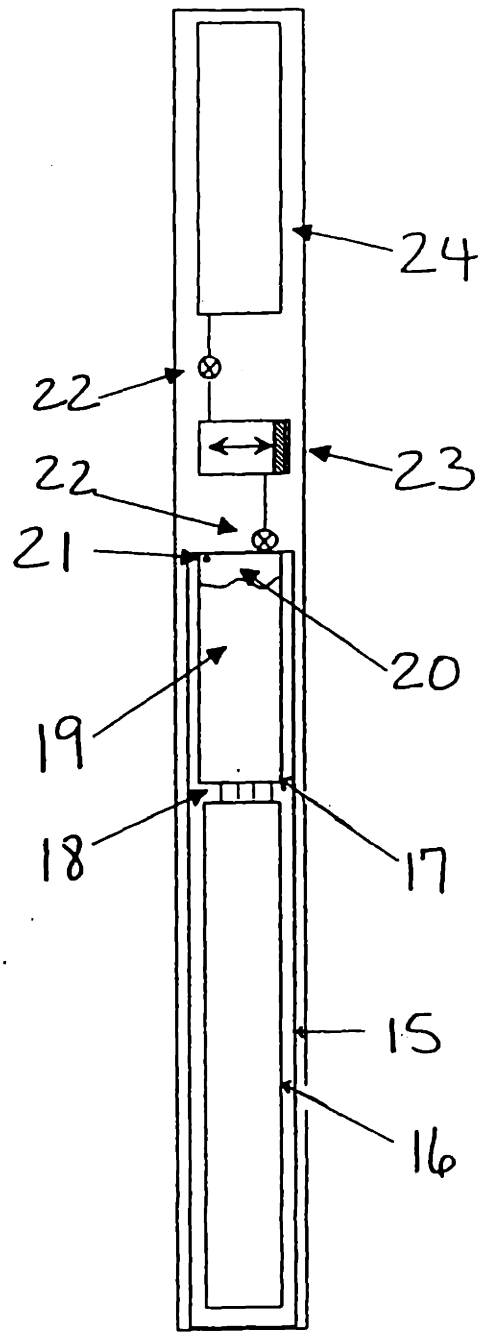

Figure 4

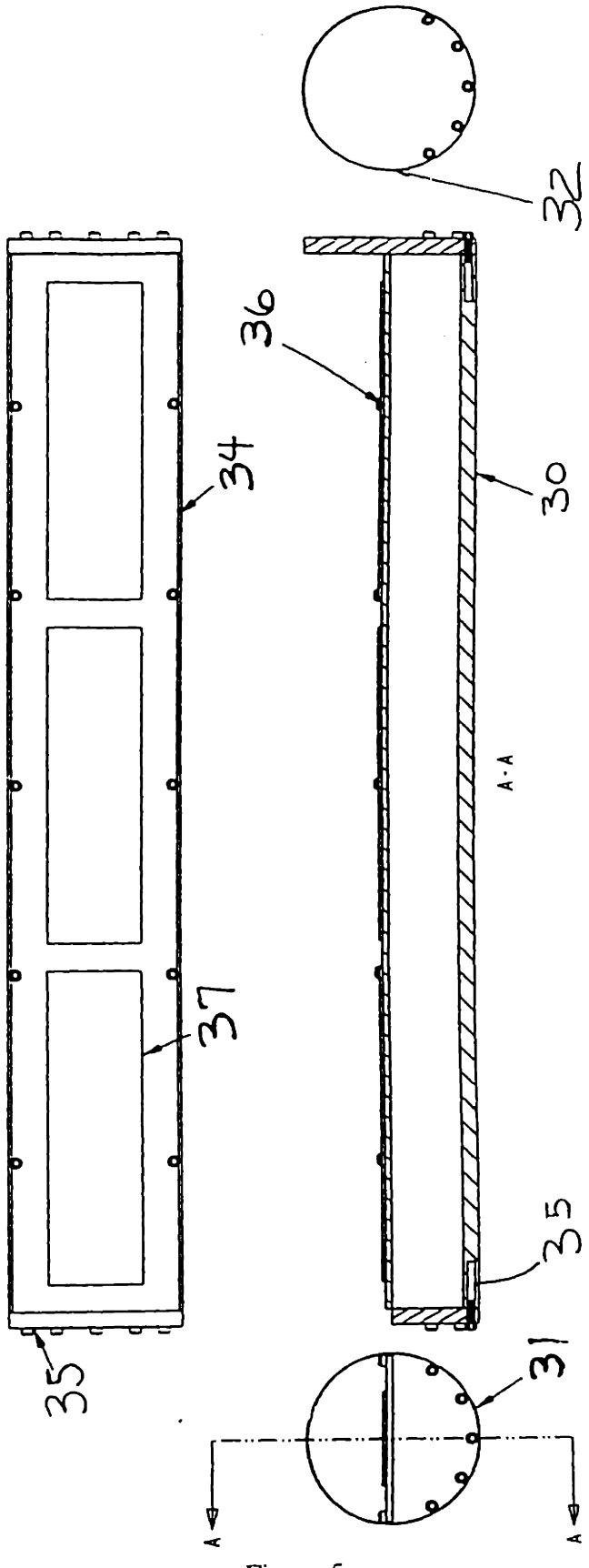

Figure 5

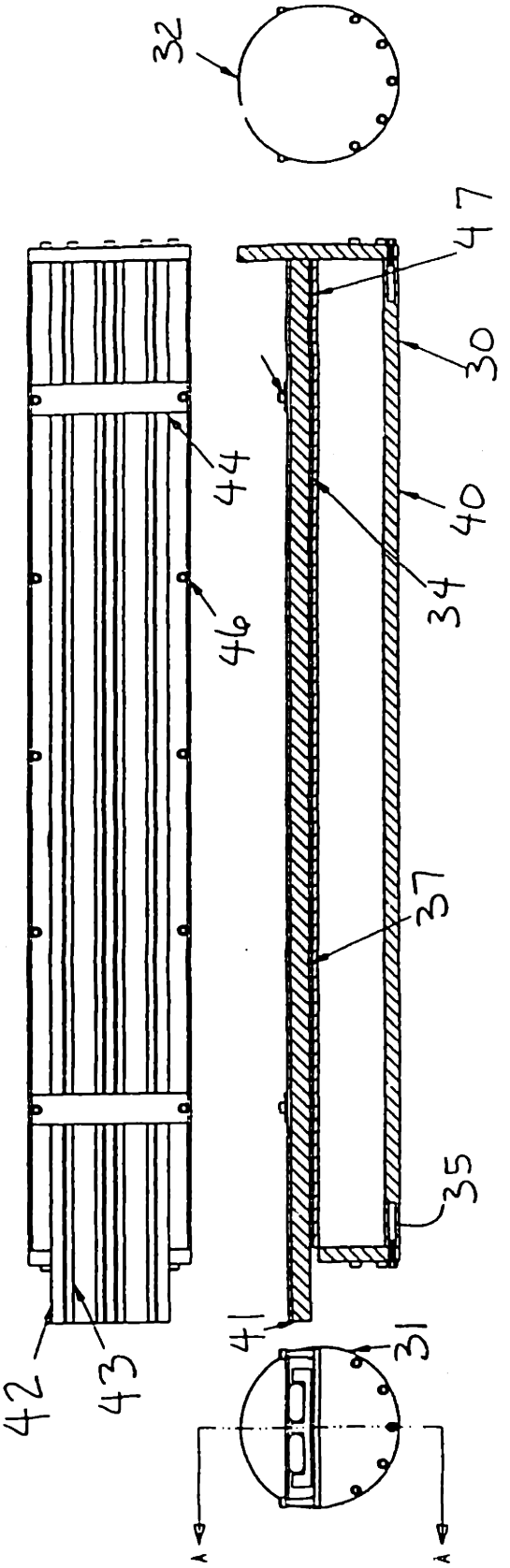

Figure 6

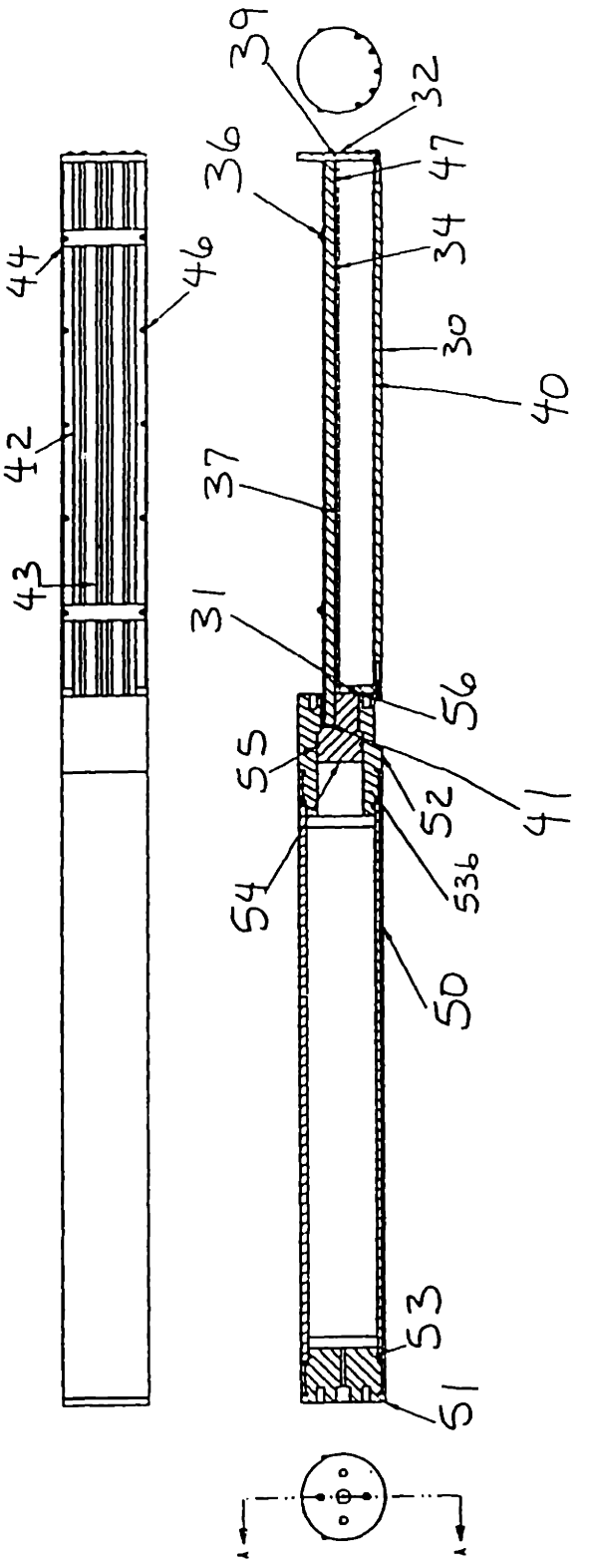

Figure 7

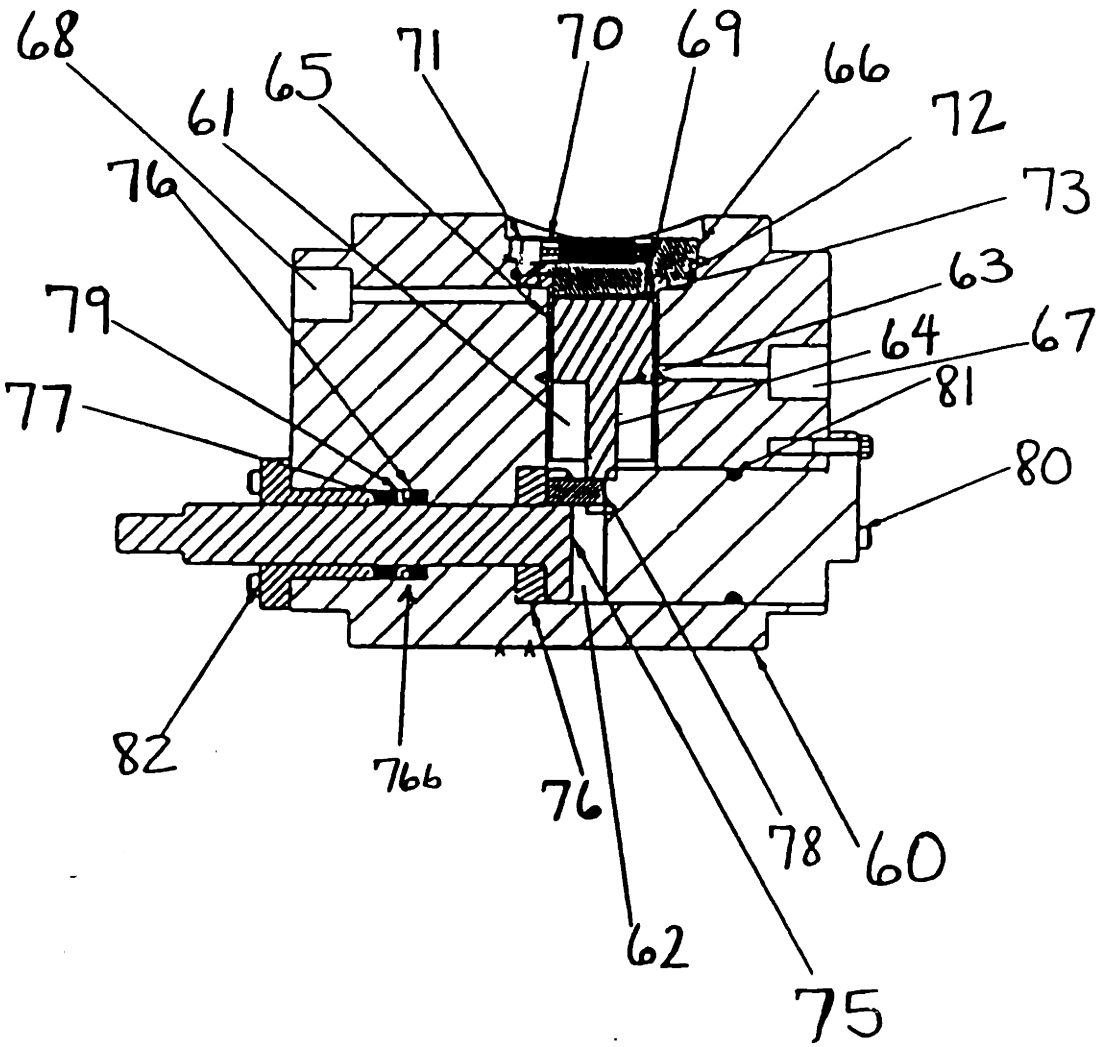

Figure 8

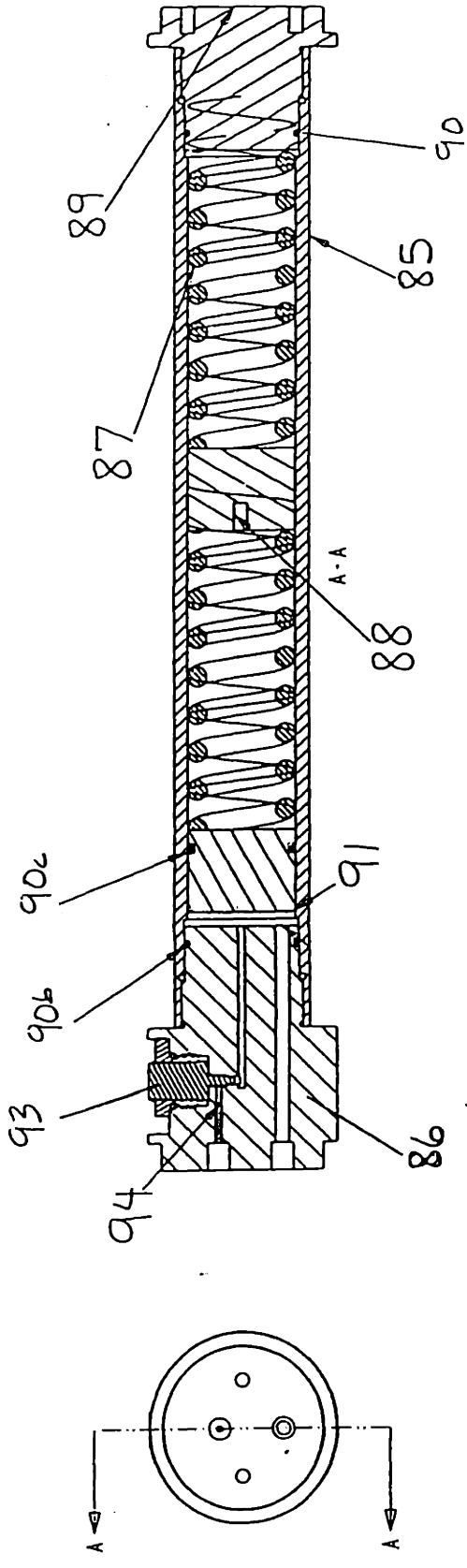

Figure 9

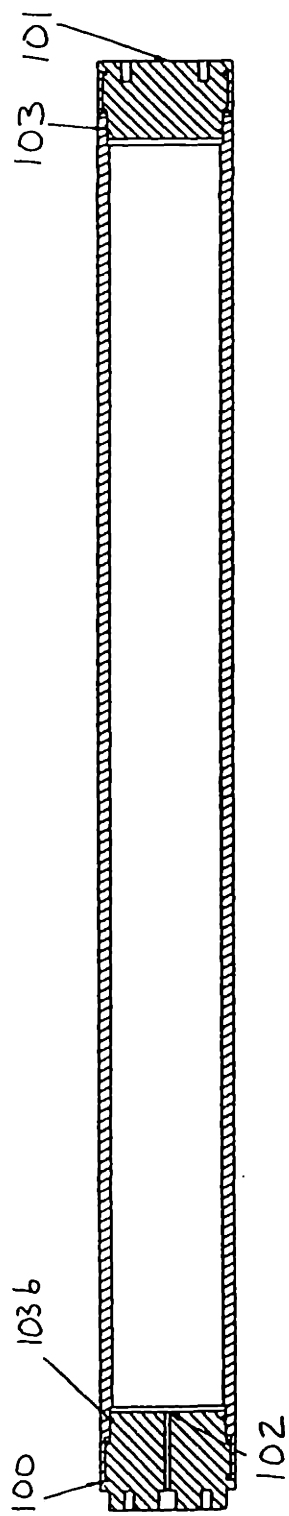

Figure 10

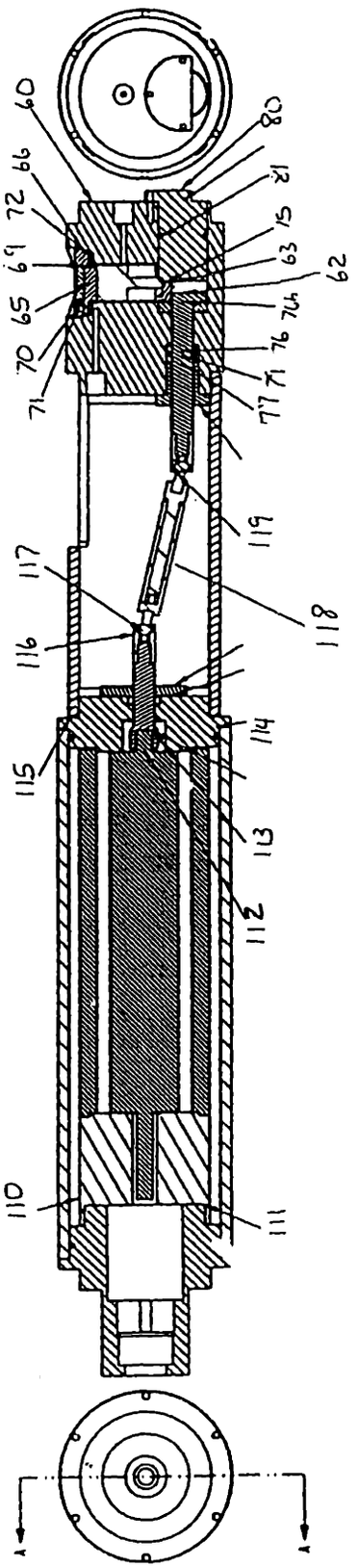
60
80
66
72
82
69
15
63
62
65
74
70
76
71
71
77
119
117
118
116
114
115
113
112
110
111

Figure 11

References

1) Ardic, Hifzi. Schlumberger Wireline & Testing Marketing Manager. Personal Interview. 13 January 1995.

2) Avallone, E.A. and T. Baumeister III, eds. Mark's Standard Handbook for Mechanical Engineers. New York: McGraw-Hill Book Co., 1978.

3) Barger, J.P. and W.M. Rohsenow and K.M. Treadwell. "Turbo Conditioning Systems with Vapor Compression Cycles." General Electric Co. Report No. AAT-321156 AE 32 (February 1955).

4) Bennett, Gloria, A. "Active Cooling for Downhole Instrumentation: Preliminary Analysis and System Selection." Los Alamos National Laboratory Report LA-11102-MS (March 1988).

5) Bennett, Gloria, A. Active Cooling for Downhole Instrumentation: Miniature Thermoacoustic Refrigerator. Ph.D. Diss. University of New Mexico, 1991. Ann Arbor: UMI 1991. 9215048.

6) Blanton, R.W. "New Capabilities in Pyroflasks." Symposium on High-Temperature Well-Logging Instrumentation, Los Alamos National Laboratory Report LA-10745-C (June 1986): 36.

7) Brown, Royce N. Compressors: Selection and Sizing. Houston, Tx: Gulf Publishing Co., 1986.

8) Cerro-Alloy: Physical Data and Applications. CerroMetal Products Co. Bellefonte, Pa. 1995.

9) Cravalho, E.G. and J.L. Smith, Jr. Engineering Thermodynamics. Cambridge, Ma.: MIT, 1981.

10) Followay, J. Schlumberger Wireline & Testing Senior Engineer. Personal Interview. 10 January 1995.

11) Fox Manufacturing Co. Sales Department. Phone Conversation. 22 February 1996.

12) Fredrickson, A.G. and R.B. Bird. "Non-Newtonian Flow in Annuli-Extrusion of Molten Plastics and Flow of Drilling Muds in Annular Spaces." Industrial and Engineering Chemistry. Vol 50, No. 3 (March 1958).

13) Goldsmid, H.J. Thermoelectric Refrigeration. New York: Plenum Press, 1964.

14) Gray, G.R. Composition and Properties of Oil Well Drilling Fluids, Fourth Edition. Houston, Tx.: Gulf Publishing Co., 1981.

15) Griffith, P. MIT Professor of Mechanical Engineering. Personal Interviews. February-May 1995.

16) Gyftopoulos, E.P. and G.P. Beretta. Thermodynamics: Foundations and Applications. New York: Macmillan Publishing Co., 1991.

17) Hazen, Gary. Schlumberger Wireline & Testing Senior Engineer. Personal Interview. 13 January 1995.

18) Head, Elton. Schlumberger Wireline & Testing Scientific Advisor. Personal Interview. 6 January 1995.

19) Higley, H.B. All About Engines. Glenwood, Illinois: Harry B. Higley & Sons, Inc., 1992.

20) Incropera, Frank P. and D.P. Dewitt. Fundamentals of Heat and Mass Transfer, Third Edition. New York: John Wiley & Sons, 1990.

21) Jaroska, Miles. Schlumberger Wireline & Testing Technical Consultant. Personal Interview. 12 January 1995.

22) Karlekar, B.V. Thermodynamics for Engineers. Englewood Cliffs, N.J.: Prentice-Hall, 1983.

23) Lee Company Technical Hydraulic Handbook. The Lee Company Technical Center: Westbrook Conn., 1989.

24) Lienhard, John H. A Heat Transfer Textbook. Englewood Cliffs, N.J.: Prentice-Hall, 1987.

25) Mathison, R.D., Jr. Schlumberger Wireline & Testing Project Manager. Personal Interview. 14 January 1995.

26) Nelson, J.F. So You Want to Build a Live Steam Locomotive. Cadillac, Michigan: Wildwood Publications, 1974.

27) Nevrekar, Dipti V. Cold Heat Exchanger and Sample Electronics for a Downhole Active Cooling System. B.S. Thesis. MIT, 1996.

28) Oldroyd, J.G. "A Rational Formulation of the Equations of Plastic Flow for a Bingham Solid." Proc. Camb. Phil. Soc. Vol. 43 (1947) pp.100-105.

29) Parsons, Mike. Schlumberger Wireline & Testing Department Manager. Personal Interview. 3 March 1996.

30) Pichot, Pierre. Compressor Application Engineering: Volume 1. Houston, Tx.: Gulf Publishing Co., 1986.

31) Pitts, D.R. and L.E. Sisson. Schuam's Outline of Theory and Problems of Heat Transfer. New York: McGraw-Hil', Inc., 1977.

32) Pop, Julian J. "Pressure Drops Associated with Running a Logging Tool/Cable Out of a Borehole Filled with Drilling Fluid." Internal Schlumberger Report. Houston, Tx., 1982.

33) Rice, J. ed. Steam & Stirling Engines You Can Build: Book 2. Transverse City, MI.: Village Press, Inc., 1993.

34) Sundquist, Wayne. Schlumberger Wireline & Testing Project Manager. Personal Interview. 12 January 1995.

35) ITI Thermoelectric Product Catalog and Technical Reference Manual. International Thermoelectric, Inc. Chelmsford, Ma., 1992

36) Thermophysical Properties of Matter-The TPRC Data Series. New York: IFI/Plenum, 1979.

37) United States Department of Energy. Mechanical Refrigerator for Deep Well Sonde Electronics: Phase I. Santa Monica, Ca., 1977.

38) United States Department of Energy. Mechanical Refrigerator for Deep Well Sonde Electronics: Phase II. Santa Monica, Ca., 1979.

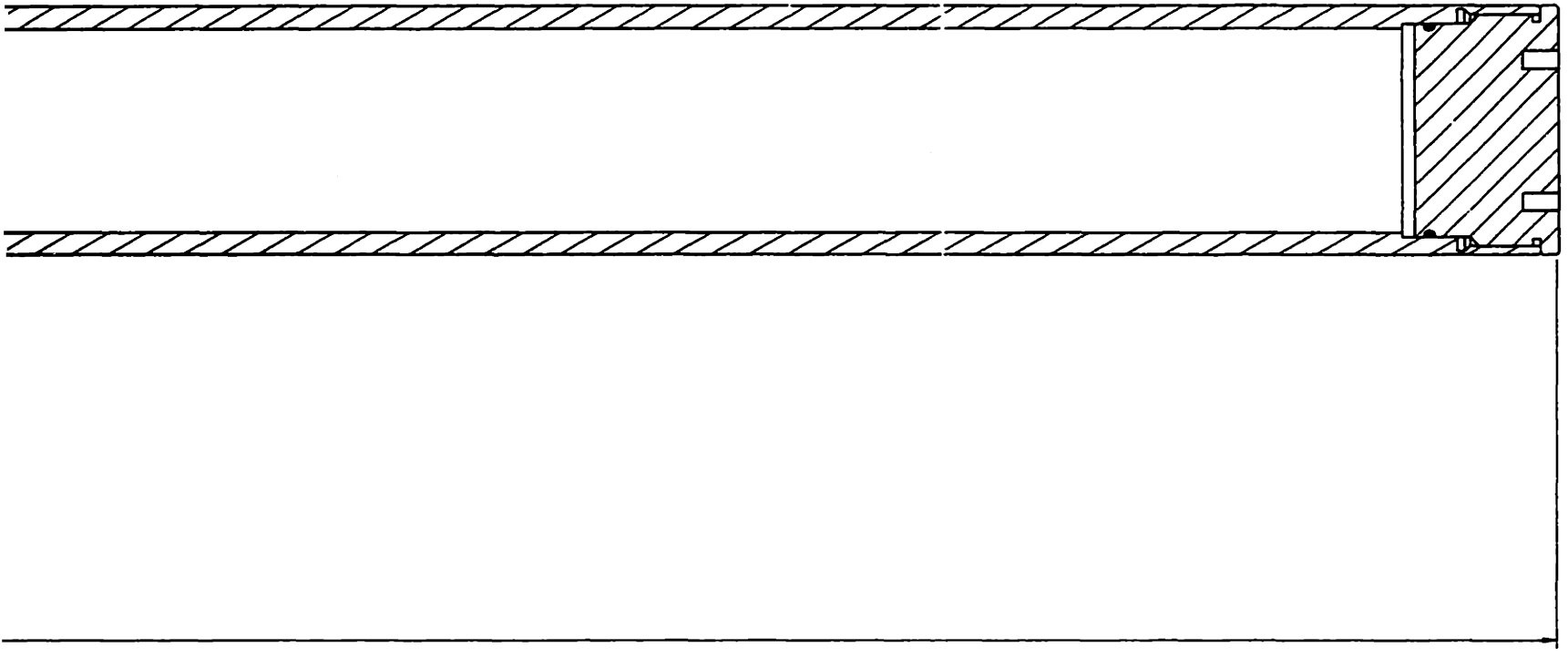

Figure 9.1: Prototype Assembly Drawing

FINISH OR TREATMENT		DET / QTY	MATERIAL
UNLESS OTHERWISE SPECIFIED SURFACE FIN 125 RMS X ± .01 XX ± .010 XXX ± .0005 ANGLES ± .05 INSIDE CORNERS .030 R MAX DIMENSIONS ARE IN INCHES REMOVE BURRS BREAK EDGES .005 - .015 CONCENTRICITY .005 TIR DIMENSIONS INCLUDE APPLIED FINISHES	CONFIDENTIAL AND TRADE SECRET DO NOT DISCLOSE USE OR REPRODUCE WITHOUT PRIOR WRITTEN APPROVAL FROM SCHLUMBERGER		SCHLUMBERGER WELL SERVICES A DIVISION OF SCHLUMBERGER TECHNOLOGY CORPORATION
	DRN A. Flores 21-Nov-96		Cooler Assembly
	DES ENGR A. Flores		
	MFG ENGR A. Flores		
	PROJ ENGR A. Flores		
		SIZE S	DRAWING NUMBER HPC / DWG NO TCOOLERASM / REV AB
		SCALE 100%	SHEET

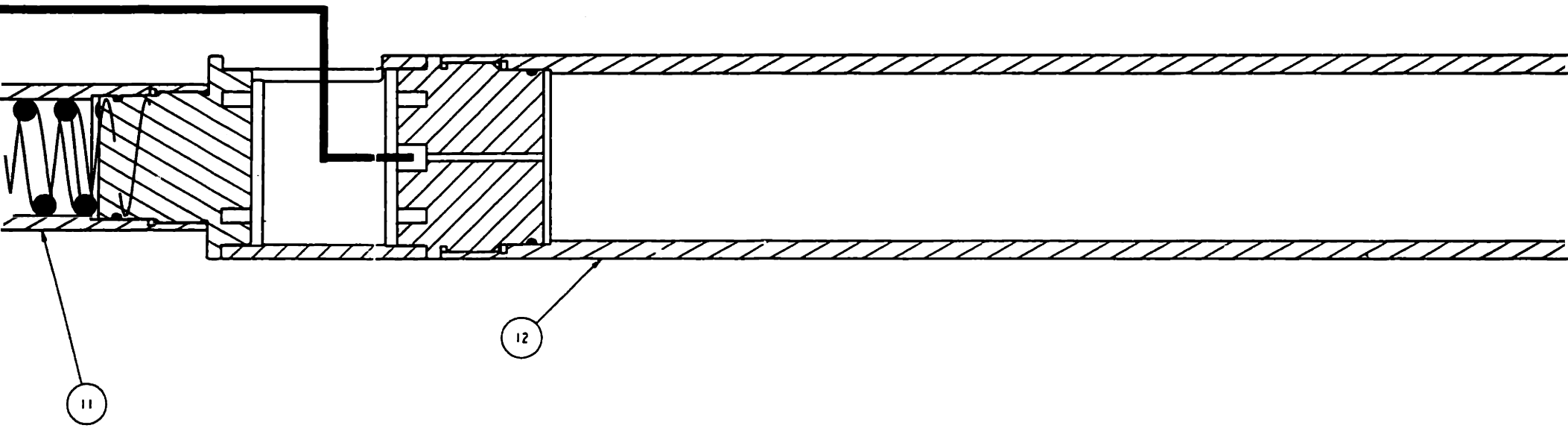
11
12

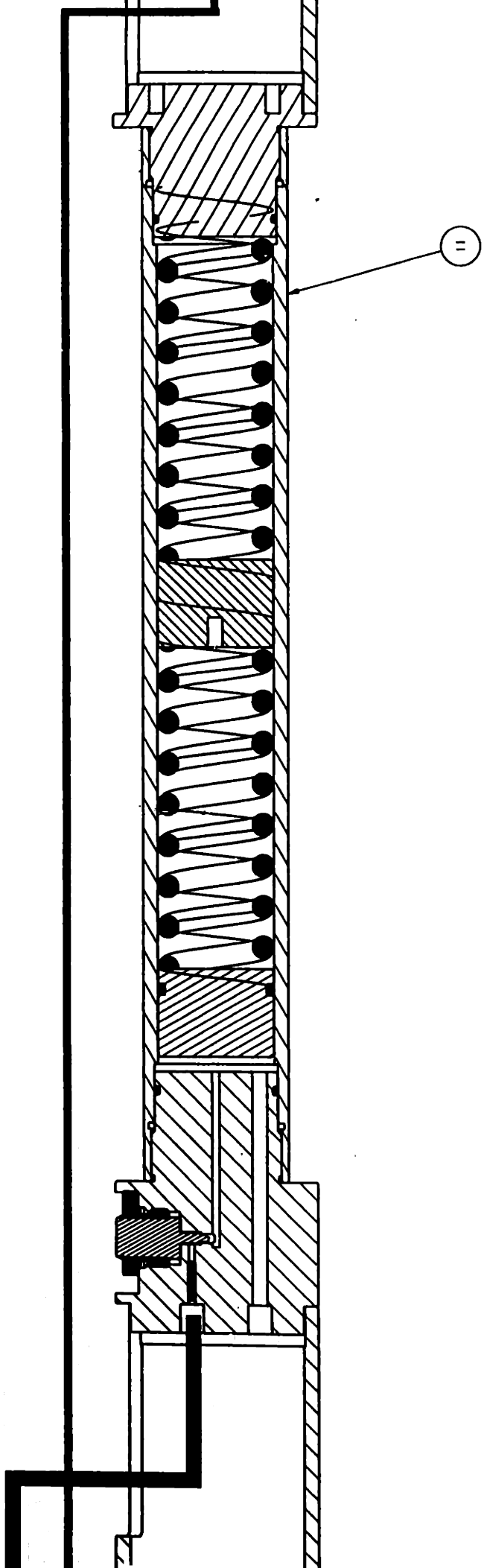

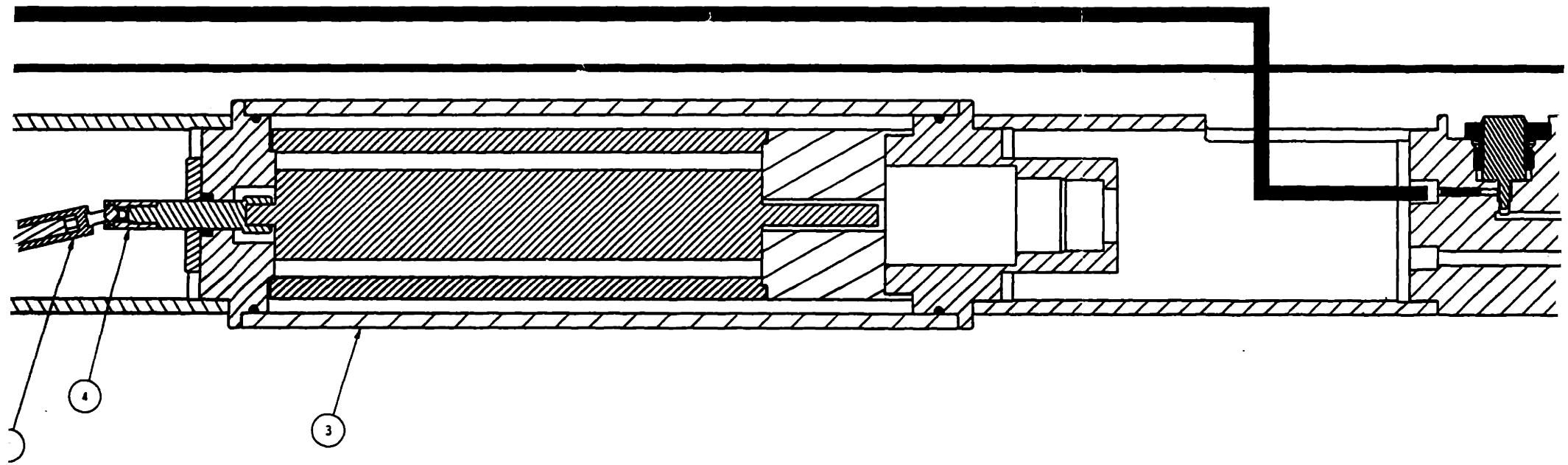
4
3

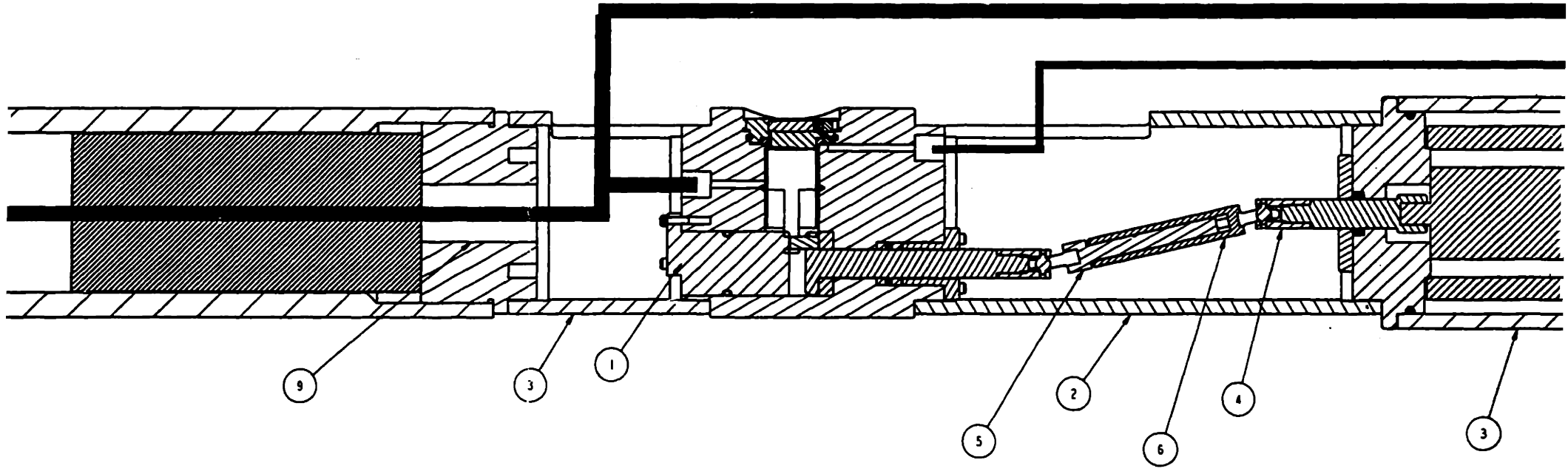

A - A

189.45

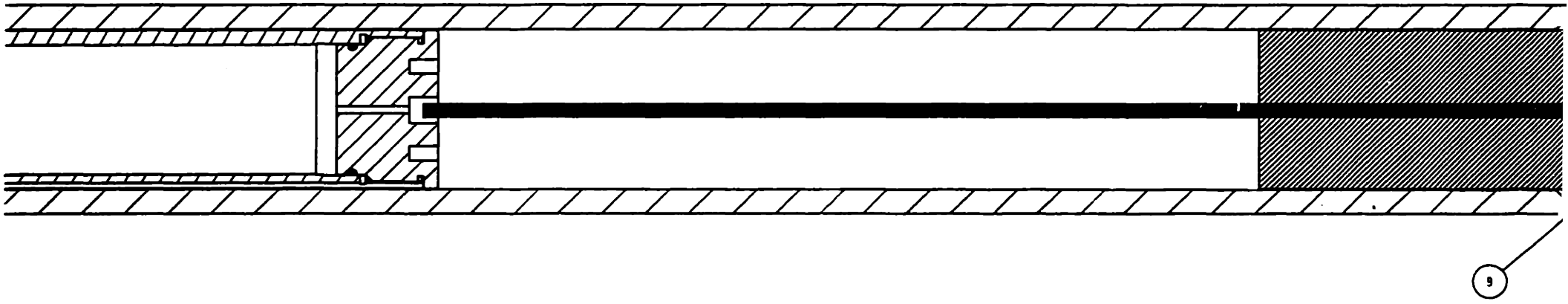
9

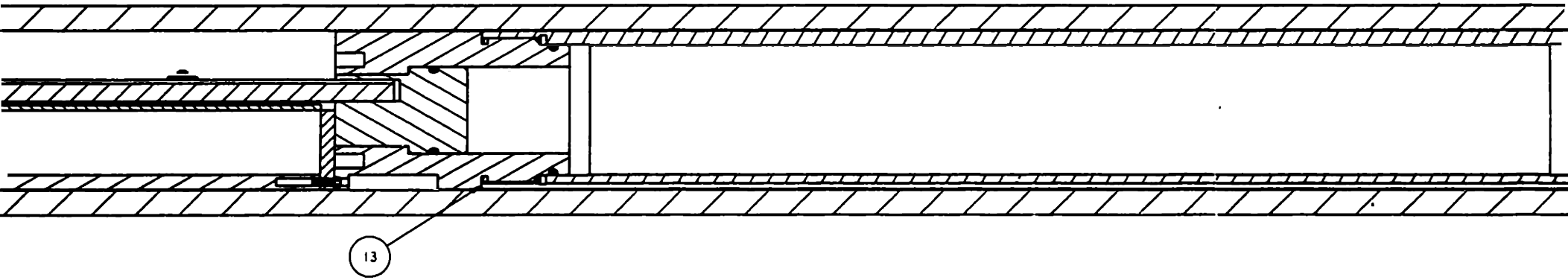
13

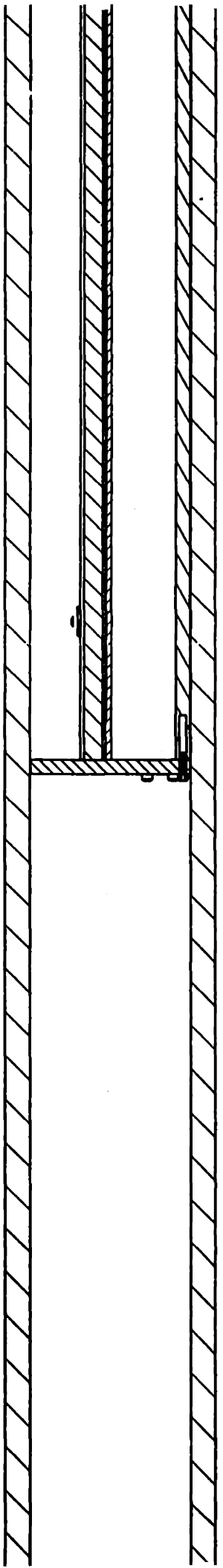

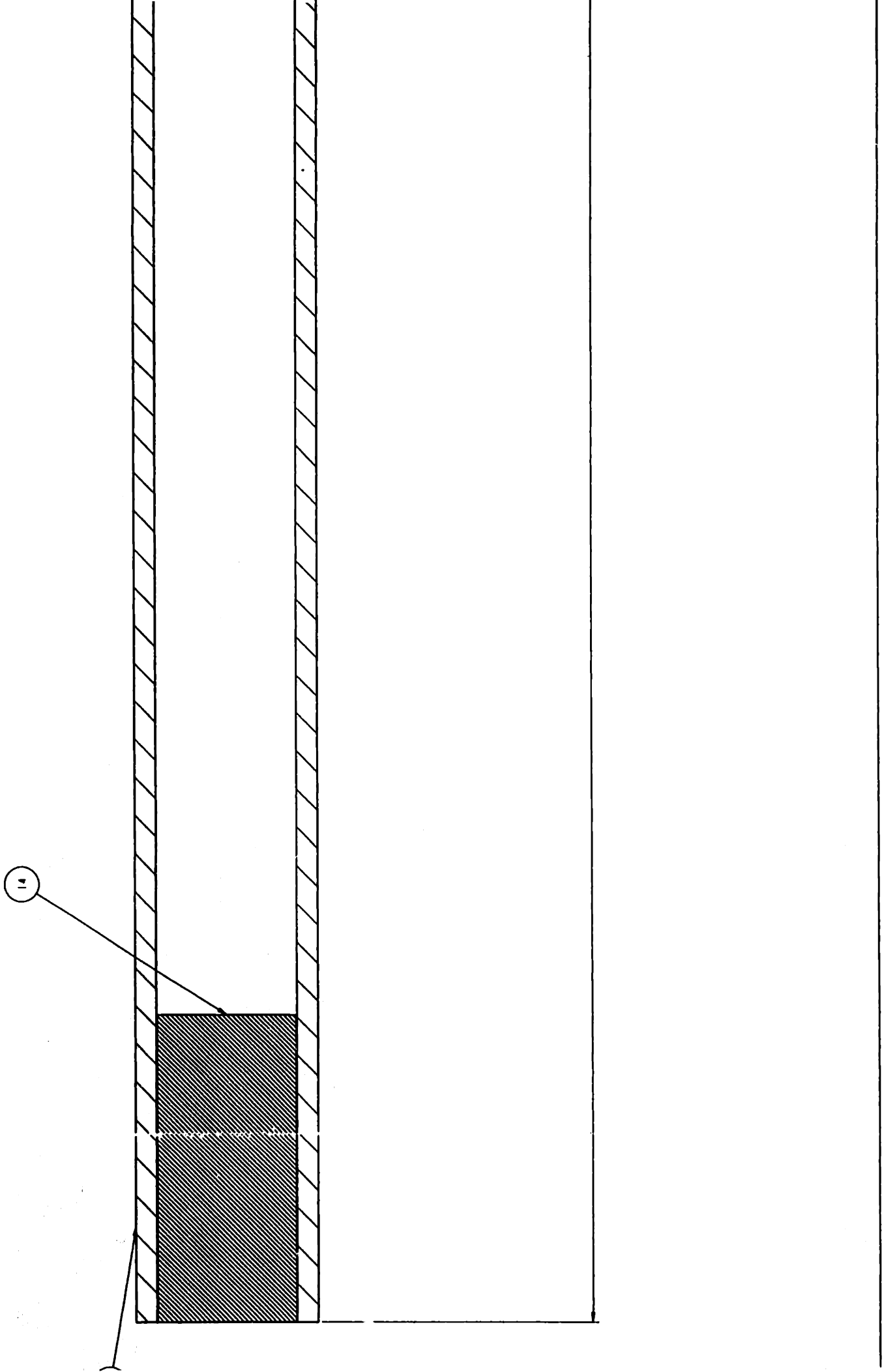

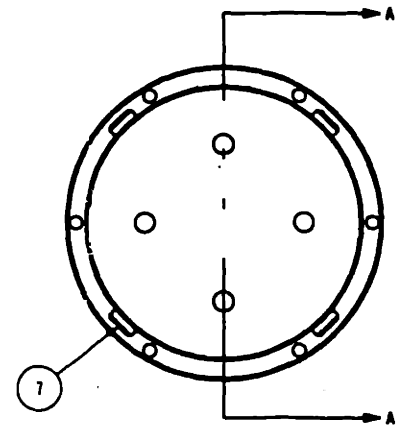

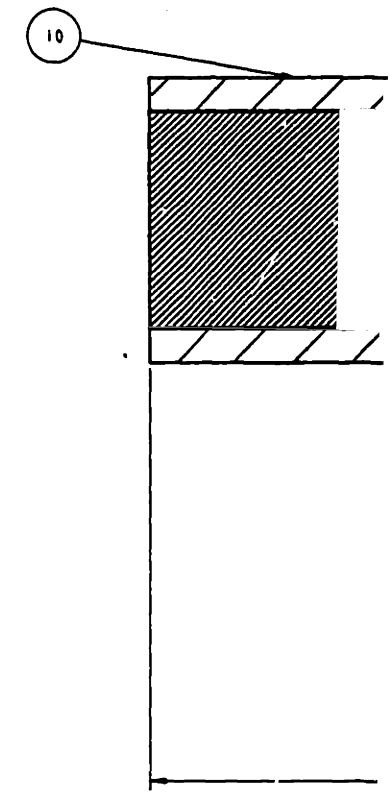

PRODUCT PARTS LIST				
ITEM	LVL	PART	QTY	TITLE
1	2	TOOL2	1	Compressor Assembly
2	2	ASPACER	2	ASSEMBLY SPACER
3	2	MOTORAS	1	Motor Assembly
4	2	UNIV-END	2	Boston Gear Universal Joint End
5	2	UNIV-MAL	1	Boston Gear Universal Joint
6	2	UNIV-FEM	1	Boston Gear Universal Joint
7	2	B013002	32	SCREW, SOC HD 1/4-20 X 3/8 STL
8	2	ASPACER2	2	ASSEMBLY SPACER
9	2	LUBEEND2	1	LUBRICATOR/FLASK JOINT
10	2	DFLASK	1	UDFH Flask
11	2	LUBESYS	1	Force Feed Lubrication Assembly
12	2	UPPERTANK	1	Upper Tank/Hot Heat Exchanger Assembly
13	2	LOWERTANK	1	Lower Tank, Sample Electronics, and Cold Heat Exchanger Assembly
14	2	TEFLON	2	Teflon Shavings